AD-A109 679   ESL INC SUNNYVALE CA   F/G 20/14
               PLACES QUICK-LOOK REPORT FOR BEACON AND AIRCRAFT EXPERIMENTS.(U)
   MAR 81 J MARSHALL, J LEHMAN, G ELSTON   DNA001-80-C-0090
UNCLASSIFIED   ESL-TM1344   DNA-5737F   NL

I ᴼᶠ 3
AD A
109679

1.0

2.8 2.5

3.2 2.2

3.6

2.0

1.1

1.8

1.25 1.4 1.6

MICROCOPY RESOLUTION TEST CHART

AD A109679

⑫
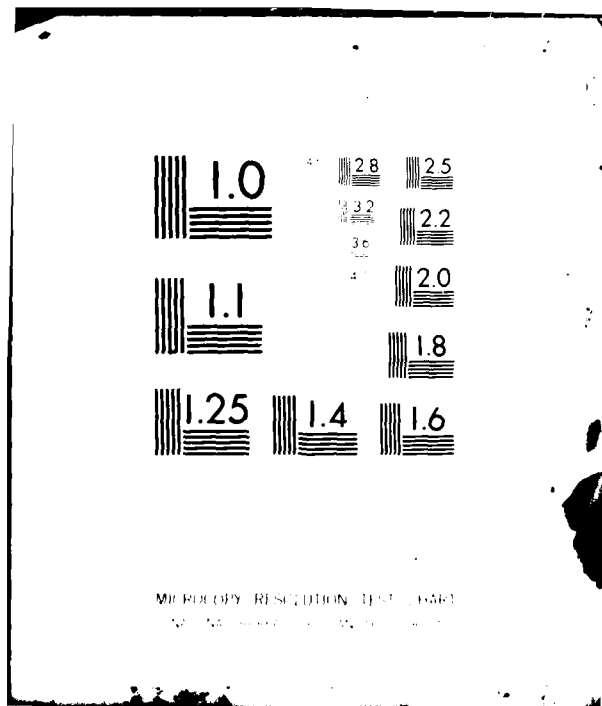
DNA 5737F

PLACES QUICK-LOOK REPORT FOR BEACON AND AIRCRAFT EXPERIMENTS

ESL Incorporated

495 Java Drive

Sunnyvale, California 94086

31 March 1981

Final Report for Period 19 December 1979—31 March 1981

CONTRACT No. DNA 001-80-C-0090

JAN 1 9 1982

Prepared for

Director

DEFENSE NUCLEAR AGENCY

Washington, D. C. 20305

01 15 82033

REPORT DOCUMENTATION PAGE		READ INSTRUCTIONS BEFORE COMPLETING FORM
1. REPORT NUMBER DNA 5737F	2. GOVT ACCESSION NO. AD-A1096 79	3. RECIPIENT'S CATALOG NUMBER
4. TITLE (and Subtitle) PLACES QUICK-LOOK REPORT FOR BEACON AND AIRCRAFT EXPERIMENTS		5. TYPE OF REPORT & PERIOD COVERED Final Report for Period 19 Dec 79 - 31 Mar 81
		6. PERFORMING ORG. REPORT NUMBER ESL-TM1344
7. AUTHOR(s) Dr. James Marshall, Jeff Lehman, Gary Elston, Wayne Solbrig		8. CONTRACT OR GRANT NUMBER(s) DNA 001-80-C-0090
9. PERFORMING ORGANIZATION NAME AND ADDRESS ESL Incorporated 495 Java Drive Sunnyvale, California 94086		10. PROGRAM ELEMENT, PROJECT, TASK AREA & WORK UNIT NUMBERS Subtask I25AAXHX638-06
11. CONTROLLING OFFICE NAME AND ADDRESS Director Defense Nuclear Agency Washington, D.C. 20305		12. REPORT DATE 31 March 1981
		13. NUMBER OF PAGES 224
14. MONITORING AGENCY NAME & ADDRESS(if different from Controlling Office)		15. SECURITY CLASS. (of this report) UNCLASSIFIED
		15a. DECLASSIFICATION/DOWNGRADING SCHEDULE N/A

16. DISTRIBUTION STATEMENT (of this Report)

Approved for public release; distribution unlimited

17. DISTRIBUTION STATEMENT (of the abstract entered in Block 20, if different from Report)

18. SUPPLEMENTARY NOTES

This work sponsored by the Defense Nuclear Agency under RDT&E RMSS Code B322080462 I25AAXHX63806 H2590D.

19. KEY WORDS (Continue on reverse side if necessary and identify by block number)

PLACES Experiment	Satellite Communications
Barium Release	Navigation
Scintillation Data	Striations
Fading Data	

20. ABSTRACT (Continue on reverse side if necessary and identify by block number)

During December 1980 the Position Location and Communication Effects Simulations (PLACES) Experiment was conducted to investigate the effects of structured ionospheric plasmas on satellite communications and navigation systems. A structured plasma environment was created by a 48 kgm barium release from a rocket launched from Eglin AFB, FL. Measurements of propagation effects on signals from the LES-8 satellite over the Pacific Ocean to a KC 135/662 aircraft operating in the Florida area were conducted (Aircraft (over)

DD FORM 1473 EDITION OF 1 NOV 65 IS OBSOLETE

20. ABSTRACT (Continued)

(Experiment) as well as measurements of the time-of-arrival spread of energy on a phase coded spread spectrum signal emanating from a rocket launched behind the barium cloud and received at specially constructed ground receiving sites in northern Florida (Beacon Experiment). This report presents a quick-look at the data measurements obtained from the aircraft and beacon experiments.

Accession For

NTIS GRA&I	X
DTIC TAB	☐
Unannounced	☐
Justification	

By
Distribution/
Availability Codes
Avail and/or
Dist   Special

A

TABLE OF CONTENTS

1

LIST OF ILLUSTRATIONS

LIST OF ILLUSTRATIONS (Continued)

LIST OF ILLUSTRATIONS (Continued)

LIST OF ILLUSTRATIONS (Continued)

LIST OF ILLUSTRATIONS (Continued)

LIST OF ILLUSTRATIONS (Continued)

LIST OF ILLUSTRATIONS (Continued)

LIST OF TABLES

SECTION 1
INTRODUCTION

1-1   GENERAL.

The Position Location and Communications Effects Simulations (PLACES)
Experiment sponsored by the Defense Nuclear Agency was conducted during December
1980 to investigate the effects of structured ionospheric plasmas on satellite
communication and navigation systems. A structured plasma environment was
created by a 48 kgm barium release from a rocket fired from Eglin AFB in northern
Florida. Signal propagation through the striated ion cloud was accomplished by
transmissions from the LES-8 satellite to a KC135-662 aircraft (Aircraft Experi-
ment) and from a second rocket fired above the barium cloud to two ground stations
located at Cape San Blas and St. George Island (Beacon Experiment). Another
rocket was fired directly through the barium cloud to measure the in-situ plasma
properties (Probe Experiment[1]). Ground optical experiments were conducted as
well[2]. This report is intended to provide a quick look at the beacon experi-
ment and aircraft experiment data.

1-2   TEST OBJECTIVES.

The primary purpose of the PLACES experiment was to measure the time-of-
arrival fluctuations and spread that are associated with radio wave propagation
through a strong scatter striated plasma environment. The measurements of time-
of-arrival spread and jitter are relevant to the strategic performance of wideband
pseudonoise SHF communications and navigation systems including NAVSTAR GPS. The
frequency domain manifestation of time-of-arrival spread is fading decorrelation
with frequency, and thus, the results of this configuration are also relevant to
wideband frequency hopping systems. The beacon experiment provided these
measurements of the time-of-arrival fluctuations and spread.

The primary purpose of the aircraft experiment was to measure the barium cloud fading channel in order to provide data for back propagation diagnostics of the plasma structure evolution. The secondary purpose was to generate real-time diagnostic information about the barium cloud plasma structure that could be used to guide the beacon rocket transmission experiment launch timing. Additionally, the aircraft experiment data is an aid to the interpretation of the beacon experiment data.

1-3   TEST CONCEPT.

A total of four 48 kgm barium releases were conducted. These releases were named GAIL (12/4/80), HOPE (12/6/80), IRIS (12/8/80) and JAN (12/12/80). Four beacon and two probe rockets were planned to be launched during this series; however, due to a sequence of events it was only possible to launch two beacon rockets and one probe rocket. Fortunately, each of these launches was successful and have provided valuable data. The aircraft experiment was successfully conducted following each release. The program was conceived and designed to ensure a high probability of success after accounting for the possibility of certain failures and this objective was met.

1-3.1   Beacon Experiment Test Concept.

The beacon experiment uses two signals transmitted from the beacon rocket. A strong scatter striated plasma environment of interest is created at VHF by the barium environment. For this reason, a VHF link at 98 MHz is used. This VHF link is biphase modulated by a pseudonoise signal at a 9.8 megachip per second rate. The beacon receiver stations, by virtue of the high rate PN modulation, perform high resolution cross-correlation measurements of the propagation channel, and in particular, measurements of its time-of-arrival fluctuation and spread properties. A C-band CW signal at 4116 MHz (98 MHz x 42) is also transmitted by the rocket in phase coherence with the 98 MHz VHF signal. This signal provides a phase and time

12

reference to remove the effects of rocket motion induced on the VHF signal, thus, leaving only propagation channel effects. The beacon rocket payload also carries a C-band transponder at 5 GHz, a telemetry transmitter at S-band, and three strobe lights to allow RF and optical tracking. While there was about a 50 percent chance that the beacon strobe lights would be visible to the unaided eye, even the intensified TV optics did not detect the beacon rockets launched during event IRIS. This was believed to be due to high cirrus clouds.

Since the rocket transmissions fall into the commercial FM band with side-lobes that spill over into the TV and aeronautical navigation bands, test planning coordination with the FCC and FAA as well as other regulatory agencies was necessary. On the air testing approval was granted for the launch window each night during December following advanced notification of a launch. In spite of the well publicized potential for interference, none was observed nor noted.

For the purposes of launching the beacon rocket and the probe rocket the cloud tracking was performed by a TV tracking station at D3 near the Cape San Blas ground receiver site and by a TV tracking station at the A-15 launch complex. The beacon rocket was to have been aimed so that its trajectory would lie 100 kilometers behind the barium cloud as viewed from a ground station. Due to the southern extreme occultation geometry achieved, it was necessary to use a 40 kilometer occultation target distance. Two adequately separated ground stations were provided to better assure occultation in spite of rocket inaccuracies. Useful occultation data was obtained at both sites on each flight, although propagation effects were generally better at one site than another, as expected.

Preliminary planning called for the launch of one probe and one beacon rocket on the first barium release. Ideally, the probe rocket penetration of the barium cloud should occur near the same time as the beacon rocket occultation. These rockets are launched after the ion cloud is both well structured and optically visible. A similar rocket launch format was planned for the third barium release. On the second release the launch of two beacon payloads was

planned. During the fourth release if all launches occurred as scheduled no payload launches would be required. Diagnostics would, however, be performed by the aircraft on this release which could have been performed considerably earlier than local sunset since the visibility requirement of the rocket beacon experiments would no longer exist. The barium clouds drift azimuth was more variable than expected, which together with real time tracking difficulties and range safety constraints resulted in fewer launches than planned. Two beacon rockets were launched during the third release (IRIS) and a probe rocket was launched during the fourth release (JAN).

1-3.2 Aircraft Experiment Test Concept.

The aircraft experiment used two UHF tone signals, one transmitted from the aircraft (doppler precorrected) to LES-8/9 and one received (doppler corrected) from LES-8/9 at the aircraft. Doppler correction is provided by a K-band reference signal generated at the satellite coherently with the UHF signal. These signals were used successfully during the STRESS experiment in 1977. The capability represented by the aircraft experiment is unique in its ability to provide data on the evolution of plasma structure that satisfy the needs of the nuclear effects community and in that it enhances the volume and quality of results, not only from a communications perspective, but also from the perspective of plasma phenomenology and propagation. It was anticipated that better quality as well as quantity of data would be obtained during the PLACES experiment than obtained during the STRESS experiment. This improvement was expected through improved real-time diagnostics and aircraft control procedures. A quick look at the data collected indicates that this improvement was achieved.

With some minor modifications, the aircraft positioning system that was used during STRESS was used during PLACES. This system consisted of radar (FPS-85) cloud tracking, aircraft position tracking, and two-way communication between the aircraft and the Central Control Facility (CCF). The aircraft was directed, via

the communications link, to the region of predicted scintillation effects. This region is the "shadow" of the barium ion cloud that has been calculated from the measured ion cloud position and the precomputed satellite position. A significant improvement in this system over that used during STRESS was the transmission of real-time diagnostic data from the aircraft to the experiment control center at the CCF. At times the real time link was the only means available to position the aircraft as the FPS-85 radar, as a result of several unrelated problems, was unable to provide proper ion cloud track information on several occasions and optical tracking was only available as a backup during the 40 minute twilight optical window.

1-4   PROGRAM PARTICIPANTS.

The PLACES program is sponsored by the Defense Nuclear Agency. The aircraft and beacon experiments were conceived and implemented by ESL Incorporated. The field operations necessary to accomplish the program experiments were planned and carried out by SRII. The collection of the satellite experiment data was a joint effort of the Air Force Wright Avionics Laboratory/AAAD, ESL, and DNA. The special tone processing hardware fabricated by ESL for the STRESS program in 1977 was used for the aircraft experiment. AFWAL provided and operated the LES-8/9 communications equipment.

The program participants and their areas of responsibility are as follows:

DNA   Program sponsorship and management

SRII   Field operations, test direction, FPS-85 radar
            tracking, TV tracking system, Ionosonde, and
            magnetometer.

ESL	Aircraft and beacon experiment design, fabrication, implementation and measurements, beacon payloads, beacon ground stations.
AFWAL/AAAD	Provide and operate LES-8/9 communications equipment, satellite scheduling, and aircraft experiment data collection.
4950th	Test aircraft support.
SLA	Rocket operations, payload integration.
Thiokol	Barium payloads.
NRL	Pulsed plasma probe rocket experiment.
AFGL	Mass spectrometer on probe rocket experiment.
TIC	Ground photography.
LASL	Intensified optics.
ESD	Satellite support.
ADTC	Eglin Test Range operation.

SECTION 2
BEACON EXPERIMENT RESULTS

2-1   INTRODUCTION.

Two beacon rockets were launched during event IRIS of the PLACES
Experiment. Successful data was recorded from each of these beacons at both
ground receiving sites, Cape San Blas (D3A) and St. George Island. The ground
receiving systems effectively measure the complex channel impulse response of
the striated barium plasma. The technique used to recover the channel impulse
response relies on the processing of the pseudorandom phase modulation of the
rocket transmitted signal. The received signal inphase and quadrature compon-
ents are hardware cross-correlated with a replica of the modulating PN sequence
in the ground station receiver. Provided the PN sequence autocorrelation is
sufficiently narrow compared to the time delay extent of the channel impulse
response, an accurate representation of the channel impulse response is realized.
The beacon experiment hardware configuration is described in Appendix A. While
the complex channel transfer function has been measured, only its magnitude is
presented herein. No other beacon rockets were launched during the PLACES
series of barium releases due to range safety and operational constraints.
Strongly contributing to these launch difficulties was the unusual northward
drift of the other three barium releases. Section 3 includes a description of
these other events.

2-2   OCCULTATION GEOMETRY.

TV track data from Eglin AFB sites D3 and A-15 were used for targeting
the simultaneous beacon rocket occultation of the D3A and St. George Island
receiving sites. The trajectory flown on Flight 1 and Flight 2 are shown on
Figures 2-1 and 2-2. The time since launch is indicated on these trajectories.
Also shown is the indicated FPS-85 radar location of the maximum density portion
of the ion cloud at the occultation time.
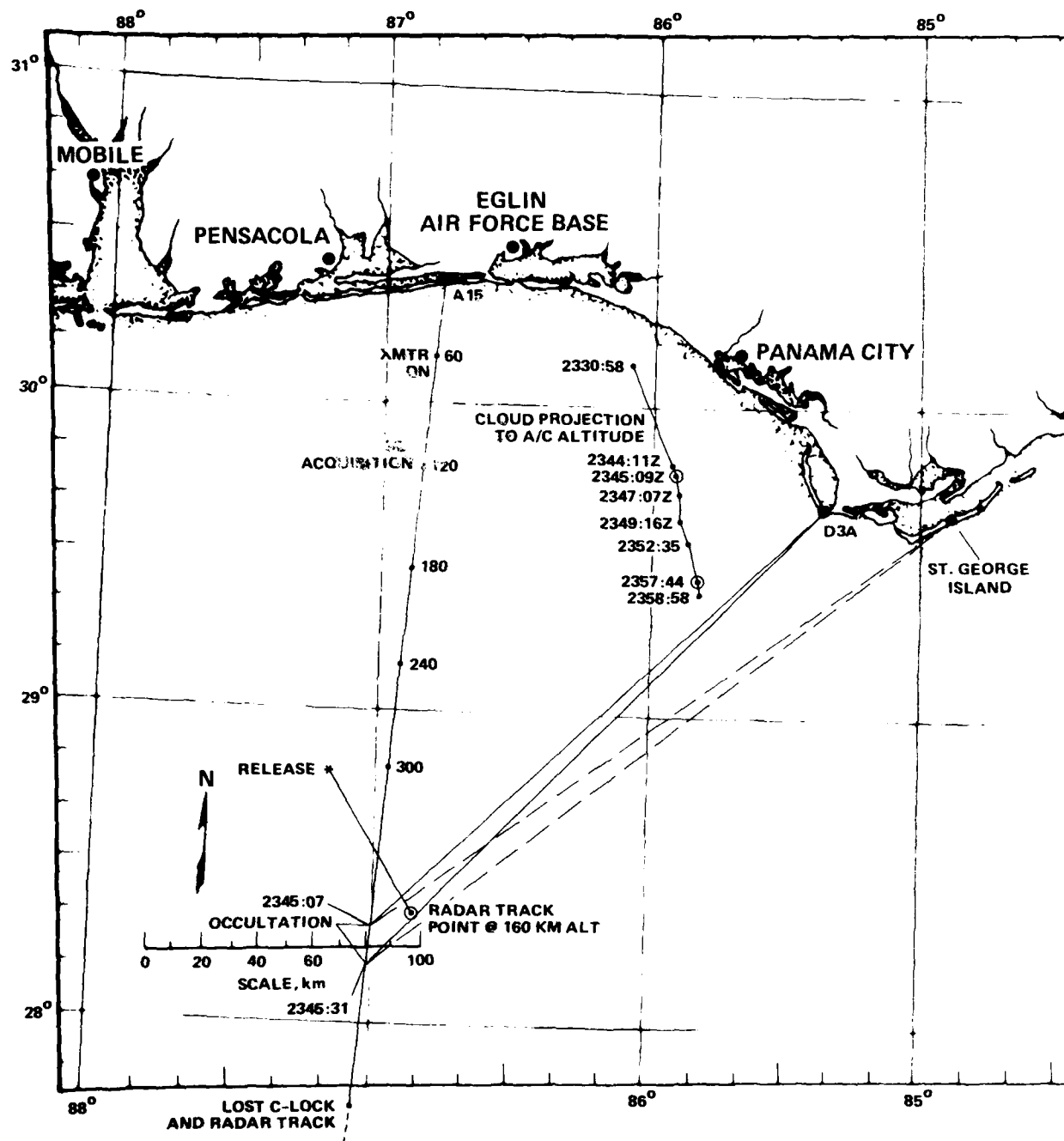
Figure 2-1. Beacon Rocket Trajectory Flight 1
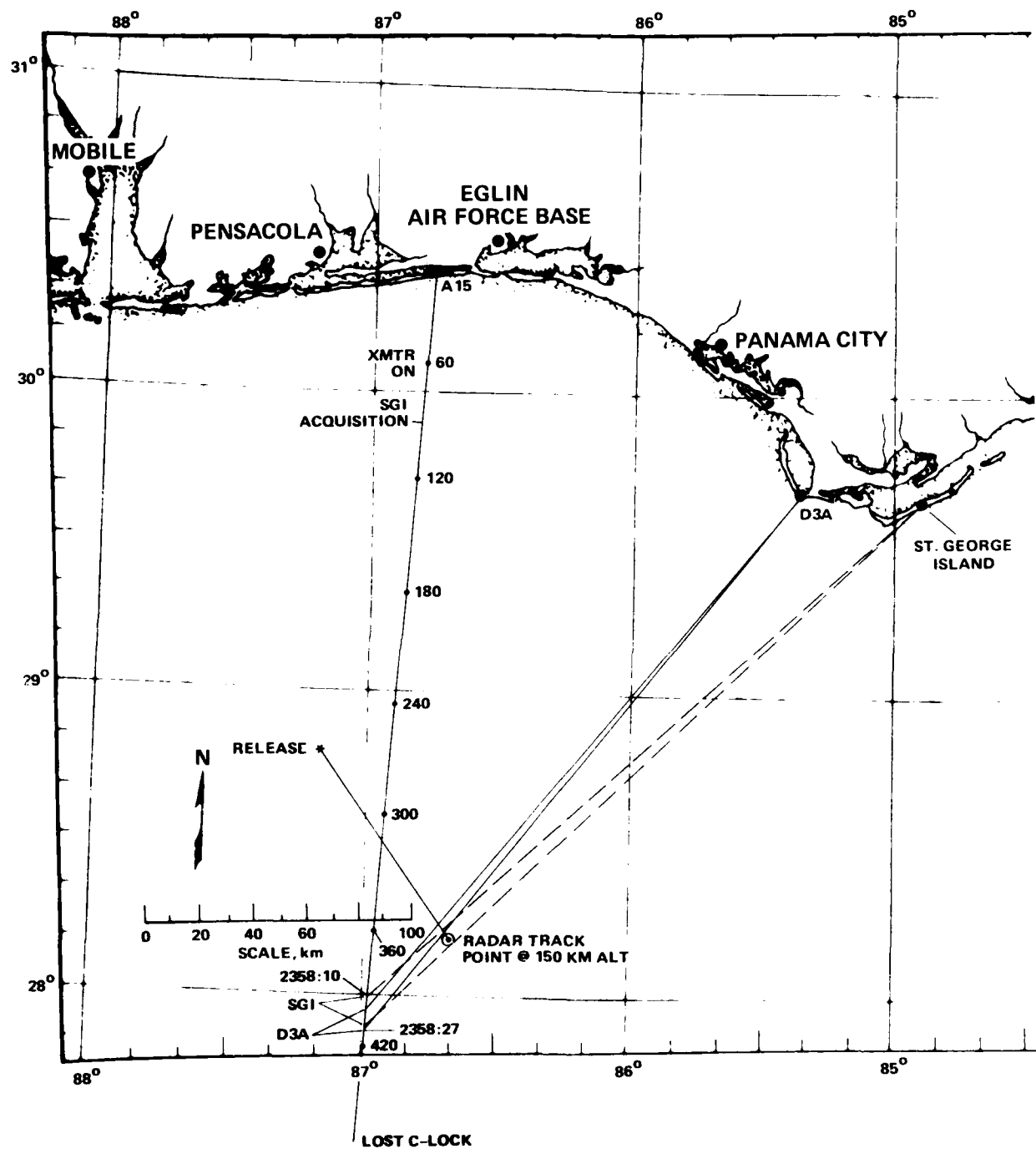
Figure 2-2. Beacon Rocket Trajectory Flight 2

Table 2-1 summarizes the launch sequence of events for both flights. Also shown are the aircraft transit times and pass number nearest the beacon occultation times. During the occultation the rocket velocity is approximately 1.44 km/s, thus, the occultation times are short.

Table 2-2 provides a summary of the occultation geometries. The site geodetic locations are also provided for reference. The peak plasma density location from the FPS-85 radar at occultation time are shown as is the peak density measured by the radar[4]. It is interesting to note that the indicated peak density values are somewhat less than for the STRESS event ESTHER; the peak density for ESTHER[5] was approximately 7.3×10^{12} m^{-3} at 30 minutes. On the other hand, the radar data also indicated the cloud is somewhat larger than ESTHER at this time. These estimates could change somewhat upon final calibration of the radar data. The aircraft data would imply the scintillation effects are at least as strong as during ESTHER (see Section 3) perhaps indicative of a larger striation extent.

The elevation angles were lower than planned due to the extreme southern occultation geometry, but were well within the design constraints of the VHF antenna. The occultation occurred nearly 60 kilometers south of the southern boundary of the intended cloud drift region. Figure 2-3 shows the anticipated cloud drift zone along with the four barium release locations and their approximate initial drift directions. Outside the northern boundary a down-leg beacon occultation could not successfully be conducted. Outside the southern boundary a 100 kilometer occultation distance could not be achieved but a 40 kilometer occultation distance was possible. As indicated, three of the four barium releases initially drifted northward. IRIS drifted southeast. Section 3 provides a description of the other releases.

Table 2-1. Launch Sequence for Beacon Experiment During Event IRIS. Times are GMT

	St. George Island	Cape San Blas	Aircraft Pass	Time
Flight 1 (Launch at 23:38:36)				
Payload on Time	23:39:38Z	23:39:38Z	5	23:38:30
Acquisition of PN Code	23:40:38	23:40:15		
Occultation Start	23:45:07	23:45:09		
Occultation End	23:45:31	23:45:30		
Loss of Signal	23:46:54	23:47:04	6	23:46:30
Payload Off Time Setting	23:48:04	23:48:04		
Flight 2 (Launch at 23:51:36)				
Payload on Time	23:52:38Z	23:52:38Z	7	23:51:50
Acquisition of PN Code	23:53:09	23:53:57		
Occultation Start	23:58:10	23:58:17		
Occultation End	23:58:25	23:58:27		
Loss of Signal	23:59:59	23:59:56	8	00:00:40
Payload Off Time Setting	00:01:03	00:01:03		

Barium Launch   23:10:00
Barium Release 23:13:06.7

Table 2-2. Occultation Geometry Summary

	Site	Occultation Time	Cloud[1] Location Lat, Lon, Alt	$N_{e_{max}}$ (m^{-3}) [2]	to Rocket			Occultation Distance (km)	Magnetic Aspect (deg)
					Elevation (deg)	Azimuth (deg)	Slant Range (km)		
Flight 1	St. George Island (29°38'36", 84°54'07")	2345:07 to 2345:31	28.350°, 86.850°, 160 km @2345:24Z	3.7×10^{12}	36.1	235.2	321.1	26.9	-42
	Cape San Blas (D3A) (29°40'00", 85°21'18")	2345:09 to 2345:30			38.2	230.1	303.3	--	-36
Flight 2	St. George Island	2358:10 to 2358:25	28.185°, 86.695°, 150 km @2358.20	2.6×10^{12}	32.6	228.4	331.1	46.0	-41
	Cape San Blas	2358:17 to 2358:27			32.9	222.6	313.6	--	-35

(1) Peak N_e point, per radar track

(2) per radar.
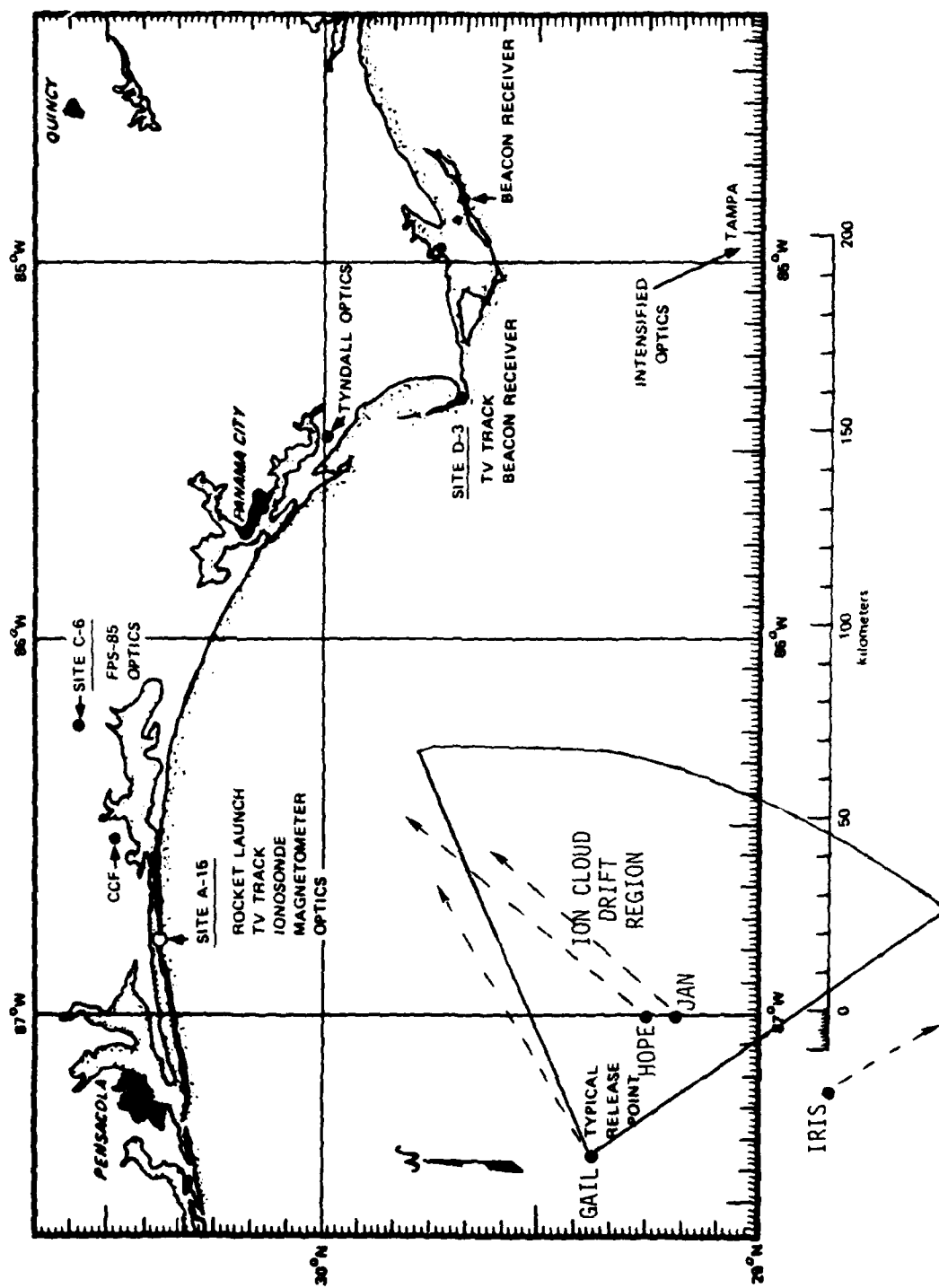
Figure 2-3. Operating Area and Initial Release Drift Directions

23

The magnetic aspect angle was also somewhat less than anticipated due to the extreme southern occultation geometry. As summarized in Table 2-2 the aspect angles were approximately 42 and 36 degrees, respectively, for the paths to the two receiving sites.

The beacon rocket on both these launches was targeted 40 kilometers behind the TV optics cloud track point. On Flight 1 the beacon rocket flew 26.9 kilometers behind the radar maximum density point. The ray path to St. George Island missed slicing the cloud through this maximum density point by approximately 1.9 kilometers. On Flight 2 the beacon rocket flew 46 kilometers behind the radar indicated maximum density point. The line-of-sight to St. George Island on this second shot appears to have passed through the maximum density point indicated by the radar. These distances behind the cloud appear within the predicted rocket trajectory dispersion anticipated.

As shown in Section 2.3, substantially less energy delay spread was noted on the second beacon occultation. While this is believed to be due to the geometry as described later in this section, it is interesting to note that the radar data indicated a 10 kilometer drop in the peak density altitude from 160 to approximately 150 kilometers altitude between the first (2345:24Z) and the second (2358:20Z) beacon occultations. The aircraft data indicated a period of lesser scintillation activity around this time as well. However, the aircraft was transiting approximately 15 kilometers north of the cloud center projection according to the real time tracking displays. On the other hand, on the first occultation strong fading was noted by the aircraft at a 12 kilometer northward miss distance. Aircraft passes approximately 20 minutes after the second occultation again show strong long lasting scintillation effects. It may be that during the time of the second occultation the indicated radar track point was somewhat north of the true cloud center; this needs to be investigated further. If so, the lesser delay spread on the second beacon occultation would be much easier to explain.

The occultation geometry for St. George Island is shown in Figure 2-4 for Flight 1. Also shown are a few data points from the FPS-85 radar cloud track from which a rough estimate for the 10^6 cm^{-3} electron density contour has been sketched. The contour is for the maximum density 160 kilometer altitude plane. Note that the TV optics track point as obtained from the aircraft positioning data agrees well with the radar location of the cloud center. That is, the aircraft projection data reprojected to a 160 kilometer altitude along the path to the LES-8 satellite closely matches the radar data. The actual TV track altitude was not available for comparison.

The line-of-sight path to St. George Island is shown in Figure 2-4 at several times of interest. The intersection of the path with the 160 kilometers altitude plane is indicated by the transition from the solid to dotted line. The four paths show the time at which the first caustic ray is evident in the data, the time at which the first striation object is traversed (the time at which the energy from the first ray is no longer delayed relative to the direct path signal), the time at which the maximum electron content (signal delay) is observed, and the time at which the signal exits the cloud. The rocket altitude at these times is also indicated. For instance, at the time the path enters the cloud, the rocket was at an altitude of 194.3 kilometers and when the path exited the cloud the altitude was 163.3 kilometers. Various altitude points are shown along each ray path as well. The rocket trajectory data was taken from the FPS-16 radar beacon tracking data. There were three FPS-16 radars tracking the beacon rocket. Two of these agree within 50 meters while the third differs by no more than 500 meters.

As a further aid to visualize the manner in which the line-of-sight path slices through the cloud, a line is shown indicating the 160 kilometers altitude point along the magnetic field lines that pass through the ray path. This illustrates, for instance, that field lines through the 10^{12} m^{-3} density contour are not cut until around the time the first object is traversed. It
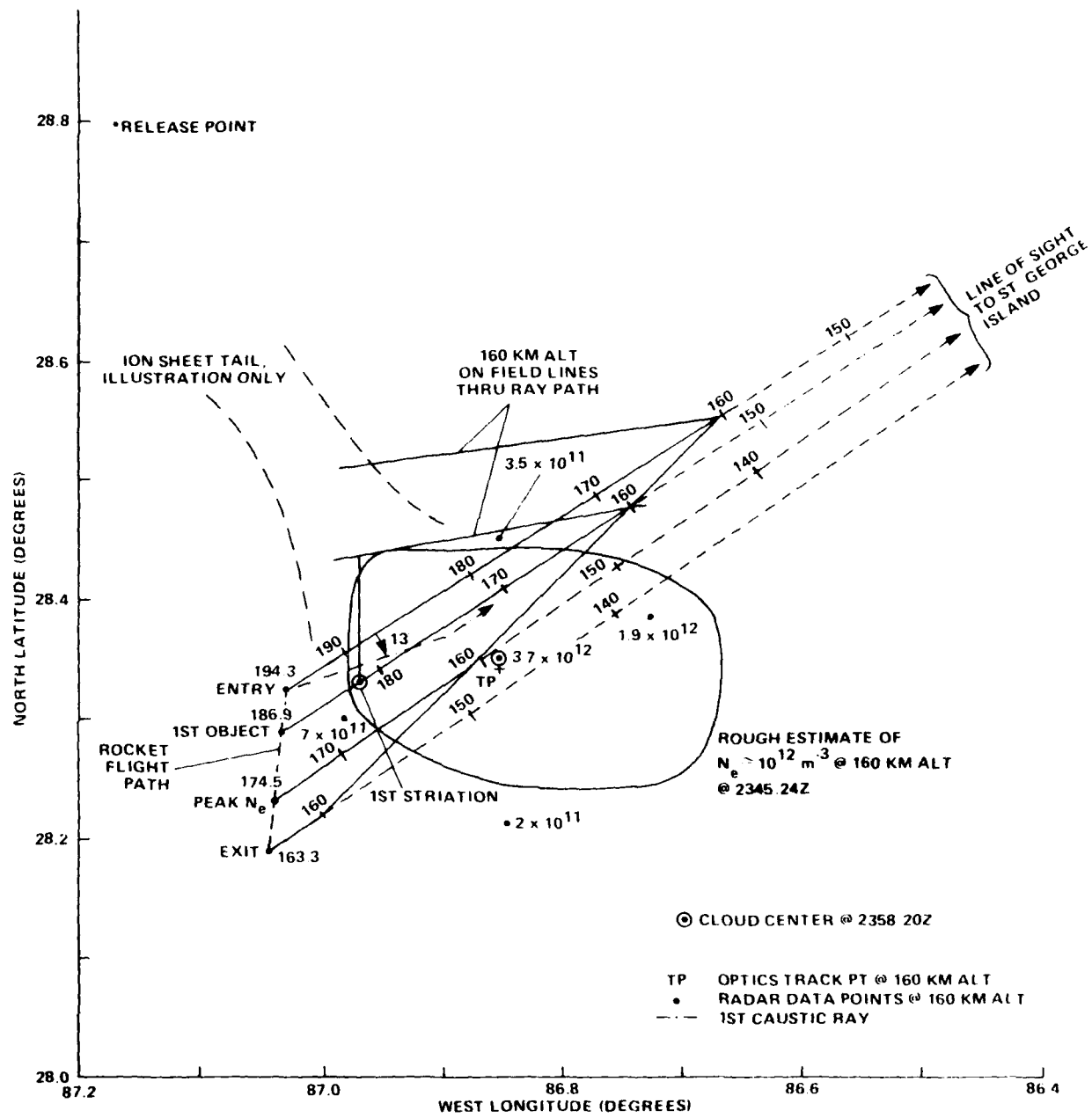
Figure 2-4. Occultation Geometry for St. George Island, Beacon Flight 1

is also from this view that it can be seen that the line-of-sight path to St. George Island missed slicing the cloud at its maximum density point by approximately 1.9 kilometers.

The occultation geometry for Cape San Blas (Site D3A) is shown in Figure 2-5. This figure shows that the path to Cape San Blas sliced the cloud somewhat more toward the tail, missing the radar track point by 3.5 to 4 kilometers.

The position of the first object can be estimated from the first object crossing times and noting the point at which the paths to D3A and St. George Island cross (since the declination of the field lines is very small). This is labeled on Figures 2-4 and 2-5 as the first striation. The field line through this point is sketched down to the 160 kilometer altitude point. This first striation is traversed at approximately 181 kilometers altitude along the path to St. George Island and approximately 176 kilometers altitude along the path to D3A.

It is also possible to roughly estimate the refraction associated with the first caustic. The first ray was observed at a delay of approximately 3 microseconds (a measurement limit). We assume as much as 4 to 5 chips (each 0.1 microsecond) is due to gross plasma delay (see Section 2-3). The excess geometrical path length of the bent ray is then approximately 500 meters. If we assume the ray bending occurs approximately 20 kilometers from the rocket, then the geometry can be solved to show approximately 13 degrees of bending as illustrated on Figure 2-4 by the dot-dash line. It is interesting to note that this places the source of the ray bending in the vicinity of the first striation as seen from St. George Island.

An interesting comparison of this geometry data with the aircraft experiment data can be made. The aircraft transited the ion cloud shadow
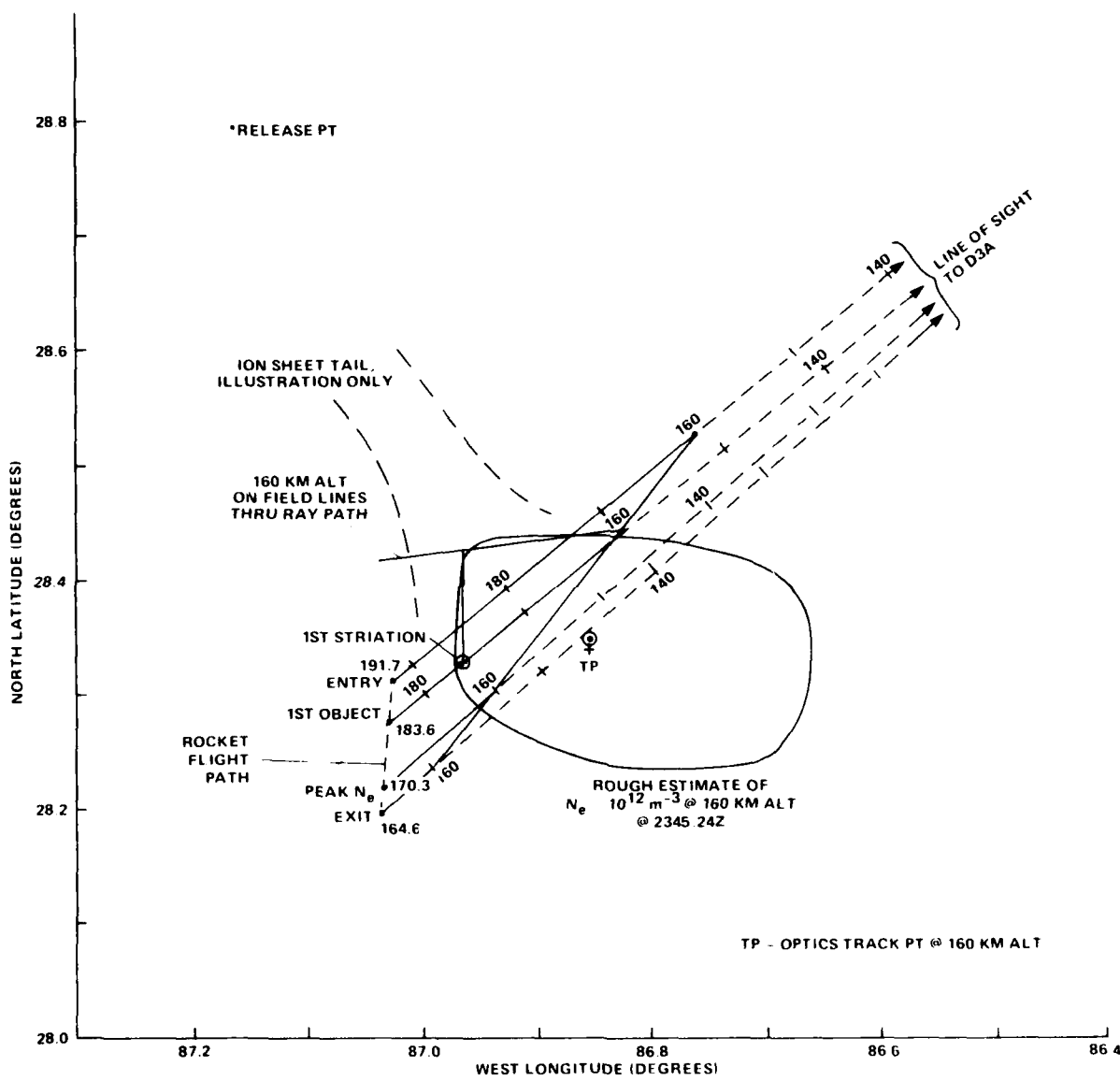
Figure 2-5. Occultation Geometry for Cape San Blas, Beacon Flight 1

approximately 5 minutes 33 seconds prior to the beacon occultation and again 2 minutes 37 seconds after the beacon occultation. From the real time tracking display the relative positions of the FPS-85 cloud center track point and the aircraft position from the FPS-16 radar track can be determined. From this data the intersection of the path connecting the aircraft and the satellite with the cloud geometry can be determined. This is shown in Figure 2-6 for the pass prior to occultation and in Figure 2-7 for the pass following occultation. The shape of the ion cloud contour shown is that roughly estimated from the radar data at the time of occultation. The center has been translated to correspond with the real time display data at the time of the aircraft transit 5 minutes earlier and 2 minutes later. There is some room for error in that the radar track altitude may not be 160 kilometers at these times, however.

The propagation path cut the field line through the cloud center approximately 173 kilometers in altitude. The aircraft propagation path slice through the 160 kilometer altitude plane is nearly orthogonal to the beacon slice because of the near vertical transit of the rocket as opposed to the constant altitude transit of the aircraft. Nonetheless, some of the same field lines are cut.

As the aircraft takes approximately 2 minutes to traverse the fading region, the position of the cloud center will move appreciably with respect to the cloud contour shown. The motion of the cloud center during the transit is indicated by the arrow through the cloud center. The position of the ray path at the beginning and end of the pass corrected for the relative cloud motion are also shown. In effect, relative to the contour drawn, the fading begins somewhat further south (the cloud was further north) and the fading ends further north (the cloud has moved south). The aircraft was in level flight throughout the fading intervals shown.
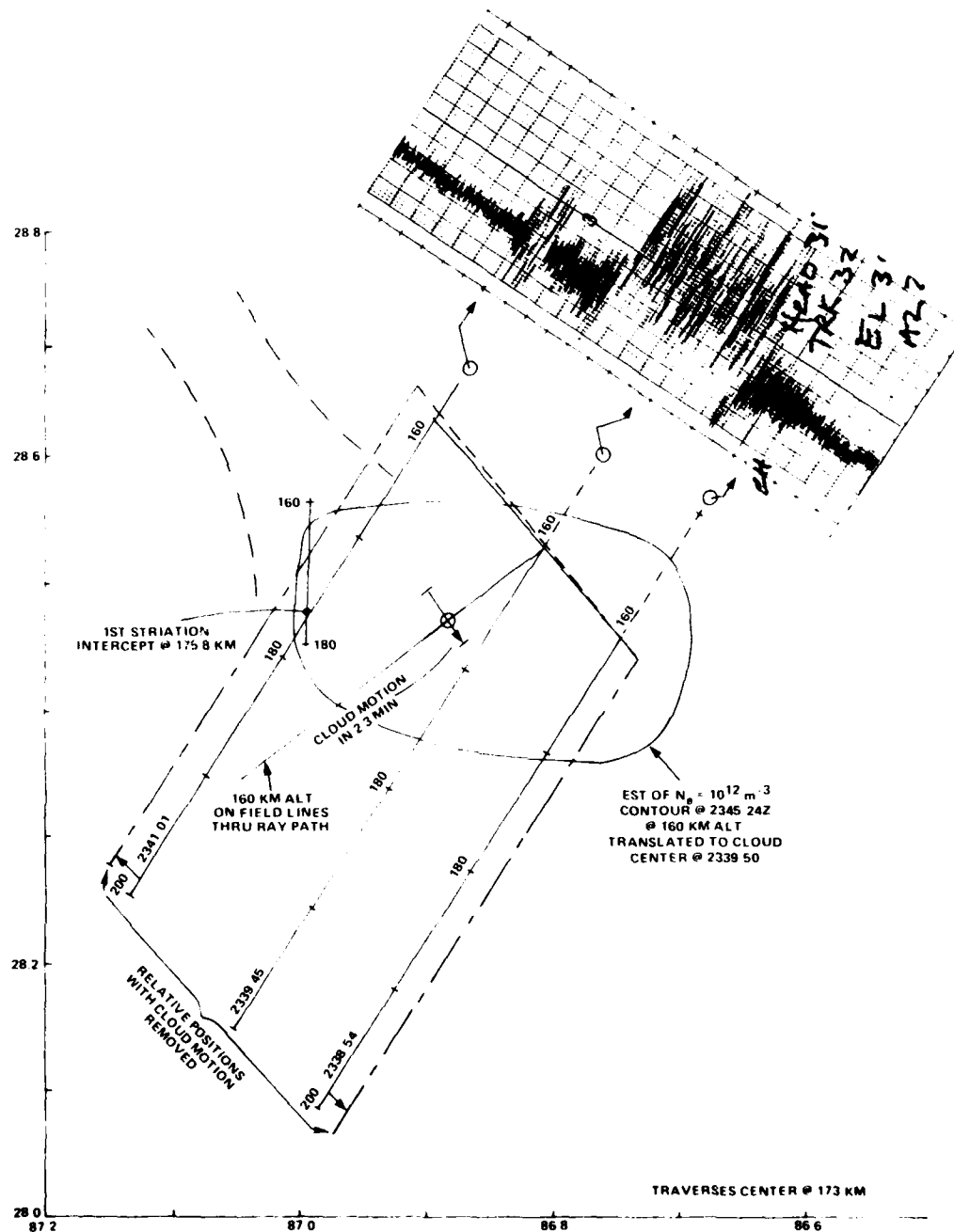
Figure 2-6. Aircraft Occultation Geometry @ 23:39:50Z
(5^m33^s Before Occultation)
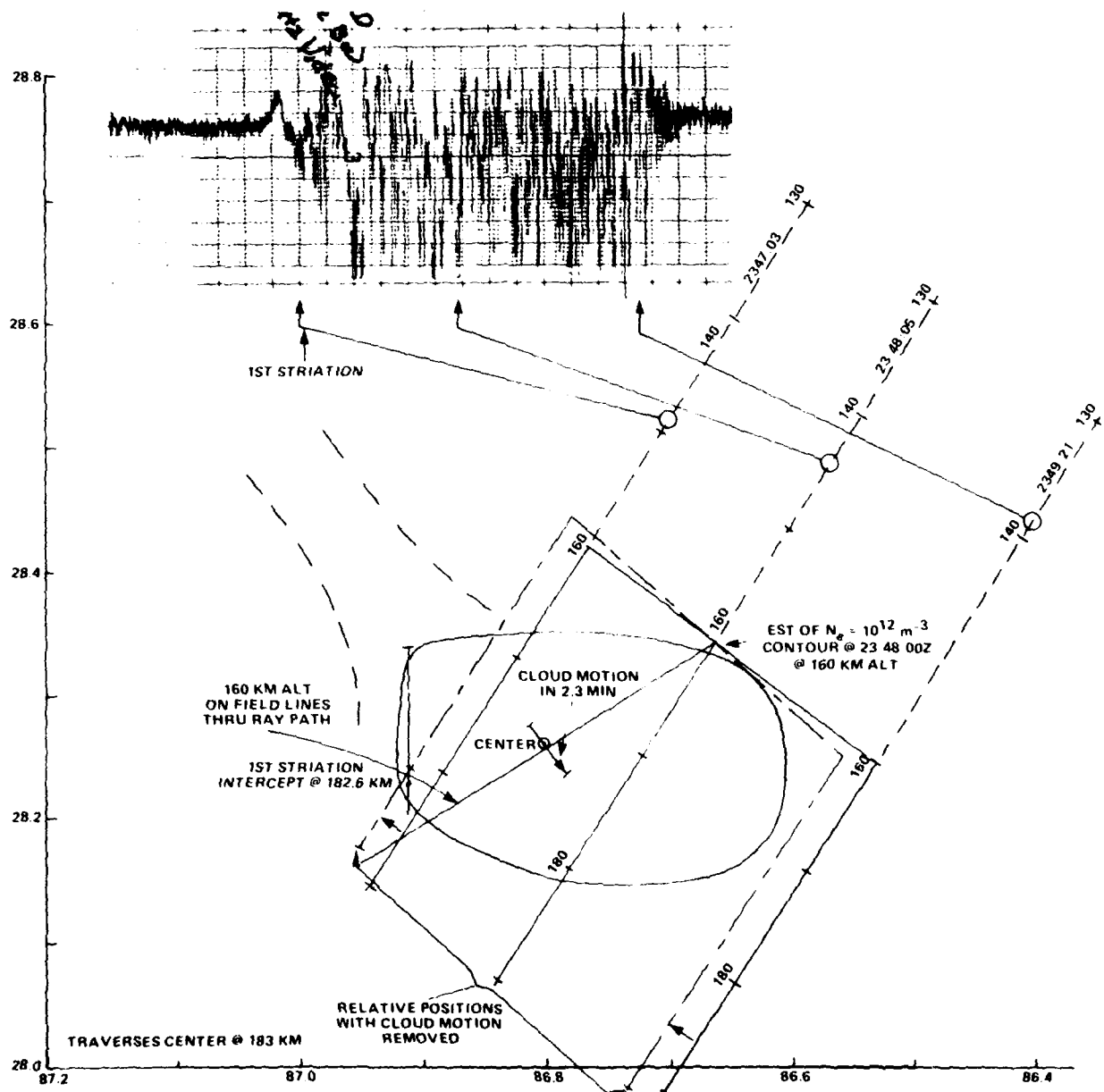
Figure 2-7. Aircraft Occultation Geometry @ 2348Z
(2^{m}37^s After Occultation)

There appears to be reasonable correlation between the contour drawn (appropriate to 5 minutes 33 seconds later) and the observed fading. Further, it appears that there is evidence that striation development is taking place. The aircraft in Figure 2-6 appears to traverse the first striation object seen by the beacon receivers at the northern end of its pass. The path cuts this field line approximately 175.8 kilometers in altitude. Between this object and the main body of the striations there are no structure effects evident in the fading data. In Figure 2-7 fading is observed over the entire aircraft transit of the cloud.

In Figure 2-7 the path traverses the center field line at an altitude of 183 kilometers, approximately 10 kilometers higher than during the earlier transit. It would appear that the first striation object would have been traversed at approximately 183 kilometers in altitude. This geometry can be refined following a more detailed reduction of the radar data.

Figure 2-8 is a photograph of the IRIS release near the time of the first occultation. The neutral cloud can be seen in the upper left-hand corner. In this view the striations appear to be on the southeast side of the ion cloud. As the strobe lights on the rocket are not visible in this photograph, nor were they observed on the TV tracking system for either launch, it is difficult to tell exactly where the rocket trajectory cut the striations. Through triangulation techniques it is anticipated that the rocket path across this view can be determined at a later date. In this view the rocket trajectory makes an angle of 59 degrees with the horizontal, going from the upper right to the lower left side. As a rough guess, the trajectory probably cuts this view such that the lower part of the trajectory exits the cloud near the apparent bend or knee where the striations blend into the background ion cloud.

The occultation geometry for the second beacon is shown in Figures 2-9 and 2-10 for St. George Island and Cape San Blas, respectively. The cloud

32
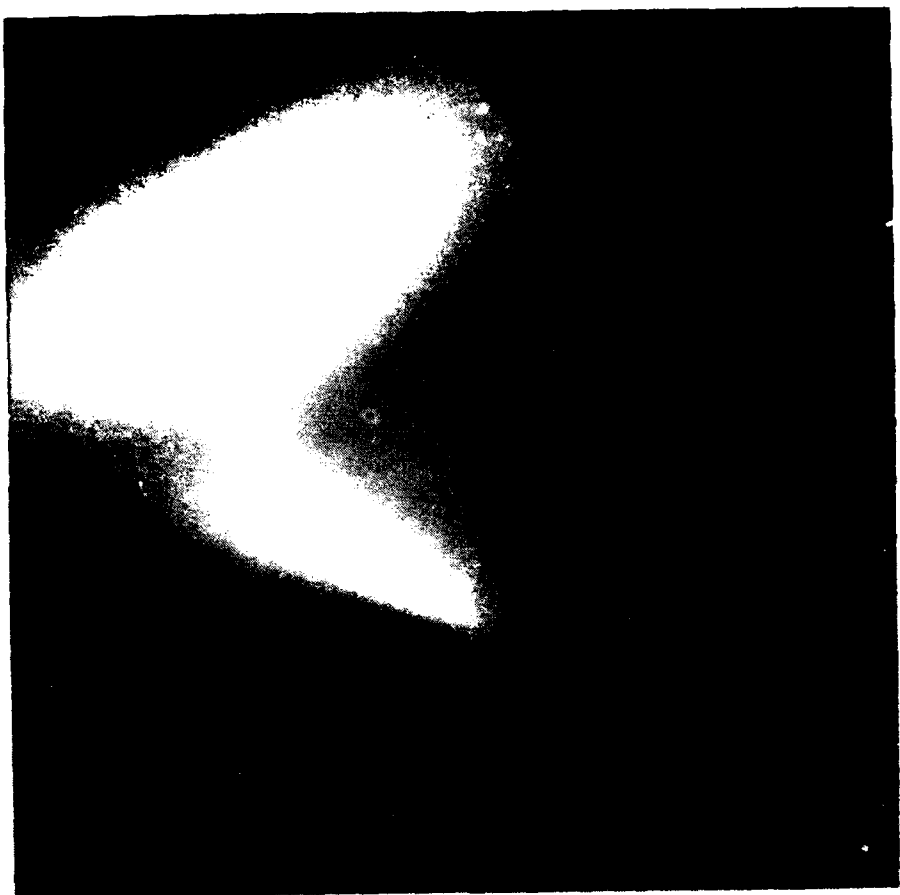
Figure 2-8.   View of IRIS from St. George Island
Near Occultation, Flight I
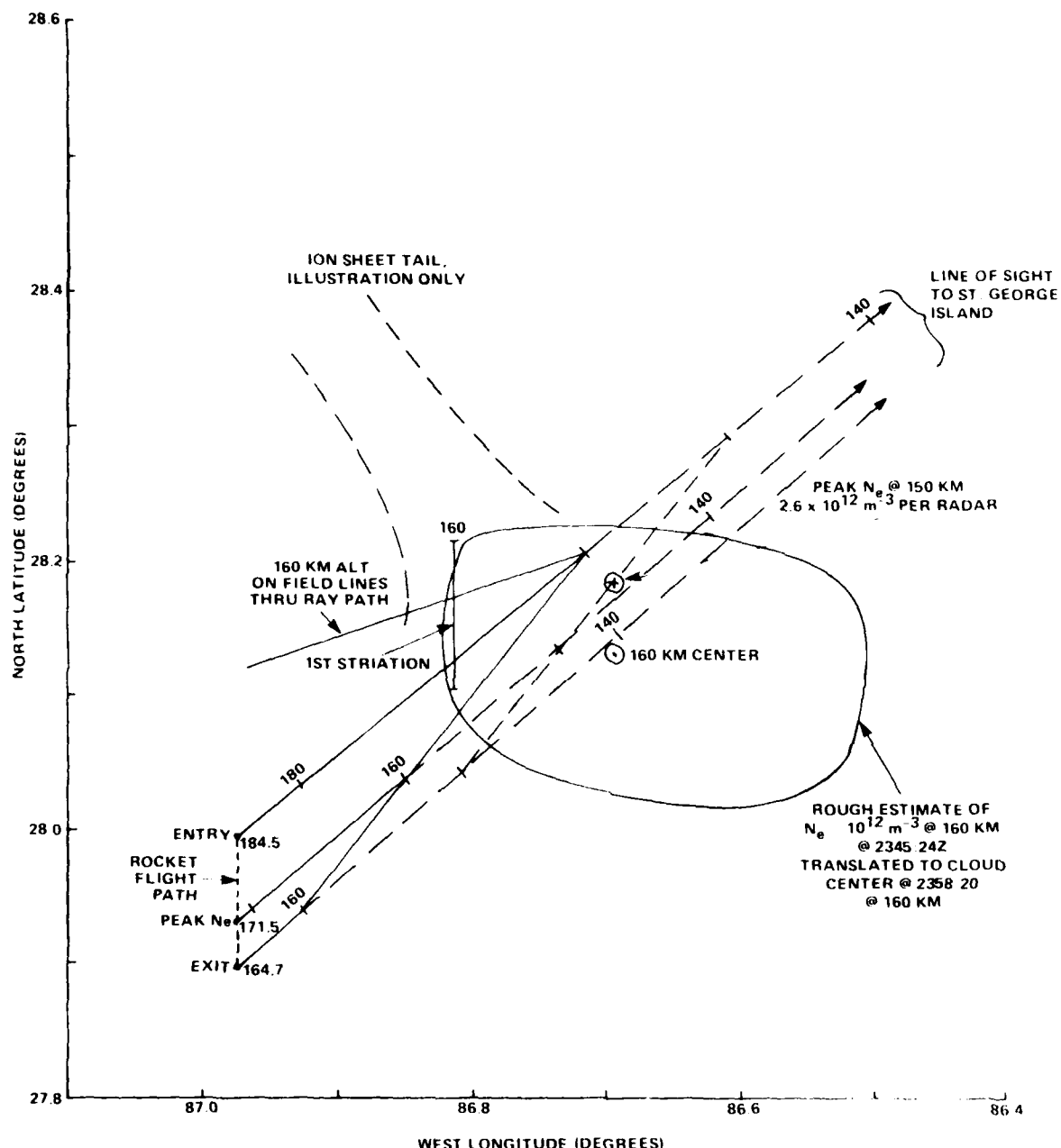
Figure 2-9. Occultation Geometry for St. George Island,
Beacon Flight 2
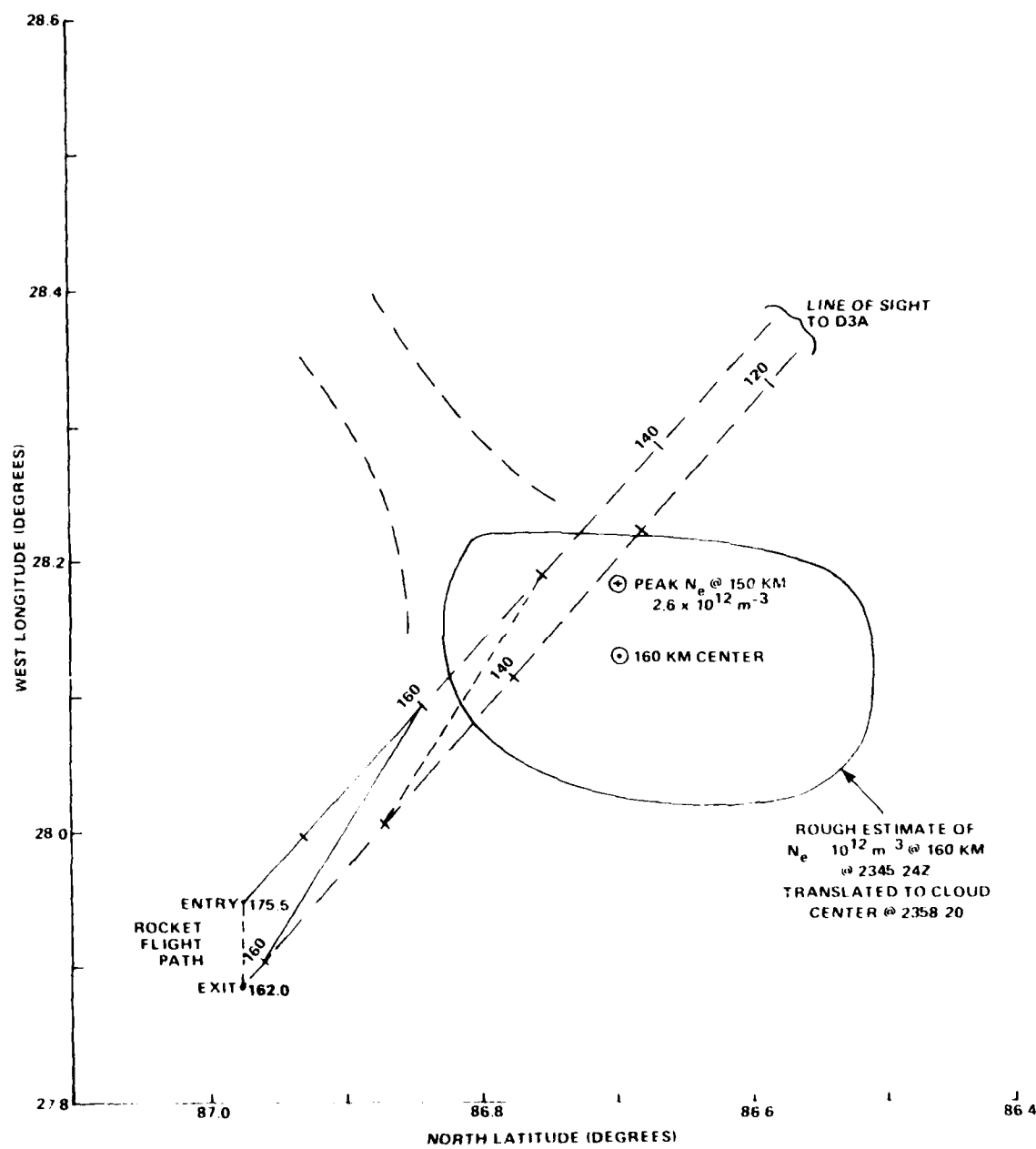
Figure 2-10. Occultation Geometry for Cape San Blas,
Beacon Flight 2

contour shown is that derived for the first occultation and is at 160 kilometers altitude. As discussed earlier, the radar data indicated a drop in peak density altitude from 160 to approximately 150 kilometers in altitude between the first and second occultations. The peak density point at 150 kilometers in altitude is shown as well as the intersection of the beacon line-of-sight path with the 150 kilometer altitude plane.

Figure 2-9 shows that the beacon path cut the 150 kilometer altitude center track point exactly on the path to St. George Island. However, the peak integrated electron content (peak signal delay) occurred somewhat after transiting the indicated center. In comparing Figure 2-4 with Figure 2-9, it would appear that the occultation geomtry was not that dissimilar. However, the second occultation occurred approximately 6 kilometers further back toward the release point. Additionally, the path cuts a slice of the cloud a few kilometers to the south of the first striation object identified on the first occultation. This occultation clearly does not result in as long a distance through the cloud as did the first occultation. If most of the striation development were to the northeast side, then this trajectory would have occulted fewer striations.

The occultation geometry for Cape San Blas, Flight 2, shown in Figure 2-10 shows that the striations were cut very low in altitude. This more than likely accounts for the weak fading and small delay spread observed on this path.

Data pertinent to the system performance during occultation is provided in Table 2-3. The antenna coupling geometry is summarized as are the acquisition times of the receiving equipment. The beacon rocket transmission equipment and both sets of ground station receiving equipment performed flawlessly. The signal-to-noise ratio was somewhat less than anticipated due to the extreme southern occultation coupling geometry and due to a substantially higher RFI environment than measured during the site survey 4 months earlier. The interference power was approximately 4.3 dB higher at St. George Island and

Table 2-3. Occultation Data Summary

	Site	Antenna Angle off Boresight VHF (deg) El	Antenna Angle off Boresight VHF (deg) Az	Antenna Angle off Boresight C-Band (deg)	Rocket Aspect Angle (deg)	Acquisition[3] Time(s) C-Band φ-Lock	Acquisition[3] Time(s) VHF Code	RFI[1] (dBm)	SNR[2] VHF (dB)	SNR[2] C-Band (dB)	Electron Content (cm^{-2}) Cloud	Electron Content (cm^{-2}) Total
Flight 1	St. George Island	-13.9	-22.8	-13.9	41	58	60	-65.3	-32 (32.9)	30$^+$	8.2x10^{12}	9.0x10^{12}
	Cape San Blas (D3A)	-11.8	-17.9	-6.8	36	~35	37	-67.9	-33 (36.6)	--	6.7x10^{12}	--
Flight 2	St. George Island	-17.4	-29.6	-17.4	43	29	31	-65.3	-33	--	7.9x10^{12}	--
	Cape San Blas	-17.1	-25.4	-10.1	38	~77	79	-67.9	-33	--	4.9x10^{12}	--

(1) Total power in 20 MHz

(2) Field estimate; ( )-theoretical

(3) Time from transmitter on time.

6.3 dB higher at Cape San Blas. Even so the VHF SNR in the 200 Hz measurement
bandwidth is a respectable 32 to 33 dB. This can be enhanced further during
the processing of these signals.

The integrated electron content measured at each ground site is also
shown in Table 2-3. The contribution of the background ionosphere is small as
indicated. Figure 2-11 shows the measured electron content over the entire
trajectory along the path to St. George Island for the first beacon. Figure
2-12 provides an expansion of this measurement during the time of occultation.
Also indicated is the general nature of the delay spread of the received signal.
Figure 2-13 shows the corresponding measurement taken at Cape San Blas. These
plots were constructed in the field from the raw data and can be refined at a
later date. Figure 2-14 is a plot of the measured electron content during the
second beacon occultation at St. George Island. For these figures the inte-
grated electron content has been calculated based upon the time-of-arrival shift
in the received signal at each instant in time.

2-3   BEACON EXPERIMENT DATA REVIEW.

Two beacon rockets were launched during event IRIS of the PLACES
Experiment. Successful data was recorded from each of these beacons at both
the Cape San Blas ground station and the receiving station located on St. George
Island. Table 2-1 provided a detailed event chronology of the beacon experiment.

2-3.1   St. George Island Beacon 1.

As anticipated, occultation of the first beacon was initially obtained
at St. George Island. The magnitude of the impulse response recorded is
graphically reproduced in Figure 2-15. This figure represents data collected
over the time interval from 23:45:01.8 to 23:45:34.2, where time is represented
as the third dimension. During this me interval approximately 12,960 samples

38

ST GEORGE ISLAND
IRIS BEACON = 1

Figure 2-11. Measured Electron Content for St. George Island, Beacon #1

39
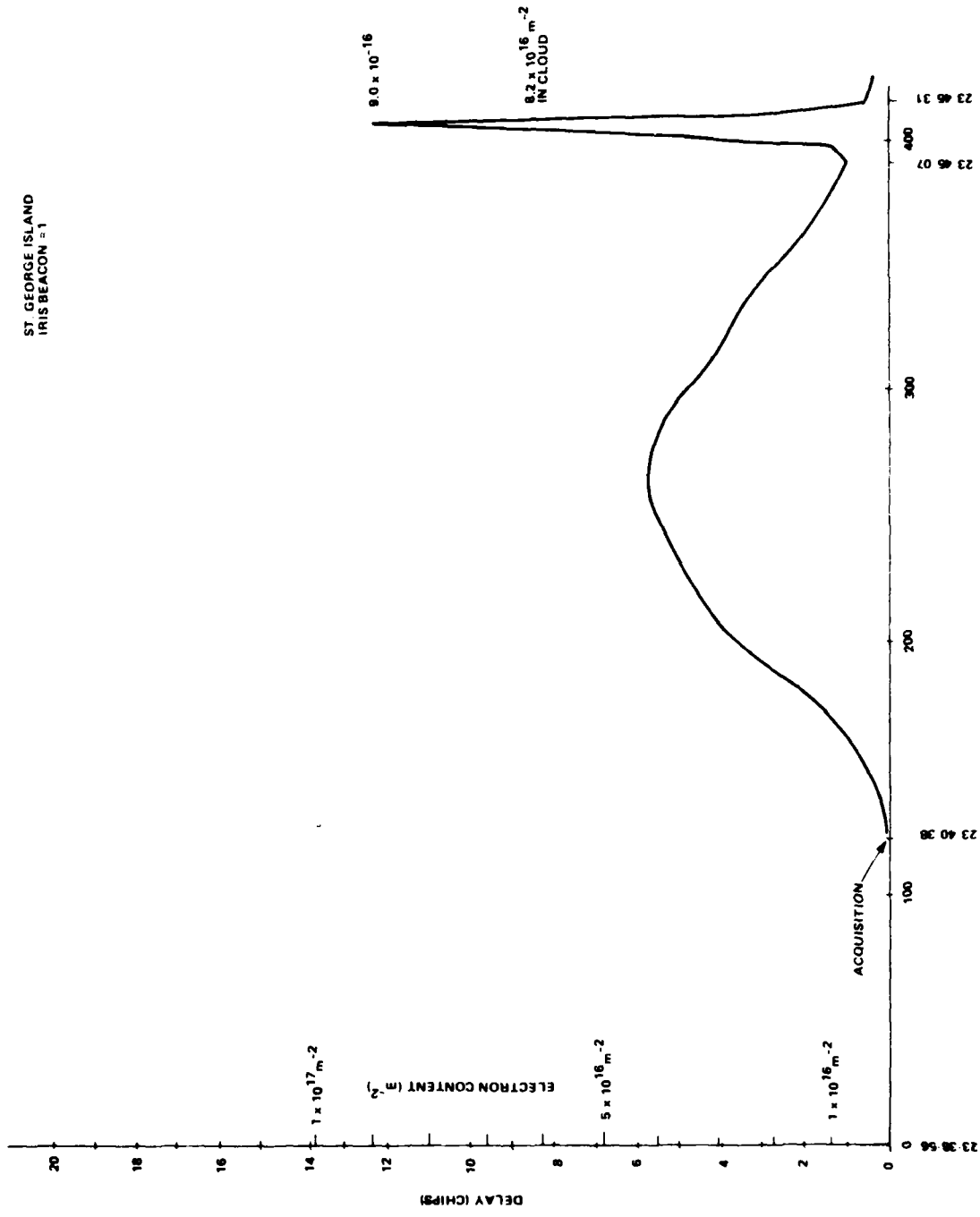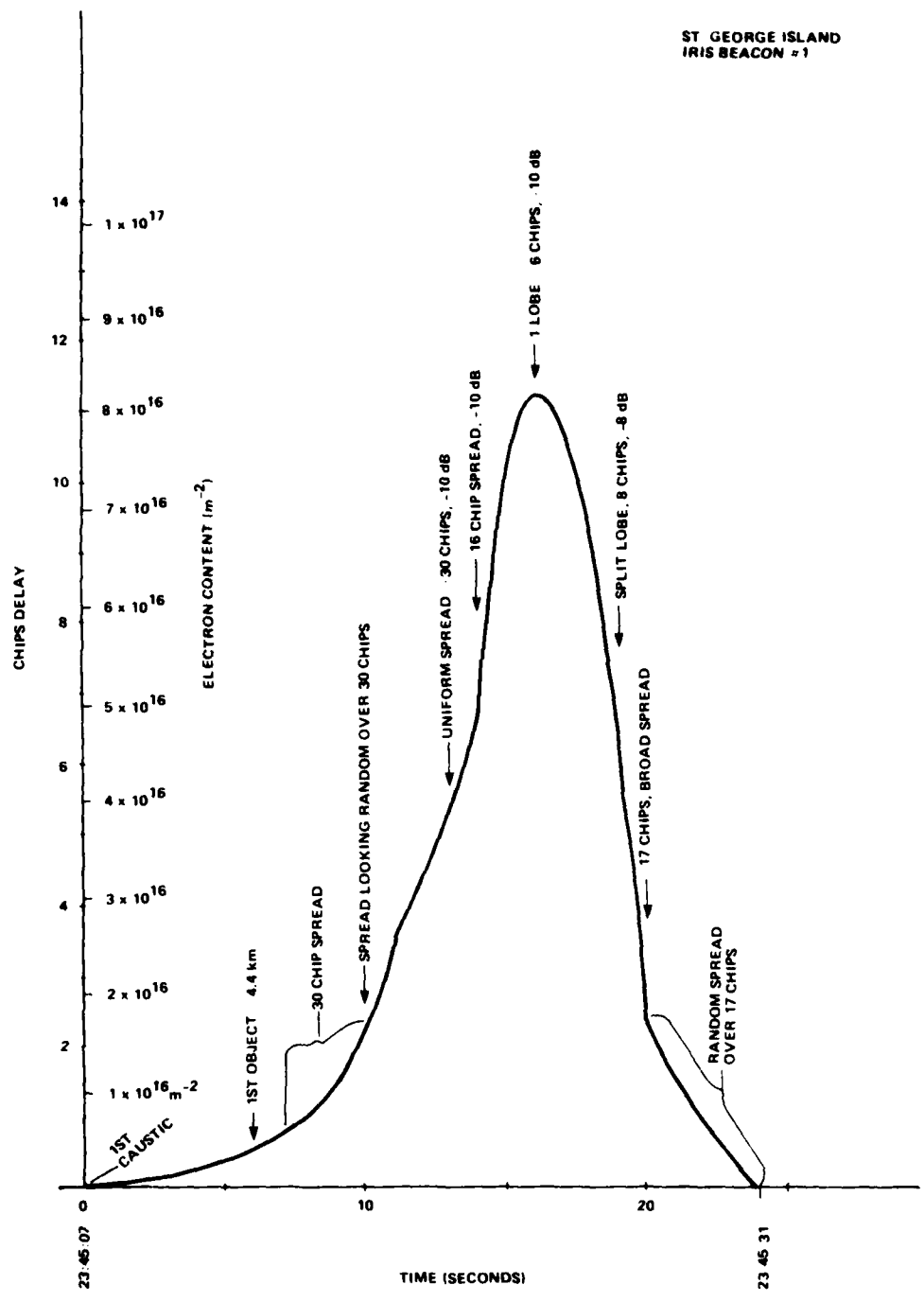
Figure 2-12. Measured Electron Content During Occultation, St. George Island, Beacon #1
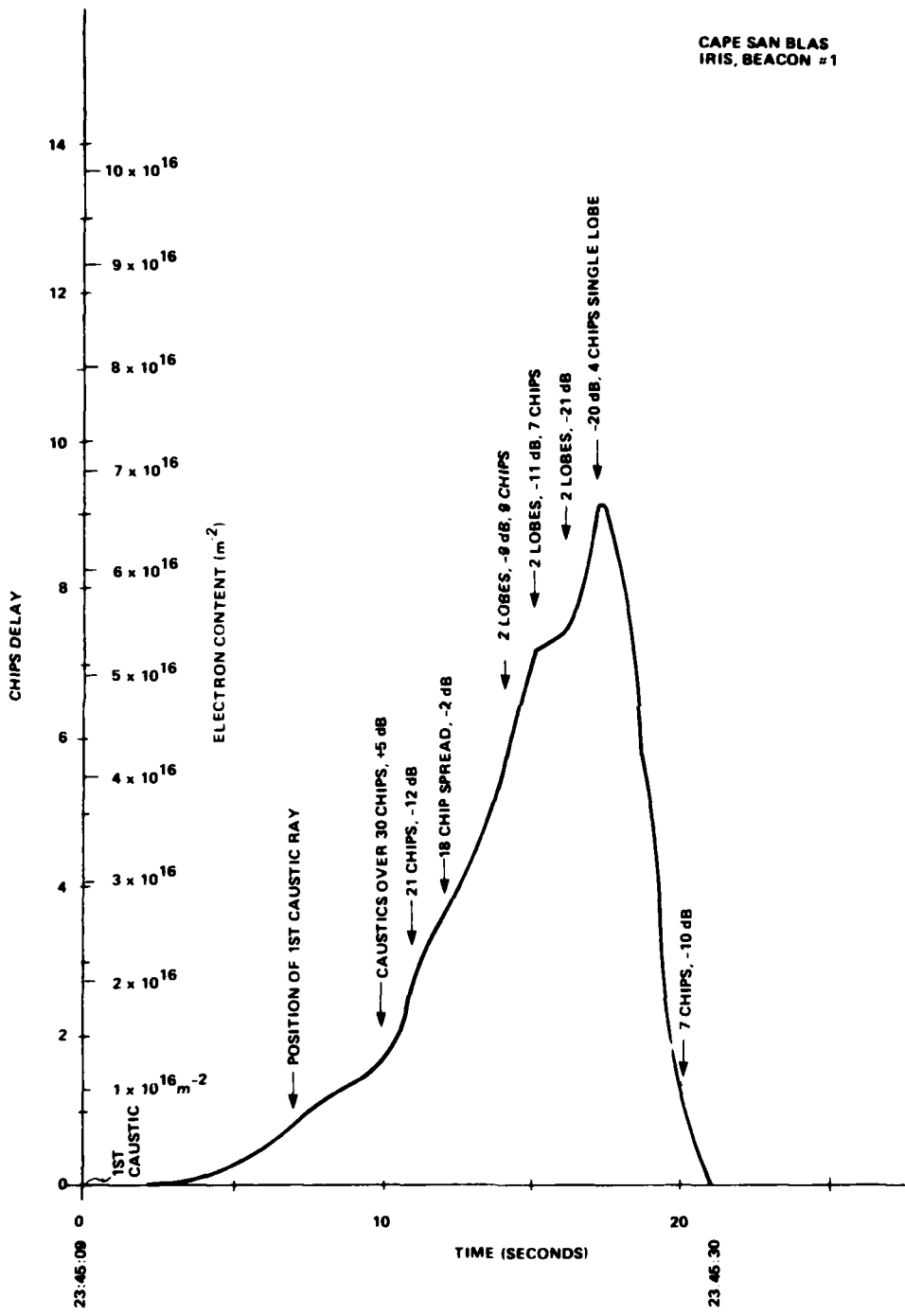
Figure 2-13. Measured Electron Content During Occultation, Cape San Blas, Beacon #1

41
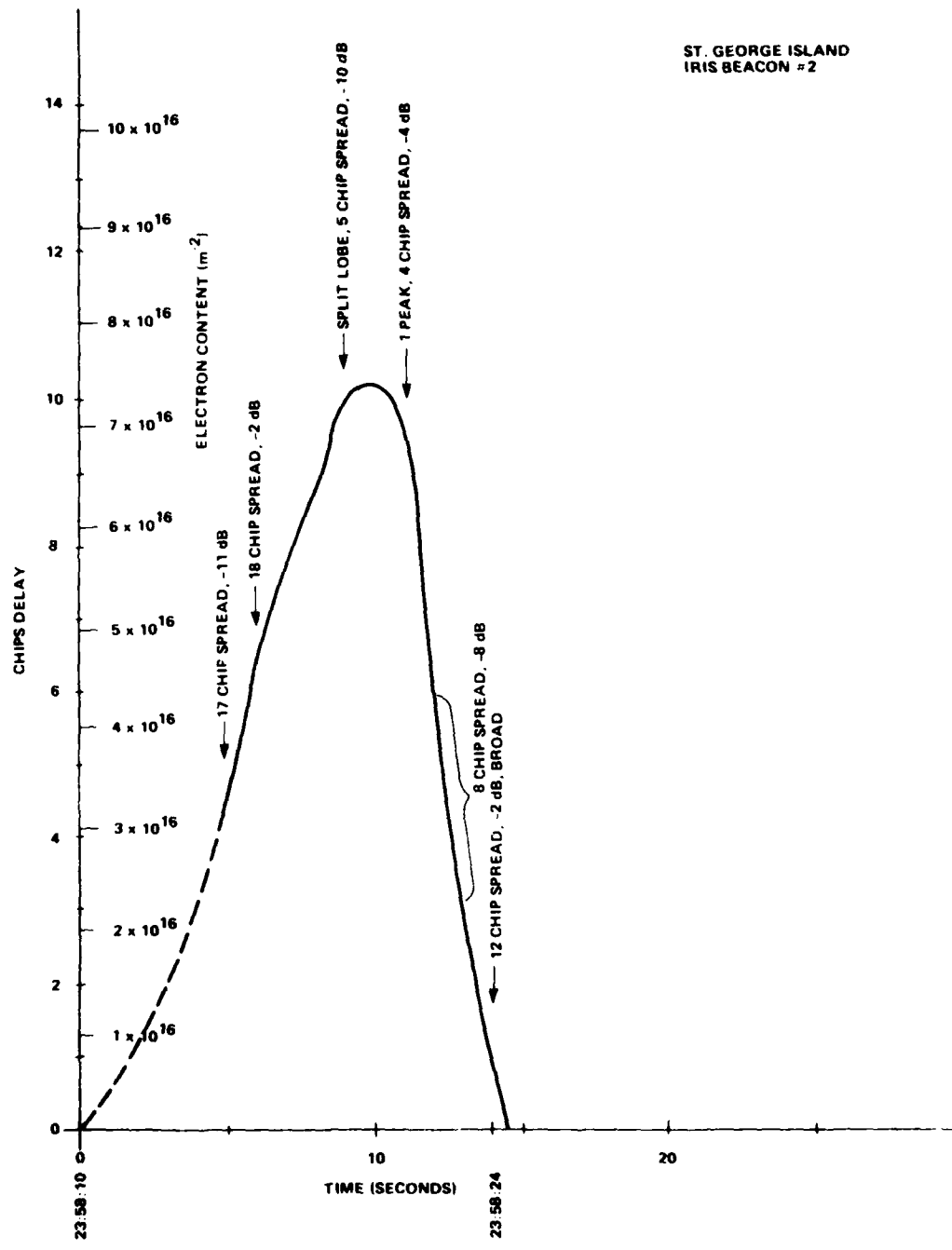
Figure 2-14. Measured Electron Content During Occultation, St. George Island, Beacon #2

DELAY AXIS - CHIPS
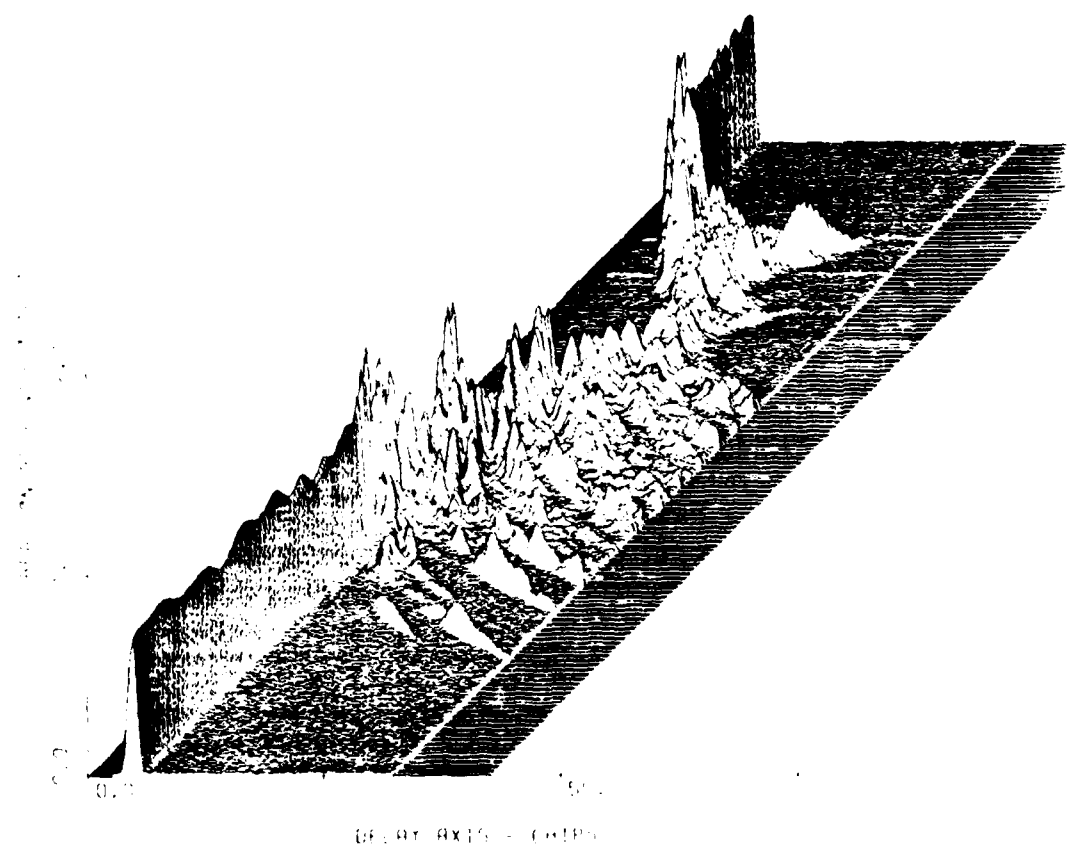
Figure 2-15.   Energy Delay Profile, St. George Island First Beacon,
               Time Span from 23:45:1.8 to 23:45:34.2

of the impulse response were taken by the receiving hardware. For plotting purposes 32 of these responses were averaged to produce each of the 400 horizontal scans presented in the figure.

Beginning from early time, the immediate features evident in the recorded response are the refracted ray caustic contributions appearing at late delays. From this first appearance in Figure 2-15 there appears to be significant energy in these components to delays even greater than the 30 chip measurement window. As expected, the relative delay of these caustics decreases as the transmitter approaches the cloud. This is a result of the decreasing difference in distance to the receiver between the beacon rocket direct path and the caustic ray paths refracting from the cloud. During occultation, when the rocket is behind the barium plasma, many caustic paths appear to merge giving a more random appearance to the delay spread. As the rocket flight continues identifiable caustics again appear, spreading energy to about 23 chips of delay on emergence from occultation.

A rough symmetry in time-of-arrival delay of the direct path is noticed for this data evidenced by a characteristic semicircular pattern in delay about the center of occultation. This symmetry in the integrated electron content profile is much greater than that observed in the other occultation data collected.

Samples of the energy delay profile (magnitude of the channel impulse response) are shown in Figures 2-16 through 2-19 sampled approximately each 0.5 second. Near the time of maximum integrated electron content when the line-of-sight path to St. George Island passes through the center of the striations (~2345:23), the signal exhibits a significant defocusing and delay spread. Near this time a delay spread of greater than 10 chips (~1 microsecond) occurs. This is probably a good initial estimate for the amount of spreading due to the random scattering imposed by the striations. In comparing this response with the unperturbed signal prior to occultation, it is apparent that a net time-of-

44
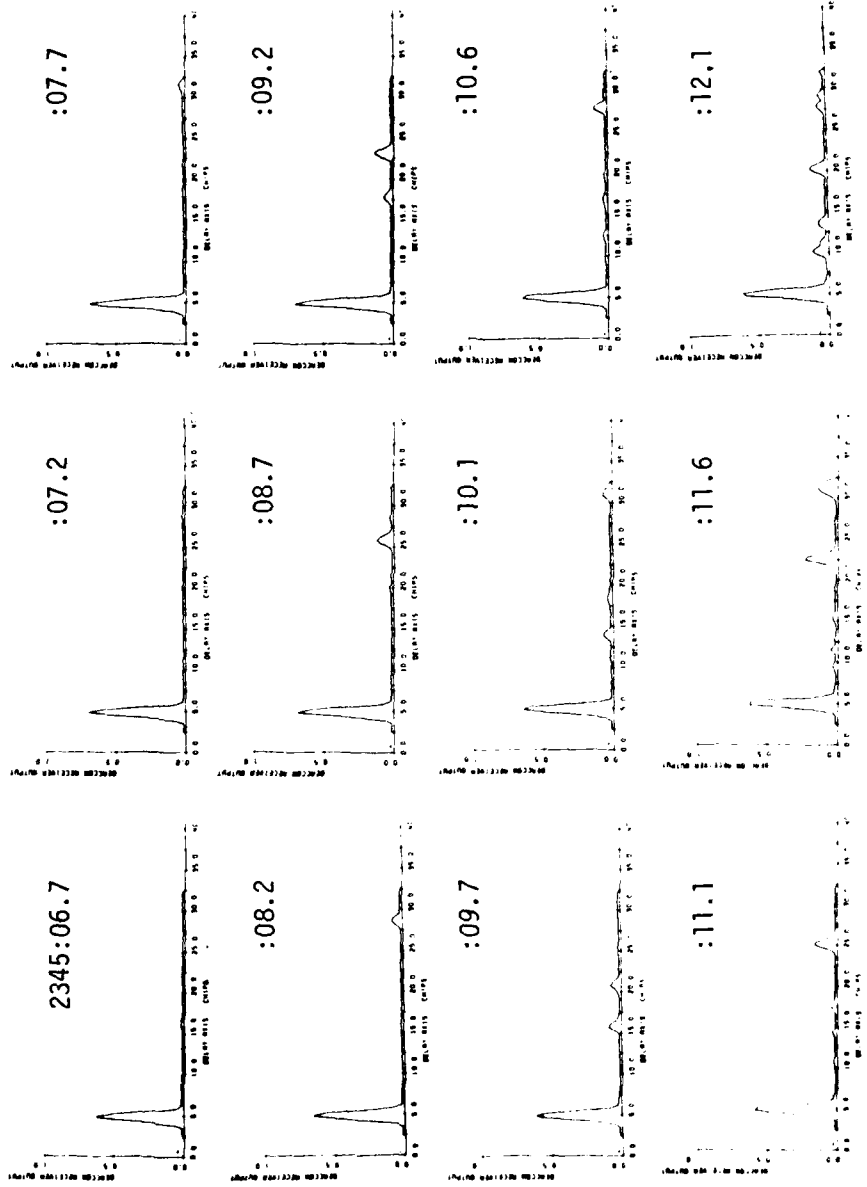
Figure 2-16. Energy Delay Profile Between 2345:06.7 and 2345:12.1, St. George Island

45
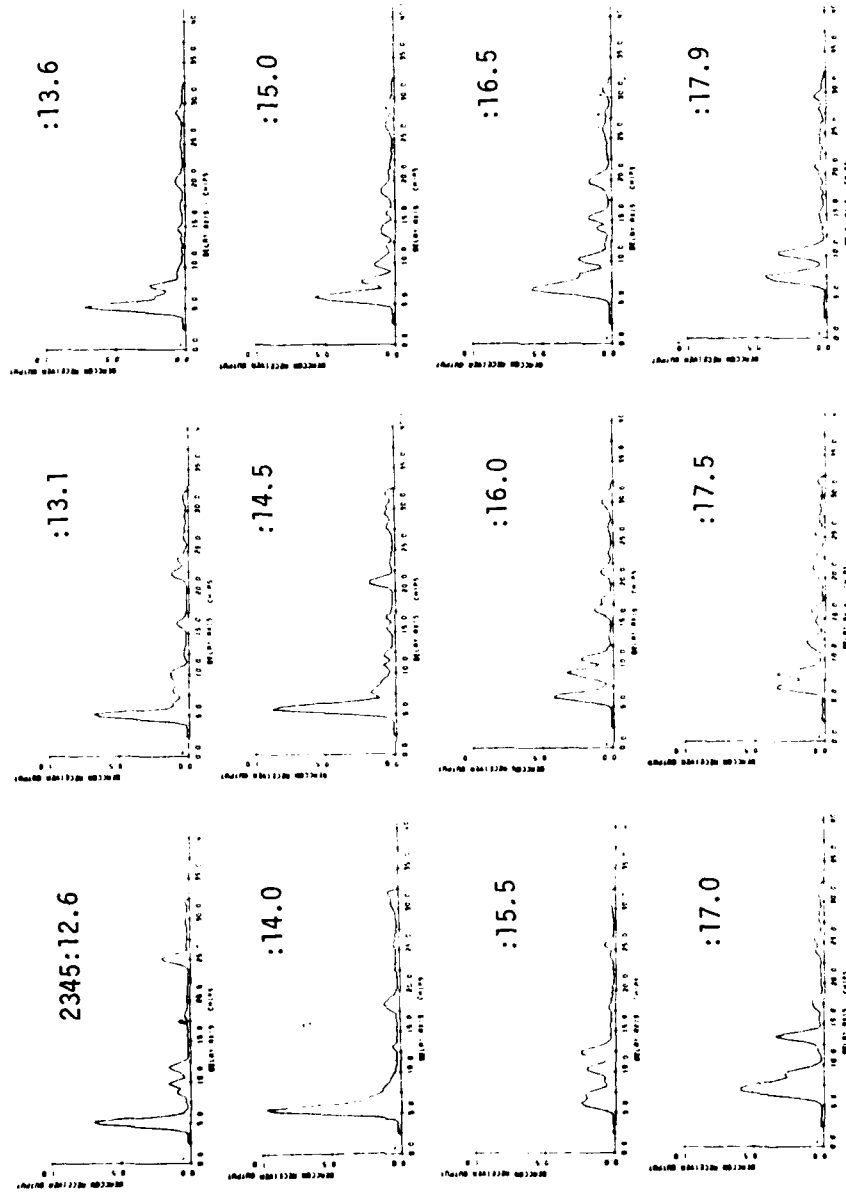
Figure 2-17. Energy Delay Profile Between 2345:12.6 and 2345:17.9, St. George Island
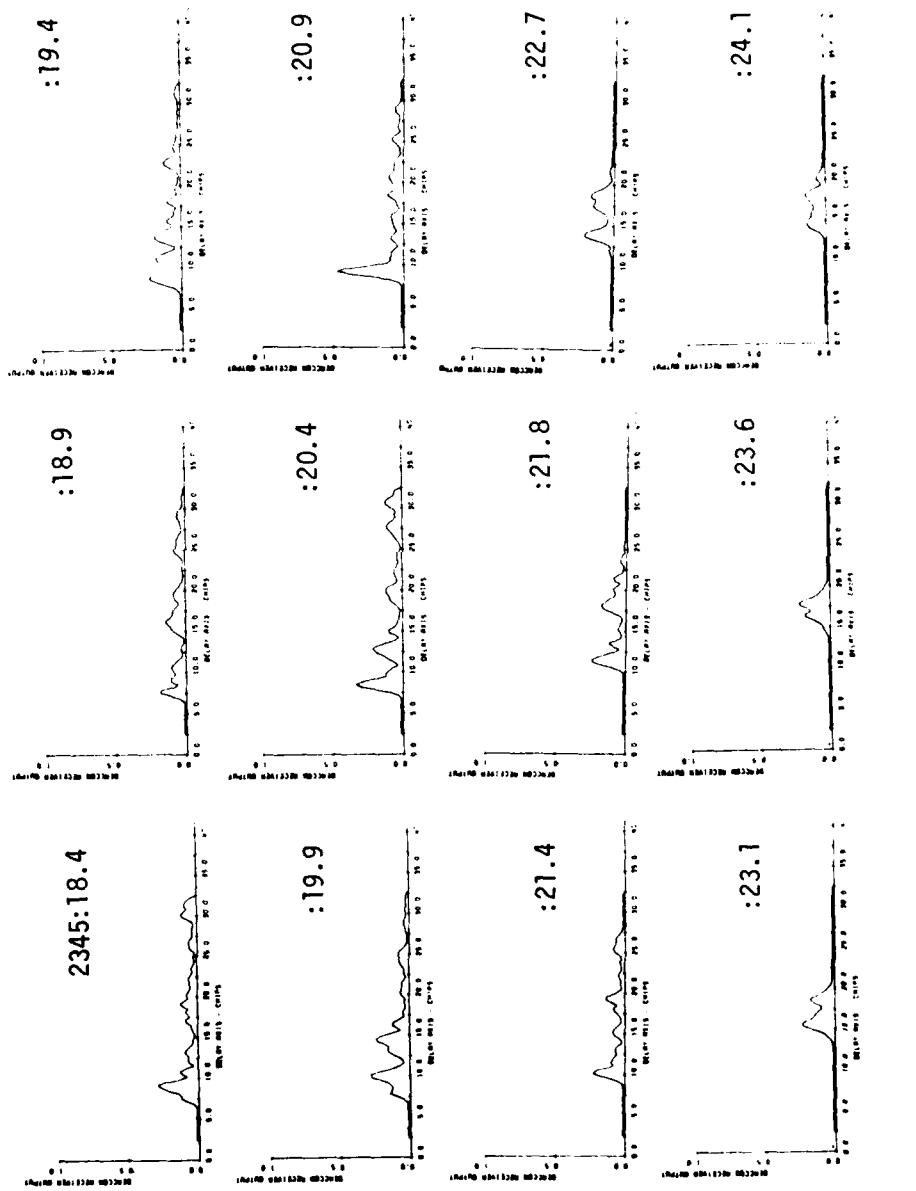
Figure 2-18. Energy Delay Profile Between 2345:18.4 and 2345:24.1,
St. George Island
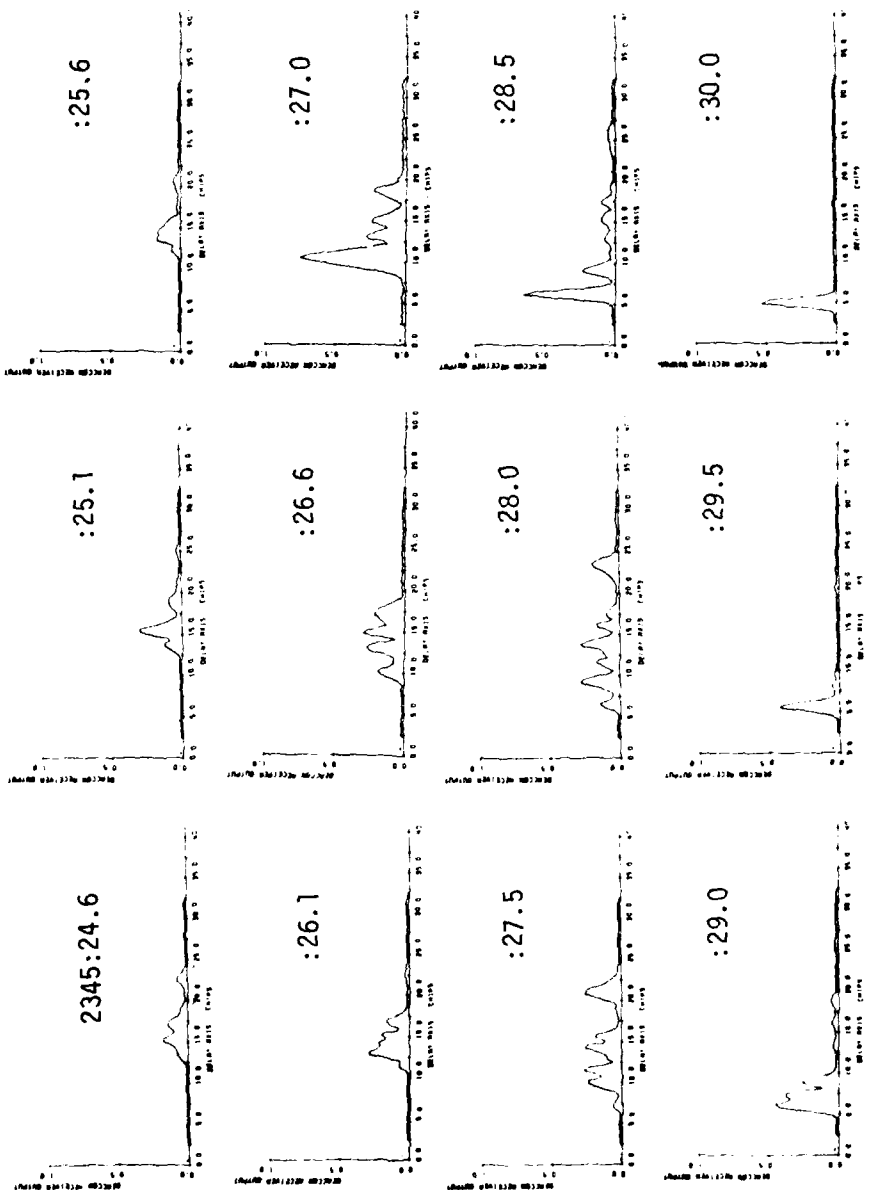
Figure 2-19. Energy Delay Profile Between 2345:24.6 and 2345:30.0, St. George Island

arrival delay of about 13 chips (~1.3 microseconds) has been added by the gross electron content of the barium ion cloud. Most strikingly apparent in these figures is the large delay spread that occurs and the potential implications to PN code tracking system design. There is some broadening of the cross-correlation of the received signal due to hardware imperfections and due to the signal dispersion imposed by the ionosphere and barium plasma; this will be removed during planned future signal processing.

2.3.2   Cape San Blas Beacon 1.

Figure 2-20 shows the impulse response recorded at Cape San Blas for the first beacon rocket. The time span for this figure is 23:45:00.4 to 3:45:32.9, and it was plotted in the same manner as Figure 2-15. The SNR for this data was measured at 32.7 dB preceding occultation. Well defined caustics are apparent in this data on approach to the cloud, though none appear as the beacon rocket exits from the cloud. It is believed this is due to the manner in which the path exits the bottom of the cloud.

Snapshots of the channel measurements taken approximately every 0.5 second are provided in Figures 2-21 through 2-24 for the Cape San Blas receiving site. At times the signal displays significant energy spread over nearly 20 chips; for instance, between 2345:20 and 2345:22Z. A better measure of the random component of the delay spread is probably 8 to 10 chips as measured near the maximum of the integrated electron content along the path (near 2345:26).

2.3.3   St. George Island Beacon 2.

The occultation was achieved for the second beacon rocket from St. George Island beginning at 23:58:10. The impulse response recorded for this event is shown in Figure 2-25 over a time period from 23:58:01.2 to 23:58:33.7. Again a slight symmetry is noted to the delay pattern for this receiver geometry. In this case the initial caustic energy does not show up at large delays
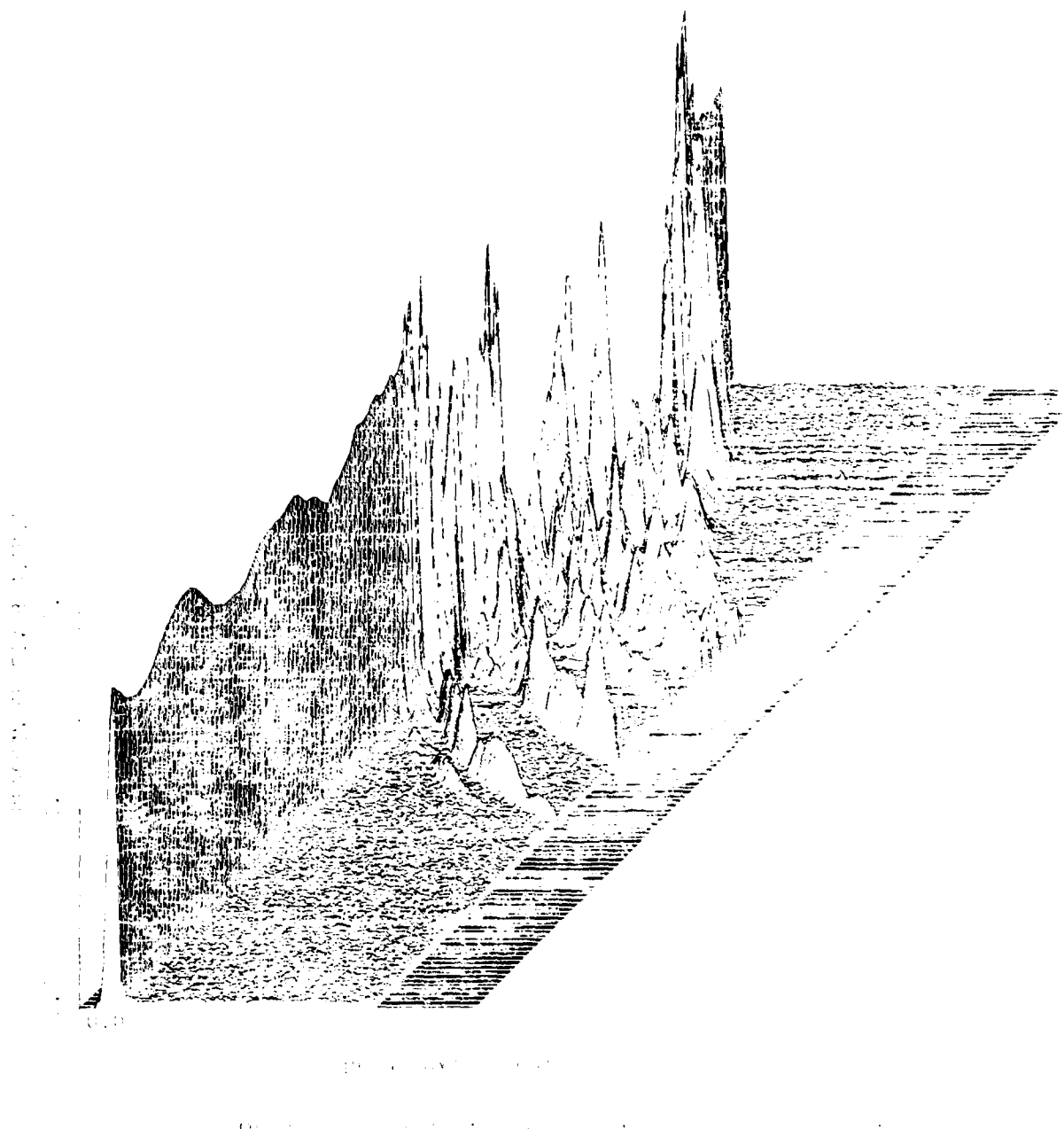
Figure 2-20.   Energy Delay Profile, Cape San Blas, First Beacon
Time Span from 23:45:00.4 to 23:45:32.9
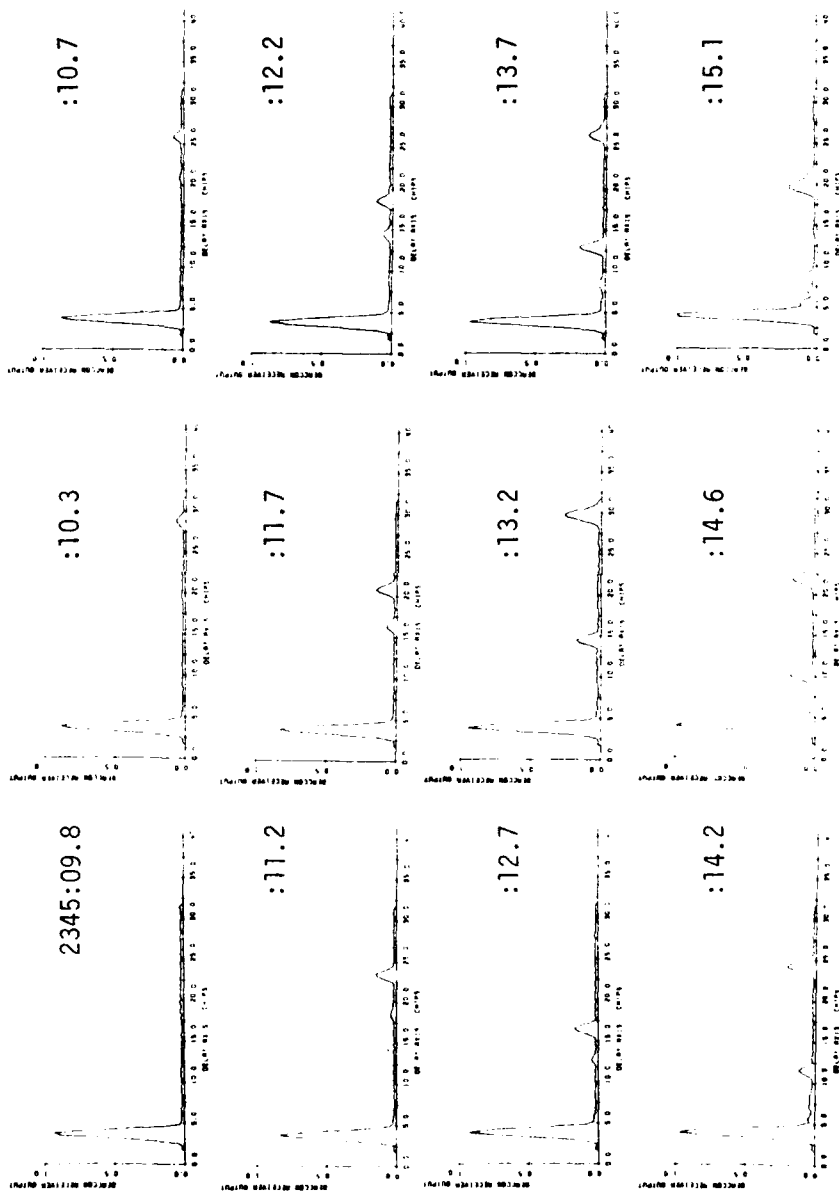
Figure 2-21. Energy Delay Profile Between 2345:09.8 and 2345:15.1,
Cape San Blas
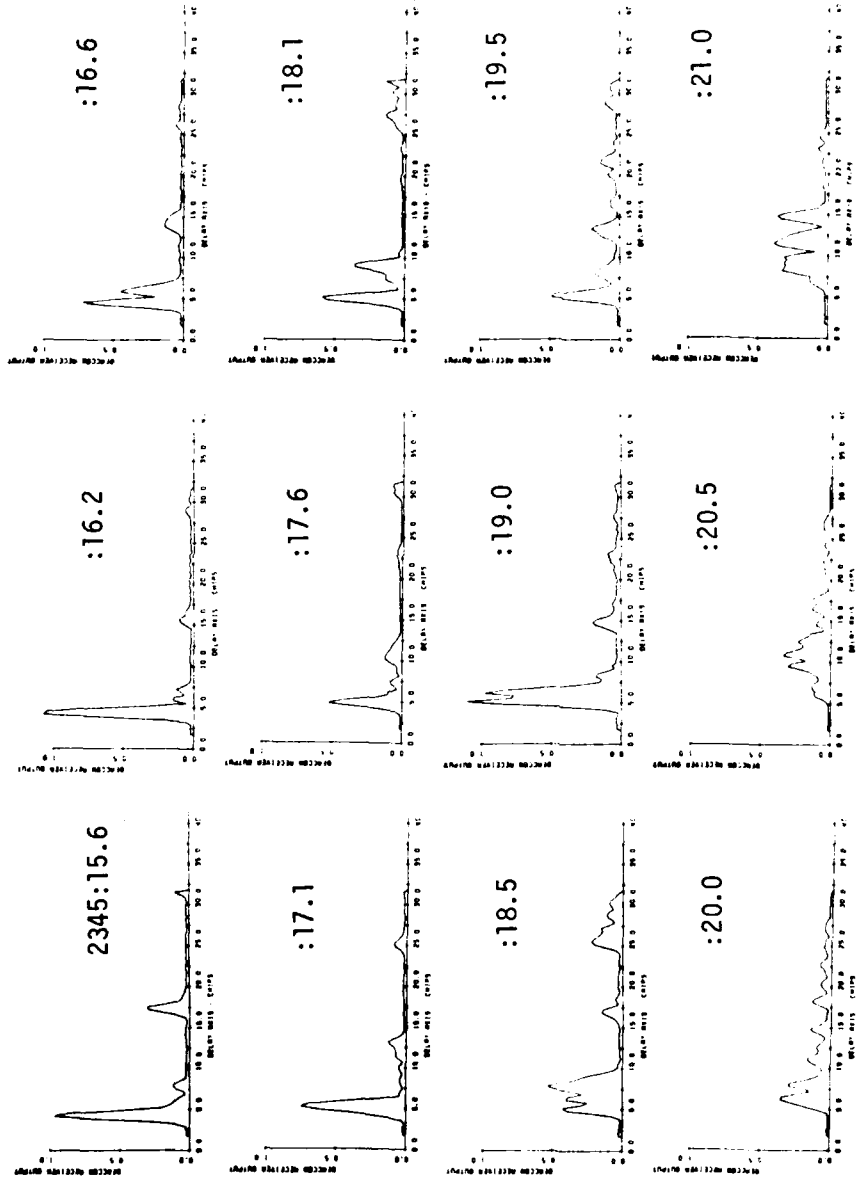
Figure 2-22. Energy Delay Profile Between 2345:15.6 and 2345:21.0, Cape San Blas

52
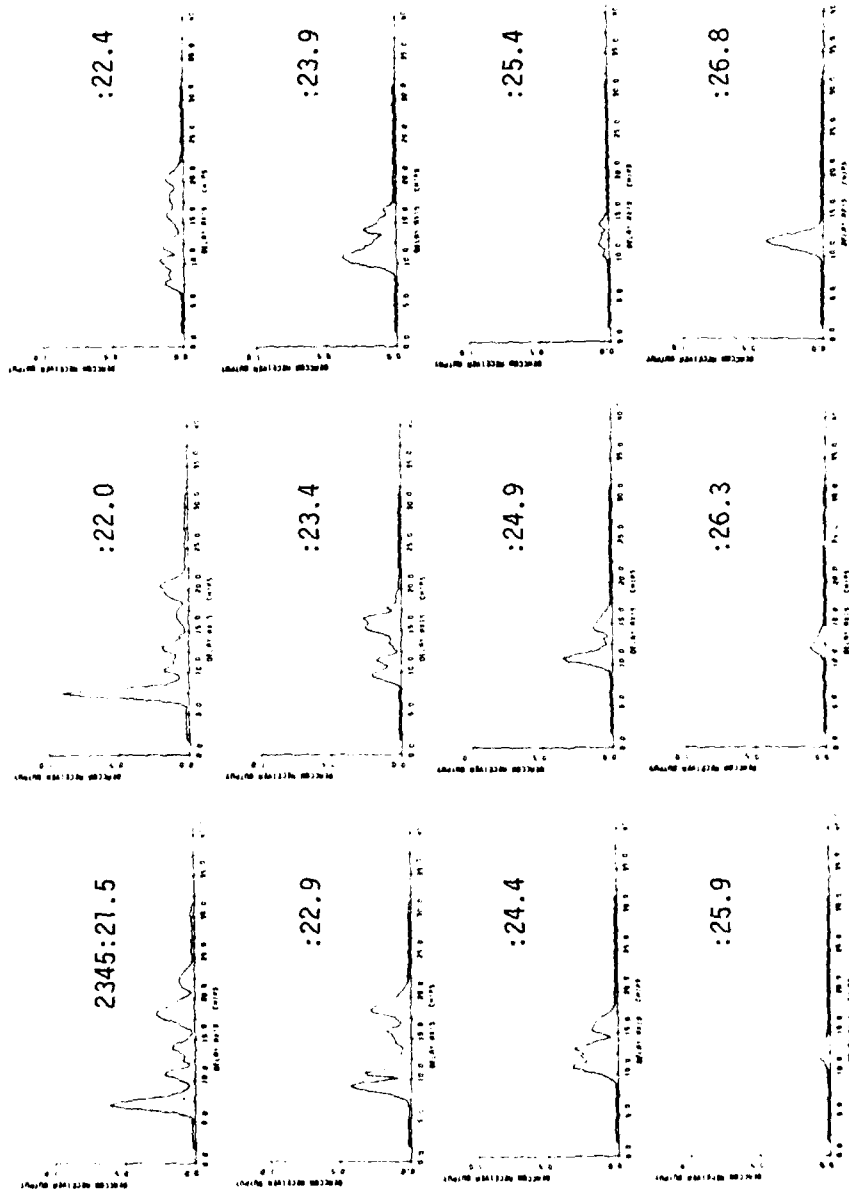
Figure 2-23. Energy Delay Profile Between 2345:21.5 and 2345:26.8, Cape San Blas
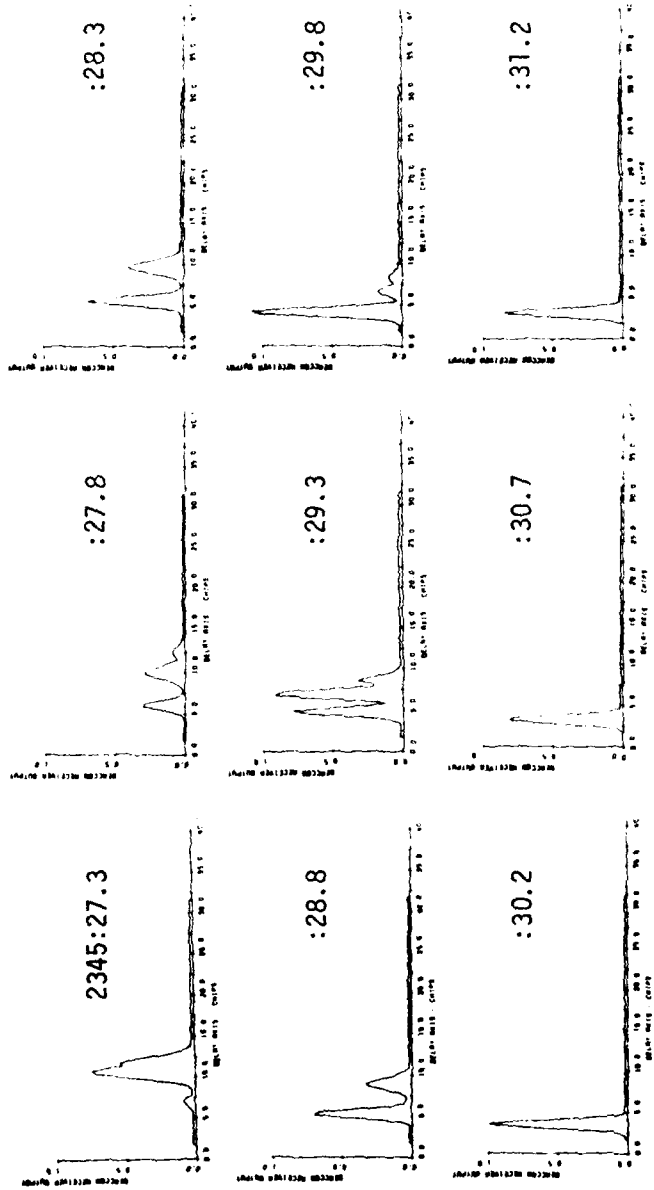
Figure 2-24. Energy Delay Profile Between 2345:27.3 and 2345:31.2, Cape San Blas

DELAY AXIS - CHIPS

PULSE DELAY PROFILE - ST. GEORGE IAL.
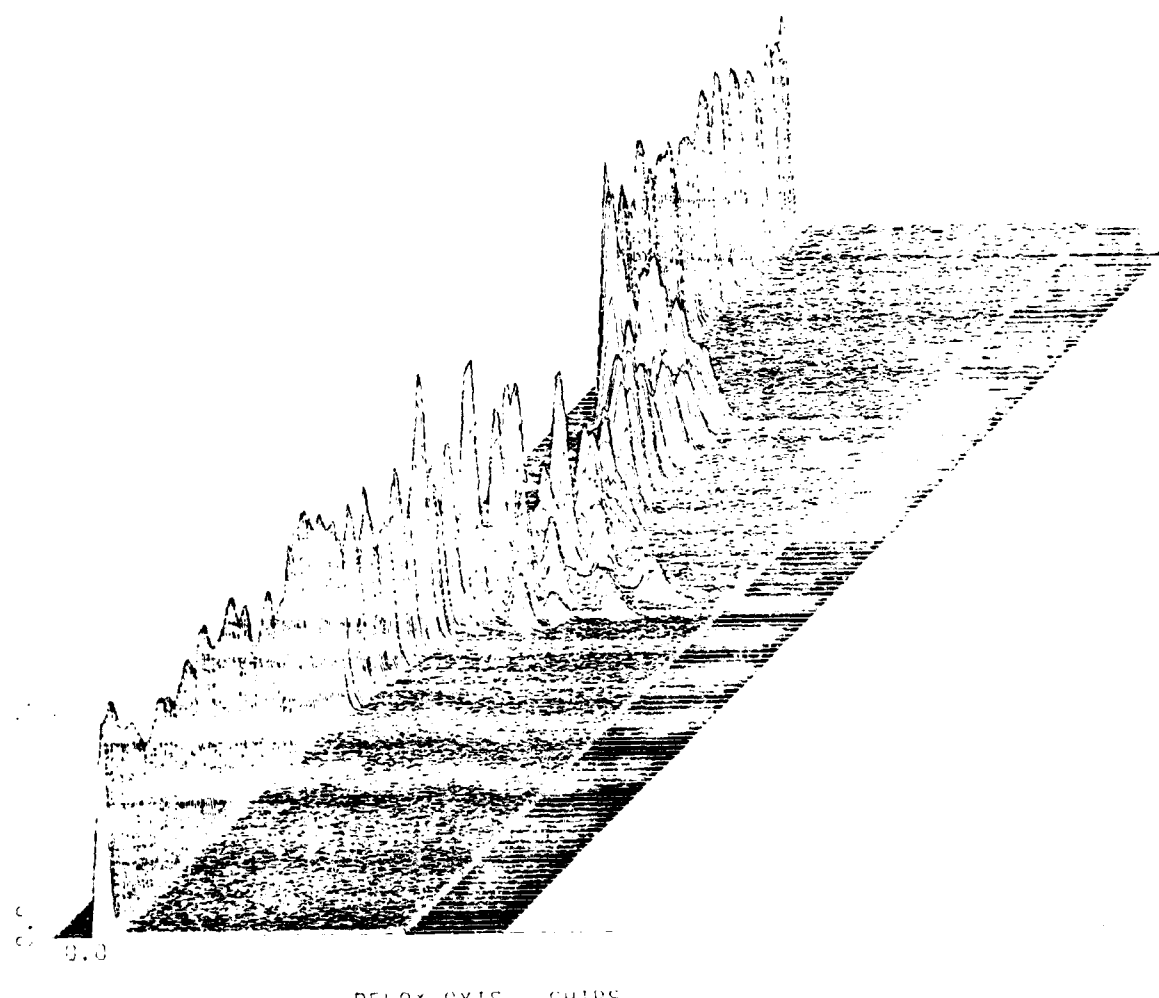
Figure 2-25.   Energy Delay Profile, St. George Island, Second Beacon
Time Span from 23:58:01.2 to 23:58:33.7

as it did for the first beacon nor is the delay spread as large. The maximum delay seen is approximately 26 chips for the caustics occurring on approach to the cloud. The defocusing that occurs behind the cloud center is also less (compare the amplitudes of Figure 2-19 to Figure 2-15). As the two rockets reached the cloud only 13 minutes apart it is doubtful that these differences are due to cloud aging. Rather, the weaker effects experienced for the second beacon seem to point to interaction with a weaker and/or less developed portion of the cloud. This perspective is consistent with the geometry interpretation given earlier in Section 2.2.

A cyclic pattern to the amplitude shown on Figure 2-25 can be noticed prior to occultation. Upon close examination of the data this appears to occur at a frequency of approximately 0.2 Hz, which corresponds closely to the coning rate expected of the rocket vehicle. When viewed on a logarithmic scale the magnitude of this effect is seen to be approximately ±2 dB. This is of the correct magnitude for a coning effect of about ±8 degrees. The line-of-sight to the receiving sites makes an angle of approximately 40 degrees with the rocket axis. As the rocket cones about this angle the VHF antenna pattern varies by approximately 2 dB (see Appendix A). It is anticipated that this effect can be removed to a first order in future processing of the data. This behavior is also apparent in the second beacon recording from Cape San Blas. The observed signal variation for the first occultation was less than 1 dB.

The impulse response patterns presented here are difficult to describe or categorize due to the complexity of the real barium environment. The primary effects are expected to arise from the striations themselves, but the gross plasma itself can also significantly disturb the channel impulse response.

In an effort to examine the contributions of the gross plasma to the measured signal characteristics, a quick effort was made to model the gross plasma along the path to St. George Island for this second occultation. To

accomplish this the integrated content was approximated from the time-of-arrival delay of the main lobe of the impulse response. Expressed as a phase at the beacon frequency, the resulting estimate of integrated phase appears in Figure 2-26. Numerical propagation calculations using the PATS code were performed across a 20 MHz bandwidth with 98 MHz center frequency using this environment. The propagation geometry used was patterned after an estimate of that which existed for the second beacon at St. George Island. The results of these propagation calculations were then assembled to provide a prediction of the transfer characteristic of the environment. This transfer function was then Fourier transformed to yield the predicted impulse response. The results of this simulation appear on the top of Figure 2-27. Figure 2-27 also provides a detailed view of the response actually recorded (bottom) which includes the striation effects as well as the gross plasma effects.

The unsymmetric nature of the plasma in the plane cut by the ray path is apparent in the caustic components showing up on approach to the medium but not on exit. In reference to Figure 2-26, this is apparently due to the steep phase encountered as the path enters the barium cloud. Also apparent in Figure 2-27 are two distinct sets of caustics in the simulated environment where four are initially visible in the actual data. This seems to indicate that there was some structuring of the plasma occulted. It is also noted that the measured impulse response delay spread is considerably greater through the center of the occultation region than occurs for the unstructured plasma simulated. A separation of the random striation effects from the gross plasma effects are planned in future processing.

Figures 2-28 and 2-29 provide some interesting snapshots of the measured data during the occultation. Figure 2-28 provides an example of a situation in which there is a rapid fluctuation or jitter in the time-of-arrival of the peak signal energy. Figure 2-29 on the other hand shows data that exhibits a progression from a discrete signal delay to a broad continuum of delayed energy
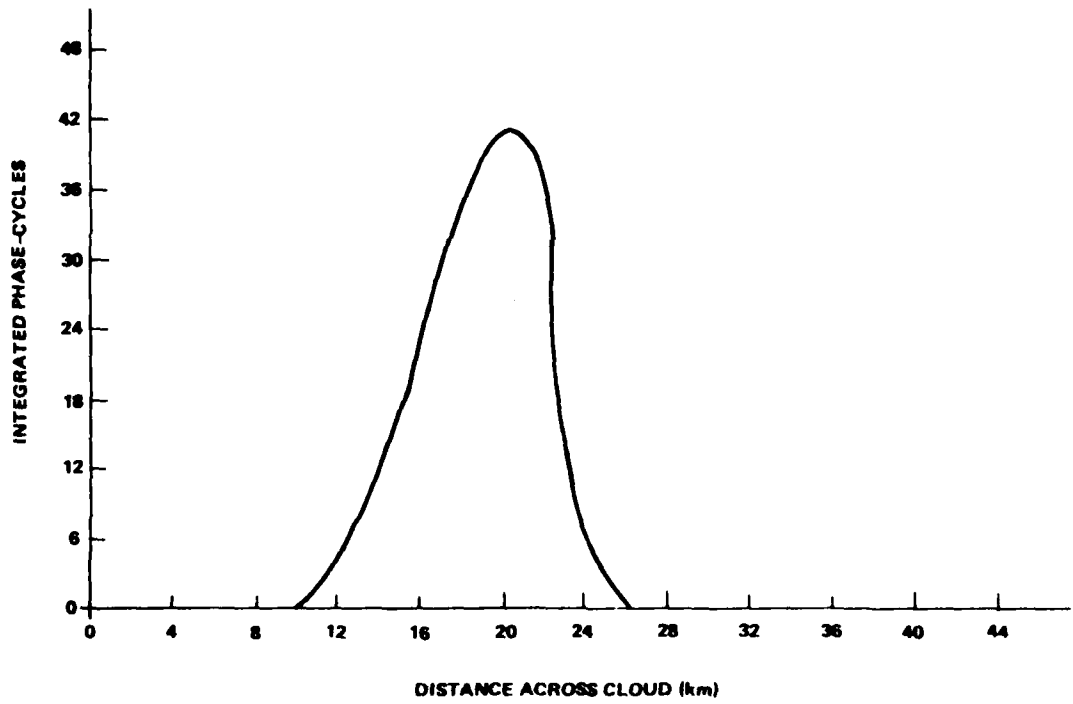
Figure 2-26. Estimated Integrated Phase of the Gross Plasma, St. George Island, Second Beacon
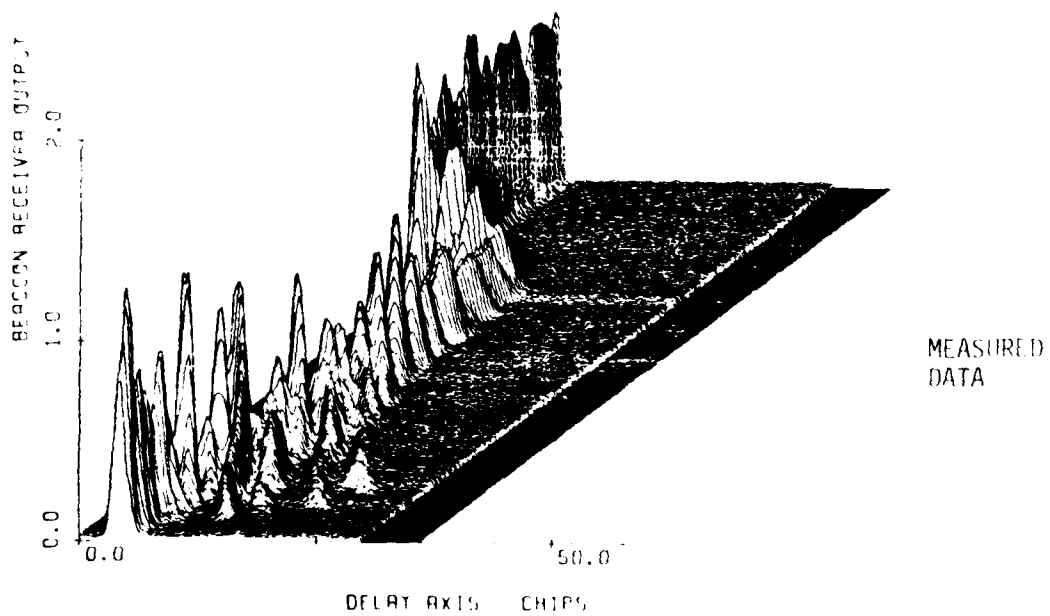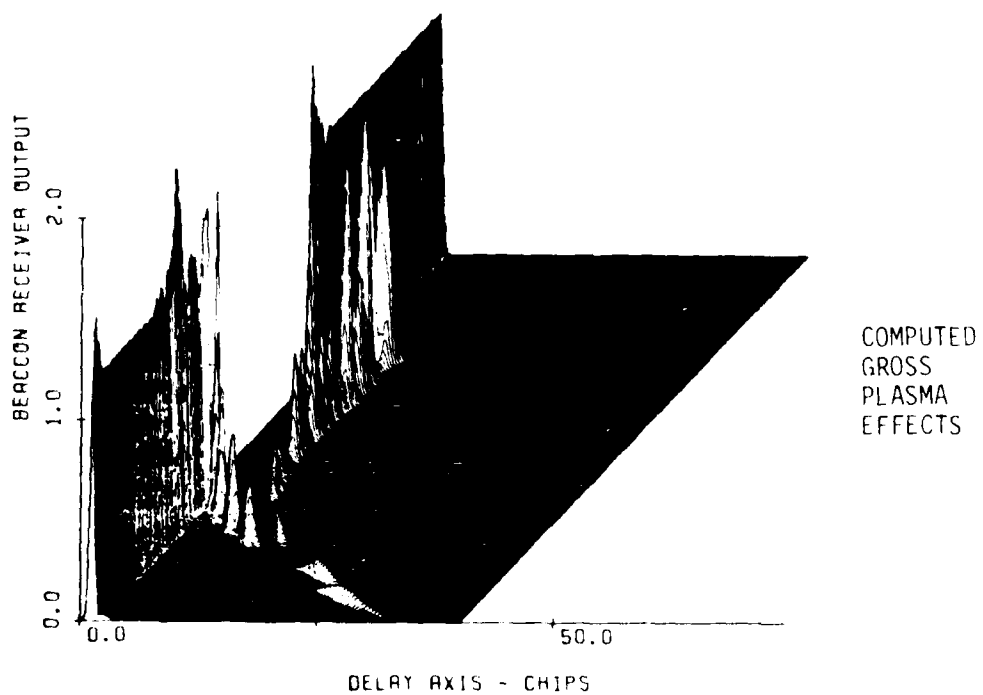
Figure 2-27. An Estimated Impulse Response for the Gross Barium Cloud as
Seen at St. George Island for the Second Beacon Rocket (top)
and the Actual Data Recorded (bottom)

59
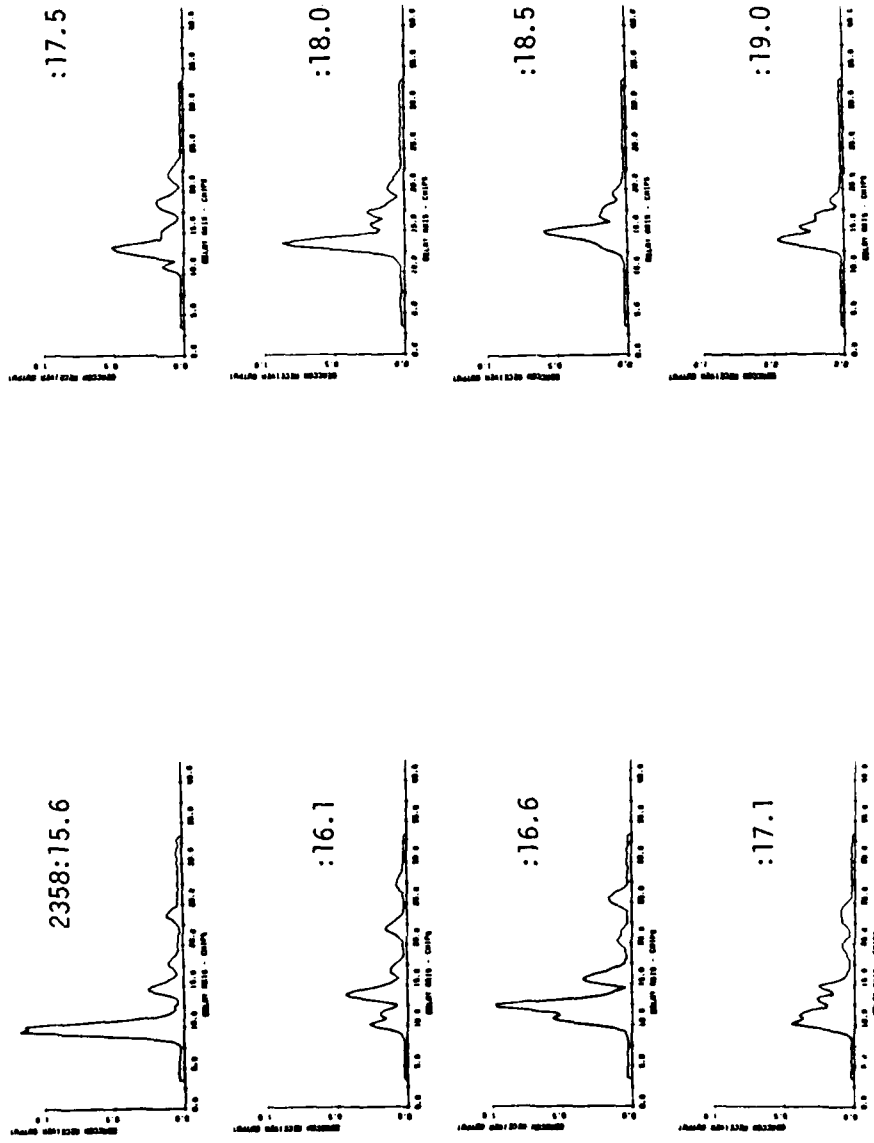
Figure 2-28. Energy Delay Profile Between 2358:15.6 and 2358:19.0, St. George Island, Second Beacon
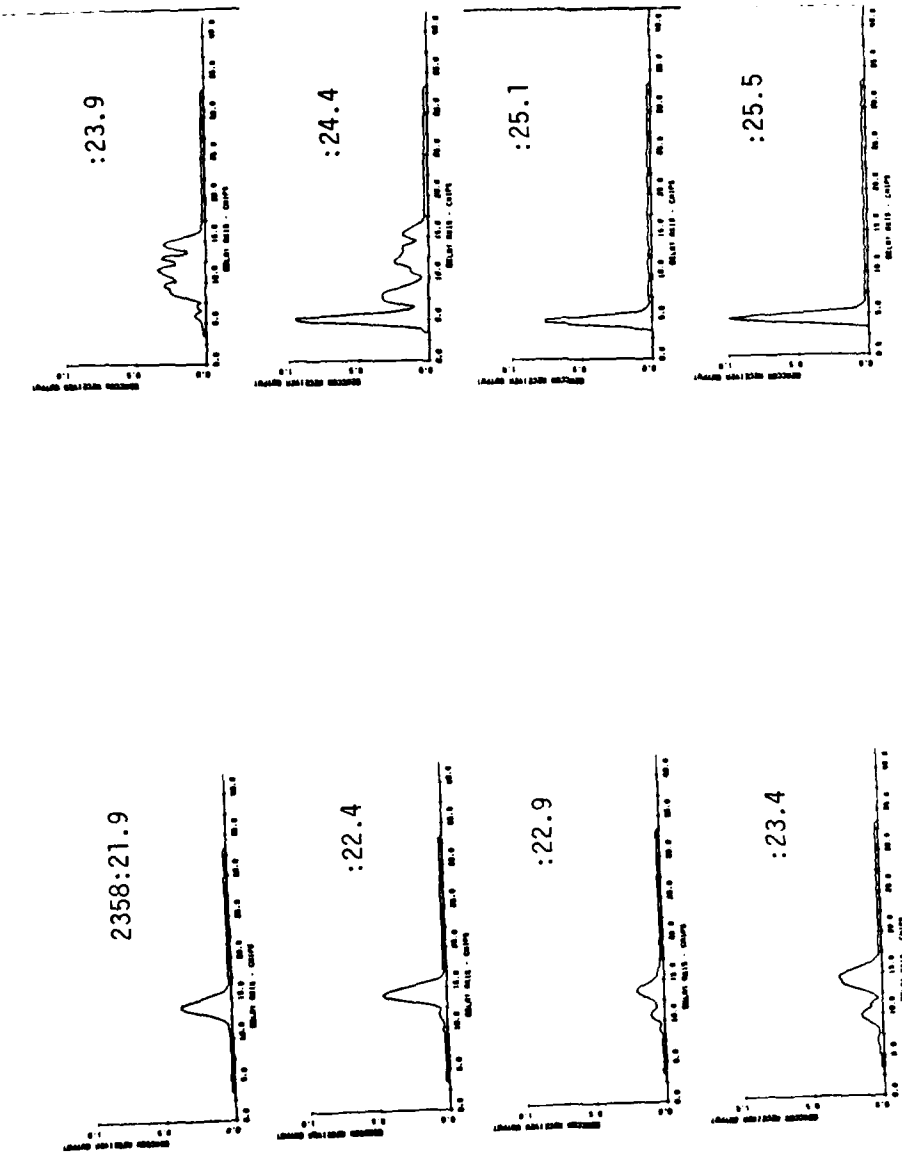
Figure 2-29. Energy Delay Profile Between 2358:21.9 and 2358:25.5, St. George Island, Second Beacon

and then an abrupt transition to a discrete carrier delay as the signal exits the cloud. Eith of these situations would present tracking difficulties to spread spectrum receivers, especially if these variations were to occur as rapidly as presented here.

2-3.4 Cape San Blas Beacon 2.

The data from the second beacon rocket as recorded at Cape San Blas appears in Figure 2-30. The time span plotted extends from 23:58:05.4 to 23:58:37.9. As caustics were not evident as the path entered the cloud, an adjustment in the measurement window (time delay tracking of the signal) was made that resulted in a partial loss of signal upon exit of the ion cloud. As shown, the signal abruptly shifted back and largely out of the measurement window at 2358:25. A few seconds later (at 2358:30) the measurement window was shifted to again encompass the signal. Based on the time of occultation at St. George Island, the occultation at Cape San Blas should occur within several seconds of 23:58:18. Notably absent at this time (or any other time) are the discrete caustic rays observed in the other occultation data. The evidence of the cloud is apparent, however, in the increasing time-of-arrival (chip) delay beginning at about 23:58:18. This data indicates only a marginal intersection of the beacon signal path with the barium plasma occurred.

Figure 2-30 does indicate some weak fading did occur. Thus, some weakly striated material may have been occulted. Figure 2-31 shows a sample of the weakly fading signal. This figure is a 50 millisecond average taken at time 2358:23.3.

2-4 CONCLUSIONS.

The primary purpose of the beacon experiment was to measure the time-of-arrival jitter and spread (or frequency selective properties) produced by a striated plasma. In this regard the experiment has been highly successful. An

62
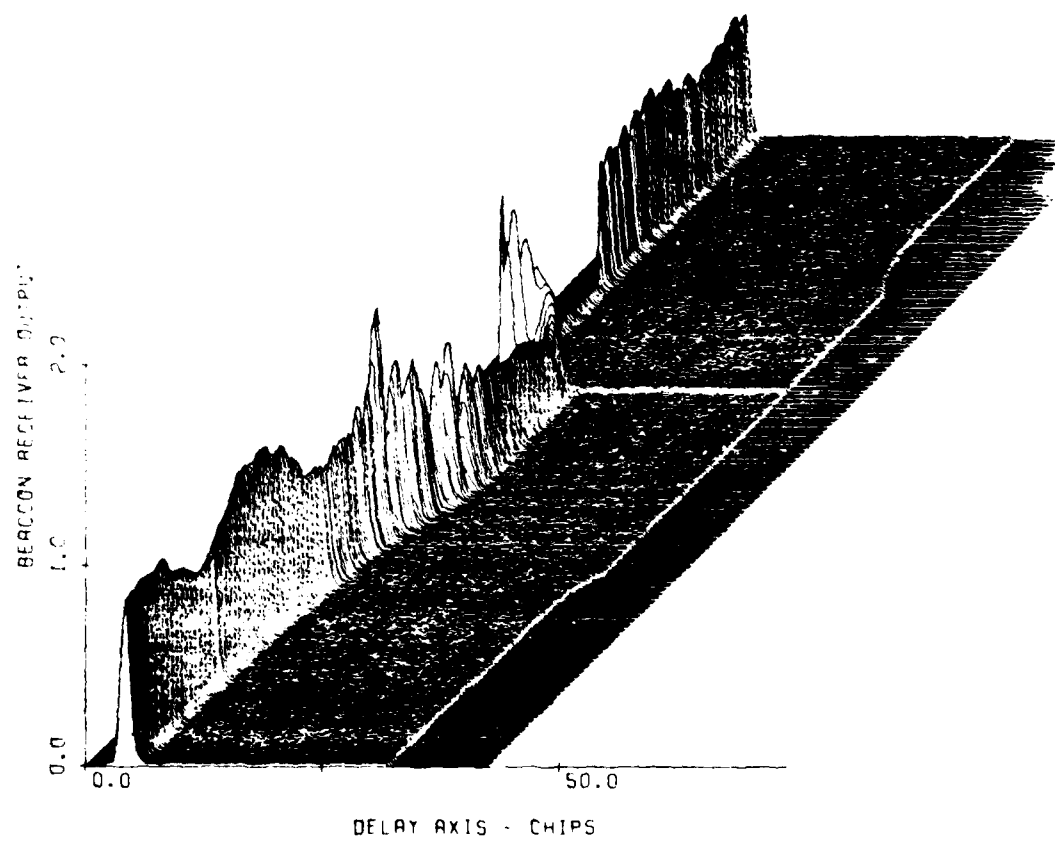
Figure 2-30. Pulse Delay Profile, Cape San Blas, Second Beacon
Time Span from 23:58:05.4 to 23:58:37.9

63
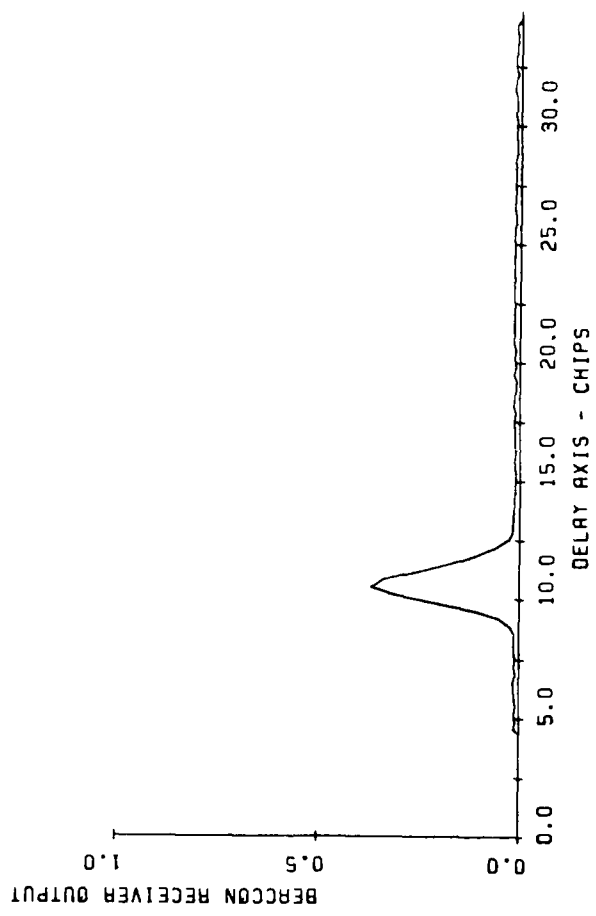
Figure 2-31. Detail of the Impulse Response for Cape San Blas During Occultation. Second Beacon, Time of 23:58:23.3

accurate understanding of the relation between the plasma structure and these parameters is important to the understanding of the performance of spread spectrum PSK systems and high data rate systems operating through a striated ionospheric plasma. Even without this detailed understanding, the data is directly relevant to system performance. The data indicates the potential for loss of code lock and false lock as well as the usual difficulties in operating through fading environments.

The agreement of the PLACES beacon experiment data with theoretical relations for the time-of-arrival jitter and spread remain to be tested. A cursory review of the data would suggest that a geometrical approach based on angular spectrum arguments will successfully account for the measured energy delay profile and as well as the spectrum of the signal at each component of delay. This geometrical interpretation would explain the basic cause of the signal time-of-arrival jitter and spread as the geometric increase in path length produced by the plasma angular scattering. The data measured is of high quality and should facilitate the theoretical interpretation of the measurements.

SECTION 3
AIRCRAFT EXPERIMENT RESULTS

3-1   INTRODUCTION.

The aircraft signals used to probe the barium plasma environment were the same as those used in 1977 during the STRESS experiment as diagrammed in Figure 3-1. A UHF tone (~250 MHz) and a k-band (~38 GHz) reference signal are synthesized from a common oscillator at the satellite and transmitted down to the KC 135/662 aircraft transiting the barium cloud shadow. The K-band signal is used as a phase reference to remove the effects of the aircraft motion leaving only the phase imparted by the barium cloud ionization. The total phase shift imparted by the barium plasma to the K-band signal is generally less than 100 degrees, a factor of 152 less than the UHF signal. This K-band signal is also used to precorrect an uplink UHF tone (~340 MHz) so that it arrives at the satellite with zero doppler. At the satellite this signal is split into inphase and quadrature components, each component one bit sampled at a 50 kHz rate and these samples are sent down to the aircraft on the K-band signal using a 100 Kbps DPSK mode.

At the aircraft both the UHF uplink and downlink tone data are recorded. The downlink tone data was sent over an FM link through the FLTSATCOM satellite to the B-4 receiving site at Eglin AFB and then sent over a microwave link to the CCF where it was digitized, computer processed and displayed in real time.

This experiment configuration differs from the STRESS Test 3 configuration only in that the uplink tone processor is on the aircraft rather than at the Roof Top Facility (RTF) at AFWAL. While a much lower gain antenna is available on the aircraft than at the RTF for receipt of the K-band data signal, the satellite dish antenna can be pointed directly at the aircraft. In this way, as anticipated, fewer difficulties are encountered with loss of K-band phase lock (and thus loss of doppler correction on the downlink data). (During STRESS the K-band satellite
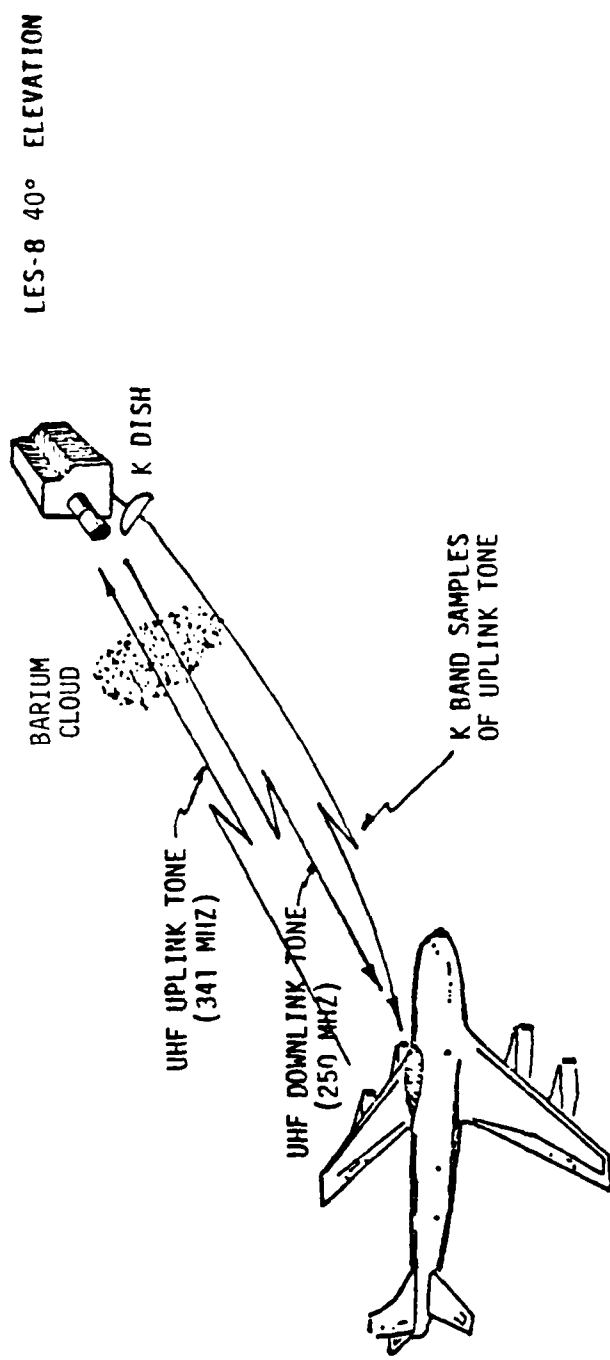
Figure 3-1. PLACES Aircraft Experiment

dish antenna was pointed halfway between the aircraft in Florida and the RTF in Ohio resulting in frequent loss of K-band phase lock.) The equipment configuration used during the experiment is described in Appendix B.

3-2   AIRCRAFT EXPERIMENT OVERVIEW.

The aircraft experiment employed LES-8 throughout the experiment. LES-8 and LES-9 were in nearly identical orbital positions. The uplink and downlink tone processing equipment built by ESL under the STRESS program performed reliably. There was no apparent degradation over the past 3 years in the overall signal quality. In fact, 2 or 3 dB of SNR improvement appears to have been realized, possibly through a combination of more favorable geometry and hardware/antenna changes on the aircraft. A quick look at the downlink C/KT indicated approximately 51 dB-Hz compared to 46 to 47 dB-Hz measured during STRESS.

Table 3-1 summarizes the aircraft data recorded. Both uplink and downlink data are available except during periods when K-band phase lock was lost. Without K-lock the uplink tone data is lost. A detailed summary for each release for each pass is provided in the subsequent sections. The real time processing software generally worked reliably. Occasional computer crashes did occur but were generally quickly corrected by the highly efficient CCF programming staff. Loss of K-lock would result in loss of phase lock in the real time processing software, but again this only presented minor difficulties. The greatest difficulties were encountered with the FPS-85 radar tracking data. Only during event IRIS was useful cloud data obtained consistently for positioning the aircraft. Without the real time relay link through the FLTSATCOM and the associated aircraft position displays it would not have been possible to position the aircraft and obtain fading data on the other three events. Figure 3-2 illustrates the quality of the real time fading display. The phase data will be enhanced through proper windowing and processing of the data as recorded on the aircraft.

Table 3-1. A/C Data Summary

RELEASE	RELEASE TIME	RELEASE ALTITUDE	RELEASE LOCATION	NO. OF PASSES	DATA PERIOD
GAIL 12/4/80	2307:36Z	178.1 km	~29.37°, ~87.37°	32	2307:10 --- 0148 0136 LAST STRONG FADING (R+2:29)
HOPE 12/6/80	2307:37Z	179.4 km	~29.25°, ~87.0°	33	2307:40 --- 0206 0113 LAST STRONG FADING (R+2:06)
IRIS 12/8/80	2313:07Z	179.6 km	28.799°, 87.166°	31	2329 --- 0205 0150 LAST FADING DATA (R+2:37)
JAN 12/12/80	2313:42Z	184.3 km	29.166°, 86.993°	35	2314:06 --- 0200 0157 LAST STRONG FADING (R+2:43)
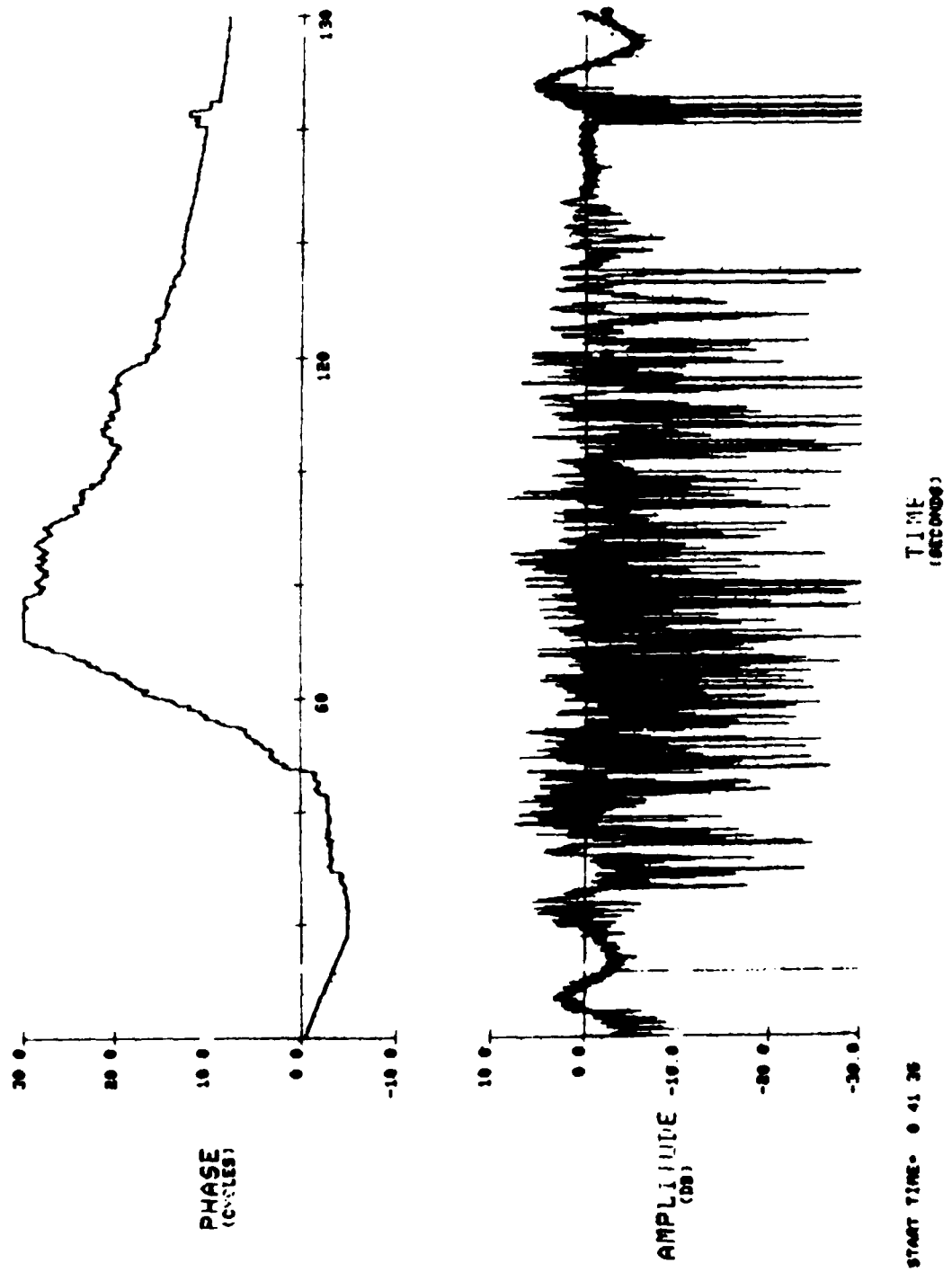
Figure 3-2. Real Time Fading Display for Event JAN at R+1^{h}28^m

70

The following sections describe the aircraft experiment results for the four PLACES barium releases, GAIL, HOPE, IRIS, and JAN. The discussion includes the cloud tracking data, the aircraft location data correlated with periods of intense fading, and samples of the uplink and downlink test results.

3-3   TEST RESULTS FOR GAIL.

The barium cloud for the first experiment, GAIL, was released on 4 December 1980 at 23:07:36Z. It was released at an altitude of 178.1 kilometers approximately 87.37°W, 29.37°N. The projection at release of this cloud from the LES-8 satellite down to the 10.668 kilometer aircraft altitude is 86°14'36"W, 31°25'43"N. This is slightly southwest of the planned projection of 86°11'31"W, 31°31'1"N. The cloud quickly moved northeast from this point, stopped for a few minutes, then moved southwest at a slower pace for the rest of the experiment. The apparent projection from the satellite to the aircraft operating altitude appears to follow a somewhat different pattern due to the satellite motion as shown in Figure 3-3. The cloud projection was about 1 degree south and 1 degree west of the release point at R+2 hours 28 minutes.

The early time cloud drift was more northerly than previously observed. This northerly drift in conjunction with an optical tracking error resulted in the apparent cloud drifting outside the range safety firing limits for the beacon and the probe before striations were clearly evident.

The optical tracking system uses two ground sites to follow the cloud, and from these locates the cloud position. During this release, the D3A ground site tracked the neutral cloud, not the striated ion cloud, causing the projection of the ion cloud position to be significantly northeast of its actual position. The FPS-85 radar was not working from release (R) to R+20 minutes due to a cable failure. The tracking error is clearly evident in the large jump in the cloud projection point around 2347Z when the track was switched from optics to radar. The aircraft tracking
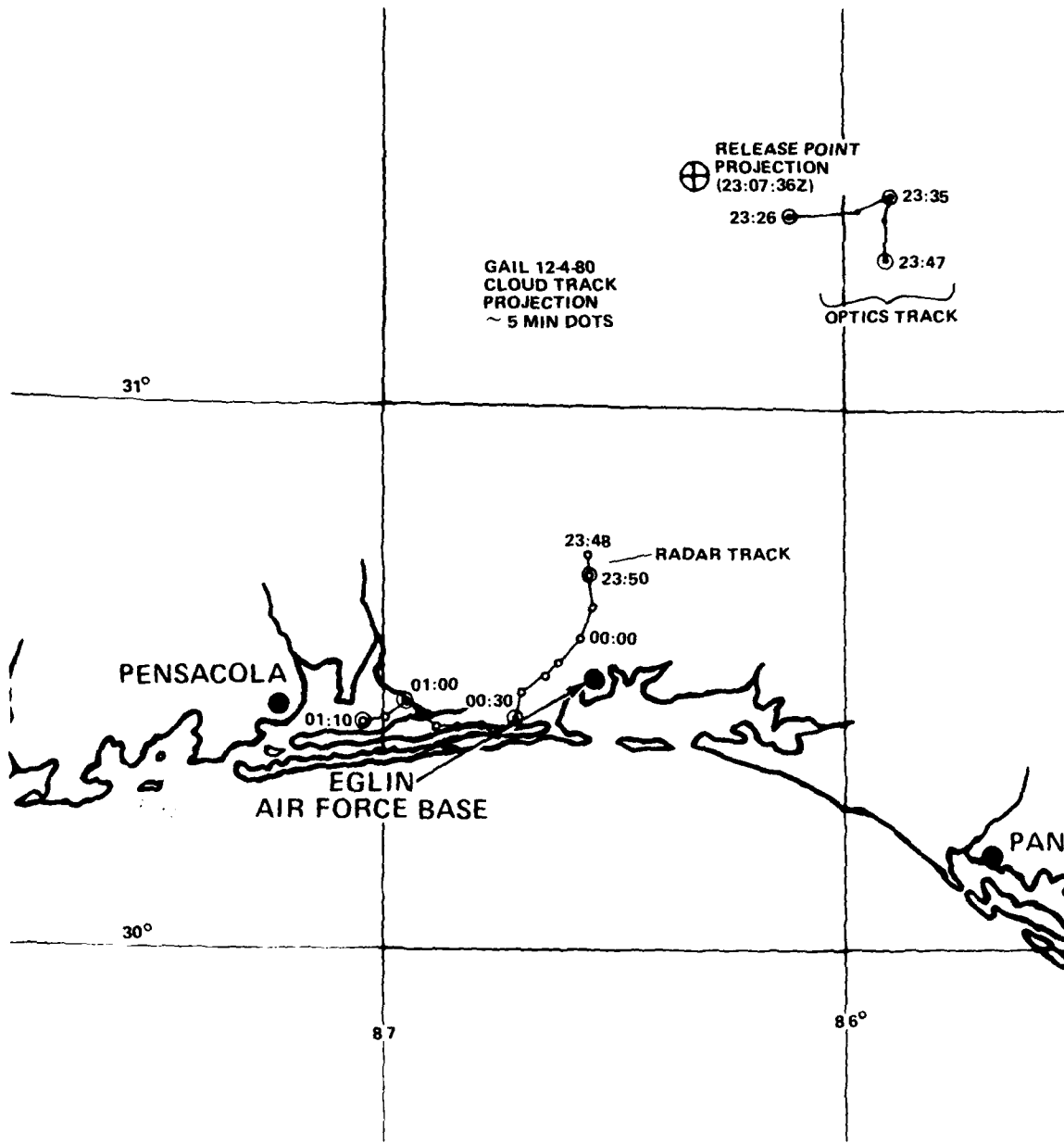
Figure 3-3.   Ion Cloud Track Projection for GAIL

radar was held for missile tracking for the first 21 minutes; thus, the aircraft position during this time must be derived from the less accurate onboard INS data. As a further complication, the radar provided the projection data using the LES-9 ephemeris rather than LES-8. These difficulties resulted in no useful data until approximately 1 hour after release. Figure 3-4 shows the aircraft ground track which reflects the difficulty in obtaining good projection data.

Figures 3-5, 3-6, and 3-7 show the aircraft ground track during each hour and also show the periods of strong (deep) fading. Since the radar projection was south of the true projection, the first pass of the aircraft through the radar track around 0000Z resulted in no fading and the aircraft was vectored north back toward the last optics track data. It was along this flight path that strong fading was observed (see Figure 3-6). From that point on the real time aircraft track display and real time fading display were used to position the aircraft.

A total of 32 passes were made with fading seen as late as R+2 hours 45 minutes. A summary of these passes is given in Table 3-2. Uplink tone data is available when the K-band signal is in phase lock. Moderate to strong fading was seen during 18 of the 19 passes between R+50 minutes and R+1 hour 32 minutes. Weak fading and diffraction ringing were observed between R+1 minute and R+50 minutes. During most of this first 50 minutes, the aircraft was following the incorrect optics track point projection data causing it to traverse the high altitude, low-ion density part of the cloud, northeast of the cloud center. Only weak fading was seen during the last two passes. Uplink data is available for 12 of the 32 passes while downlink data is available for all 32 passes.

The data received from each of these releases shows the expected progression of effects from diffraction ringing, large defocusing from the background ion cloud, large defocus with superimposed fading from developing striations, and eventually random fading at late times. Representative data are described below.

73
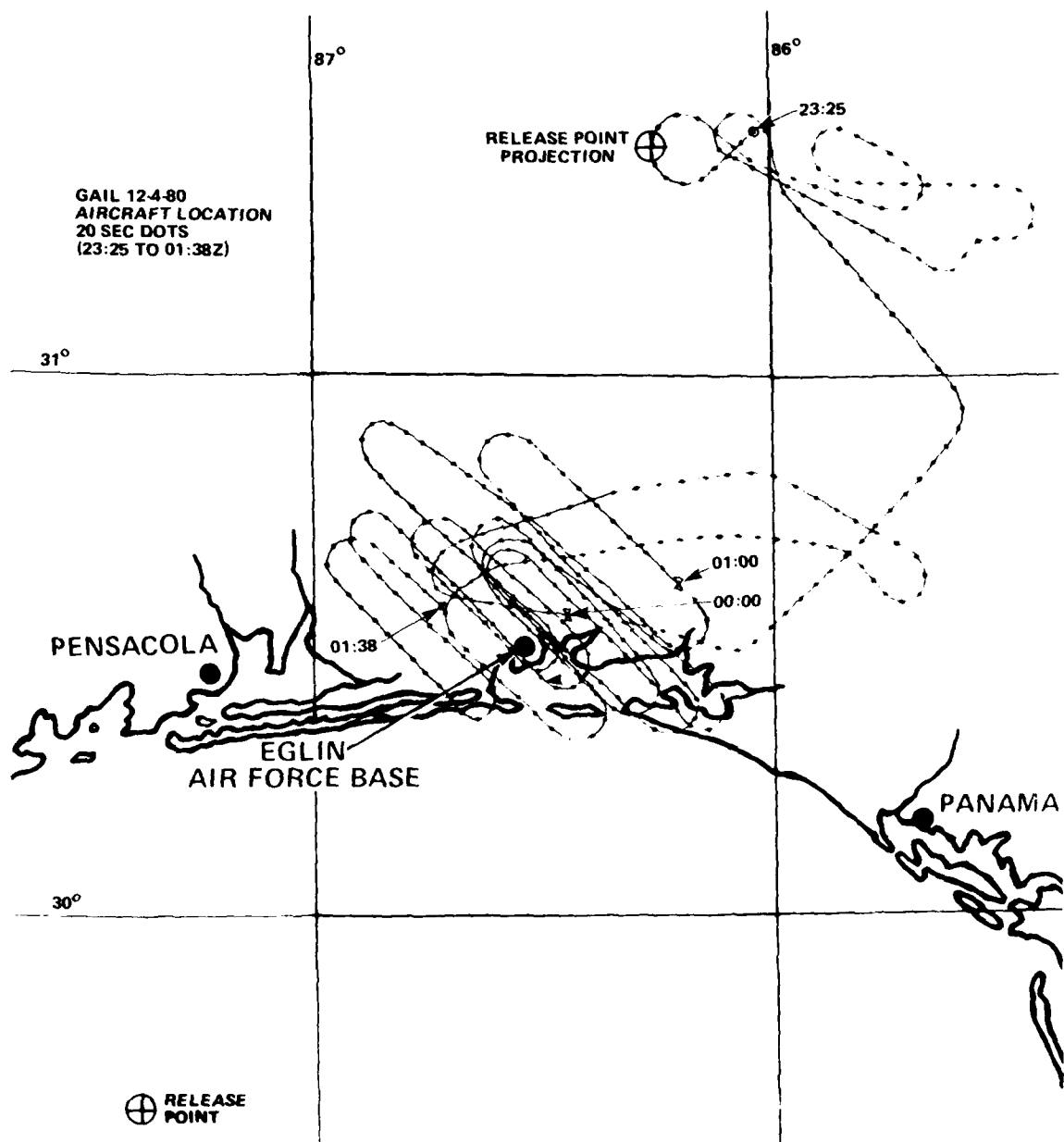
Figure 3-4. Aircraft Ground Track for GAIL

74
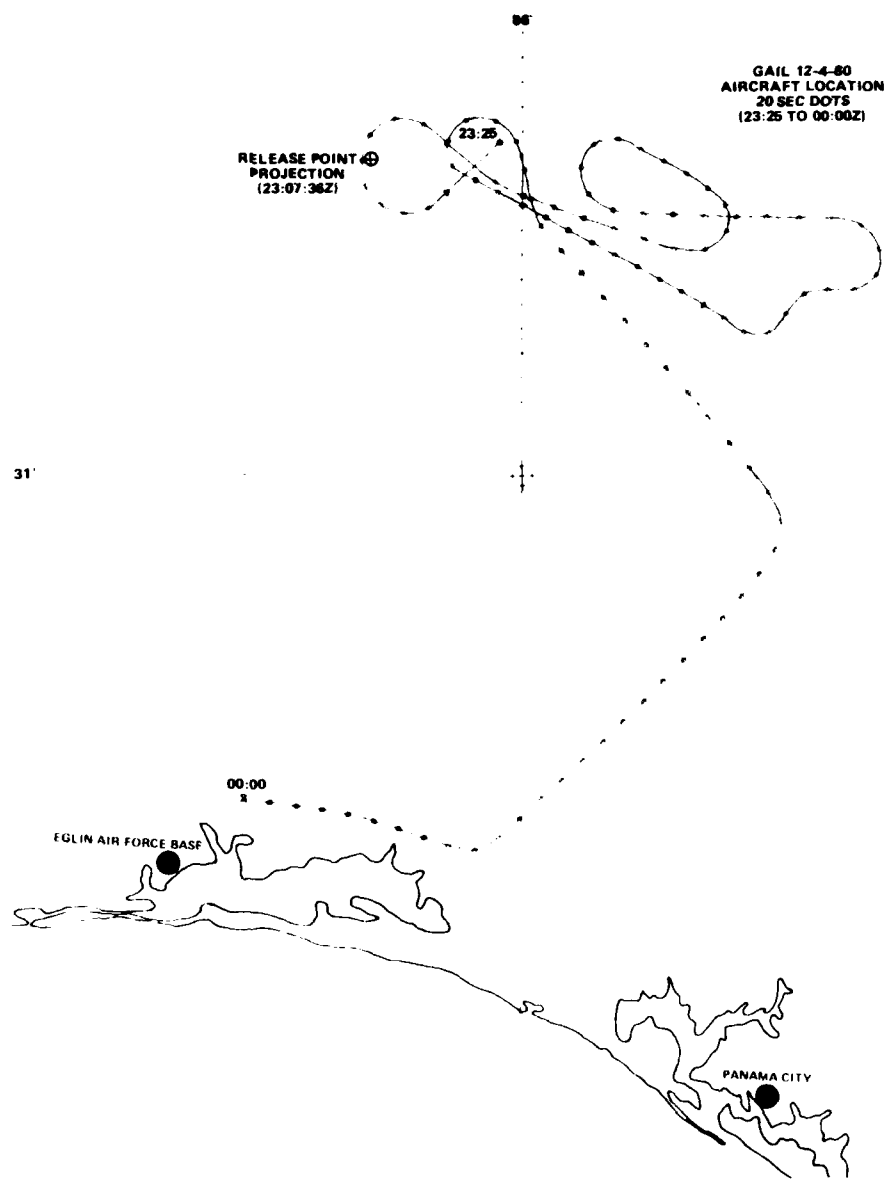
Figure 3-5. Aircraft Ground Track for GAIL from 23:25 to 00:00Z
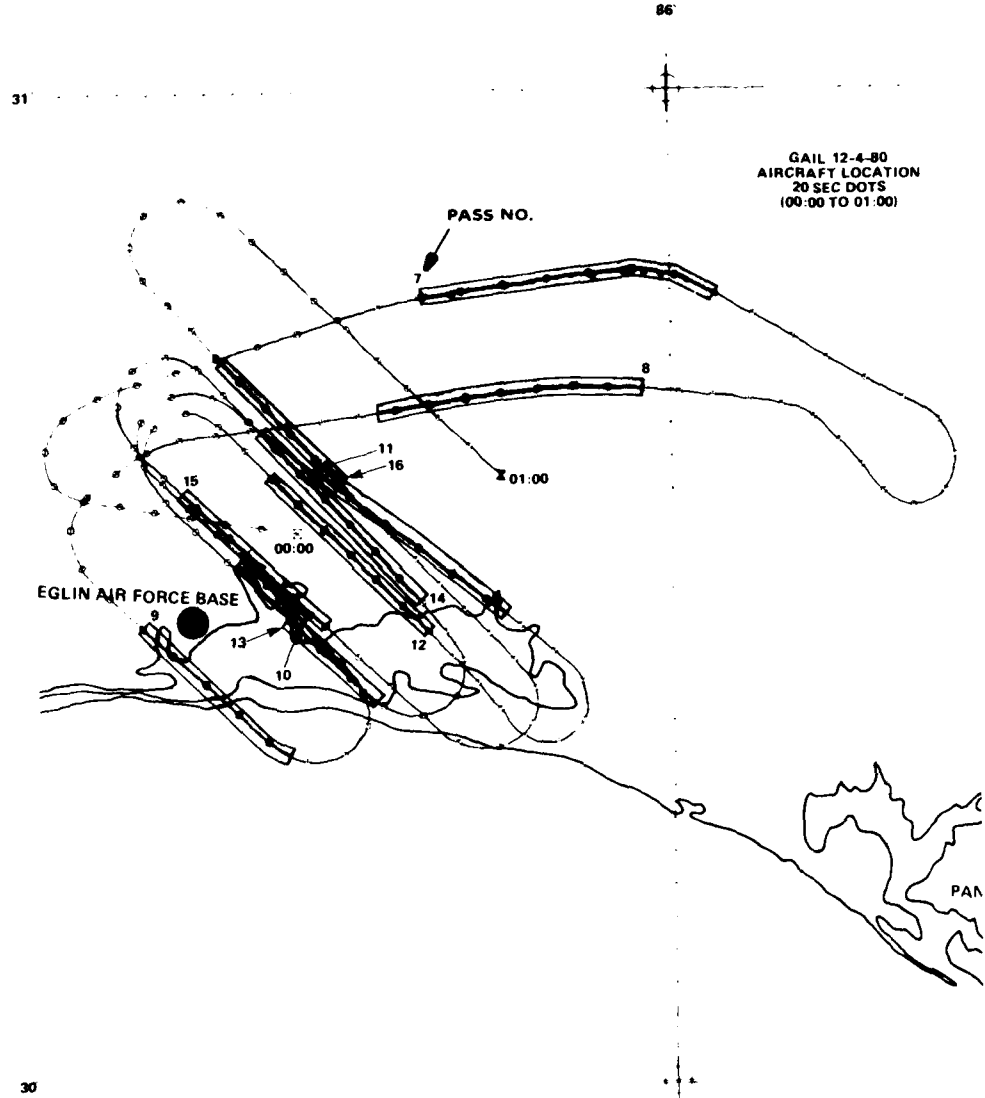
Figure 3-6. Aircraft Ground Track for GAIL from 00:00 to 01:00Z.
Periods of Deep Fading are Shaded

GAIL 12-4-80
AIRCRAFT LOCATION
20 SEC DOTS
(01:00 TO 01:37)

01:00

01:37

EGLIN AIR FORCE BASE
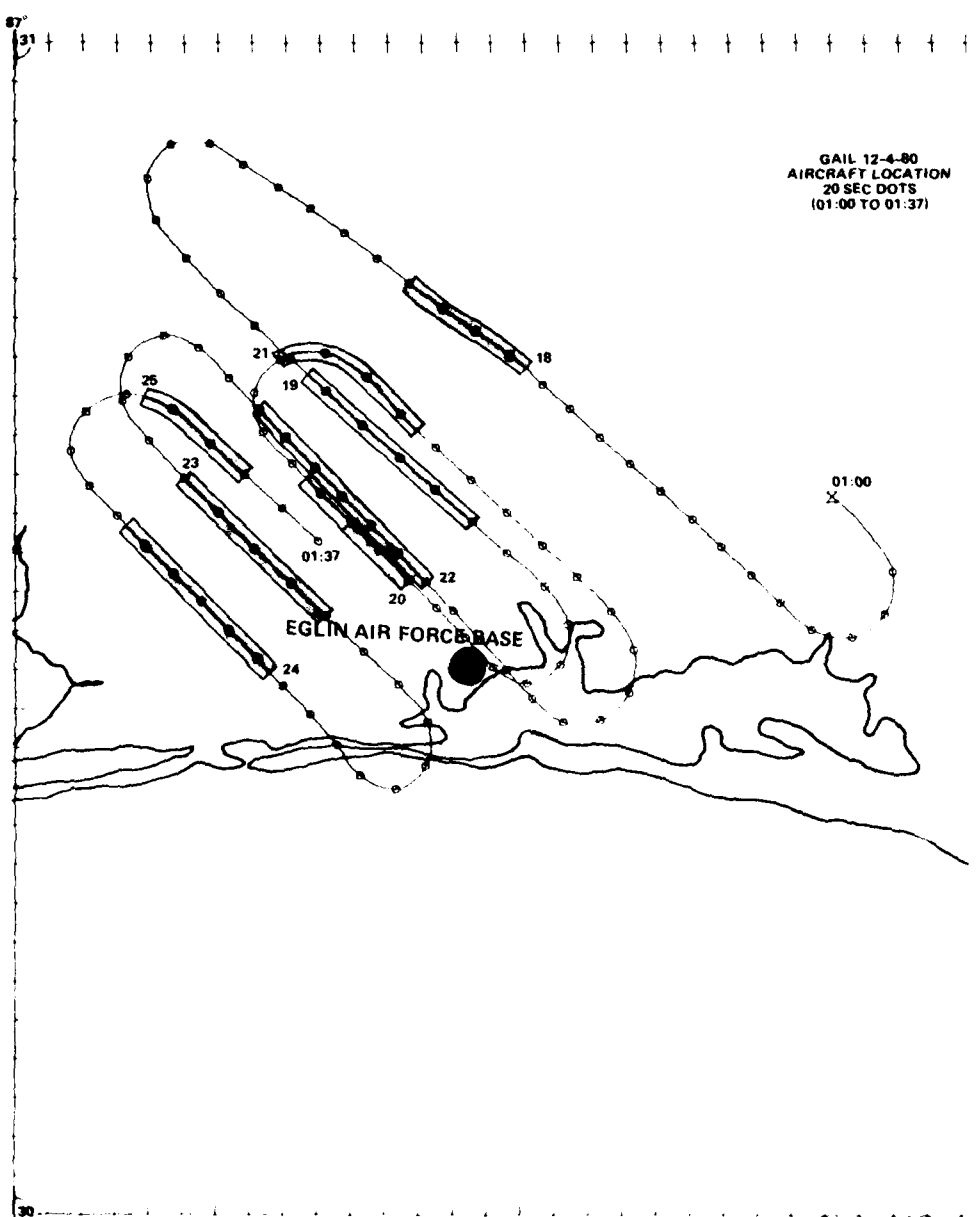
Figure 3-7.   Aircraft Ground Track for GAIL from 01:00 to 01:37Z.
Periods of Deep Fading are Shaded

Table 3-2. Aircraft Data Summary for GAIL

Pass No.	Time	K-Lock[1]	Comments
-3	23:07:40-23:09:30	Yes	Diffraction ringing
-2	23:11:50-23:13:30		Diffraction ringing
-1	23:17:40-23:19:30		Weak fading
0	23:24:00-23:26:20		Weak fading
1	23:29:50-23:31:40		Weak fading
2	23:32:40-23:34:20		Weak fading
3	23:35:30-23:37:30	No	Weak fading
4	23:41:40-23:43:20		Weak fading
5	23:48:20-23:50:10		Weak fading
6	23:59:00-00:02:00	No, manual[2] doppler correction	Weak fading
7	00:06:00-00:08:40	No, manual[2] doppler correction	Strong fading
8	00:14:20-00:17:10	Yes	Strong fading
9	00:20:20-00:22:30		Moderate fading
10	00:23:40-00:25:40		Moderate fading
11	00:29:40-00:30:40		Strong fading
12	00:33:00-00:35:50		Strong fading
13	00:37:50-00:39:10		Moderate fading
14	00:41:30-00:44:00	No	Strong fading
15	00:46:30-00:48:30		Strong fading
16	00:49:40-00:55:30		Strong fading, three pieces to cloud
17	00:57:20-01:00:00	No, manual[2] doppler correction	Weak fading
18	01:04:40-01:06:30	No, manual[2] doppler correction	Strong fading

Table 3-2. --Continued

Pass No.	Time	K-Lock[1]	Comments
19	01:10:40-01:12:10	No, manual[2] doppler correction	Strong fading
20	01:14:40-01:16:20	No, manual[2] doppler correction	Strong fading
21	01:17:30-01:18:50	No, manual[2] doppler correction	Strong fading
22	01:23:20-01:25:40	No, manual[2] doppler correction	Strong fading
23	01:27:20-01:29:20	No, manual[2] doppler correction	Strong fading
24	01:32:00-01:34:00	No, manual[2] doppler correction	Strong fading
25	01:35:20-01:36:40	No, manual[2] doppler correction	Strong fading, short interval
26	01:39:30-01:42:00	No, manual[2] doppler correction	No fading
27	01:42:00-01:46:00	No, manual[2] doppler correction	No fading/possibly weak fading
28	01:48:00-01:52:00	No, manual[2] doppler correction	No fading/possibly weak fading

[1]Loss of k-lock implies loss of uplink tone data.

[2]Manual doppler correction on downlink tone.

Two examples of early time passes are given in Figures 3-8 and 3-9 taken from the real time strip charts onboard the aircraft. These passes show early time diffraction or multipath ringing characterized by oscillating amplitude fluctuations. This diffraction ringing was noted almost immediately following each release. This can be contrasted to the strong deep fading seen in Figure 3-10 for Pass 11 which shows what we term strong fading characteristic of well developed striations. The last strong fading of the night for GAIL is shown in Figure 3-11. It is interesting to note the coarseness or slower fading that results at late time.

3-4   TEST RESULTS FOR HOPE.

The second barium release called HOPE occurred on 6 December 1980, at 23:07:37.4. It was released at an altitude of 179.4 kilometers at an approximate latitude and longitude of 29.25°N and 87.0°W. This release point was about 5 minutes southwest of the planned release point. This cloud appears to have moved north-northeast for a few minutes, stopped, then moved south-southwest at a moderate velocity for the rest of the night. The cloud projection was located about 2 degrees south and 1.5 degrees west of release at R+2 hours 38 minutes. A plot of the available cloud projection data is shown on Figure 3-12. The aircraft ground track is shown on Figure 3-13.

Optical track data was used until about R+55 minutes with radar track data being used for the remainder of the experiment. The optics track located the cloud somewhat north of the radar track. The radar track appears to have been more consistent with the observed fading. As shown on Figure 3-13 the aircraft was vectored nearly 0.5 degree south of the optics track around 0000Z. Figures 3-14, 3-15, and 3-16 show the aircraft ground track for each hour period. The intervals of strong fading are indicated by the shading.
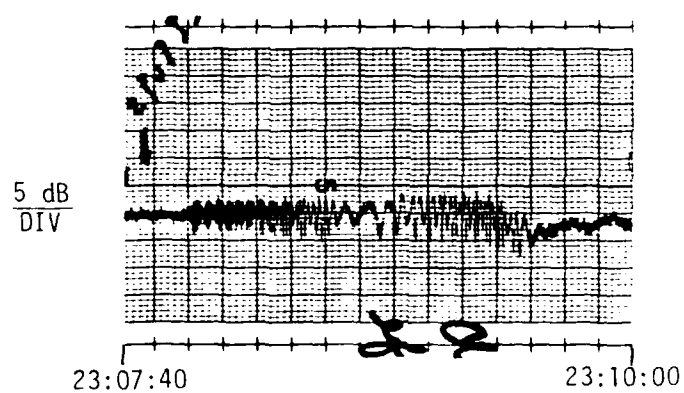
Figure 3-8.   Downlink Fading on GAIL Pass 3, R+1 Minute

$\frac{2}{DIV}\ dB$

23:11:50   23:13:40
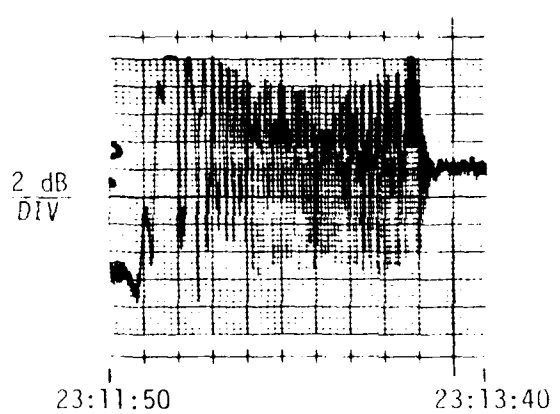
Figure 3-9.   Downlink Fading on GAIL Pass 2, R+5 Minutes
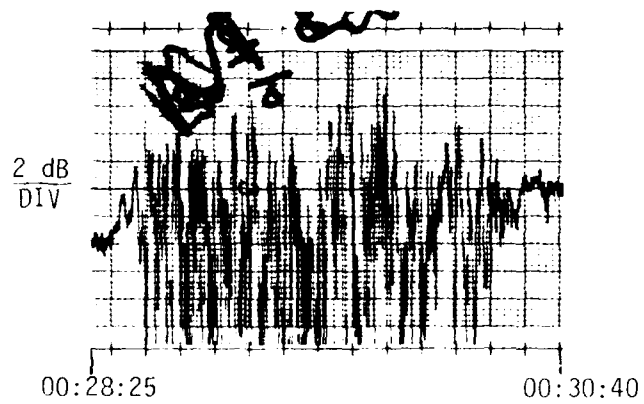
Figure 3-10. Downlink Fading on GAIL Pass 11, $R+1^h25^m$

$$\frac{2 \text{ dB}}{\text{DIV}}$$

01:31:42   01:34:10
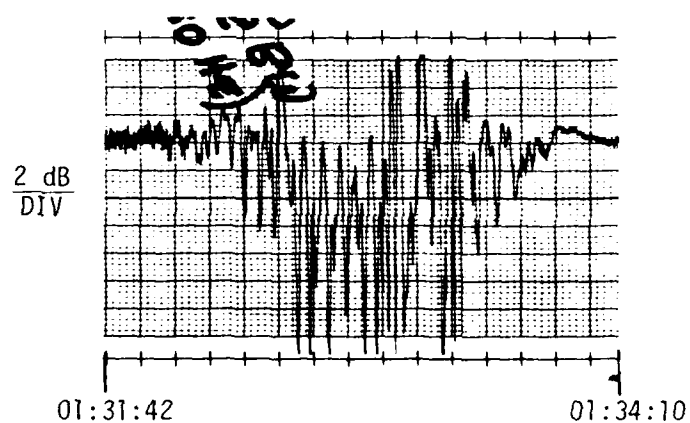
Figure 3-11. Downlink Fading on GAIL Pass 24, $R+2^h25^m$
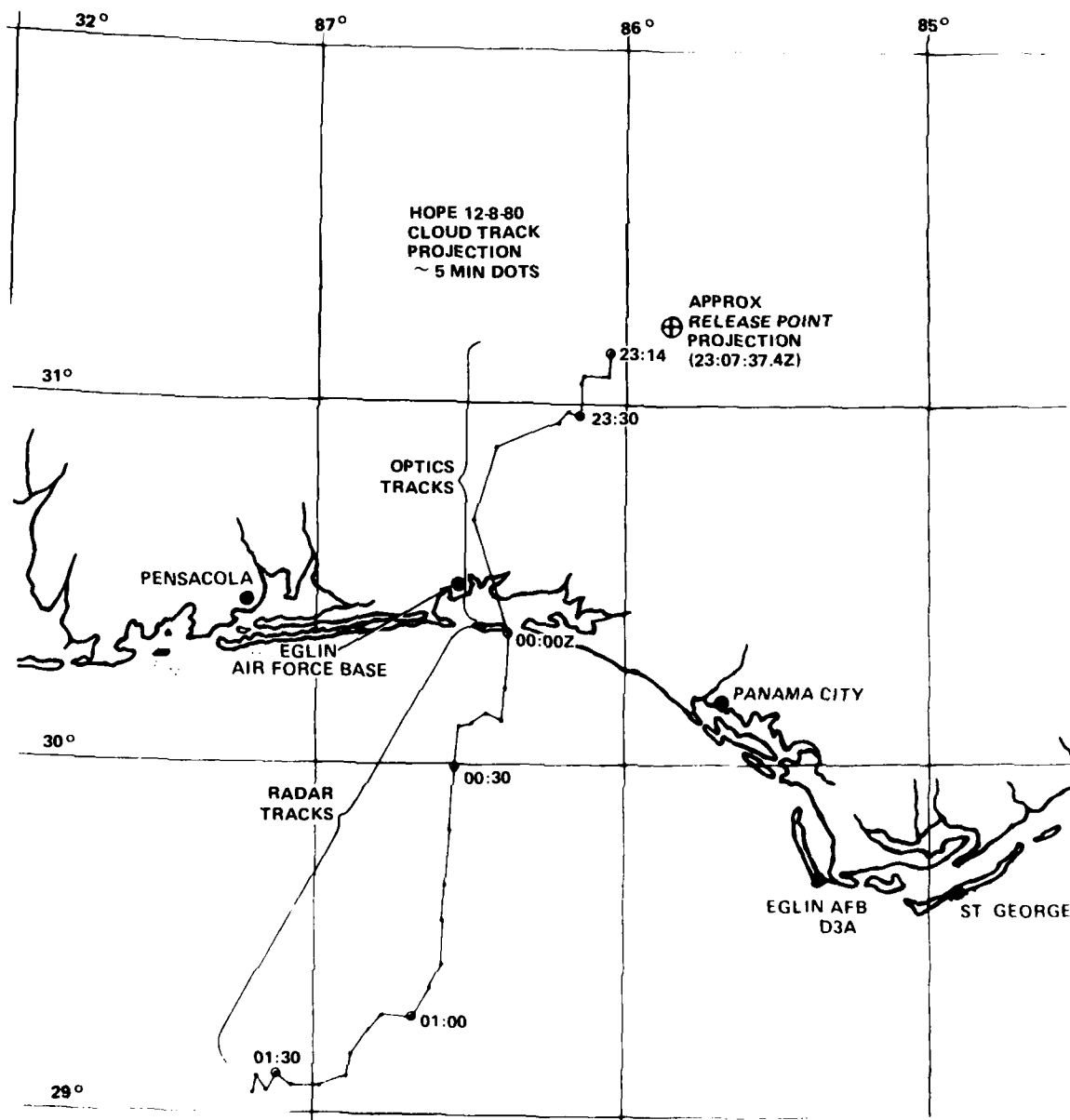
Figure 3-12. Ion Cloud Track Projection for HOPE
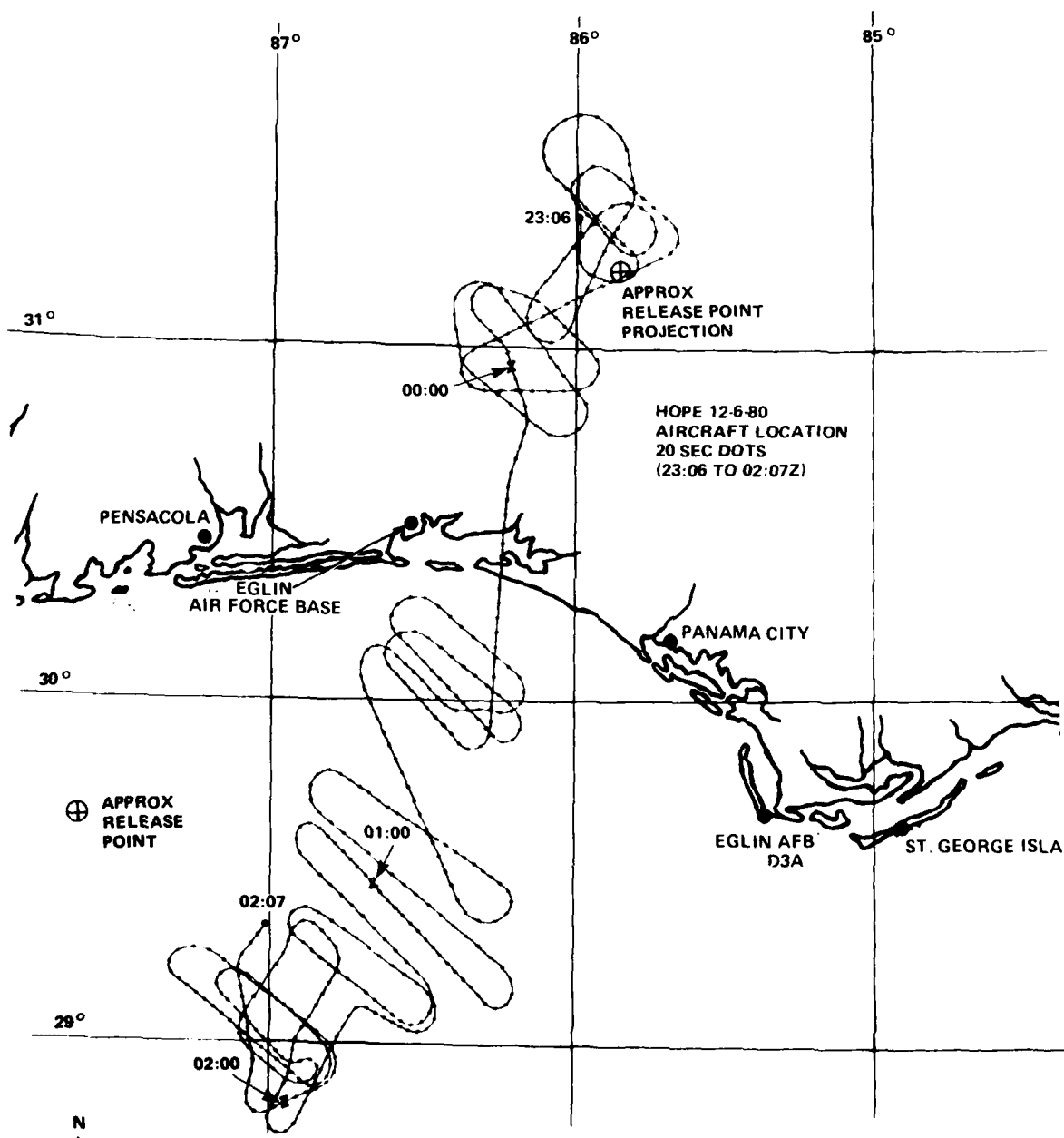
Figure 3-13. Aircraft Ground Track for HOPE
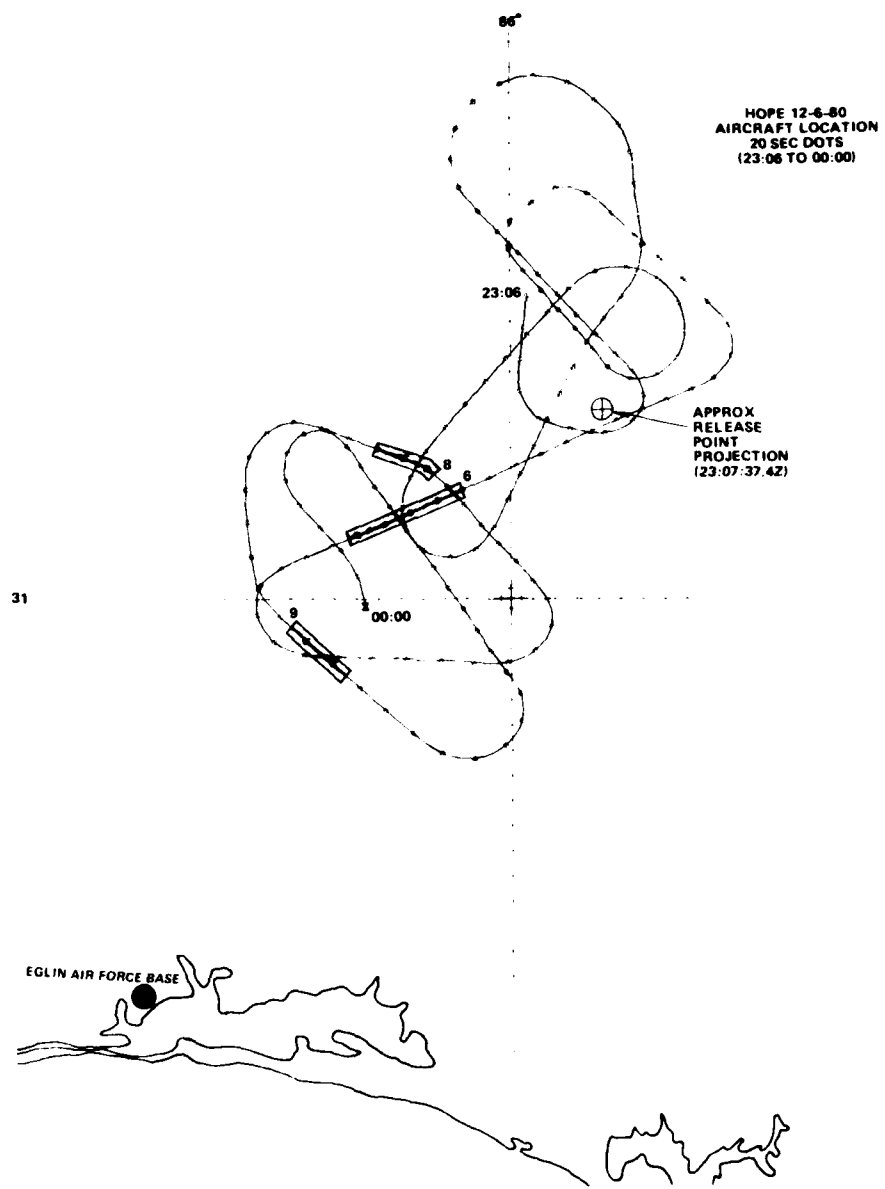
Figure 3-14. Aircraft Ground Track for HOPE from 23:06 to 00:00Z.
Periods of Deep Fading are Shaded
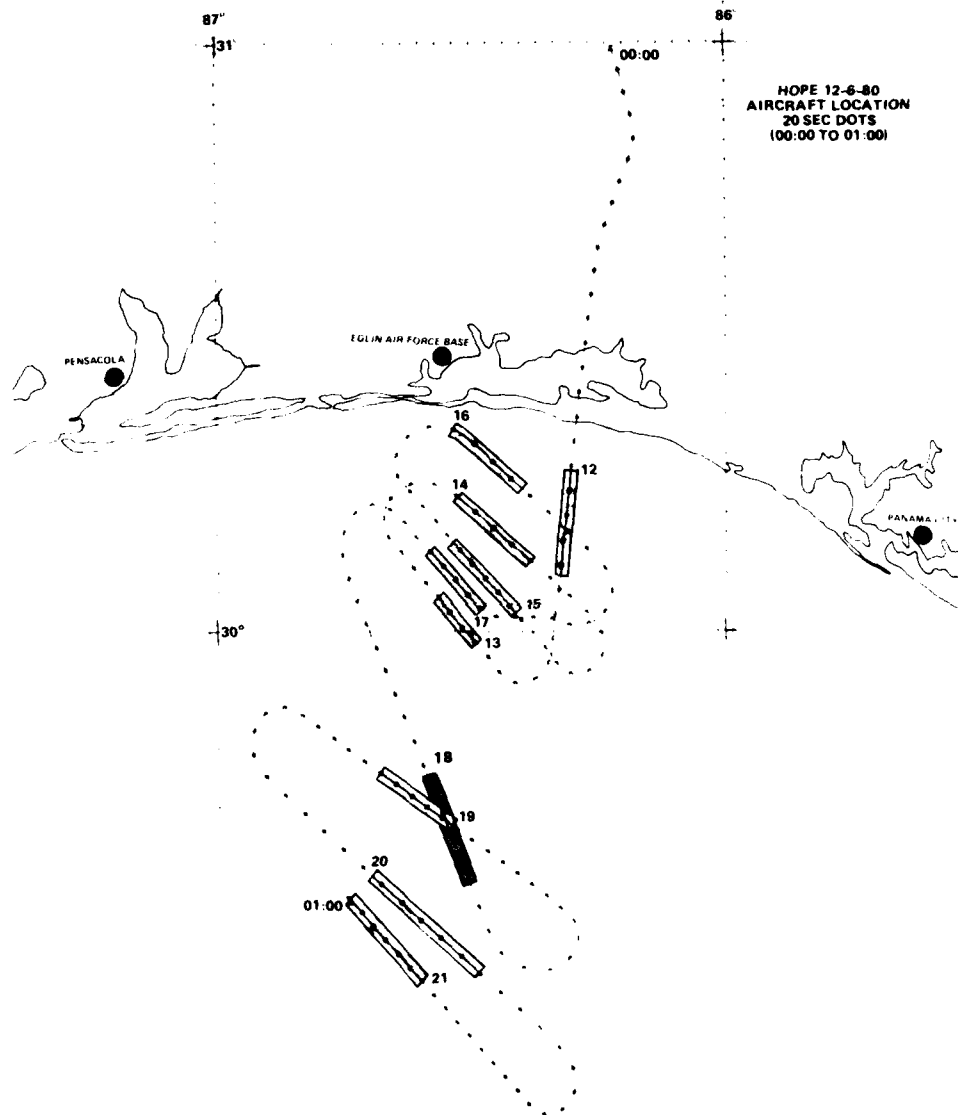
Figure 3-15. Aircraft Ground Track for HOPE from 00:00 to 01:00.
Periods of Deep Fading are Shaded
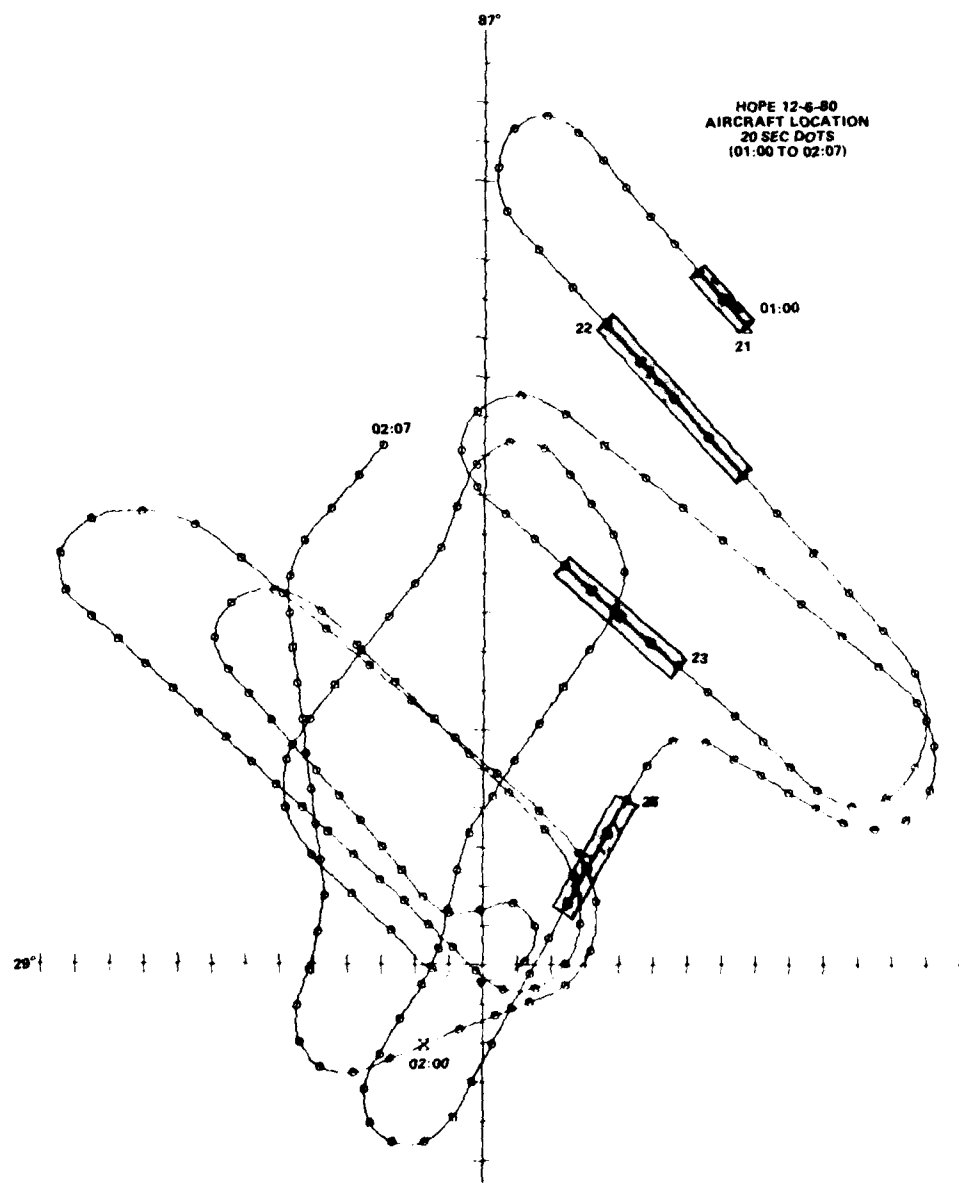
Figure 3-16. Aircraft Ground Track for HOPE from 01:00 to 02:07.
Periods of Deep Fading are Shaded

The ion cloud from HOPE drifted more northerly than during GAIL and again resulted in an inability to launch a beacon or a probe rocket.

A total of 33 passes were made during this release with 14 showing moderate to strong fading. A summary of all of the passes is given in Table 3-3. The last pass ended at R+2 hours 57 minutes while the last pass with moderate fading observed ended at R+2 hours 22 minutes. The first 11 passes, which were between release and R+55 minutes, showed strong fading in only two passes and diffraction ringing in one. These passes were made while the aircraft followed the optics cloud track. The time between R+55 minutes and R+1 hour 3 minutes was spent catching up with the cloud which was south of the aircraft. Twelve of the next 15 passes showed moderate to strong fading yielding the total of 14 good passes. Pass 26 is interesting because it shows only one deep fade that may be due to a single object. The last seven passes showed weak fading or no fading.

Uplink data is available for 32 of the 33 passes and downlink data is available for all 33 passes. K-band lock was lost during part of one pass making the uplink data questionable during that pass. Occasionally, as noted, a loss of lock indication was obtained, but, the uplink data appeared unperturbed.

A few samples of the data from HOPE are given in Figures 3-17 through 3-21. These data have been preliminary computer processed for this quicklook report. Additional processing is planned. Pass 1 shown in Figure 3-17 shows an unusually large defocus of nearly -20 dB with some diffraction ringing at the edges. The depth and duration of this defocus, lasting approximately 75 seconds is remarkable. Defocusing of this magnitude was not observed during the prior STRESS experiment and is believed to be due in part to the alignment of the propagation path and the ion cloud drift (stretching) direction. If the initial stretching direction was approximately along 40 degrees azimuth and since the azimuth to the satellite at early times was approximately 210 degrees, then the ray path would make an angle of about 10 degrees with the stretching direction of the cloud.

90

Table 3-3. Aircraft Data Summary for HOPE

Pass No.	Time	K-Lock	Comments
1	23:07:30-23:11:40	No	Diffraction ringing, large defocus of ~15 dB
2	23:17:40-23:20:00	Yes	No fading
3	23:22:00-23:24:00		Weak diffraction ringing
4	23:27:30-23:29:10		Very little fading
5	23:30:50-23:32:20		Very little fading
6	23:36:20-23:38:40	?, uplink OK	Strong fading, large defocus of ~15 dB
7	23:40:30-23:42:00	Yes	Little fading
8	23:45:00-23:47:00		Strong fading, partially in turn
9	23:49:50-23:51:30		Moderate fading
10	23:54:00-23:57:00		No fading
11	00:00:00-00:01:00		No fading
12	00:05:40-00:07:50		Moderate diffraction ringing
13	00:10:00-00:12:00		No fading
14	00:14:00-00:16:20		Strong fading
15	00:18:20-00:21:40		Strong fading
16	00:23:30-00:15:00		Strong fading
17	00:29:00-00:31:20		Strong fading
18	00:36:30-00:38:00		Little fading
19	00:42:30-00:45:20		Strong fading
20	00:50:00-00:52:10		Strong fading first minute
21	00:56:00-01:02:00		Strong fading in 00:59:20 to 01:01:20
22	01:04:30-01:06:20		Strong fading
23	01:10:50-01:12:40		Moderate fading
24	01:15:30-01:17:00	?, uplink OK	Moderate fading
25	01:21:00-01:23:20	Yes	Weak fading
26	01:28:20-01:29:30		One deep fade

Table 3-3. --Continued

Pass No.	Time	K-Lock	Comments
27	01:34:00-01:36:00	Yes	Weak fading
28	01:36:00-01:37:00		Weak fading
29	01:39:20-01:41:10		Weak fading
30	01:44:00-01:45:00		No fading
31	01:49:00-01:53:00		No fading
32	01:53:00-01:55:00		No fading
33	02:02:00-02:04:00		Weak fading

Figure 3 17. Downlink Fading on HOPE Pass 1, R+1 Minute

1.0

1.1

1.25   1.4   1.6

2.8   2.5

2.2

2.0

1.8
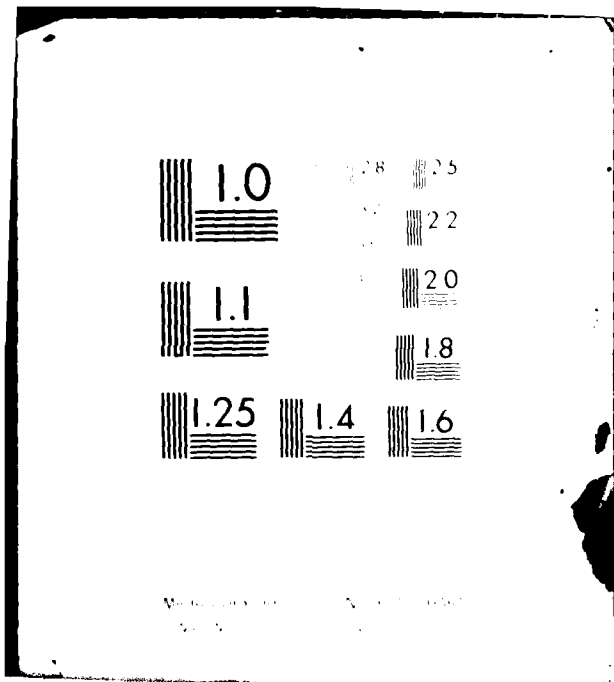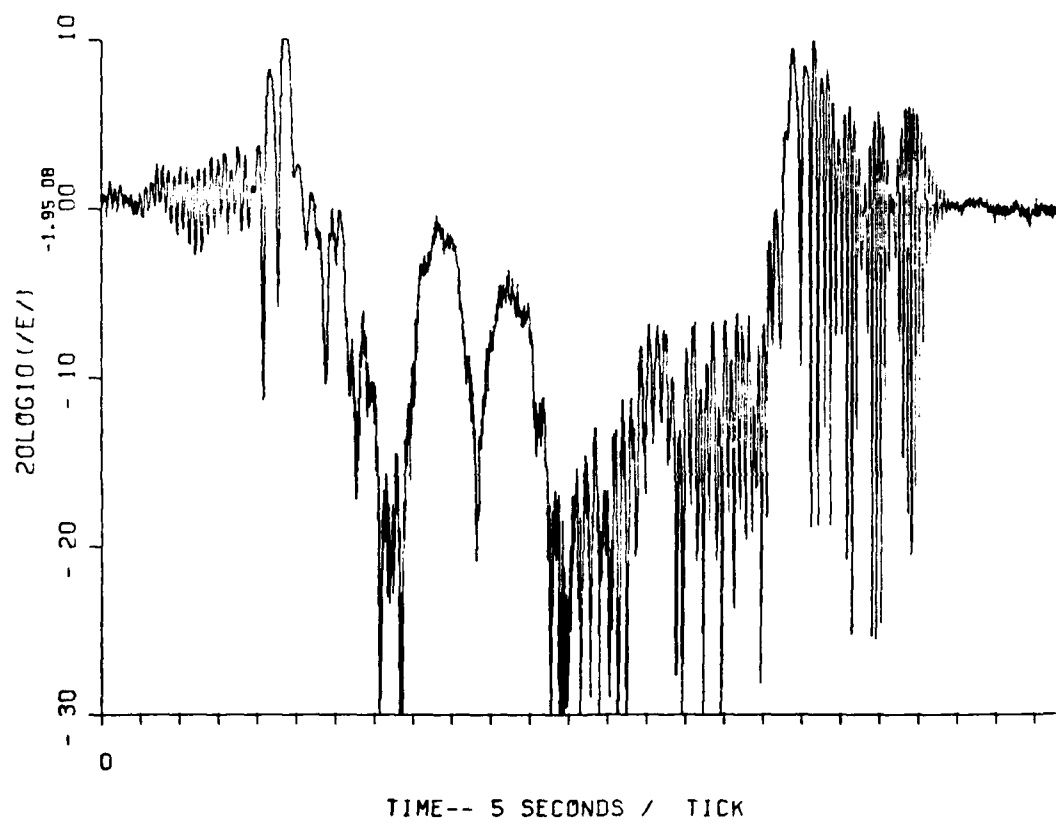
Figure 3-18.   Downlink Fading on HOPE Pass 6, R+30 Minutes
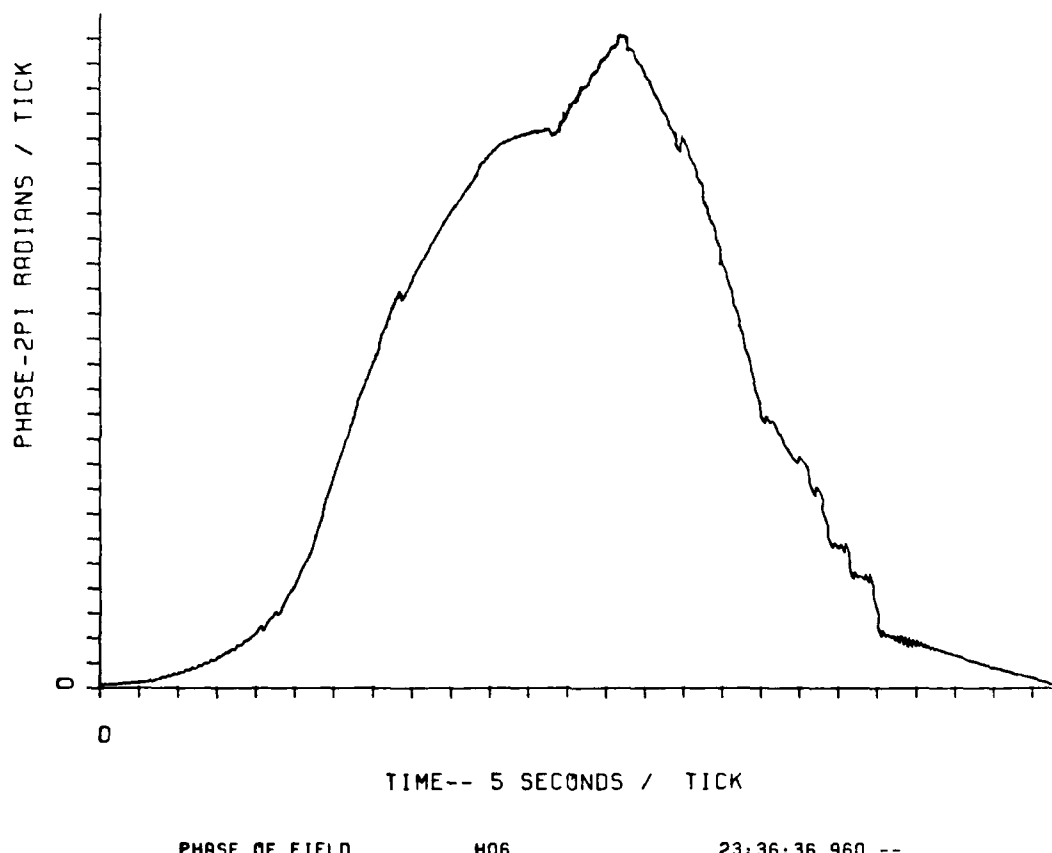
Figure 3-19.   Downlink Phase Effects on HOPE Pass 6, R+30 Minutes
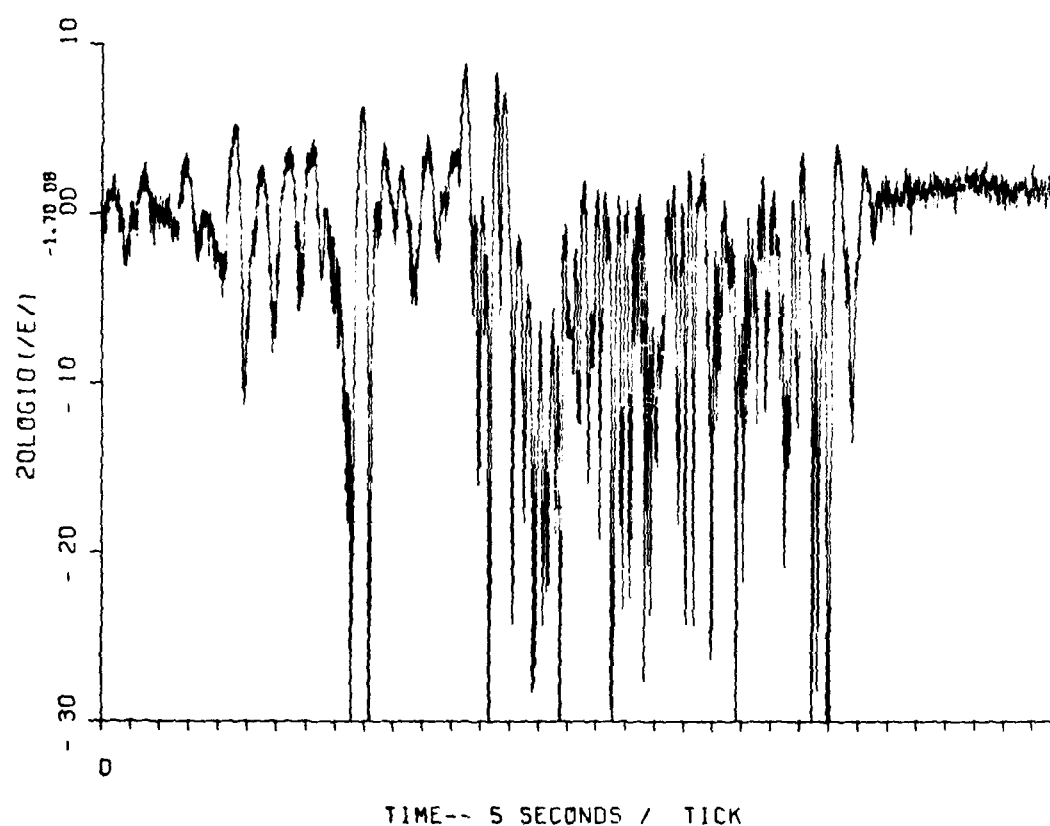
Figure 3-20. Downlink Fading on HOPE Pass 19, R+1^{h}37^m

Figure 3-21. Downlink Phase Effects on HOPE Pass 19, R+1^{h}37^m

A plot of azimuth angle and elevation angle variation from the 662 aircraft to the LES-8 satellite for all four PLACES releases is given in Figure 3-22. By far the largest component of the change with time is due to the satellite motion. The azimuth and elevation both increase by approximately 18 degrees over a typical 3 hour period. The azimuth angle typically started near 207 degrees at 2300 (GMT) and ended near 227 degrees at 0200 (GMT). Likewise, the elevation angle started near 34 degrees at 2300 (GMT) and ended near 51 degrees at 0200 (GMT). Generally, it was desired to have an elevation angle in excess of 30 degrees throughout the test.

As time progresses, Pass 6 at R+30 minutes (Figures 3-18 and 3-19) shows the development of some structuring superimposed on this still large defocus. This structuring is evident in the amplitude and phase characteristics in the latter half of the pass (cloud). Figures 3-20 and 3-21 show Pass 19 at 1 hour and 37 minutes; again, the slower fading amplitude characteristics and smaller integrated electron content (less phase windup) of the background ion cloud are evident. These figures are indicative of the processed data quality available. The processing bandwidth can be reduced to improve signal quality still further in subsequent planned processing.

3-5   TEST RESULTS FOR IRIS.

The third barium release, IRIS, was on 8 December 1980 and occurred at 23:13:06.7. It was released at an altitude of 179.6 kilometers and a latitude and longitude of 28.799°N and 87.166°W. The projection of this release point is 30°40'11"N and 85°51'24"W. The cloud projection moved in a south-southeast direction during the entire experiment and was last seen about 3 degrees south and 0.75 degrees east of the release point projection at R+2 hours 30 minutes. Plots of the cloud track projection and aircraft ground track are in Figures 3-23 and 3-24. Figures 3-25, 3-26 and 3-27 show the aircraft ground track for each hour with intervals of strong fading indicated.

AZ (DEG)
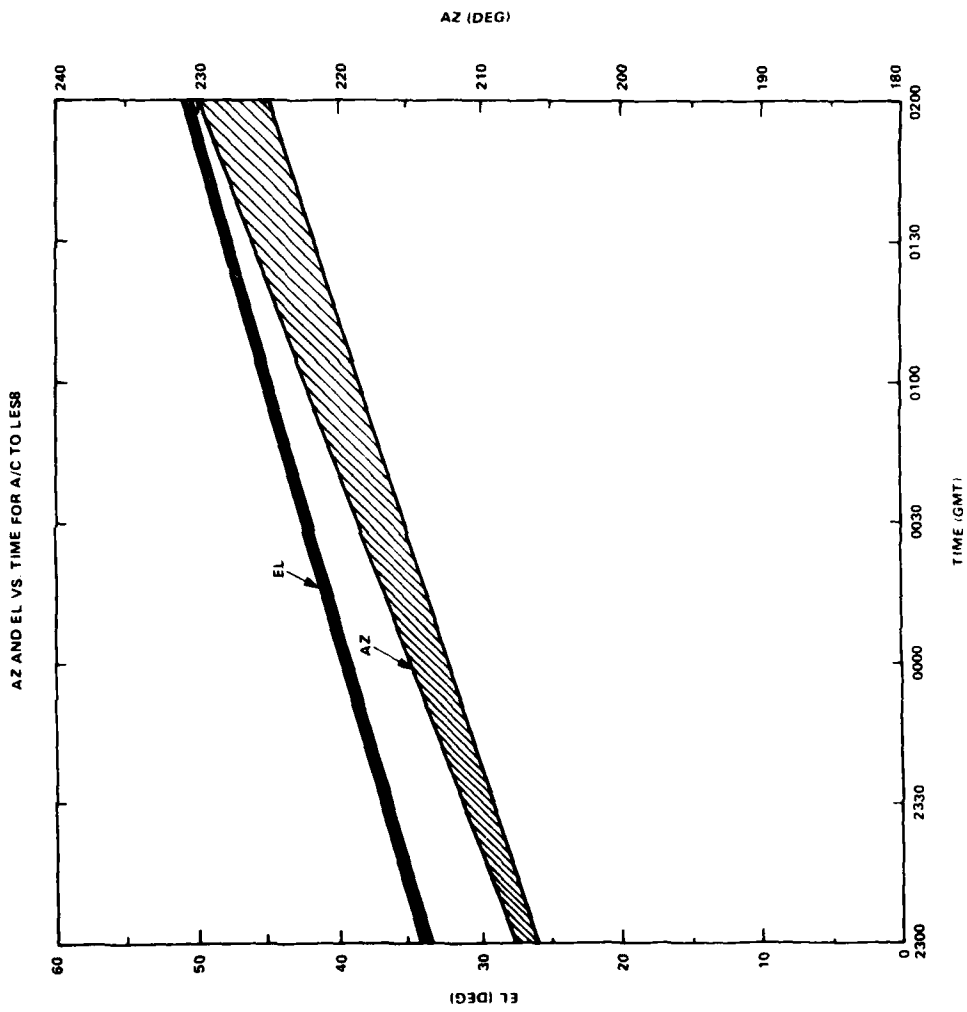
Figure 3-22. Azimuth and Elevation Angle to LES-8 Versus Time During PLACES

99
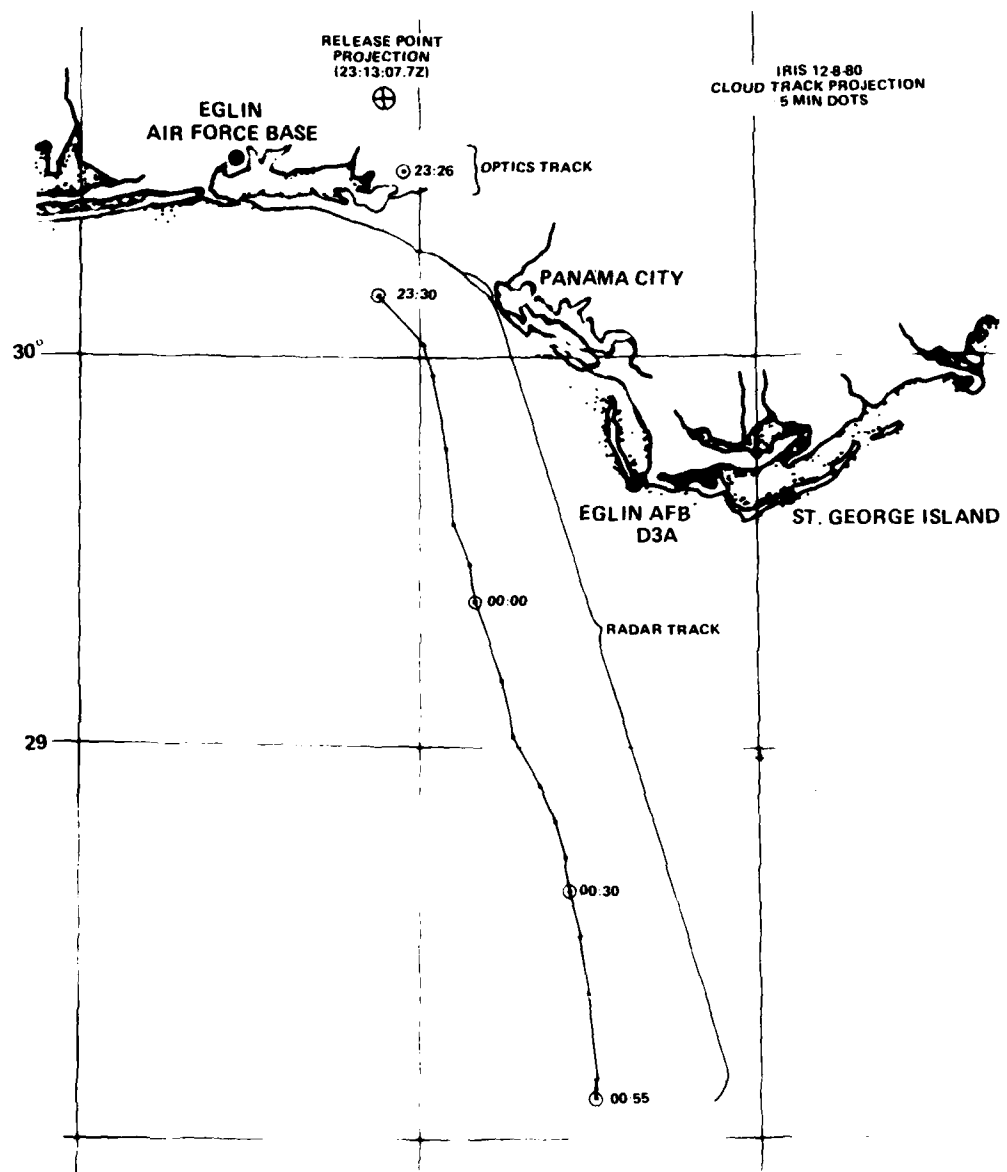
Figure 3-23.   Ion Cloud Track Projection for IRIS
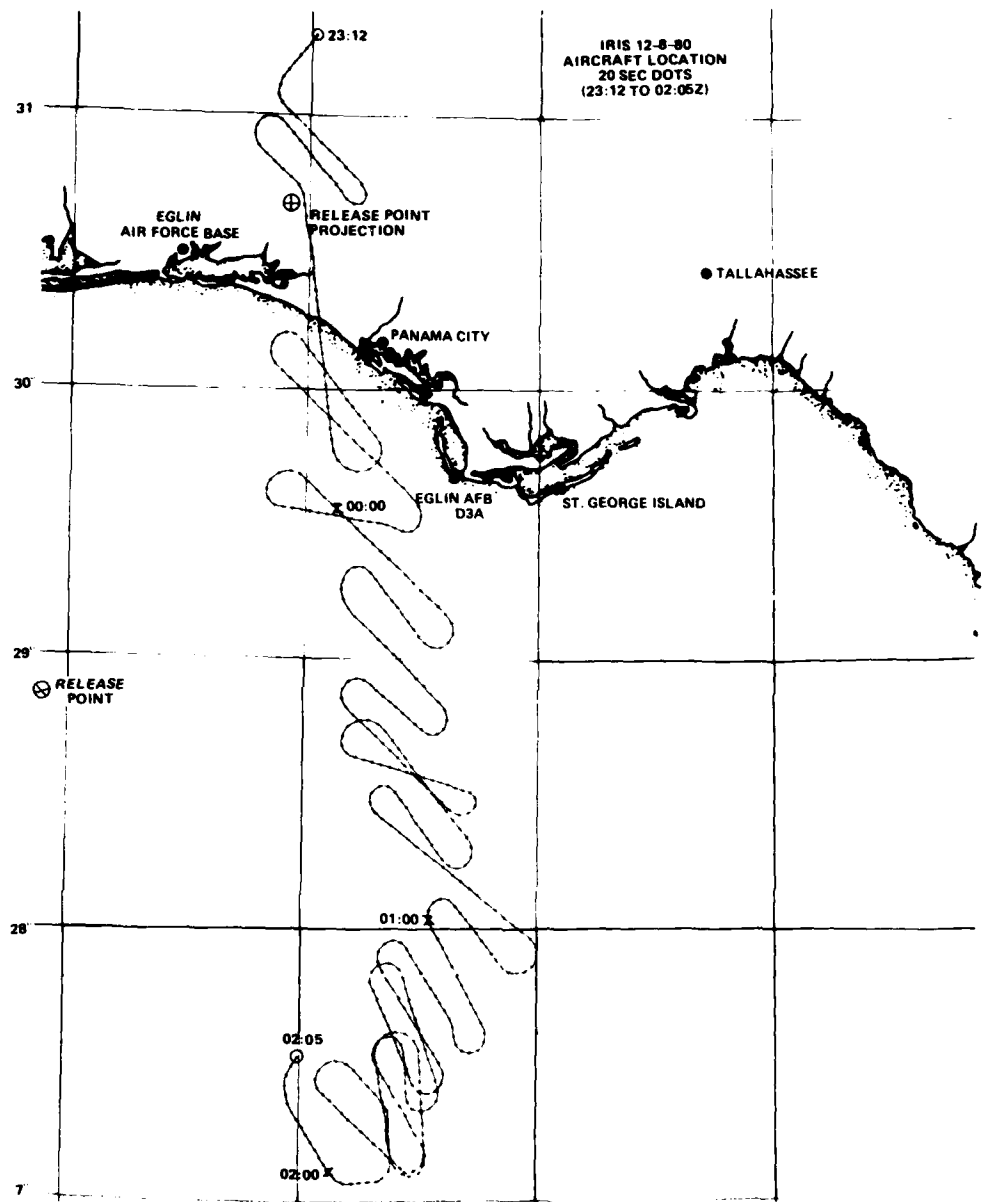
Figure 3-24. Aircraft Ground Track for IRIS
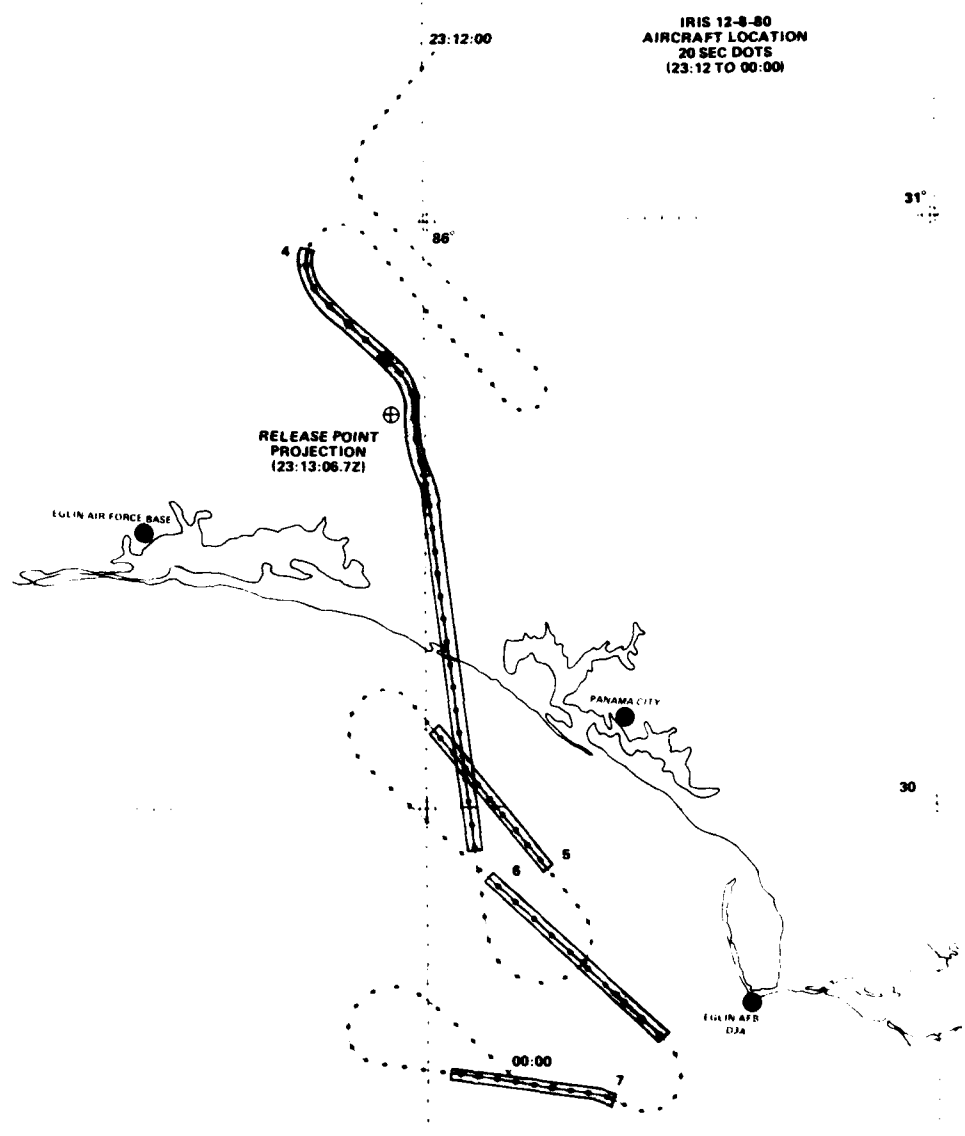
Figure 3-25. Aircraft Ground Track for IRIS from 23:12 to 00:00Z. Periods of Deep Fading are Shaded
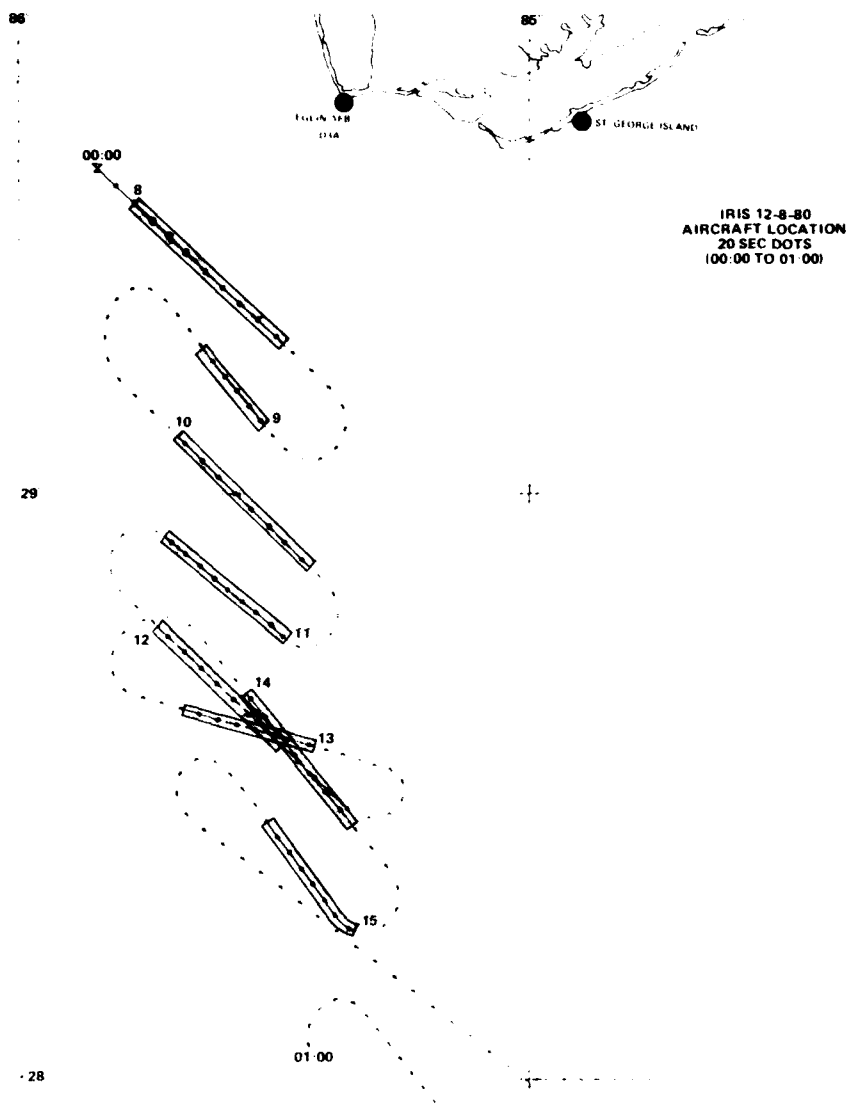
Figure 3-26.   Aircraft Ground Track for IRIS from 00:00 to 01:00Z.
Periods of Deep Fading are Shaded
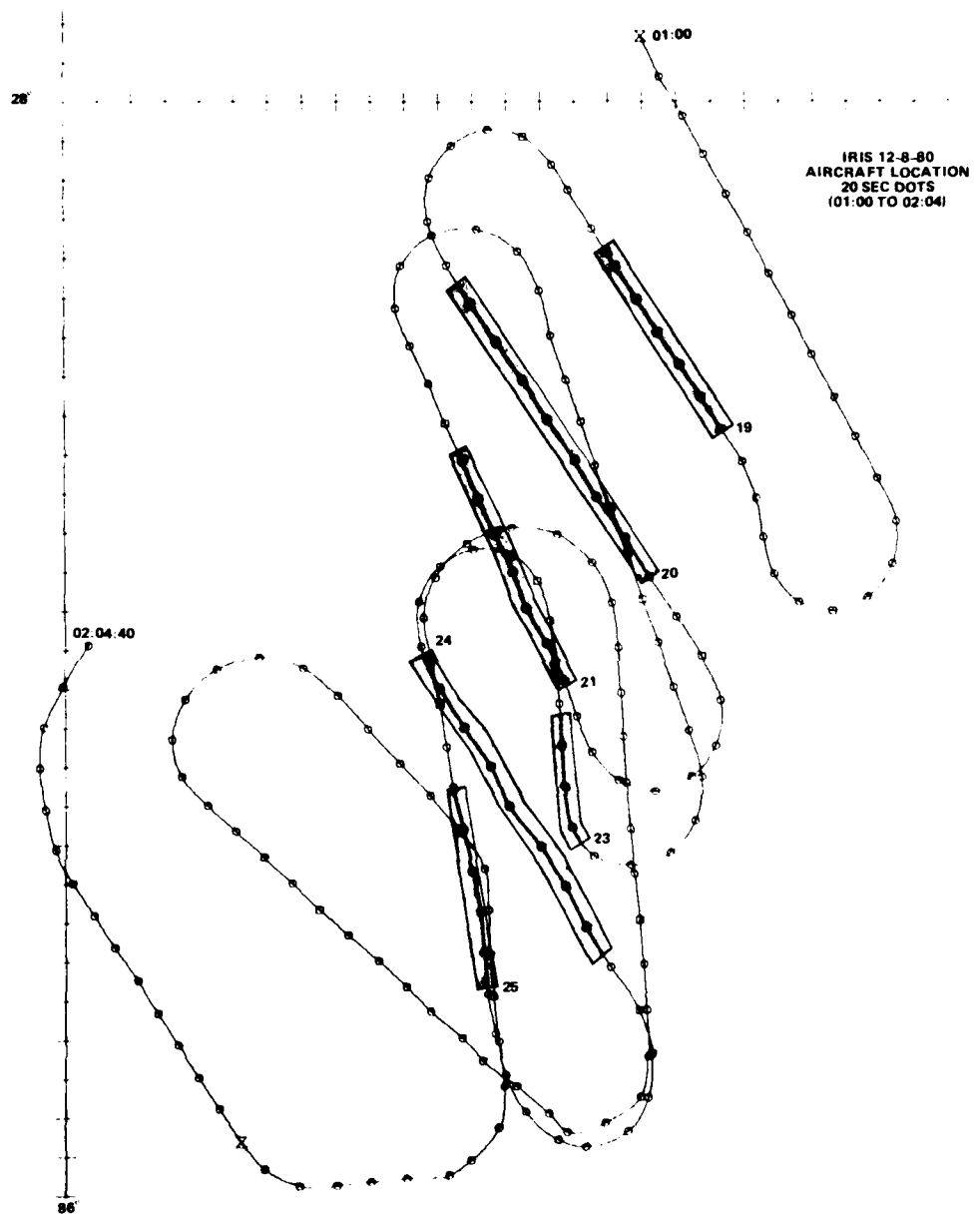
Figure 3-27. Aircraft Ground Track for IRIS from 01:00 to 02:04Z.
Periods of Deep Fading are Shaded

No cloud tracking data was available between release and R+12 minutes. Optics track data was used from R+12 minutes to R+15 minutes and radar track data was used thereafter. The release being low and west of the planned release point resulted in the radar not acquiring the release as planned. The radar track provided a consistent indication of the striation location throughout the night.

A total of 31 passes were made ending at R+2 hours 48 minutes. A summary of these passes is given in Table 3-4. The first strong fading was seen at R+16 minutes, the fourth pass. Moderate to strong fading was present during 17 of the next 22 passes with the last strong fading ending at R+2 hours 26 minutes. The last fading seen ended at R+2 hours 44 minutes during Pass 29.

Downlink data is available for all 31 passes. K-band lock was never achieved during this experiment due to an oscillator failure, consequently no usable uplink data was recorded. Manual doppler correction was used throughout the night. Prior analyses[3] have shown that the uncompensated doppler will not corrupt the phase power spectral density data, but will make processing somewhat more difficult.

Two beacon rockets were fired during this release, both resulting in good data. Because of the extreme southern drift of the cloud, a 40 kilometer occultation distance had to be used to stay within the range safety limits. The data received from both beacon rockets matches very closely with predicted data in the pre-experiment test plan. A correlation between the aircraft data and the beacon data was described in Section 2.

Sample plots of the downlink amplitude fading for IRIS are given in Figures 3-28 through 3-37. Passes 4 and 5 (R+18 minutes and R+26 minutes) shown in Figures 3-28 and 3-29 show a large -15 dB defocus with rapid deep fading indicative of structure formation. As the ion cloud was stretched southeast more perpendicular to the propagation path, this defocus is believed to be indicative of a

Table 3-4. Aircraft Data Summary for IRIS

Pass No.	Time	K-Lock	Comments
1	23:15:30-23:18:10	No, manual doppler correction	No fading
2	23:19:40-23:23:10	No, manual doppler correction	Weak diffraction ringing
3	23:25:10-23:28:20	No, manual doppler correction	No fading
4	23:29:20-23:34:20	No, manual doppler correction	Strong fading, large defocus
5	23:38:30-23:41:30	No, manual doppler correction	Strong fading, large defocus, second fading object
6	23:46:30-23:49:40	No, manual doppler correction	Strong fading
7	23:51:50-23:54:50	No, manual doppler correction	Strong fading
8	00:00:40-00:03:30	No, manual doppler correction	Strong fading
9	00:06:50-00:08:30	No, manual doppler correction	Strong fading
10	00:13:20-00:15:50	No, manual doppler correction	Strong fading
11	00:18:10-00:20:40	No, manual doppler correction	Strong fading

Table 3-4. --Continued

Pass No.	Time	K-Lock	Comments
12	00:23:20-00:26:00	No, manual doppler correction	Strong fading
13	00:30:30-00:32:50	No, manual doppler correction	Strong fading
14	00:37:00-00:39:40	Yes, no uplink tone	Weak fading
15	00:41:50-00:44:20	Yes, no uplink tone	Strong fading
16	00:48:00-00:52:00	Yes	No fading
17	00:56:00-00:58:00	Yes	No fading
18	01:00:40-01:03:40	No, manual doppler correction	No fading
19	01:07:00-01:08:50	No, manual doppler correction	Moderate fading
20	01:11:50-01:14:20	No, manual doppler correction	Strong fading
21	01:17:50-01:20:00	No, manual doppler correction	Strong fading
22	01:23:30-01:26:00	No, manual doppler correction	No fading
23	01:27:50-01:29:20	No, manual doppler correction	Moderate fading
24	01:31:30-01:34:10	No, manual doppler correction	Moderate fading
25	01:38:00-01:39:40	No, manual doppler correction	Moderate fading

Table 3-4. --Continued

Pass No.	Time	K-Lock	Comments
26	01:44:00-01:46:00	No, manual doppler correction	No fading
27	01:47:30-01:49:40	No, manual doppler correction	Weak fading
28	01:54:00-01:55:00	No, manual doppler correction	No fading
29	01:56:00-01:57-00	No, manual doppler correction	Weak fading
30	01:58:00-01:59:00	No, manual doppler correction	No fading
31	02:00:00-02:01:30	No, manual doppler correction	No fading
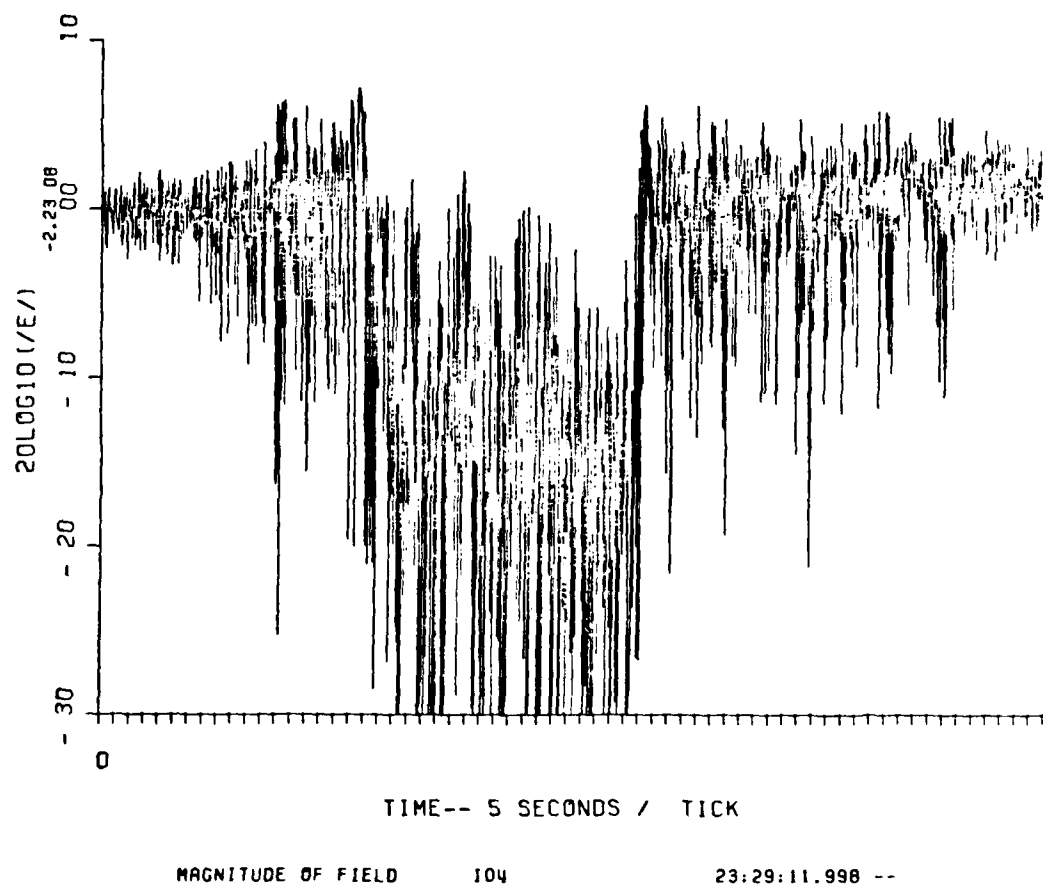
Figure 3-28. Downlink Fading on IRIS Pass 4, R+18 Minutes

109
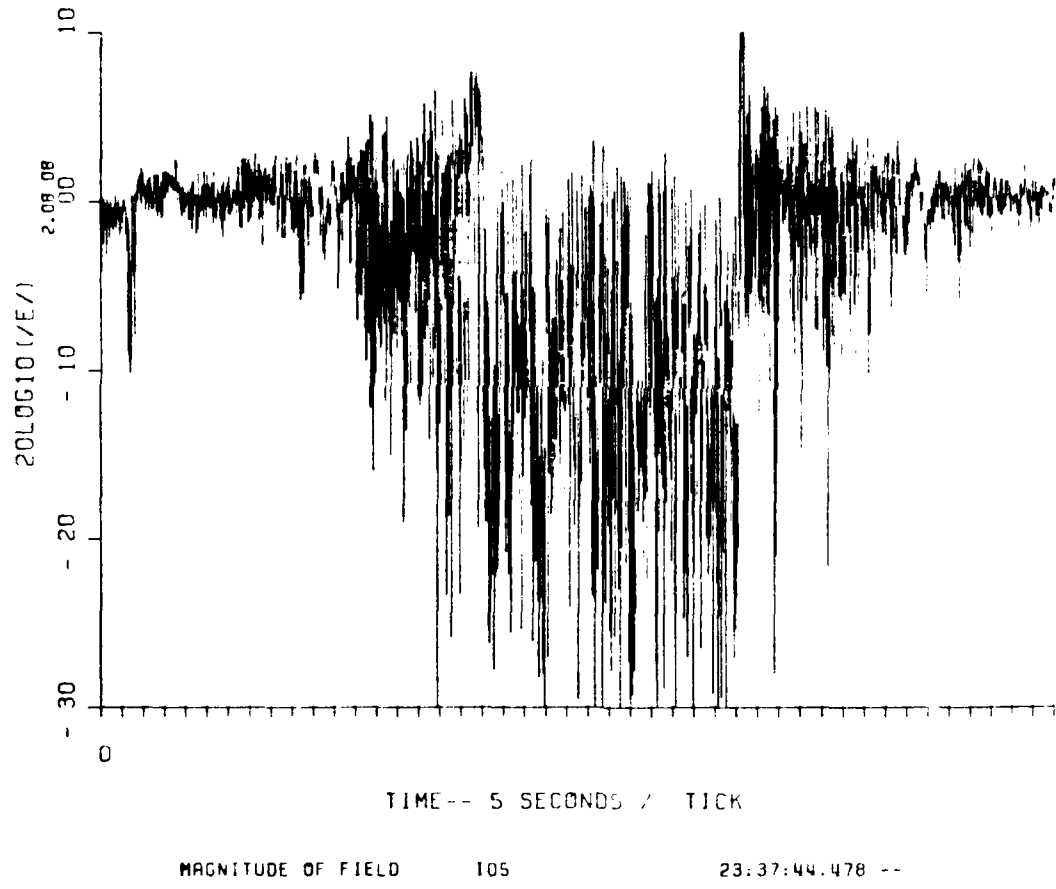
Figure 3-29. Downlink Fading on IRIS Pass 5, 2:36 Minutes
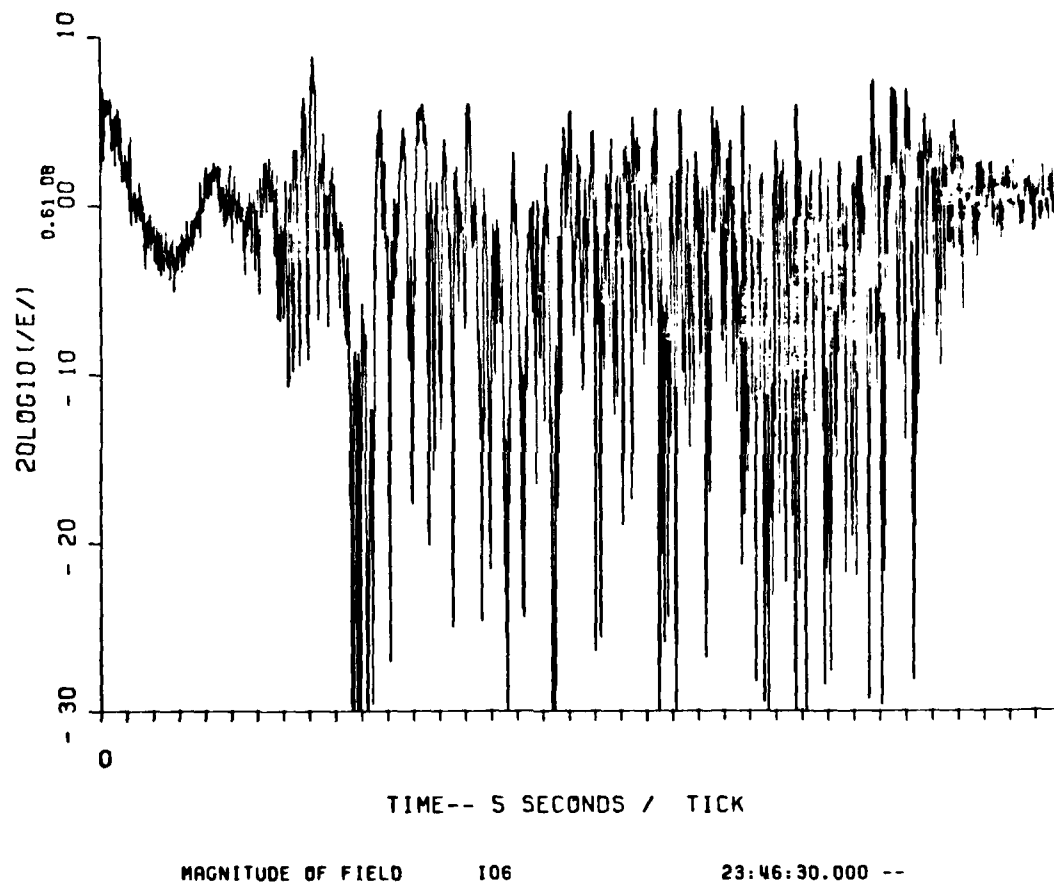
Figure 3-30. Downlink Fading on IRIS Pass 6, R+34 Minutes

111
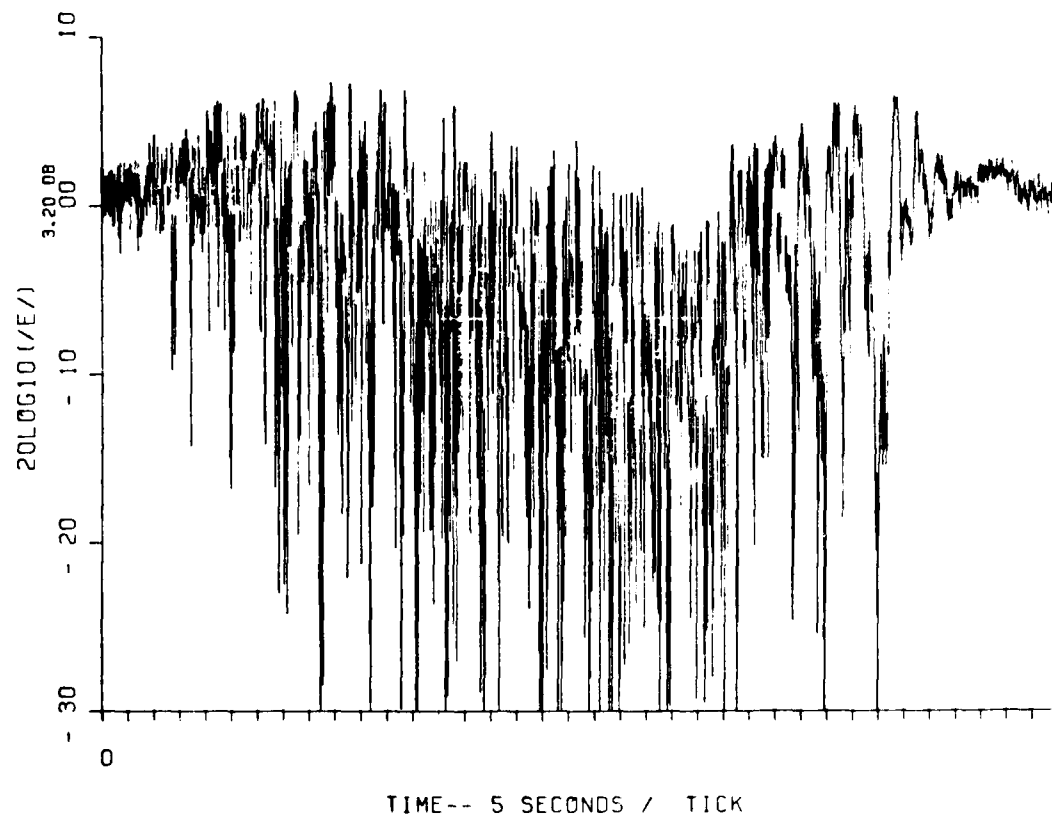
Figure 3-31.   Downlink Fading on IRIS Pass 7, R+39 Minutes

112
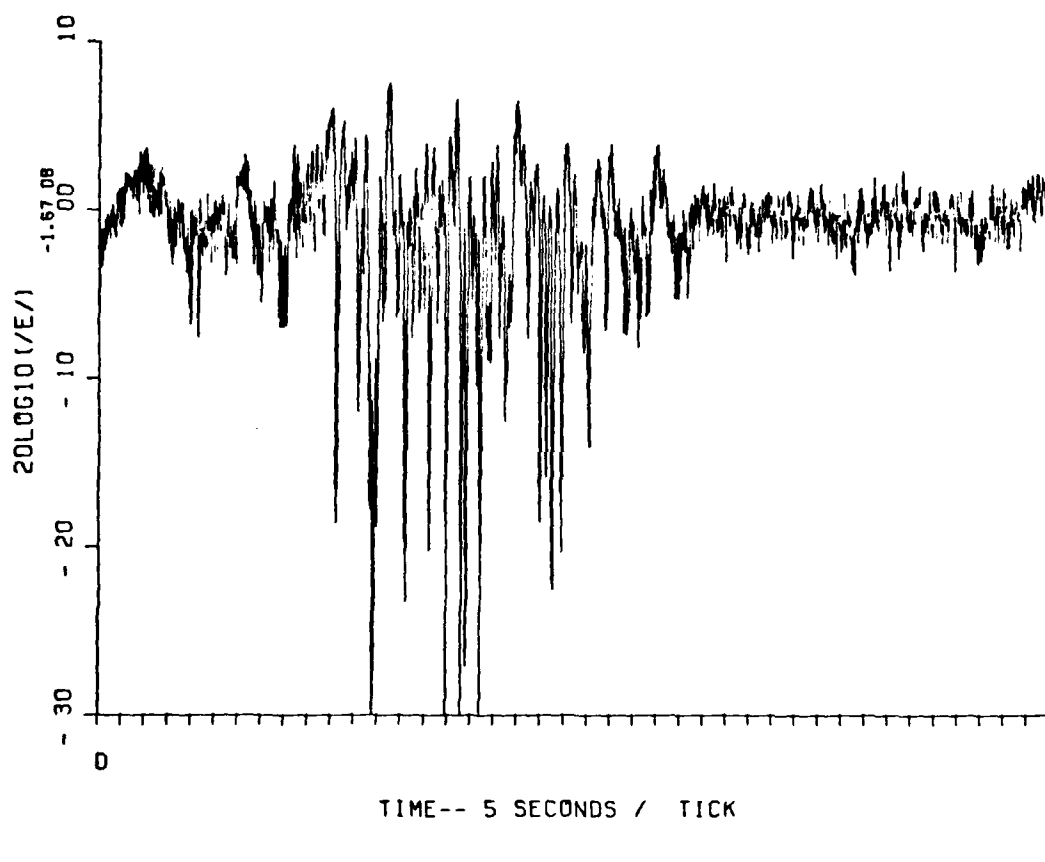
Figure 3-32.   Downlink Fading on IRIS Pass 8, R+49 Minutes

113
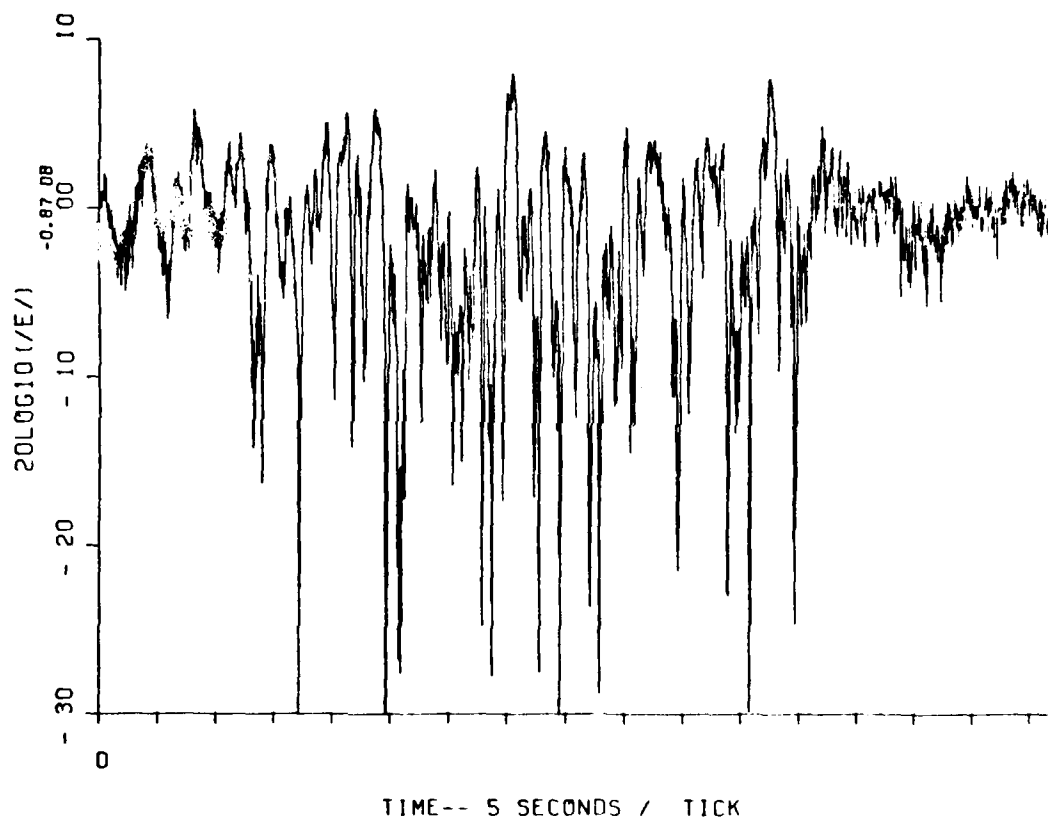
Figure 3-33.   Downlink Fading on IRIS Pass 9, R+1 hour

114
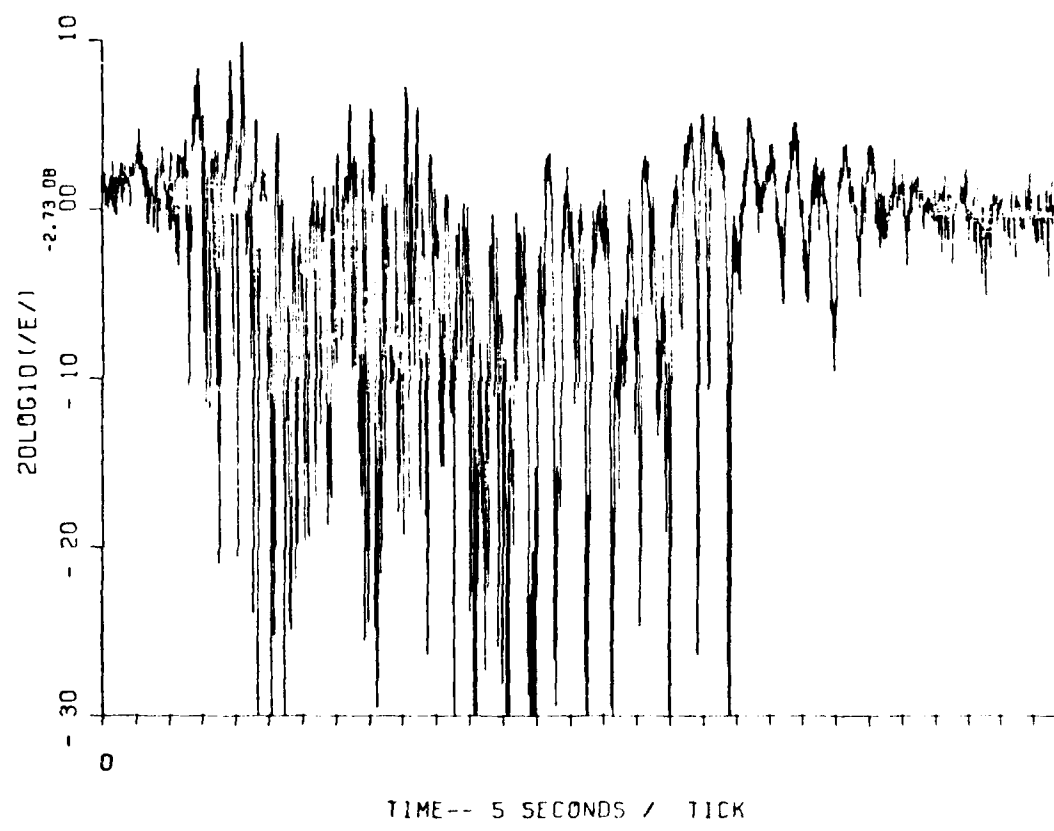
Figure 3-34.   Downlink Fading on IRIS Pass 11, R+1^{h}5^m
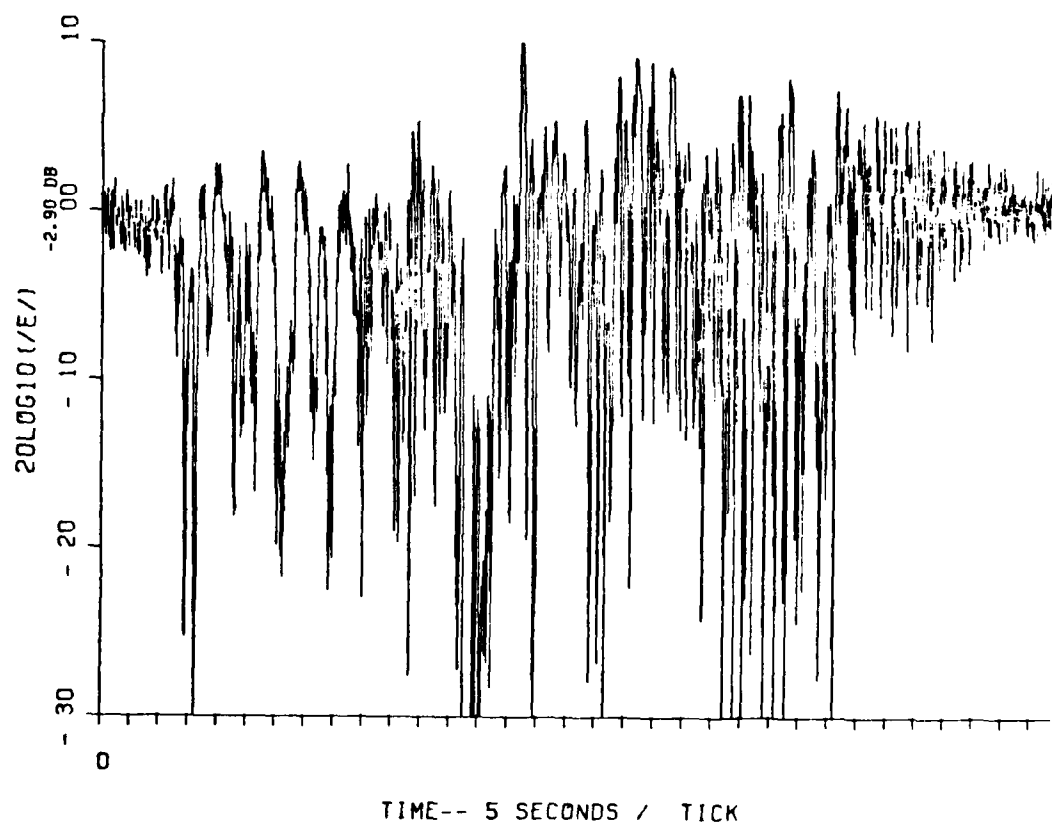
Figure 3-35. Downlink Fading on IRIS Pass 12, R+1^{h}10^m
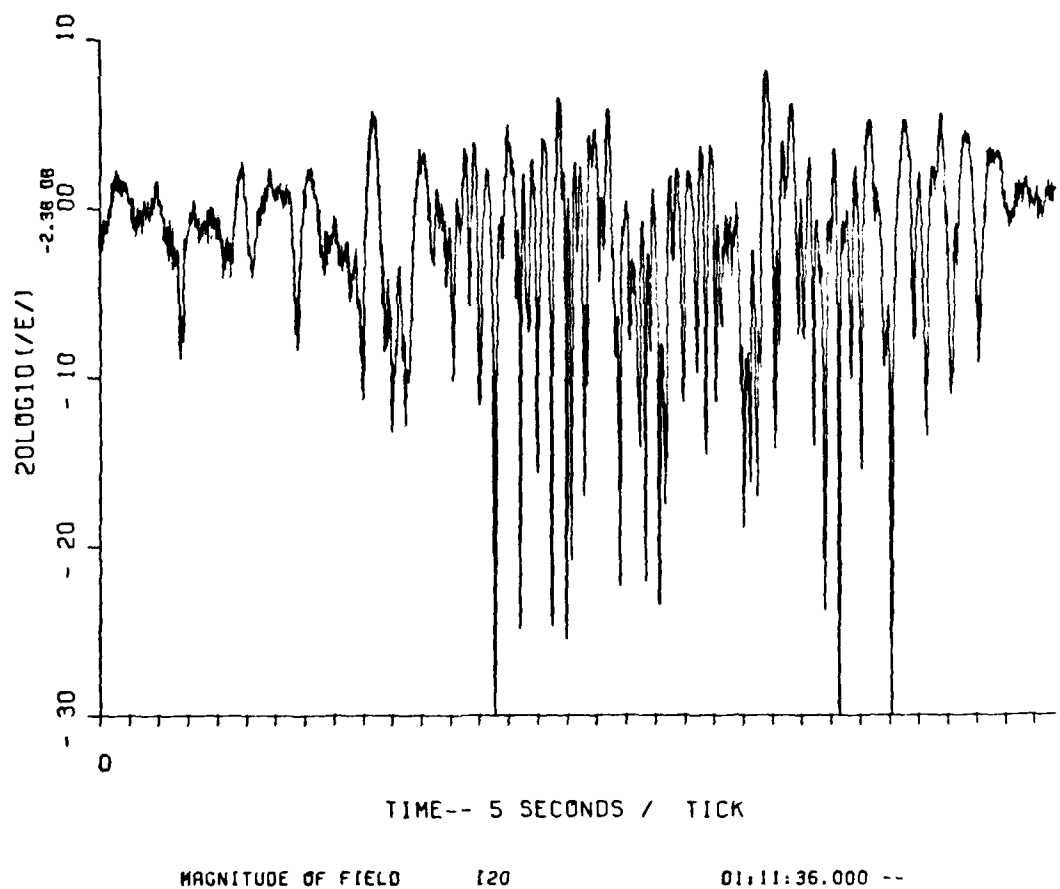
Figure 3-36. Downlink Fading on IRIS Pass 20, R+2 hours
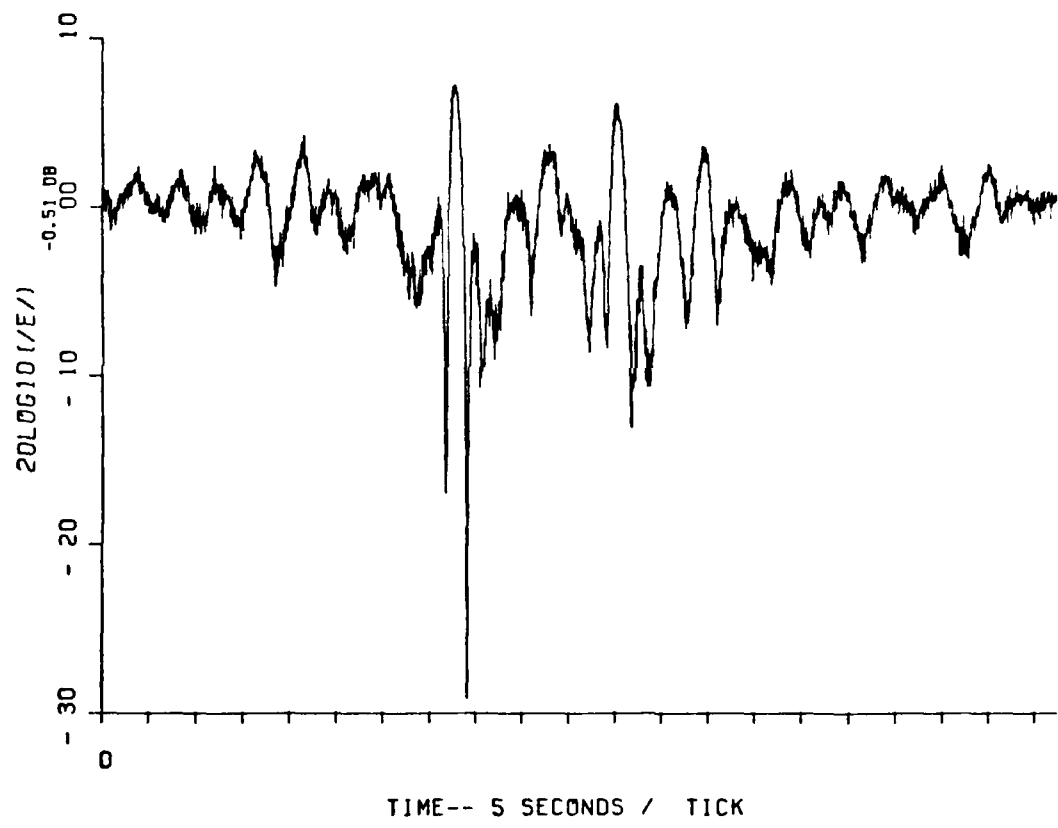
Figure 3-37.   Downlink Fading on IRIS Pass 25, $R+2^h26^m$

high ion cloud density and not a geometric artifact. While not shown here, a quick look at the phase power spectral density obtained near the first beacon occultation (Pass 5) also indicates a very strongly structured cloud. The phase PSD height at 1 Hz is approximately 5 dB higher than that obtained during the STRESS event ESTHER, Pass 10. ESTHER Pass 10 was used to originally estimate the probable magnitude of effects expected from the PLACES beacon experiment. The processing window in Figure 3-28 (Pass 5) did not cover the second fading object evident in the strip chart recording shown in Figure 2-6 (Section 2-2). The first beacon rocket occultation occurred approximately 5 minutes 33 seconds later. Pass 6 (Figure 3-30) occurred approximately 2 minutes 37 seconds after the first occultation. Pass 7 shown in Figure 3-31 occurred approximately 5 minutes before the second occultation and showed strong well developed fading along with a shallow defocus. The next pass occurred approximately 4 minutes after the second occultation and shows very little fading activity (see Figure 3-32). It is possible the aircraft passed north of the true cloud center and thus traversed the striations low on the field lines. As discussed earlier, a quick look at the radar data indicated a large drop in tracking altitude between the first and second occultations. These data need to be examined further to better establish cause and effect before reaching any conclusion. Pass 9, (Figure 3-33) while reminiscent of late time fading, is more developed than Pass 8. Pass 11 shown in Figure 3-34 indicates the presence of a well developed cloud once again. The fading on the (developing?) western side of the cloud appears slower than on the eastern side. Pass 12 shown in Figure 3-35 also shows the slower fading to the west. Figure 3-36 shows the nature of the fading observed at R+2 hours. Figure 3-37 shows the last fading seen on IRIS which occurred at R+2 hours 26 minutes.

3-6   TEST RESULTS FOR JAN.

JAN, the fourth barium release, occurred on 12 December 1980 at 23:13:42. It was released at an altitude of 184.3 kilometers and a latitude and longitude of 29.166°N and 86.993°W. This release drifted on an approximate 40° azimuth and then

stopped for a few minutes. It then drifted very slowly west for the remainder of the experiment, with its projection ending up about 1 degree west of the initial release point projection.

Optics tracking was used until approximately R+48 minutes. It gave reasonably consistent information on the cloud location during this time but the track showed some abrupt changes. Radar tracking was available for the remainder of the experiment, but was inconsistent with the fading observed. The striated portion of the ion cloud was followed using the real time fading displays and the radar tracking of the aircraft. Plots of the available cloud tracking data and the aircraft ground track are given in Figures 3-38 and 3-39. Figures 3-40, 3-41 and 3-42 show the aircraft ground track during each hour along with periods of strong fading.

A total of 35 passes were made ending at R+3 hours 33 minutes. Table 3-5 contains a summary of these passes. Diffraction ringing with large ~15 dB defocus was seen during the first three passes. Strong fading was present for all 18 passes between R+24 minutes and R+1 hour 2 minutes. Very good data was received during this time. Moderate to strong fading was present in four of the next eight passes ending at R+2 hours 44 minutes. Fading was seen as late as R+2 hours 54 minutes.

Uplink and downlink data was received for all passes. K-band lock was not lost during this release. Overall, it is believed that the highest quality data was obtained during JAN.

No beacon rockets were launched during this release. A 100 kilometer solution could not be used due to the close proximity of shipping traffic. A computer hardware failure delayed processing of a 40 kilometer solution and the cloud was outside range safety limits by the time the computer came back on line at R+36 minutes. A probe rocket was successfully launched however[1].

120
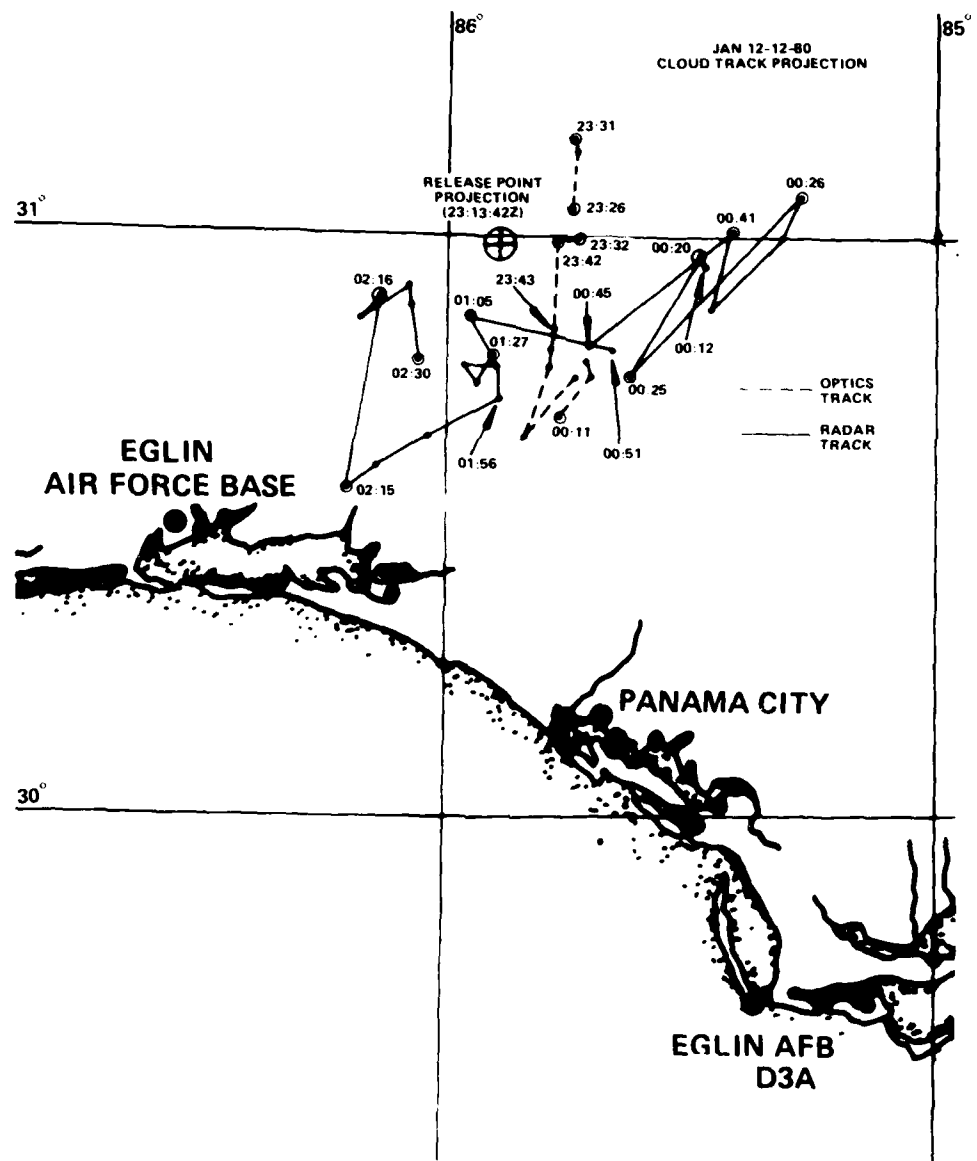
Figure 3-38. Ion Cloud Track Projection for JAN

121
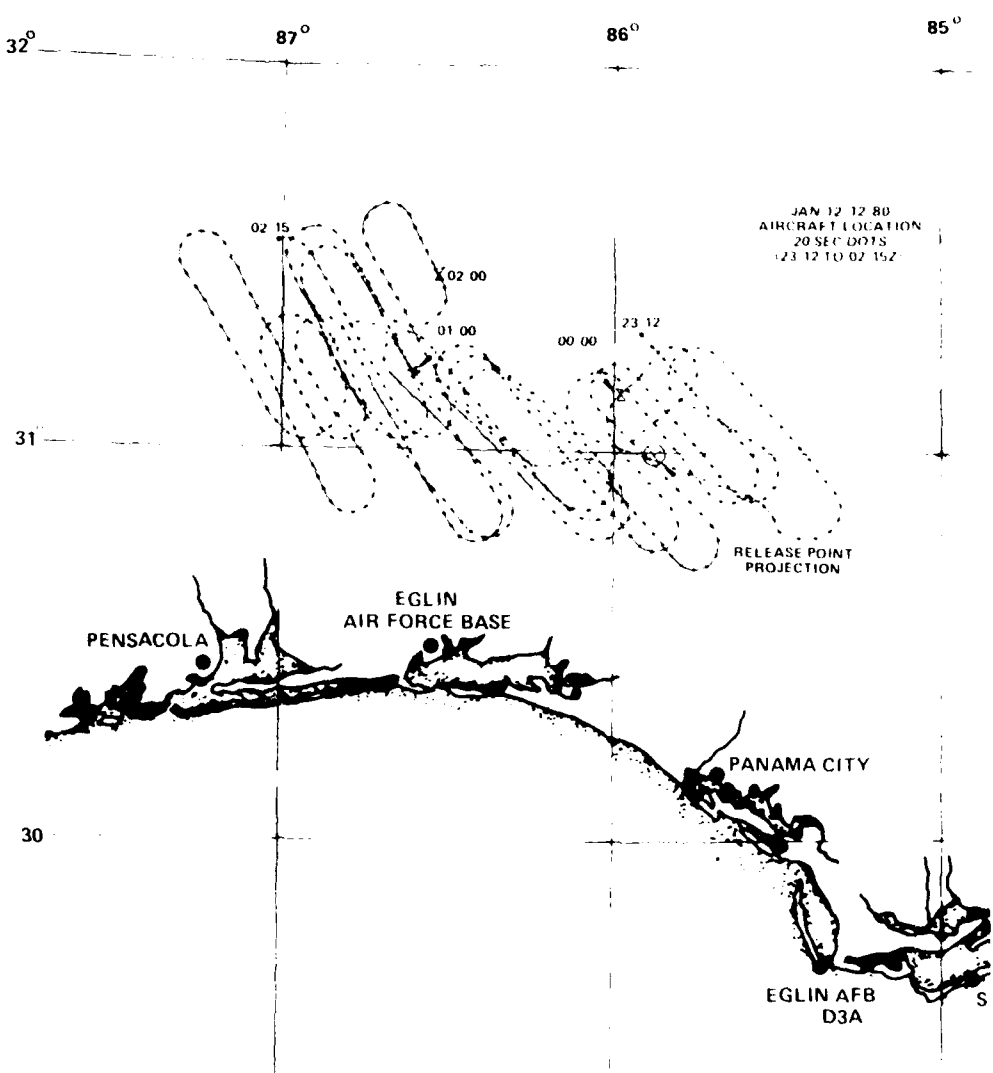
Figure 3-39. Aircraft Ground Track for JAN
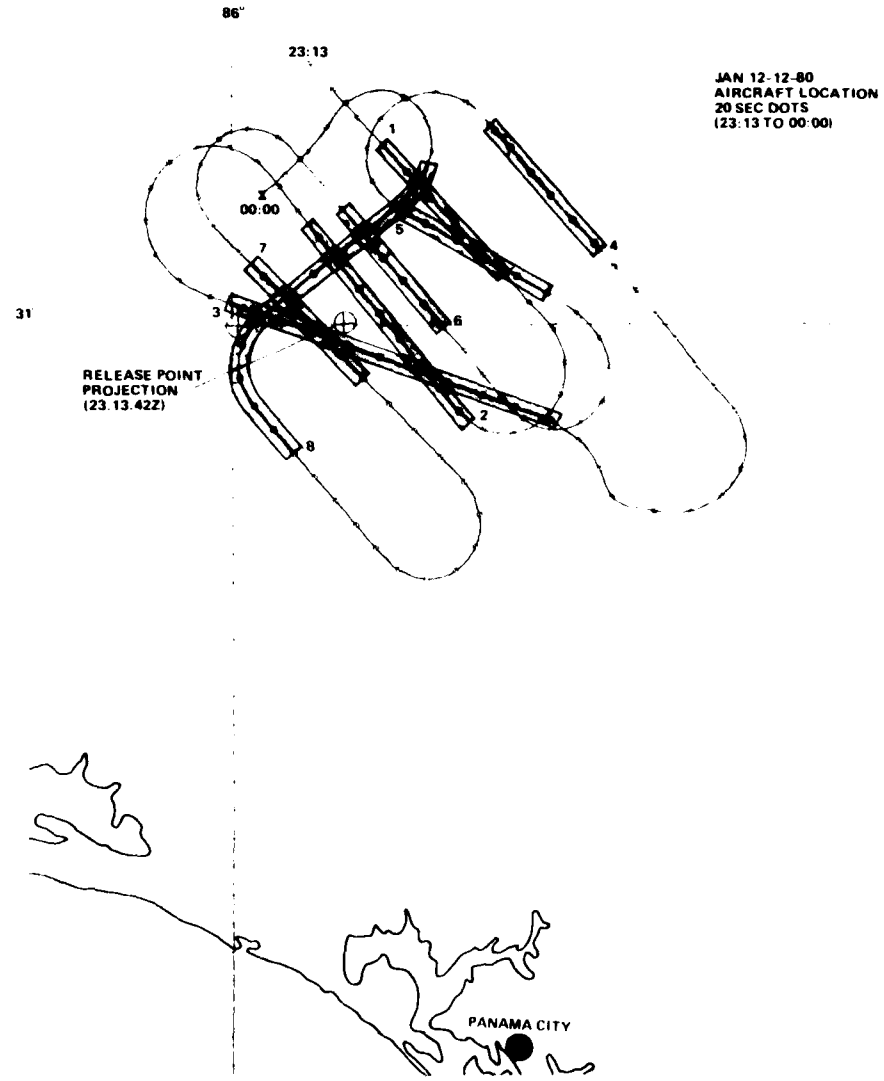
Figure 3-40. Aircraft Ground Track for JAN from 23:13 to 00:00Z.
Periods of Deep Fading are Shaded
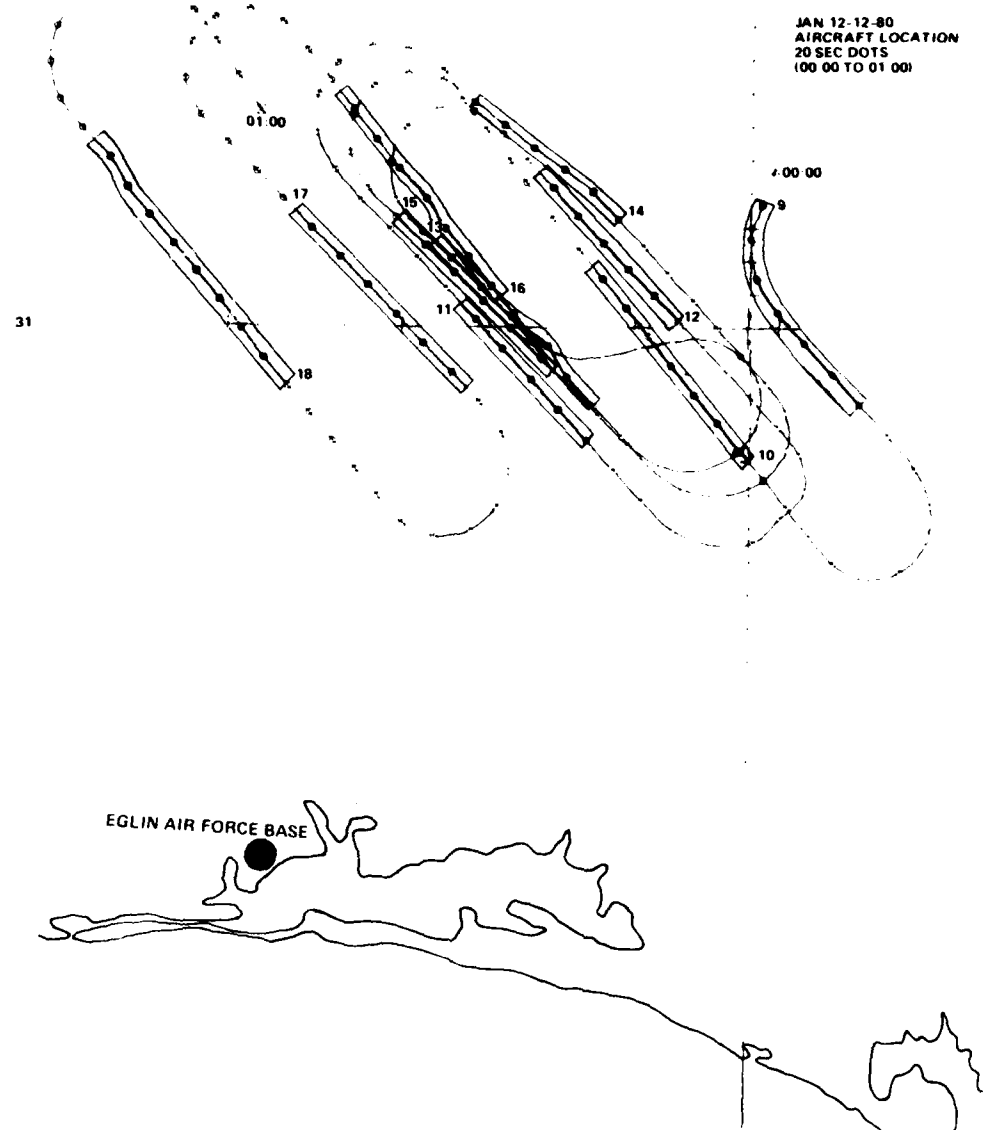
Figure 3-41.   Aircraft Ground Track for JAN from 00:00 to 01:00Z.
Periods of Deep Fading are Shaded
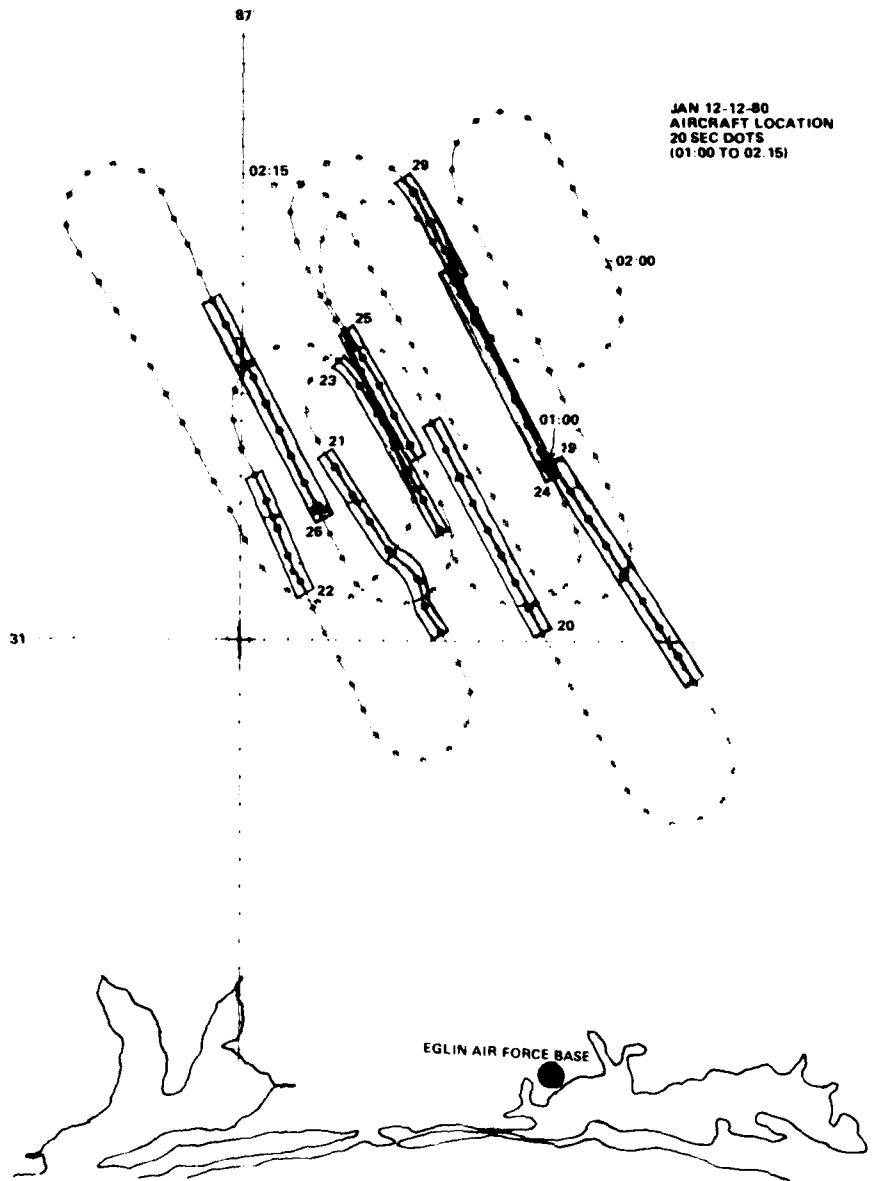
Figure 3-42. Aircraft Ground Track for JAN from 01:00 to 02:15Z.
Periods of Deep Fading are Shaded

Table 3-5. Aircraft Data Summary for JAN

Pass No.	Time	K-Lock	Comments
1	23:14:00-23:45:40	Yes	Moderate diffraction ringing
2	23:18:10-23:20:50		Diffraction ringing with large ~15 dB aefocus
3	23:24:30-23:27:30		Diffraction ringing with large ~15 dB defocus
4	23:32:50-23:34:40		Strong fading, but short
5	23:37:00-23:38:40		Strong fading
6	23:42:20-23:44:00		Strong fading
7	23:47:10-23:48:40		Strong fading
8	23:53:20-23:57:00		Strong fading
9	00:00:20-00:02:20		Strong fading
10	00:05:50-00:08:10		Strong fading
11	00:13:50-00:15:20		Strong fading
12	00:19:30-00:21:30		Strong fading
13	00:24:10-00:26:00		Strong fading
14	00:30:40-00:32:20		Strong fading
15	00:34:40-00:36:30		Strong fading
16	00:41:40-00:44:10		Strong fading
17	00:47:50-00:49:50		Strong fading
18	00:53:40-00:56:30		Strong fading
19	01:00:00-01:02:40		Strong fading
20	01:07:20-01:10:00		Strong fading
21	01:12:50-01:15:00		Strong fading
22	01:19:10-01:20:40		Weak fading
23	01:23:00-01:25:00		Strong fading
24	01:28:00-01:30:40		Moderate fading
25	01:33:40-01:35:10		Moderate fading
26	01:38:30-01:41:20		Weak fading, large focus
27	01:45:30-01:47:30		No fading

Table 3-5. --Continued

Pass No.	Time	K-Lock	Comments
28	01:51:50-01:53:30	Yes	Weak fading
29	01:55:30-01:57:00		Strong fading
30	01:59:40-02:01:20		No fading
31	02:03:20-02:07:20		Weak fading
32	02:09:30-02:14:00		No fading
33	02:20:00-02:25:00		No fading
34	02:30:30-02:37:00		No fading
35	02:39:00-02:46:50		No fading

Samples of processed amplitude and phase plots for JAN are given in Figures 3-43 through 3-59. They show the full progression of cloud development from diffraction ringing to strong deep fading, to the eventual loss of track. These figures have been processed from the uplink tone data.

Figure 3-43 shows the strong diffraction ringing that was noted about 1 minute after release on the first pass. This developed into a large defocus of -10 dB by R+6 minutes as shown in Figures 3-44 and 3-45. No structuring is evident during this pass. Again the alignment of the ion cloud stretch direction with the propagation path may influence the manifestation of the large defocus. Figures 3-46 and 3-47 show a large -20 dB defocus with some developing structure. Passes 7 and 12 in Figures 3-48 through 3-51 show the continuing development of the striation structuring effects. Figures 3-52 through 3-55 show the fading at 1 hour 30 minutes and at 2 hours after release. Figures 3-56 and 3-57 at R+2 hours 15 minutes shows what appears to be a diffusion of the striations away from the main cloud. Figures 3-58 and 3-59 show the last significant fading seen during JAN at R+2 hours 42 minutes.

The integrated electron content decreased considerably over the course of the JAN release as one would expect. This is evident in the total phase wind-up of each subsequent aircraft pass. The phase wind-up varied from 109π radians in Pass 2 to 5π radians in Pass 29 as shown in the preceeding figures. The integrated electron content is shown plotted for JAN in Figure 3-60.

$$\frac{2\ dB}{DIV}$$

23:13:45   23:15:40
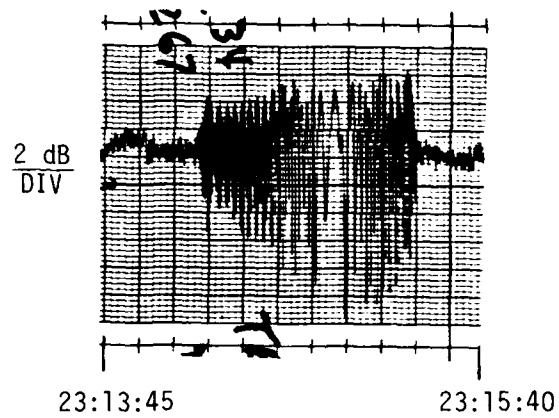
Figure 3-43.   Downlink Fading on JAN Pass 1, R+1 Minute
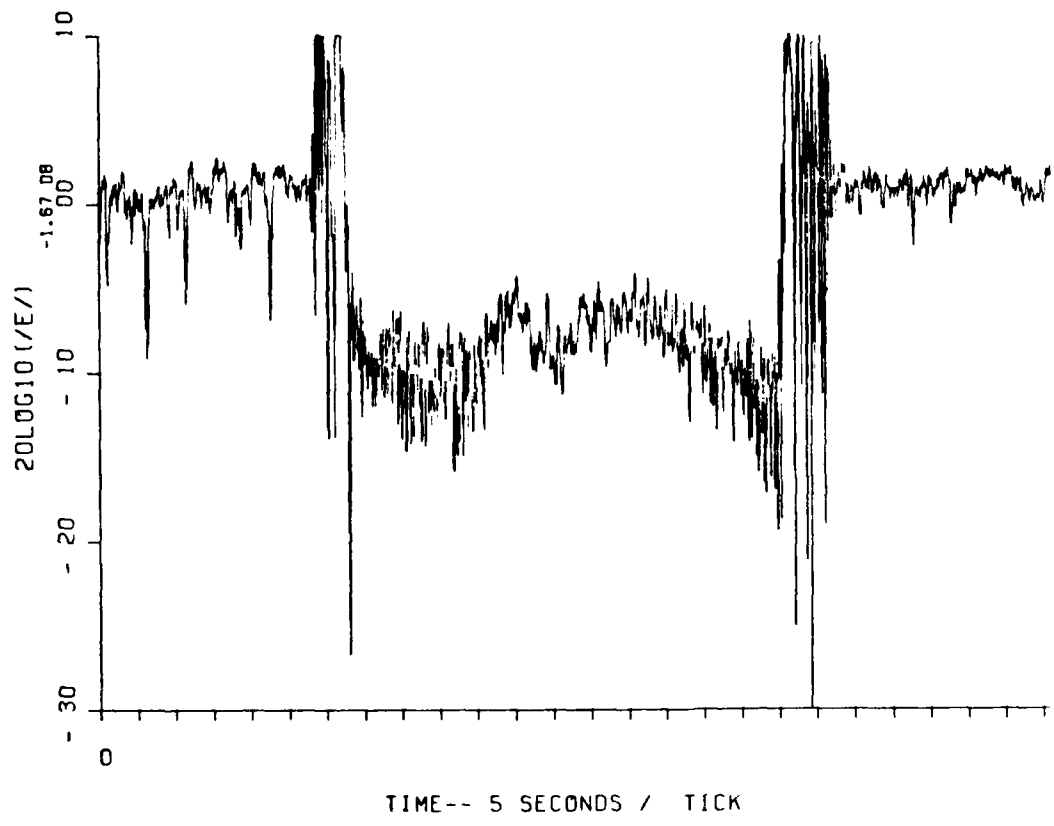
Figure 3-44.   Uplink Fading on JAN Pass 2, R+6 Minutes
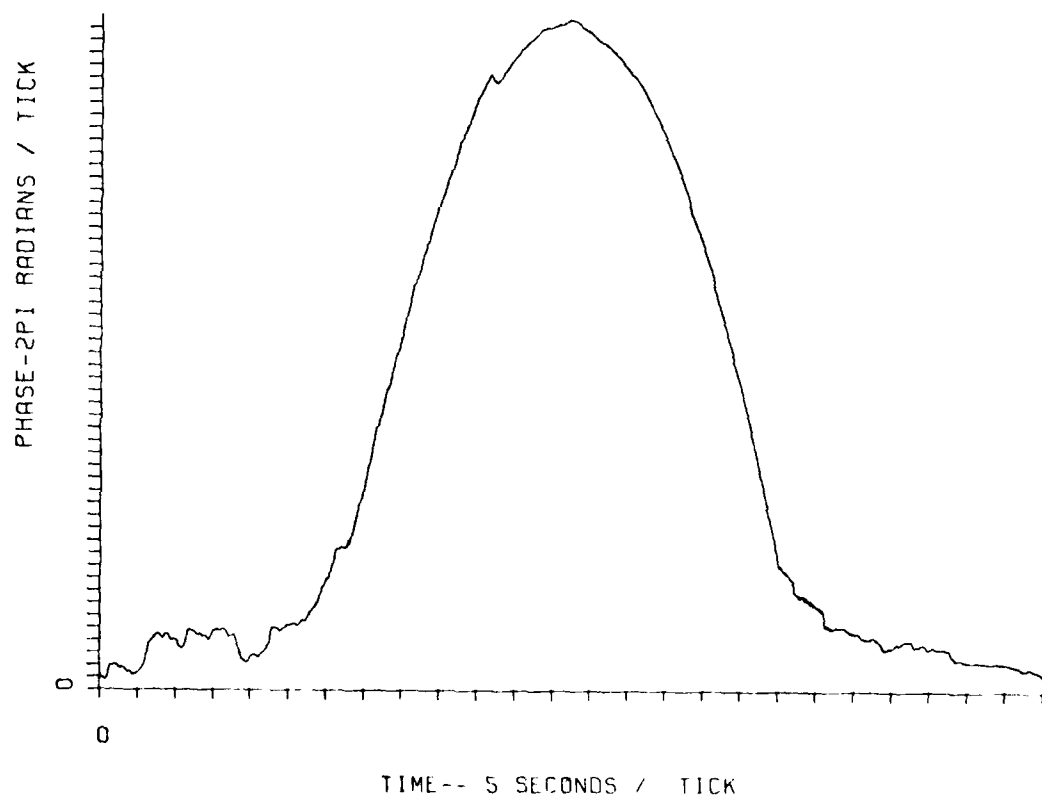
Figure 3-45.   Uplink Phase Effects on JAN Pass 2, R+6 Minutes
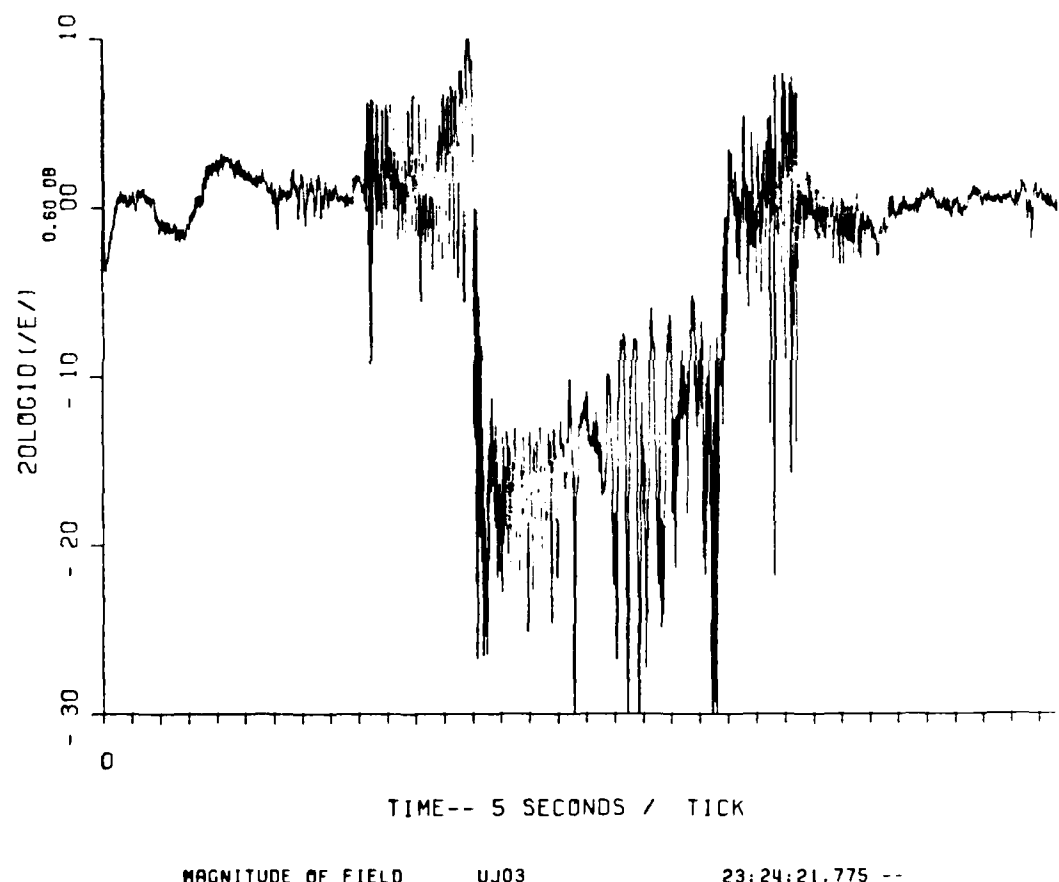
Figure 3-46. Uplink Fading on JAN Pass 3, R+13 Minutes
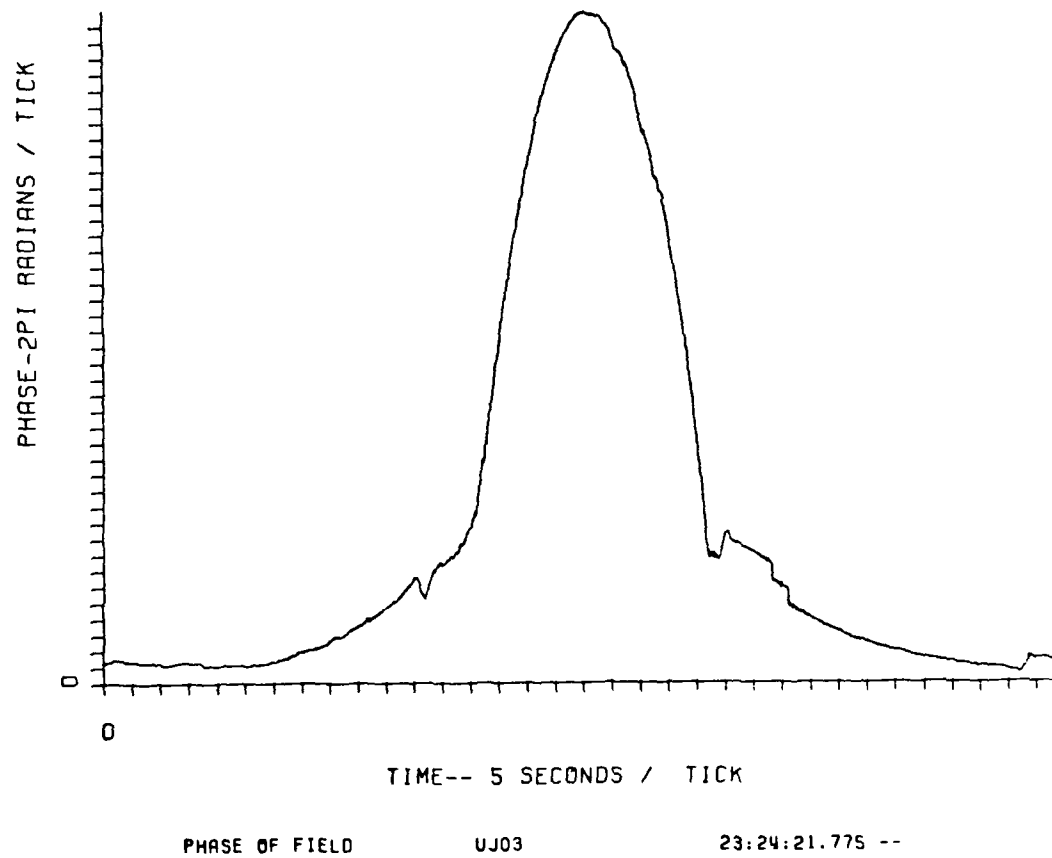
Figure 3-47. Uplink Phase Effects on JAN Pass 3, R+13 Minutes
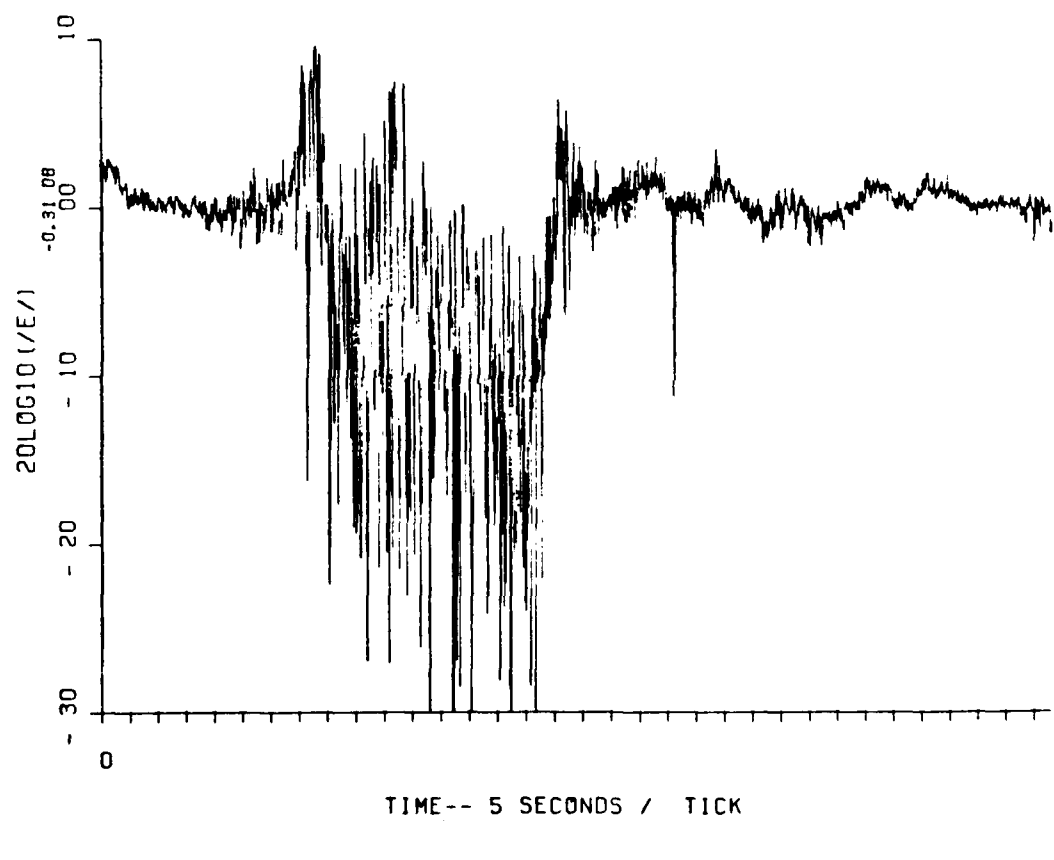
Figure 3-48. Uplink Fading on JAN Pass 7, R+30 Minutes
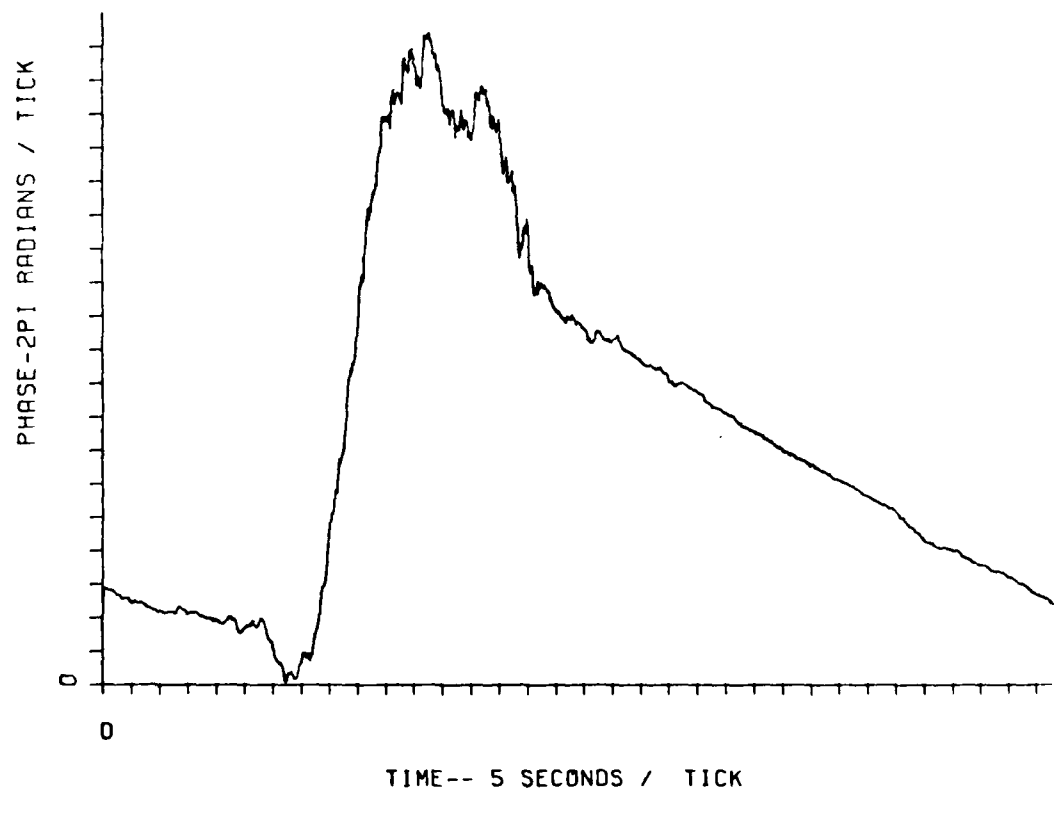
Figure 3-49. Uplink Phase Effects on JAN Pass 7, R+30 Minutes
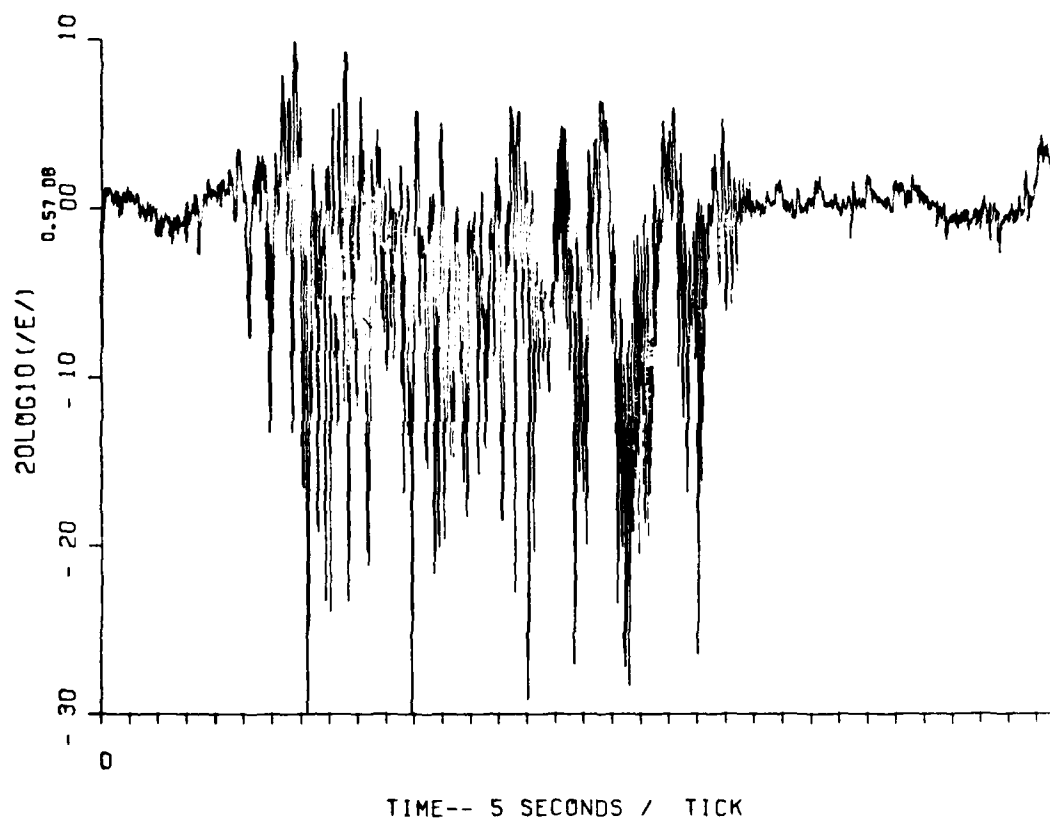
Figure 3-50. Uplink Fading on JAN Pass 12, R+1 Hour

136
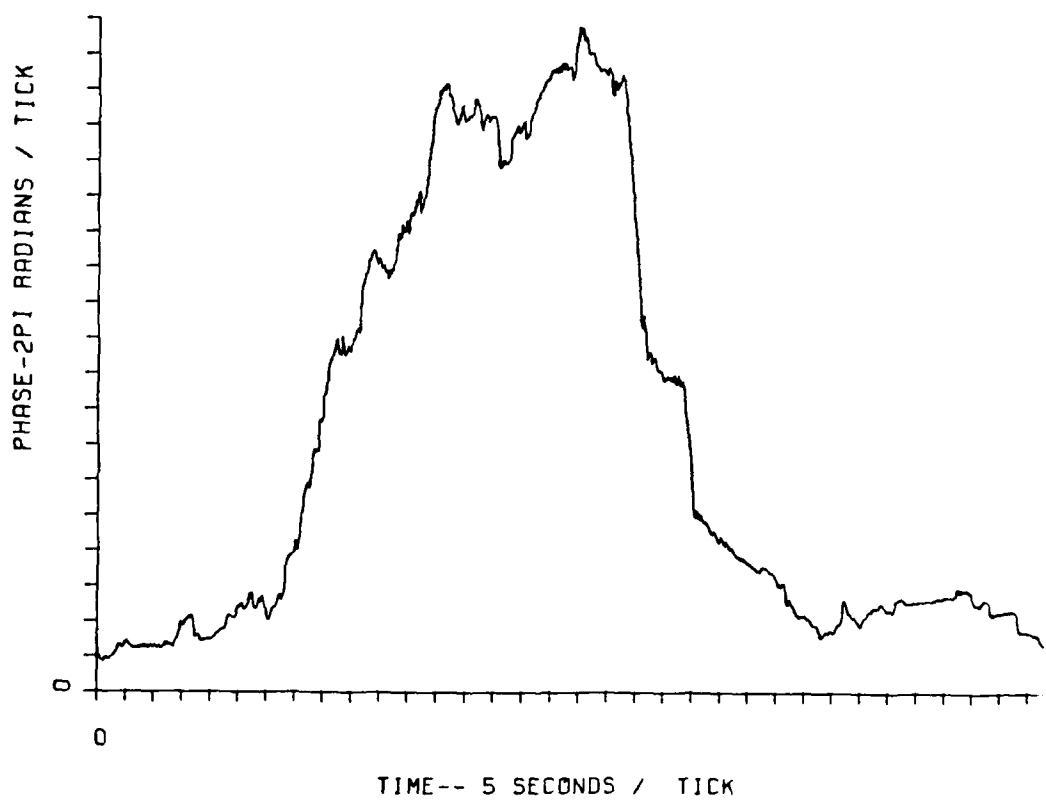
Figure 3-51.   Uplink Phase Effects on JAN Pass 12, R+1 Hour
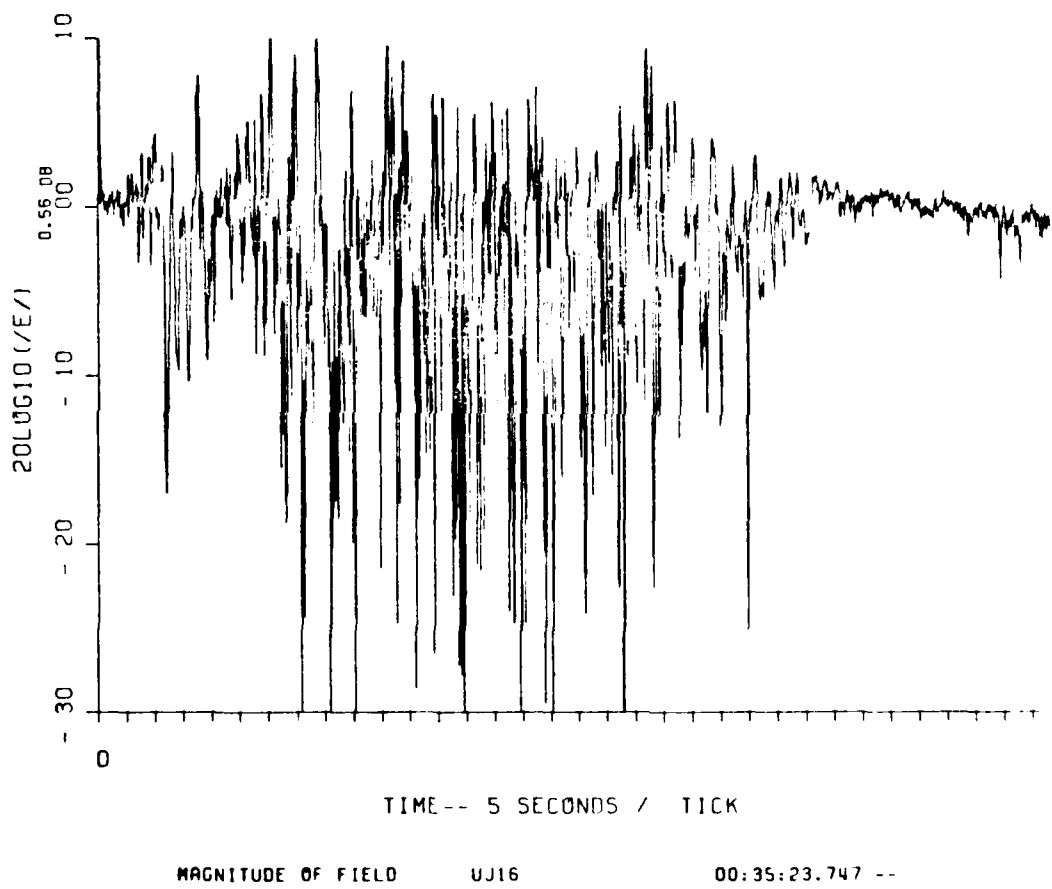
Figure 3-52. Uplink Fading on JAN Pass 16, R+1^{h}30^m
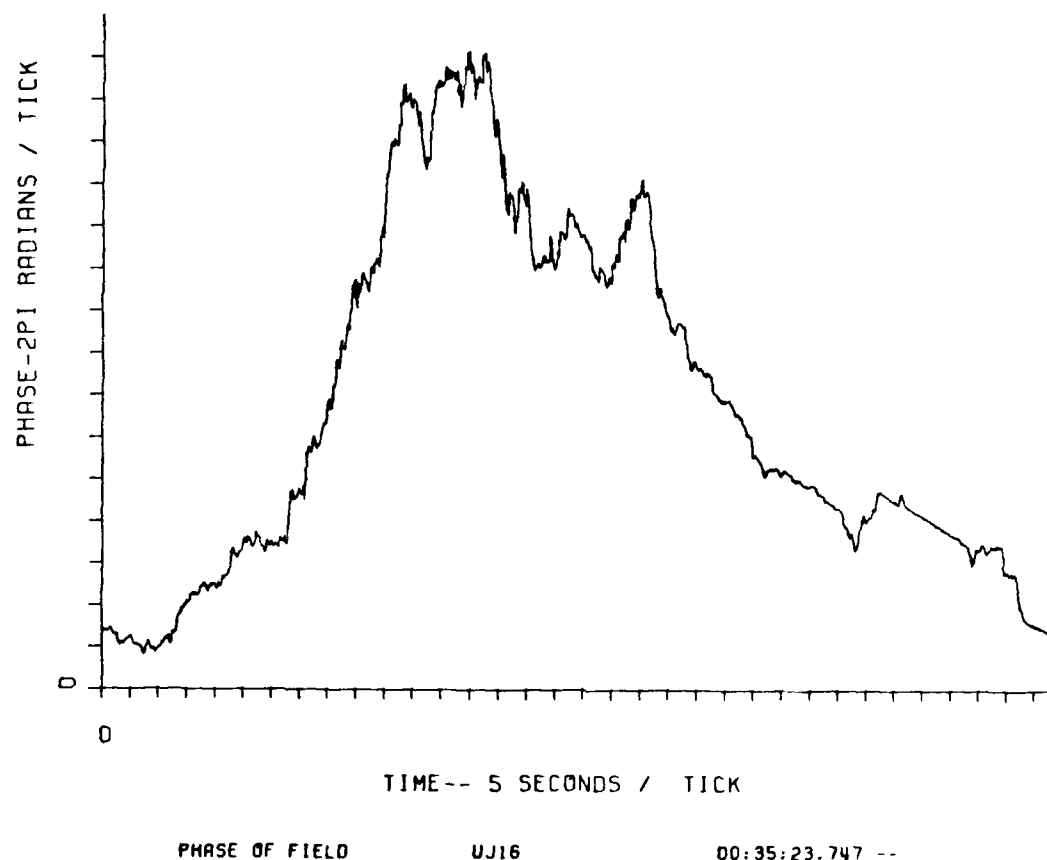
Figure 3-53. Uplink Phase Effects on JAN Pass 16, R+1^{h}30^m
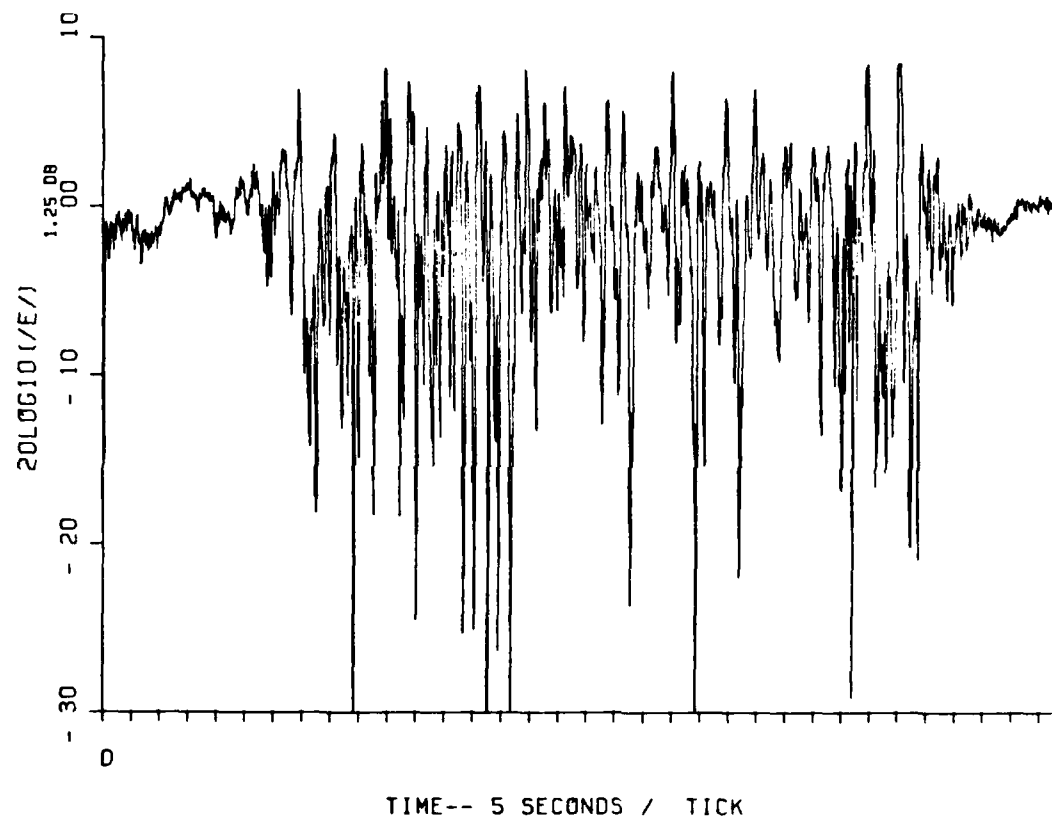
Figure 3-54. Uplink Fading on JAN Pass 20, R+2 Hours
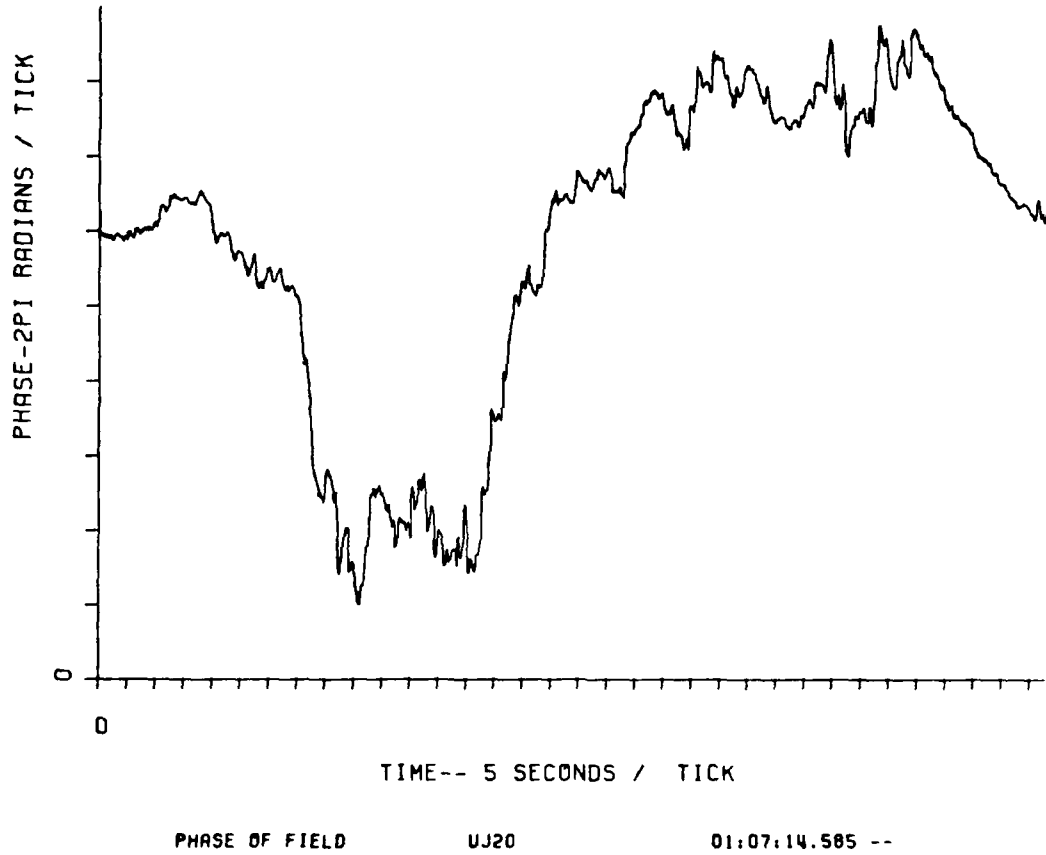
Figure 3-55. Uplink Phase Effects on JAN Pass 20, R+2 Hours

141
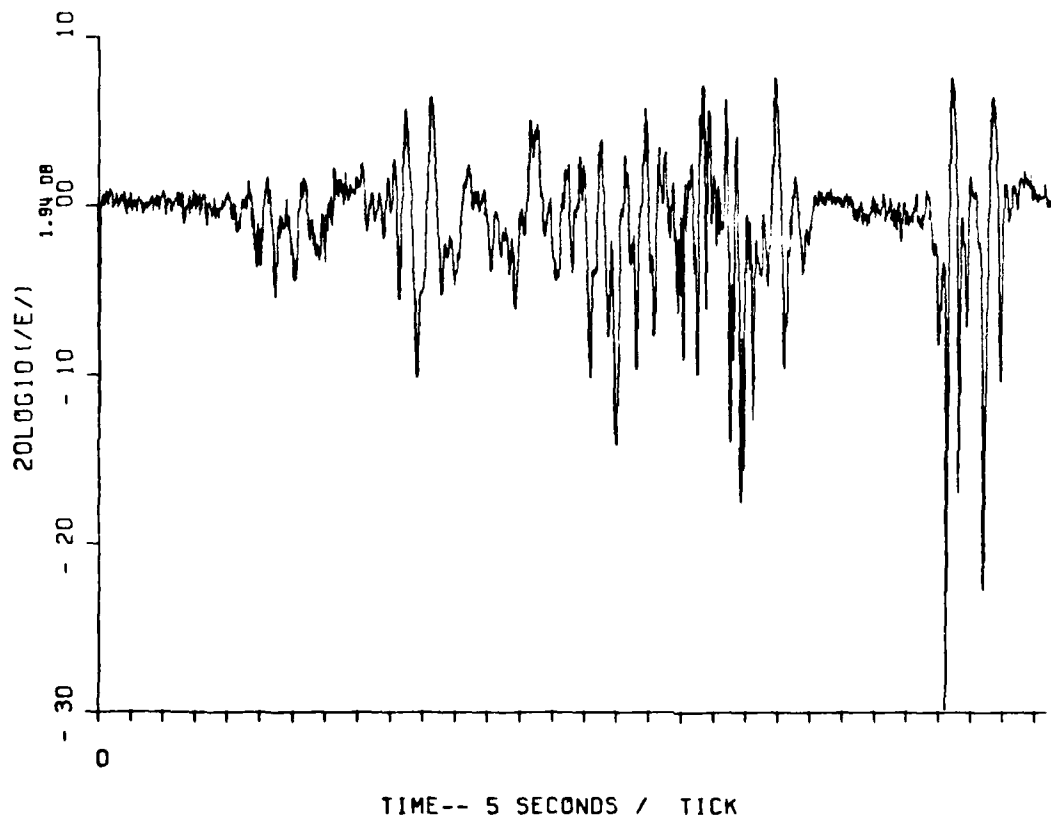
Figure 3-56.   Uplink Fading on JAN Pass 24, R+2^{h}15^m
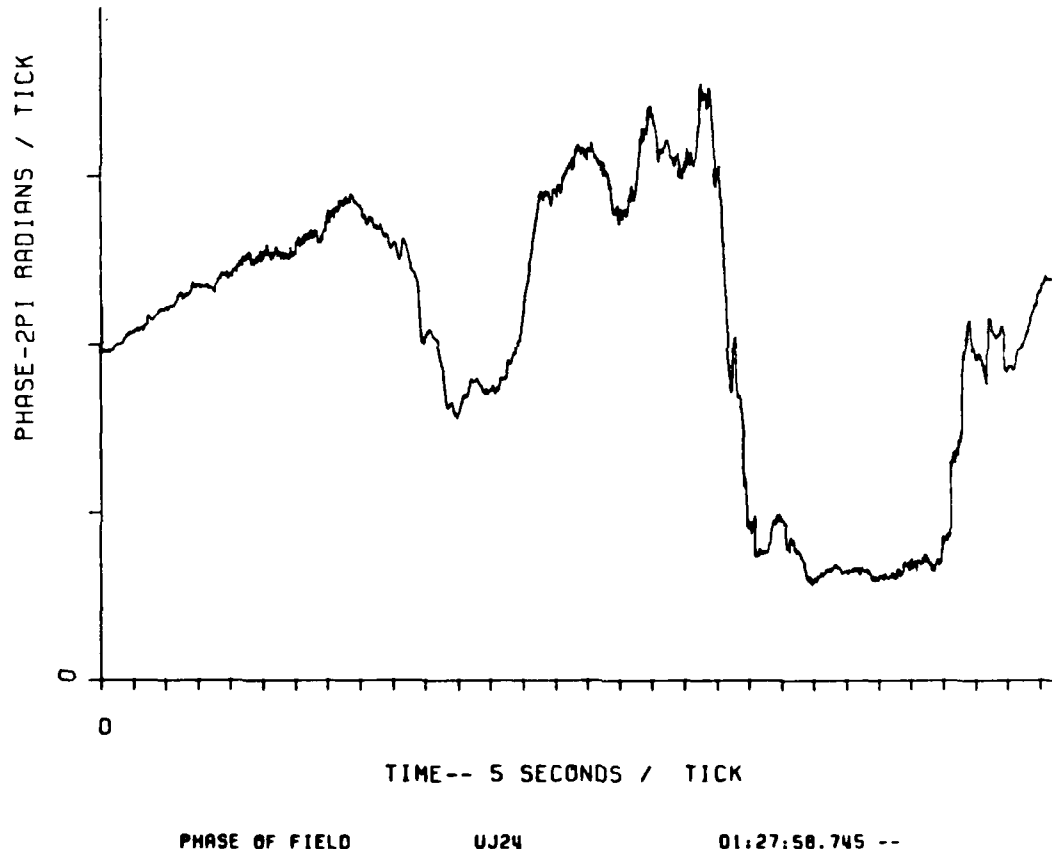
Figure 3-57. Uplink Phase Effects on JAN Pass 24, R+2^{h}15^m

143
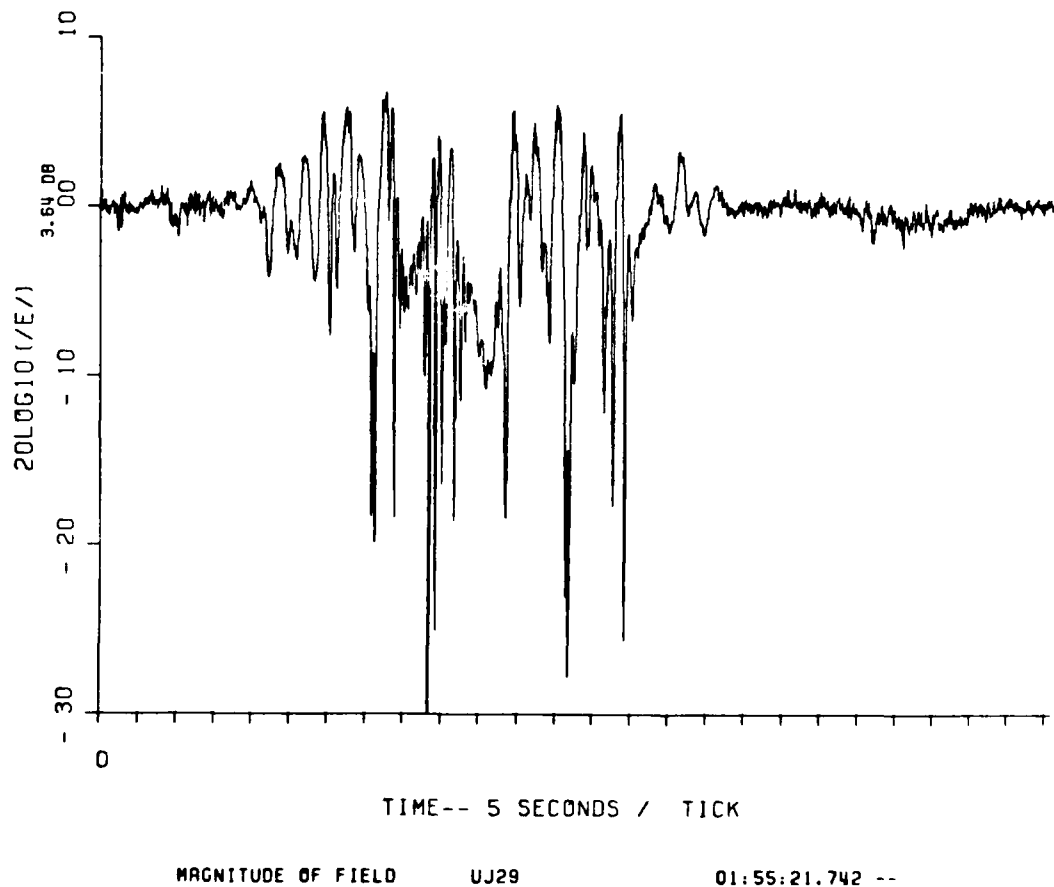
Figure 3-58. Uplink Fading on JAN Pass 29, R+2^{h}43^m

144
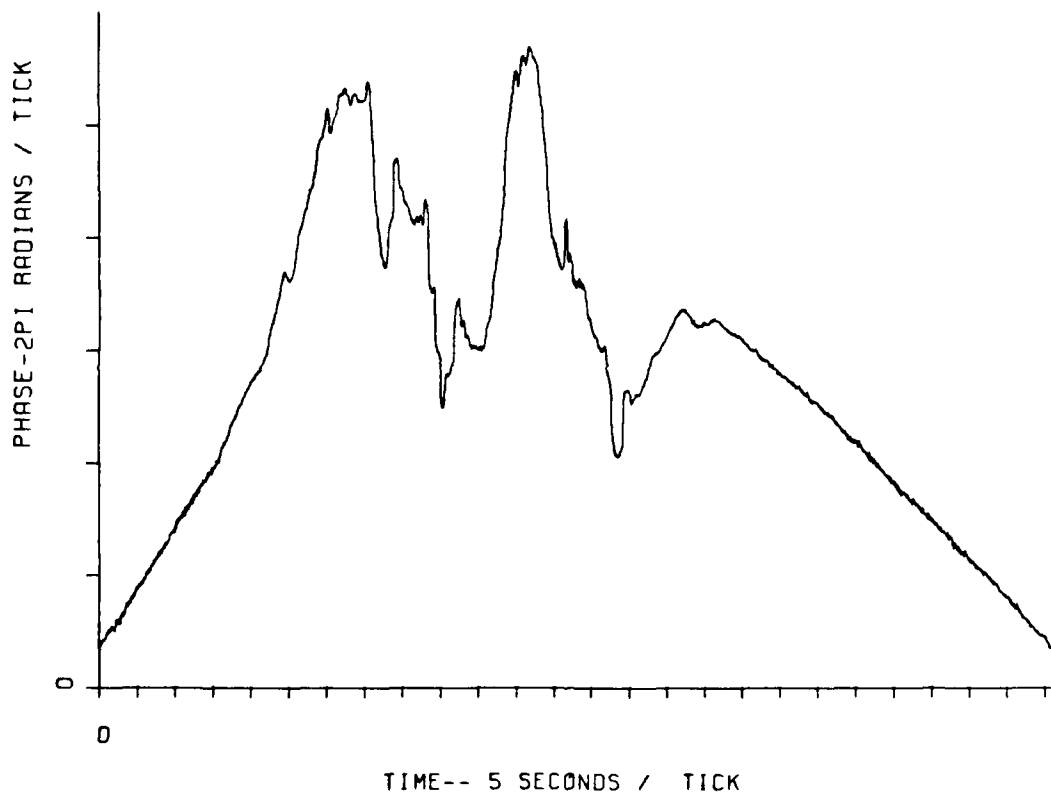
Figure 3-59. Uplink Phase Effects on JAN Pass 29, R+2^{h}43^m
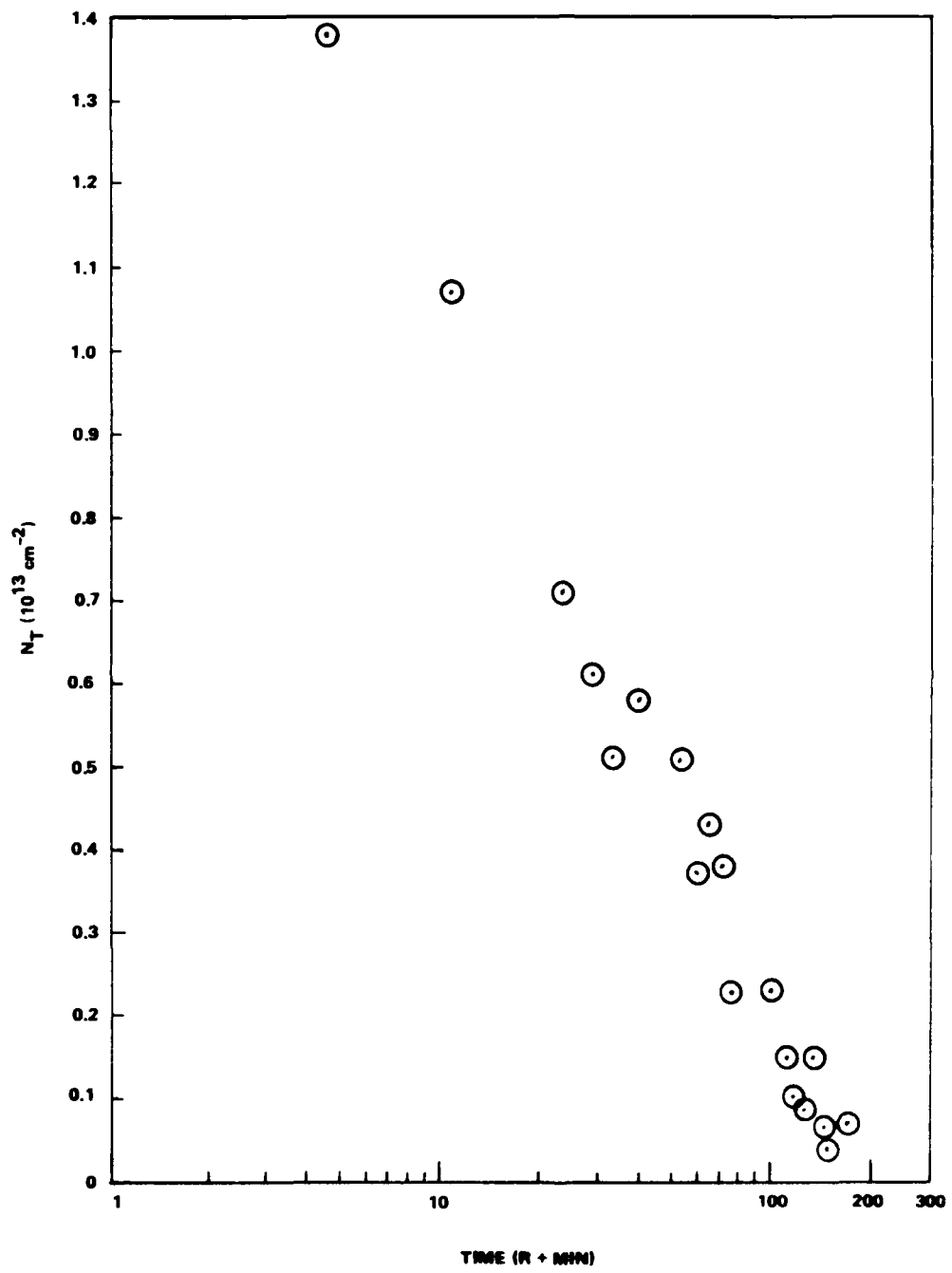
Figure 3-60. Integrated Electron Content Versus Time for JAN

3-7   CONCLUSIONS.

         The PLACES Aircraft Experiment measured the propagation characteristics
of the striated barium ion cloud using the LES-8 satellite in a manner similar to
the STRESS experiment. The primary utility of this data is to provide information
on striation evolution to late times that can aid theoretical developments.
Additionally it provides an opportunity to work in a "hands on" real world situa-
tion with satellite communication systems, striated plasmas and propagation data
that facilitates the physical interpretation of theoretical calculations/predic-
tions. This data has also been helpful in interpreting the beacon experiment
results as described in Section 2.2. The downlink tone data obtained during PLACES
is of higher quality than that obtained during the STRESS experiment of 1977. Only
limited downlink data was available from STRESS due to conflicts with higher
priority communications tests. The uplink tone data is believed to be of about
the same quality.

         The scintillation effects observed are similar to those observed during
STRESS with the exception of the long deep defocusing seen at early times. During
HOPE a -20 dB defocus lasted for approximately 75 seconds. From this it should be
obvious that even large chunks of high density plasma ($\sim 10^7$ cm^{-3}) can be important
to UHF satellite communication systems.

         The IRIS cloud moved rapidly southeast and should therefore have
resulted in a morphologically older cloud faster than seen before. Its data is
also of interest around the beacon occultation time. JAN on the other hand moved
slower than any observed before. JAN should yield the highest quality data.
Backpropagation processing of these signals to provide estimates of the integrated
plasma content through the ion cloud striations is planned during subsequent
processing. It is anticipated that this data may be able to provide insight to
current issues in striation phenomenology such as freezing. Freezing is a
postulated late-time phenomenon wherein bifurcation stops and the striations move

as a unit. The processing software and techniques for reducing the aircraft data were developed during the STRESS data reduction. This same software will be used during the PLACES data reduction.

SECTION 4
REFERENCES

[1]   E. Szuszczewicz, J. Holmes, M. Swinney; DNA/PLACES Barium Event JAN:
        Quick-Look Field Report of "In Situ" Probe Measurements; NRL Memo-
        randum Report 4476, 26 March 1981. (UNCLASSIFIED)

[2]   Dr. D. McDaniel, Position Location and Communications Effects
        Simulations (PLACES) Test Plan; SRII, September 1980. (UNCLASSIFIED)

[3]   Dr. C. Prettie, STRESS Communications and Propagation Test Results (U),
        (Unpublished).

[4]   Dr. Victor Gonzalez, Private Communication, March 1981. (UNCLASSIFIED)

[5]   Dr. Victor Gonzalez, Analysis of UHF Radar Data - STRESS Series, SRI,
        DNA 4823F, 1 December 1978. (UNCLASSIFIED)

APPENDIX A
BEACON EXPERIMENT CONFIGURATION

A-1   SIMPLIFIED THEORY OF OPERATION.

The beacon rocket transmits a 98 MHz signal V(t) that is biphase modulated by a 9.8 MHz pseudonoise code. The effects of the plasma striations on this transmission can be represented by a time varying channel impulse response $h(t,s)$. In the discussion below we let $\tilde{h}(t,s)$ represent the equivalent complex baseband channel impulse response. Additionally transmitted is a 4116 MHz reference tone $V_r(t)$ to allow removal of doppler effects from the modulated signal. By transmitting this tone at C-band the references are not significantly corrupted by effects of the barium plasma. The transmitted reference signal can be represented as

$$V_r(t) = \cos(N \omega_0 t + N \phi(t))$$

where

$N = 42 = 4116 \text{ MHz}/98 \text{ MHz}$

$\phi(t)$ is the VHF doppler phase

ω_0 is the VHF radian frequency (2π, 98 MHz).

The received reference signal is phase shifted by the plasma so that

$$\tilde{V}_r(t) = \cos(N \omega_0 t + N \phi(t) + \psi/N)$$

where

ψ = gross plasma phase shift at 98 MHz.

The transmitted VHF signal may be represented as

$$V(t) = c(t) \cos(\omega_0 t + \phi(t))$$

and the received signal is approximated by

$$\tilde{V}(t) \simeq \tilde{C}(t) \cos(\omega_0 t + \phi(t) + \psi + \theta) \ .$$

Arbitrary phase terms have been ignored since both signals are generated using a common oscillator in the rocket payload.

Figure A-1 gives an equivalent diagram of the beacon receiving system. Only a single cross-correlator output pair is shown for simplicity, operating at a delay of t. In practice nine correlators operate in parallel at delays spaced by 3-1/3 chips (0.34 microsecond). These correlations are performed 10 times for each impulse response measurement, each time incrementing the delays by 1/3 chip. The result of this measurement series is then combined to yield the complex impulse response over 90 samples with 1/3 chip resolution, for a total delay range of 30 chips (3.06 microseconds).

If we represent $\tilde{h}(t,s)$ as

$$\tilde{h}(t,s) = h_I(t,s) + j \ h_Q(t,s)$$

then the received signal $y(t)$ may be expressed as

$$y(t) \simeq c(t) \star h_I(t,s) \cos(\omega_0 t + \phi + \psi)$$

$$+ \ c(t) \star h_Q(t,s) \sin(\omega_0 t + \phi + \psi)$$

where $\star$ denotes a convolution.
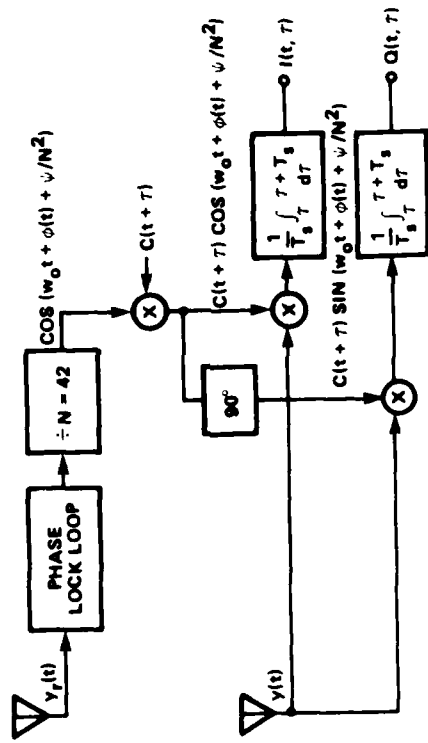
Figure A-1. Equivalent Beacon Receiver Model

The partial cross-correlator outputs are given by

$$I(t,\tau) \simeq \cos(\psi-\psi/N^2)\, \frac{1}{T_s} \int_t^{t+T_s} c(t) \star h_I(t,s) \cdot c(t+\tau)\, dt$$

and

$$Q(t,\tau) \quad \sin(\psi-\psi/N^2)\, \frac{1}{T_s} \int_t^{t+T_s} c(t) \star h_Q(t,s) \cdot c(t+\tau)\, dt \ .$$

Substituting the following in to the equations for $I(t,\tau)$ and $Q(t,\tau)$,

$$c(t) \star h_{\substack{I\\Q}}(t,s) = \int_{-\infty}^{\infty} h_{\substack{I\\Q}}(t,s)\, c(t-s)\, ds \ ,$$

and assuming the channel impulse response does not change over the code integration period T_s, so that the order of the integration may be changed, yields:

$$I(t,\tau) \sim \cos(\psi-\psi/N^2) \int_{-\infty}^{\infty} h_{\substack{I\\Q}}(t,s)\, r_t(\tau+s)\, ds$$

where

$$r_t(\tau+s) = \frac{1}{T_s} \int_t^{t+T_s} c(t-s)\, c(t+\tau)\, dt$$

where r_t is the partial autocorrelation of the code over an interval starting at time t. Likewise,

$$Q(t,\tau) \approx \sin(\psi-\psi/N^2) \int_{-\infty}^{\infty} h_Q(t,s) \; r_t(\tau+s) \; ds \; .$$

If the correlator integration time spans one code period T (0.428 seconds) then $r_t(x)$ is independent of the time t and ideally is the thumbtack function given by

$$r_t(x) = \begin{cases} 1 - \dfrac{|x|}{T_c} & |x| \leq T_c \\ 0 & |x| > T_c \end{cases}$$

where T_c is a code chip period (0.102 microseconds). Thus, r_t effectively provides a weighted average of $h_I(t,\tau)$ in a narrow window $(\pm T_c)$ about the delay τ, so that

$$I(t,\tau) \approx \cos(\psi-\psi/N^2) \; h_I(t,\tau)$$

and

$$Q(t,\tau) \approx \sin(\psi-\psi/N^2) \; h_Q(t,\tau) \; .$$

This representation is a good one provided the channel impulse response is relatively constant over (spread much more than) T_c (0.102 microseconds).

In actual fact, the code integration period is only 225 microseconds or approximately 2205 chips of the total code of length $2^{22}-1=4,194,303$ chips as it is recorded. Coherently averaging the samples can be performed during post processing to increase the integration period. The net effect of the shorter averaging period is to produce a fluctuating cross-correlation noise that depends upon the particular 2205 chip interval averaged. This results in a broad pedestal to the $r_t(x)$ function and thus to $I(t,\tau)$ whose average

value is approximately 32.2 dB below the peak signal level. The peak cross-correlation noise has been observed to be 22 dB below the peak signal level.

A-2   ROCKET TRANSMITTER SYSTEM.

The system diagrammed in Figure A-2 transmits a PN VHF signal of fairly high level (100 W) and a C-band reference CW signal (500 mW). The signals and the PN generation are established from a common reference oscillator. An isolator protects the C-band RF power amplifier from ionospheric breakdown at the C-band antenna. The VHF power amplifier system is protected by a timer set so that the VHF amplifier is turned on near 90 kilometers altitude, above the altitudes over which breakdown might be expected (50-70 kilometers). This timer also turns off the transmitter once the rocket altitude has dropped below the altitude of useful data in order to minimize commercial broadcast band inter-ference. The timer is set to turn off approximately 7 minutes after launch. The timing signals are provided actively by Sandia's portion of the payloads in the form of 28 volt pulses. The payload portion provided by ESL includes protective cannister and cannister mechanical interfaces.

It was uncertain whether the electronic subsystems of the payload package would risk malfunction through operation at altitudes lower than 90 kilometers because of conventional breakdown effects (which initiate apparently at or near a 15 volt threshold depending upon the ambient ioniza-tion level). It was for this reason that the entire payload was kept off until the 90 kilometer pulse was received from the Sandia timer interface. This causes a slight reduction in the time available to acquire the signals. It was desired acquisition be accomplished prior to an altitude of 100 kilom-eters in order to track the delay caused by the background ionosphere during the upleg of the trajectory. An acquisition period of 20 to 60 seconds was allowed for; however, there is approximately 4 minutes from turn-on to occulta-tion for typical trajectories.
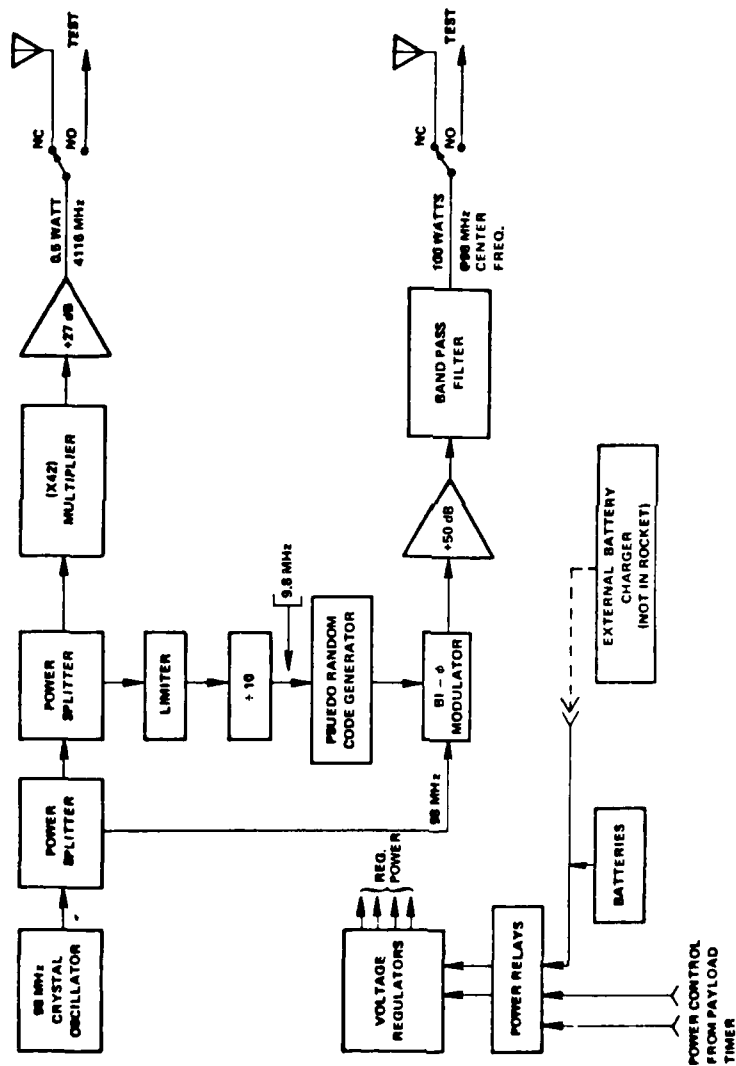
Figure A-2. Rocket Transmitter Functional Block Diagram

The entire transmitter electronics payload is also sealed to hold atmospheric pressure from launch through impact. This was done to preclude the possibility of breakdown under vacuum conditions at altitude.

The VHF signal is biphase modulated with a pseudonoise (PN) sequence at a 9.8 MHz rate as diagrammed in Figure A-2. The PN sequence is obtained by limiting a sample of the 98 MHz oscillator signal to obtain a logic signal, dividing by 10 to obtain a clock at 9.8 MHz, and using the clock to drive a digital PN sequence generator. The PN sequence obtained is used to modulate a sample of the 98 MHz oscillator and the resultant amplified to the 100W level. The 4116 MHz signal is obtained by multiplication of another sample of the 98 MHz reference, with either a straight multiplier chain or a phase-lock multiplier. The resulting 4116 MHz tone is then amplified to the 0.5W level.

Power for the payload transmitter system is supplied from an internal nickel-cadmium battery pack through a voltage regulator system. The internal batteries have sufficient capacity for a minimum of 10 minutes of system operation. The batteries are charged from an external charger as part of a system STE (Special Test Equipment) unit located at the launch complex. The STE unit also contains circuitry for the transmitter system control and monitoring. It connects to the rocket transmitter system through a Sandia interface to the umbilical cable.

Table A-1 shows the rocket transmitter system design specifications.

Each rocket transmitter system is designed to be the forward end of a complete Terrier-Tomahawk rocket system as sketched in Figure A-3. The antenna design utilizes the entire payload shell as the VHF radiator, including the nose section. The ESL supplied rocket transmitter system payload section thus has only one mechanical interface at the aft end which mates with the Sandia payload section. For proper antenna operation the entire
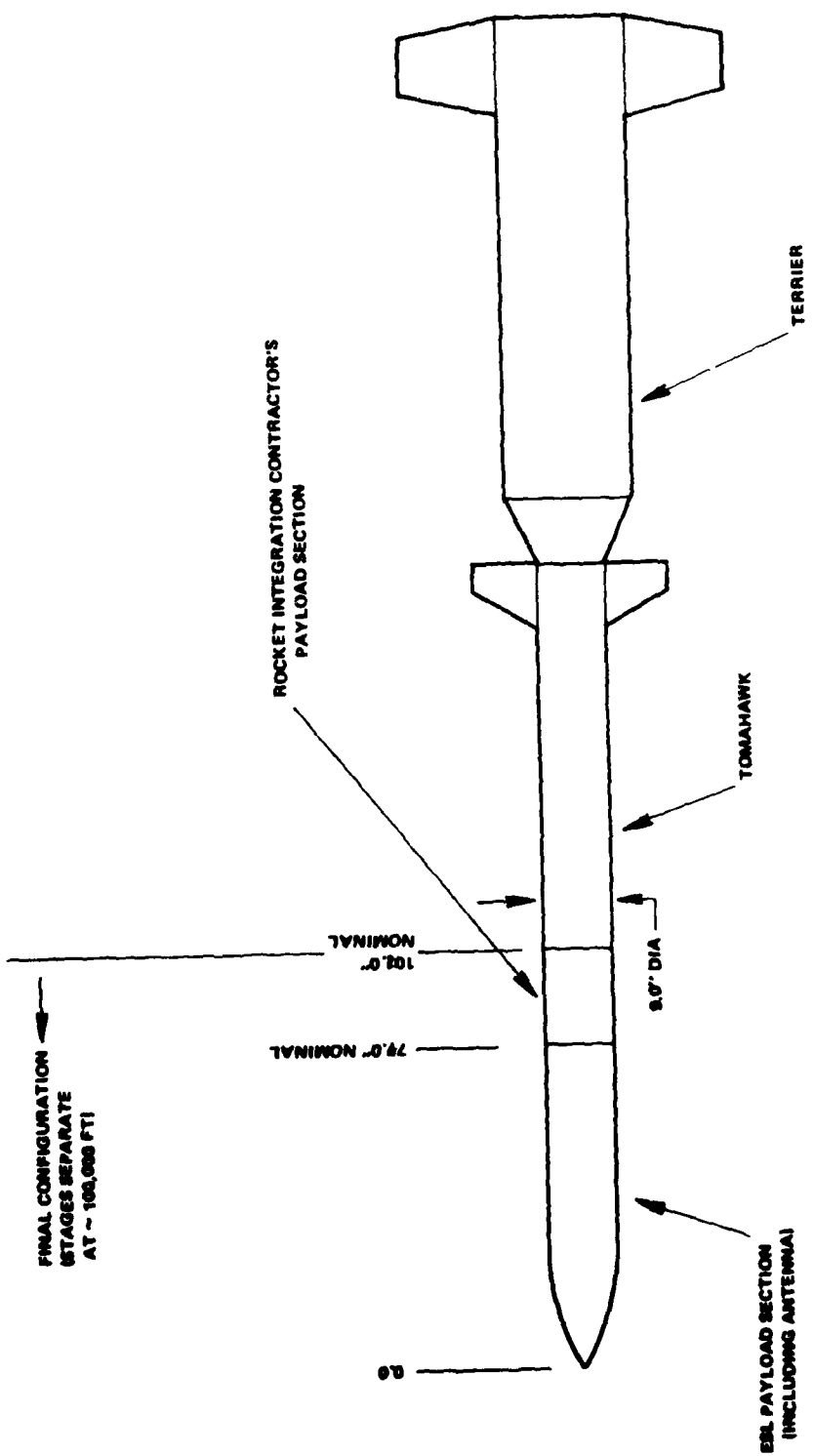
Figure A-3.   Rocket System Sketch (not to scale)

TERRIER

TOMAHAWK

ROCKET INTEGRATION CONTRACTOR'S
PAYLOAD SECTION

102.0" NOMINAL

9.0" DIA

79.0" NOMINAL

FINAL CONFIGURATION
(STAGES SEPARATE
AT ~ 100,000 FT)

9.0

BBL PAYLOAD SECTION
(INCLUDING ANTENNA)

A-9

payload is required to separate from the rocket's second stage after second stage burnout.

The rocket transmitter payload is attitude spin stabilized and conformal VHF and C-band antennas are used to reduce antenna pattern induced perturbations to the data. The conformal antenna patterns are close to spin axis symmetric. The payload skin comprises the VHF antenna. VHF and C-band radiation is linearly polarized with the electric field in the direction of the attitude vector. Figure A-4 provides more detail on the rocket antenna assembly.

Table A-1 shows the rocket transmitter system design goal specifications.

Each rocket transmitter system is designed to be the forward end of a complete Terrier-Tomahawk rocket system as sketched in Figure A-4. The antenna design utilizes the entire payload shell as the VHF radiator, including the nose section. The ESL supplied rocket transmitter system payload section thus has only one mechanical interface at the aft end which will mate with the Sandia payload section. For proper antenna operation the entire payload is required to separate from the rocket's second stage after second stage burnout.

The rocket transmitter payload is attitude spin stabilized and conformal VHF and C-band antennas are used to reduce antenna pattern induced perturbations to the data. The conformal antenna patterns are close to spin axis symmetric. The payload skin comprises the VHF antenna. VHF and C-band radiation is linearly polarized with electric field in the direction of the attitude vector. Figure A-5 provides more detail on the rocket antenna assembly.

Table A-1. Rocket Payload Transmitter Design Goal Specifications

VHF XMTR Characteristics

Signal Format	PN binary sequence biphase modulated ($\pm 90°$) onto 98 MHz carrier
PN Chip Rate	9.8 M chips per second
PN Sequence Length	$2^{22} - 1 = 4, 194,303$ chips repeated every 0.428 seconds
Center Frequency	98,000 kHz ± 1 kHz
Transmitted Power Level	100W, nominal, continuous
Antenna Gain	0 dBi nominal (linear polarization)
Emission Bandwidth	-3 dB, 8.8 MHz -20 dB, 30 MHz -60 dB, 70 MHz
Harmonic Content	-60 dBc maximum each
Spurious Outputs	-40 dBc maximum each
Operating Altitude	0-1 km, and above 90 km

C-Band XMTR Characteristics

Signal Type	Discrete frequency component
Frequency	4, 116,000 kHz ± 40 kHz
Transmitted Power Level	0.5W, nominal, continuous
Antenna Gain	0 dBi, nominal
Emission Bandwidth	-60 dB, less than 1 kHz
Harmonic Content	-40 dBc maximum each
Spurious Outputs	-40 dBc maximum each
Operating Altitude	Unrestricted
Prime Power Source	Internal batteries, sufficient for 10 minute operation, minimum
External Inputs Required	Contact closure for system turn-on (less VHF amplifier) at launch contact closure for VHF amplifier turn-on at 90 km altitude
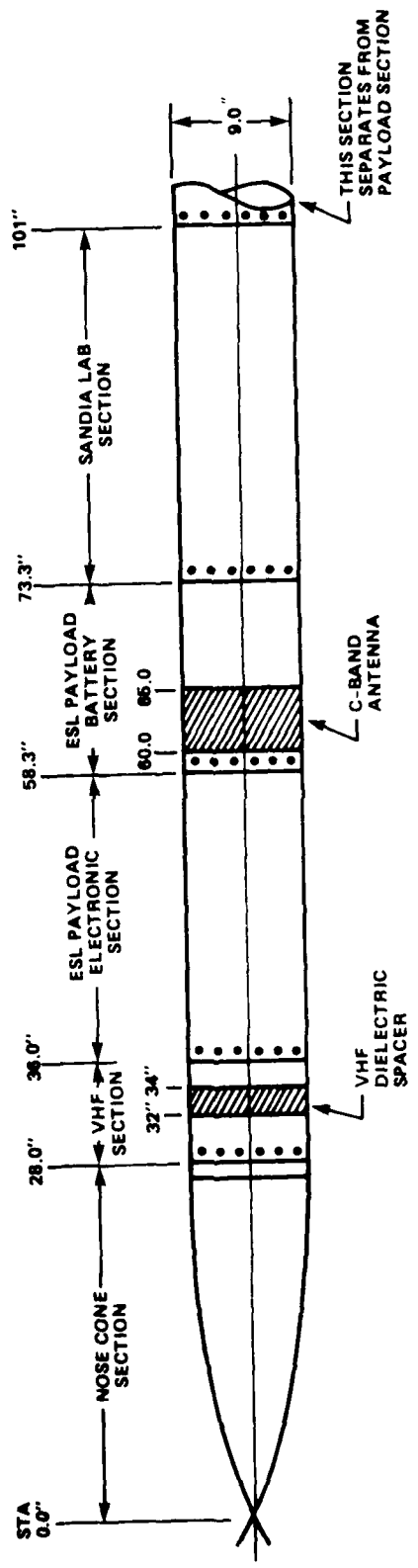
Figure A-4. PLACES Rocket Assembly, VHF and C-Band Antenna
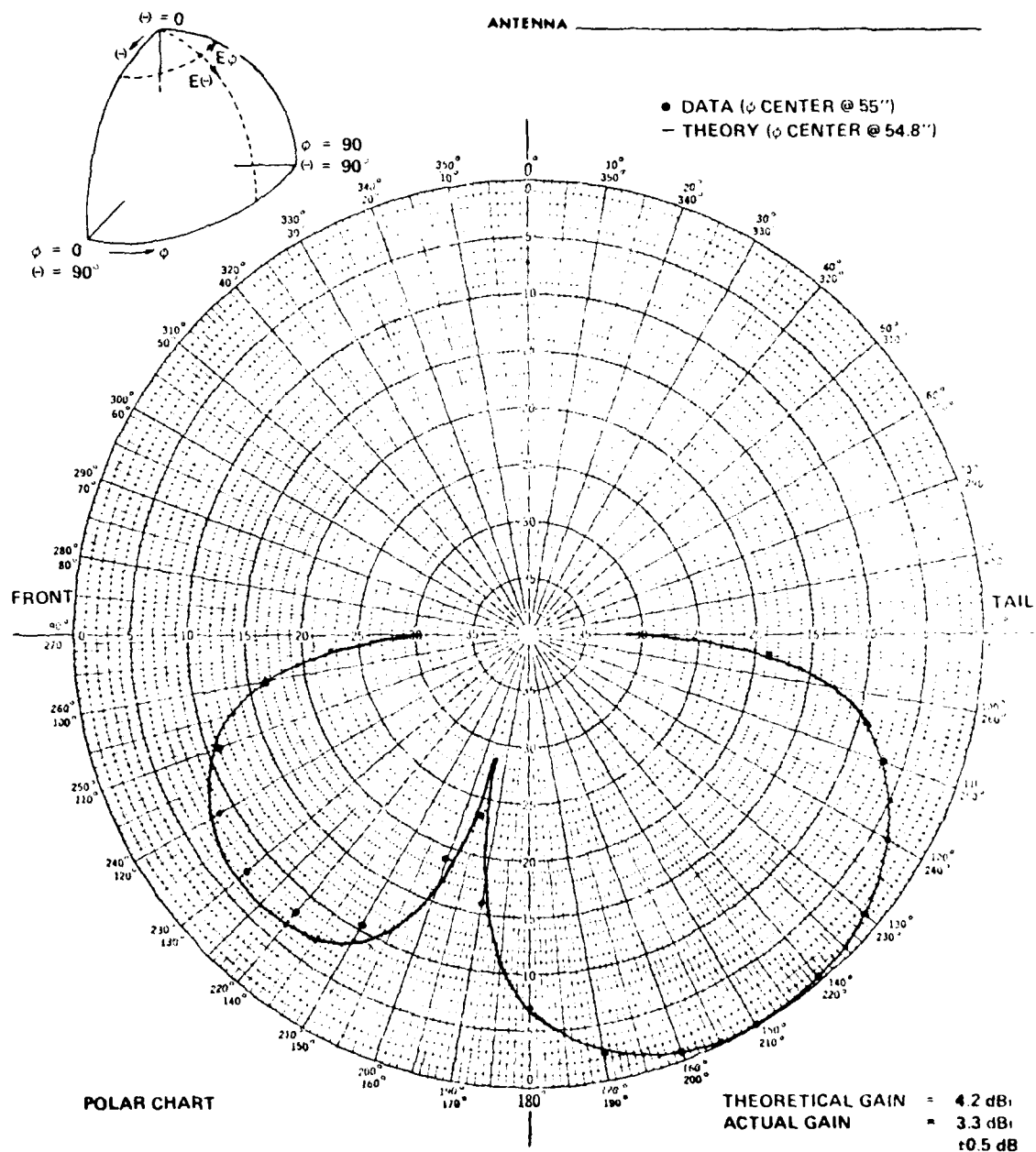
Figure A-5. VHF Rocket Antenna Pattern at 98 MHz

A-3   VHF ROCKET TRANSMITTING ANTENNA CHARACTERISTICS.

The payload skin comprises the VHF antenna which acts as an asymetric fat dipole that forces the maximum gain toward the tail of the rocket as shown in Figure A-5. The pattern data shown on this figure is plotted against a theoretical calculation performed by ESL. The phase center of the antenna is 55 inches aft of the rocket nose. The C-band antenna is effectively located at this point so that a relative phase modulation will not be imparted on the VHF data due to the rocket coning. The peak gain of the rocket antenna was measured to be 3.3 dBi ±0.5 dB.

A-4   C-BAND ROCKET ANTENNA.

The C-band rocket antenna is a microstrip wrap-around design. Figure A-6 shows the measured antenna pattern as a function of the angle off the rocket tail (aspect angle). At an aspect angle of 30 degrees the gain is approximately 1.5 dBi. While the conformal low profile antenna design results in a close to spin axis symmetric pattern, there are variations that can be seen as the rocket spins as shown in the data of Figure A-7. This figure is for a 30 degree aspect angle. Other aspect angles have shown larger gain variations with roll angle. The aspect angle varies from approximately 68 degrees to as low as 26 degrees over the rocket flight. Coning of up to 5 degrees about these nominal angles will result in aspect angles of possibly from approximately 70 degrees to 21 degrees. As shown, the C-band antenna gain is adequate over this range.

A-5   ANTENNA PHASE CENTERS AND C-BAND ANTENNA PLACEMENT.

The C-band antenna phase center is approximately 3 inches off the center of the rocket due to the wrap-around antenna shielding to the viewer by the rocket body. The phase center of the VHF antenna was found to be approximately 55 inches aft of the nose in agreement with theory. For a viewing
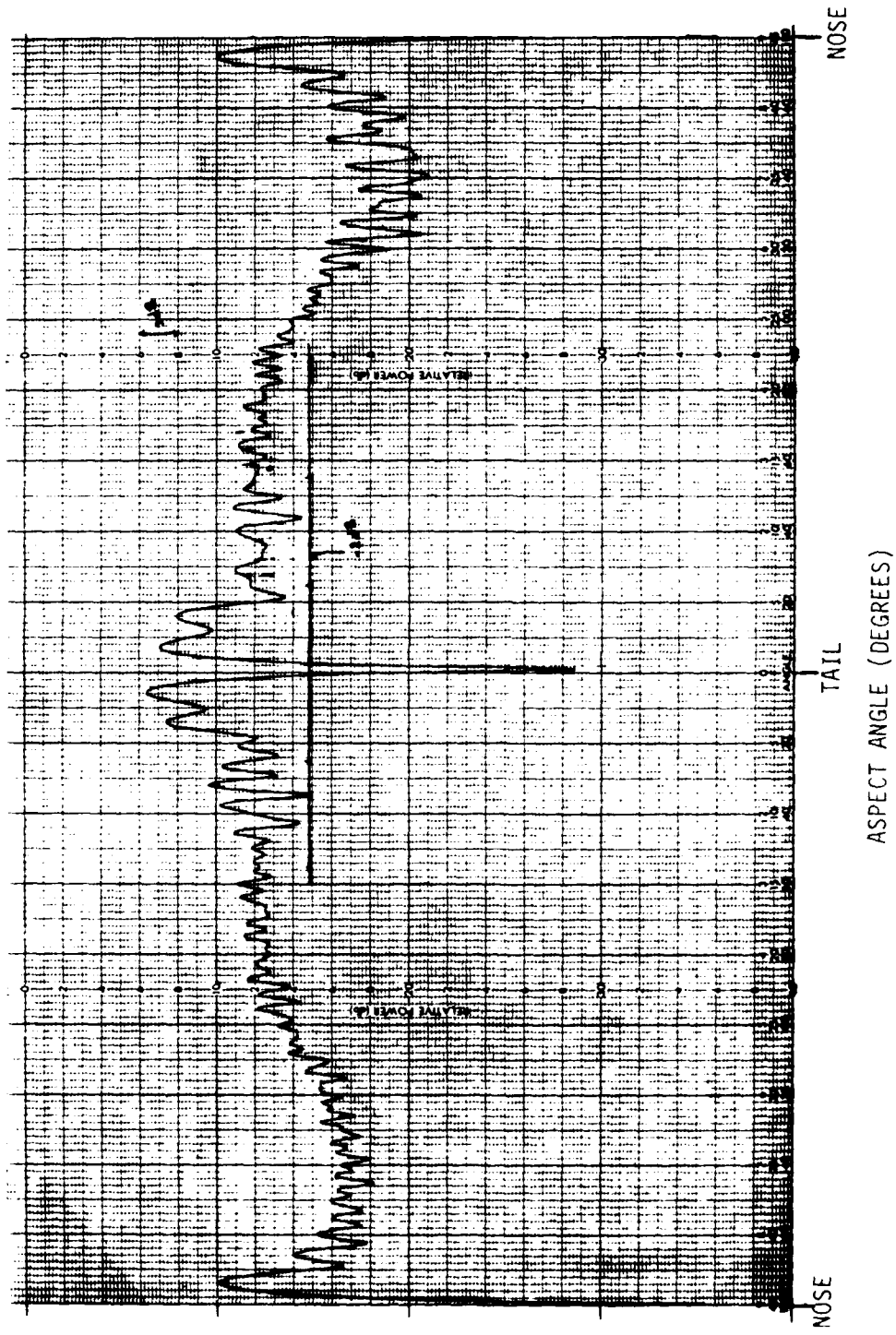
Figure A-6.   C-Band Rocket Antenna Pattern

ROLL ANGLE
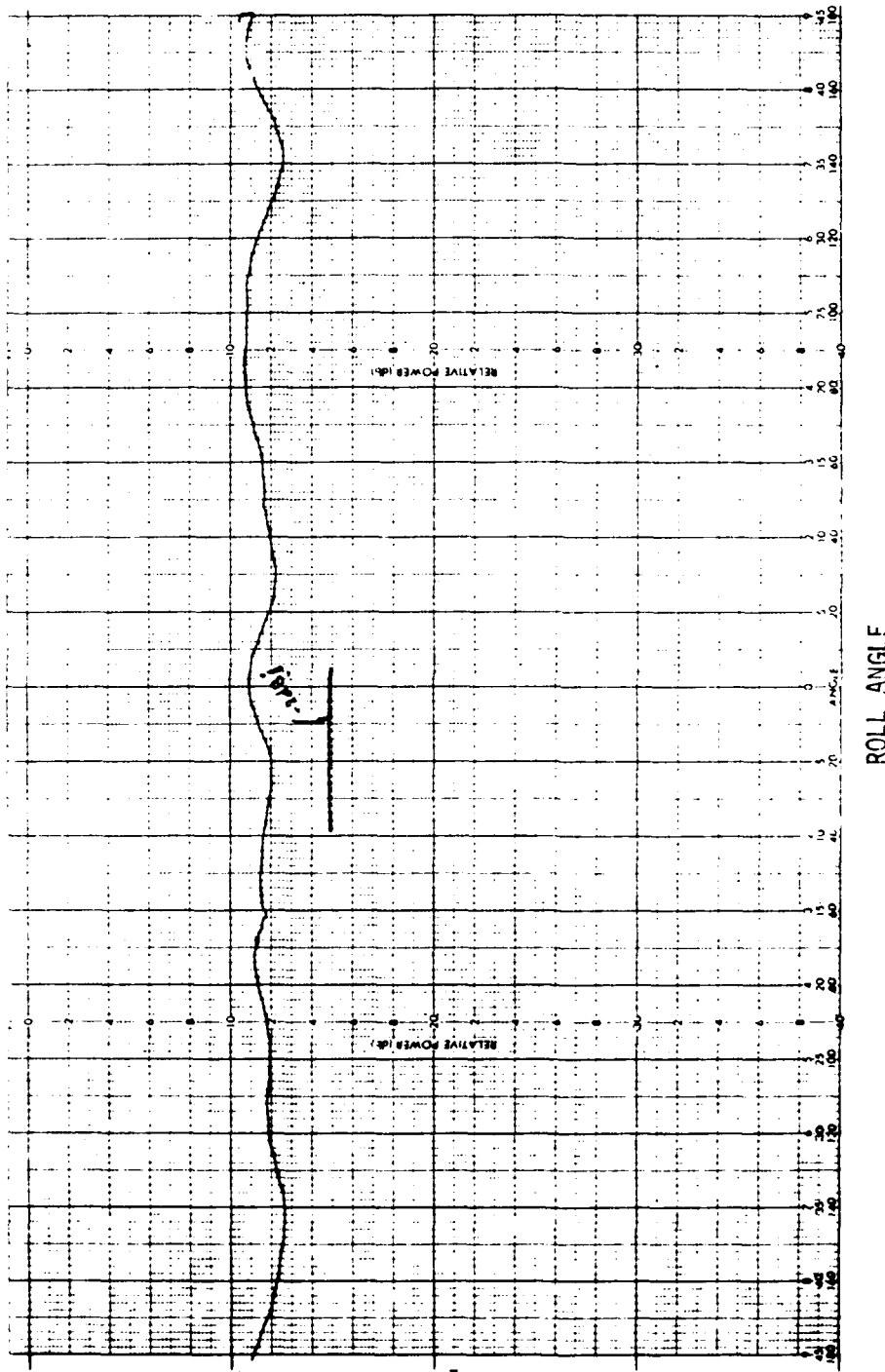
Figure A-7. C-Band Rocket Antenna Roll Pattern at 30 Degrees Aspect

A-16

aspect angle of around 30 degrees off the tail the C-band antenna should be placed approximately 60 inches from the nose so that the phase centers of the two antennas are aligned. In this way the phase variations due to rocket coning will be minimized. The actual center of the C-band antenna was placed at station 62.5 inches (see Figure A-4) which was as close to 60 inches place- ment as possible. The joint at 58.3 inches prohibited a closer placement. This favors the Cape San Blas geometry.

A-6   GROUND STATION SYSTEM.

        The purpose of the ground station system is to receive and process wideband pseudonoise (PN) VHF signals that provide a measure of the channel diagnostic data. The PN signal receiver unit shown in Figure A-8 is an RF amplifier and a converter. The output of this receiver is fed to the IF tap unit, which is the hardware module that performs the PN cross-correlation operations. This unit consists of a set of nine hardware correlators that will be swept in the dimension of relative delay to 10 delay positions each. The delay sweep positions are separated by 1/3 of a PN chip; thus, the system allows for monitoring of the channel impulse response over a 30 PN chip (or 3 microseconds) time delay range. Each hardware correlator outputs two 10-bit samples every 250 microseconds. Each 1/3 chip delay position is sampled every 2.5 milliseconds. The output samples are the result of a 225 microsecond integration; 25 microseconds are allowed for switching and integrator dump transient settling.

        The processing and control unit 1) provides the sweep control for the IF tap unit; 2) performs the initial code synchronization; 3) open-loop tracks the PN code, based upon inputs from the C-band reference signal receiver; and 4) accepts all channel and receiver diagnostic data and formats them for output to the recorder unit and the real-time display unit.
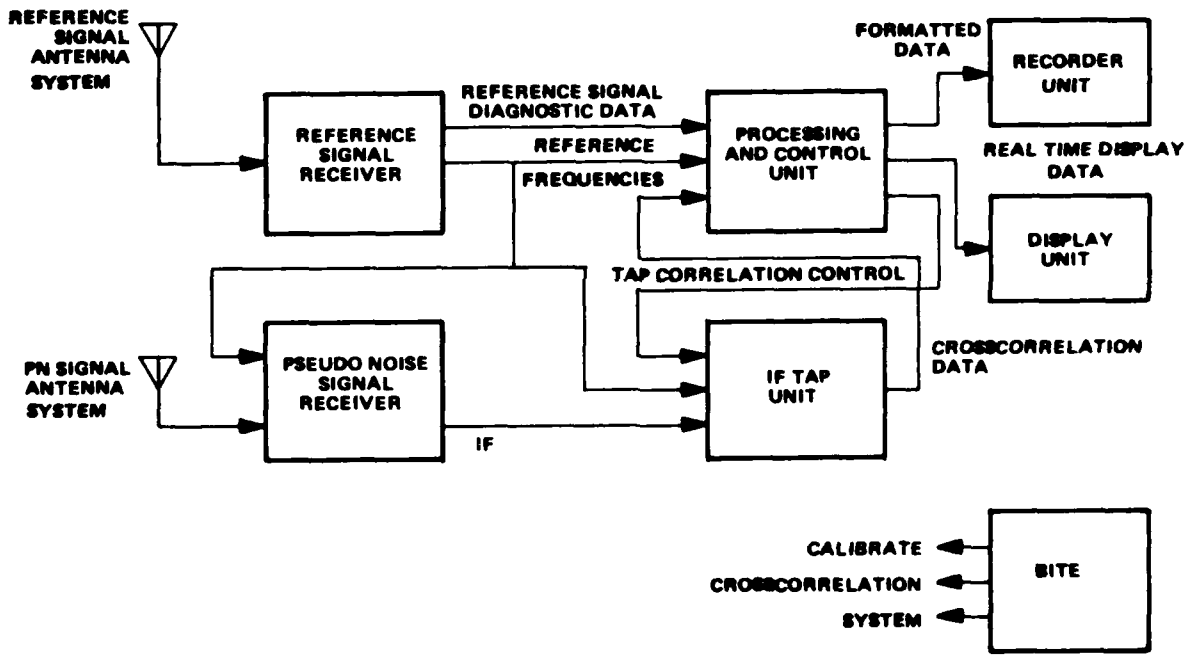
Figure A-8. Ground Station System

The sweep is performed such that each of the nine hardware correlators are at any time separated by 10/3 or three 1/3 pseudonoise chip periods. The sweep of each correlator proceeds 1/3 of a pseudonoise chip period in increasing delay for nine steps with the tenth step being a reset to the initial sweep position. The data from all 90 positions is accumulated in a buffer. Readout of this buffer to the digital tape and to the display is then made in a sequential order by delay position.

The initial code synchronization is performed by cross-correlation of the input signal with a 512 chip subsequence of the code. Once synchronization has been obtained it can be verified with the display unit. A provision in the processing and control unit has been provided that allows slewing of the entire correlator code manually for tracking out the gross time-of-arrival delay of the ionosphere. A count of the amount of slew is recorded digitally with the tap data.

The digital tape format is compatible with the reproduce functions of the system. Reproduction of the data can be performed at a rate equal to 1/8 of the initial 120 ips recording speed. This provides a feature allowing slow speed playback and display in the field for a quick look post mission analysis. Unfortunately, the record format is not a conventional IBM format and a later conversion process is required to allow further data processing and data dissemination.

A receiver unit is driven by signals from the VHF antenna system. A RHCP circularly polarized wideband antenna system is employed. The use of a circular antenna isolates the circular propagation modes of the ionosphere and reduces the risk of rocket orientation and Faraday rotation uncertainties.

The purpose of the reference signal receiver is to acquire and track the rocket C-band signal and thereby establish timing and phase references for the ground station receiving system. Integral to its implementation is a phase locked loop, with approximately 800 Hz bandwidth, to track the rocket doppler.

A-7   VHF RECEIVING ANTENNA CHARACTERISTICS.

The 98 MHz beacon receiving antennas are designed to minimize multipath interference, to maximize the rejection of RFI at the horizon and to have nearly perfect axial ratio over a broad beamwidth, and to have a flat amplitude and phase response over frequency. The antenna receives LHCP in order to minimize dispersion as a LHCP mode is phase shifted less by the ionosphere than a RHCP mode. However, either RHCP or LHCP polarization can be selected through use of the hybrid coupler on the antenna. The gain contours achieved are shown in Figures A-9 and A-10 for the horizontal and vertical polarization measurements taken at 98 MHz for unit No. 2. Figure A-11 shows the on-boresight amplitude response versus frequency. Figure A-12 shows the corresponding phase response. The physical boresight of the antenna is at 50 degrees elevation to improve RFI and multipath rejection. Figure A-11 shows the vertical polarization boresight is indeed at 50 degrees. However, due to the influence of the ground on the horizontal polarization, its effective boresight is near 40 degrees elevation (see Figure A-9). In checking the gain and phase response of the antenna it was determined that this will not create a problem to the data.

A-8   C-BAND GROUND STATION ANTENNA.

The C-band antenna design is a compromise of achieving sufficient gain for signal acquisition and sufficient beamwidth to ease the difficulty of tracking the rocket. The rocket transmits a linear polarized wave of varying orientation depending upon the rocket aspect and subsequent Faraday rotation, thus the receive polarization was chosen as RHCP. A peak linear-to-circular gain of 13.2 dBi was achieved for the ground antenna with a -3 dB beamwidth of ~26 degrees. Figures A-13 and A-14 show the antenna gain pattern as measured.
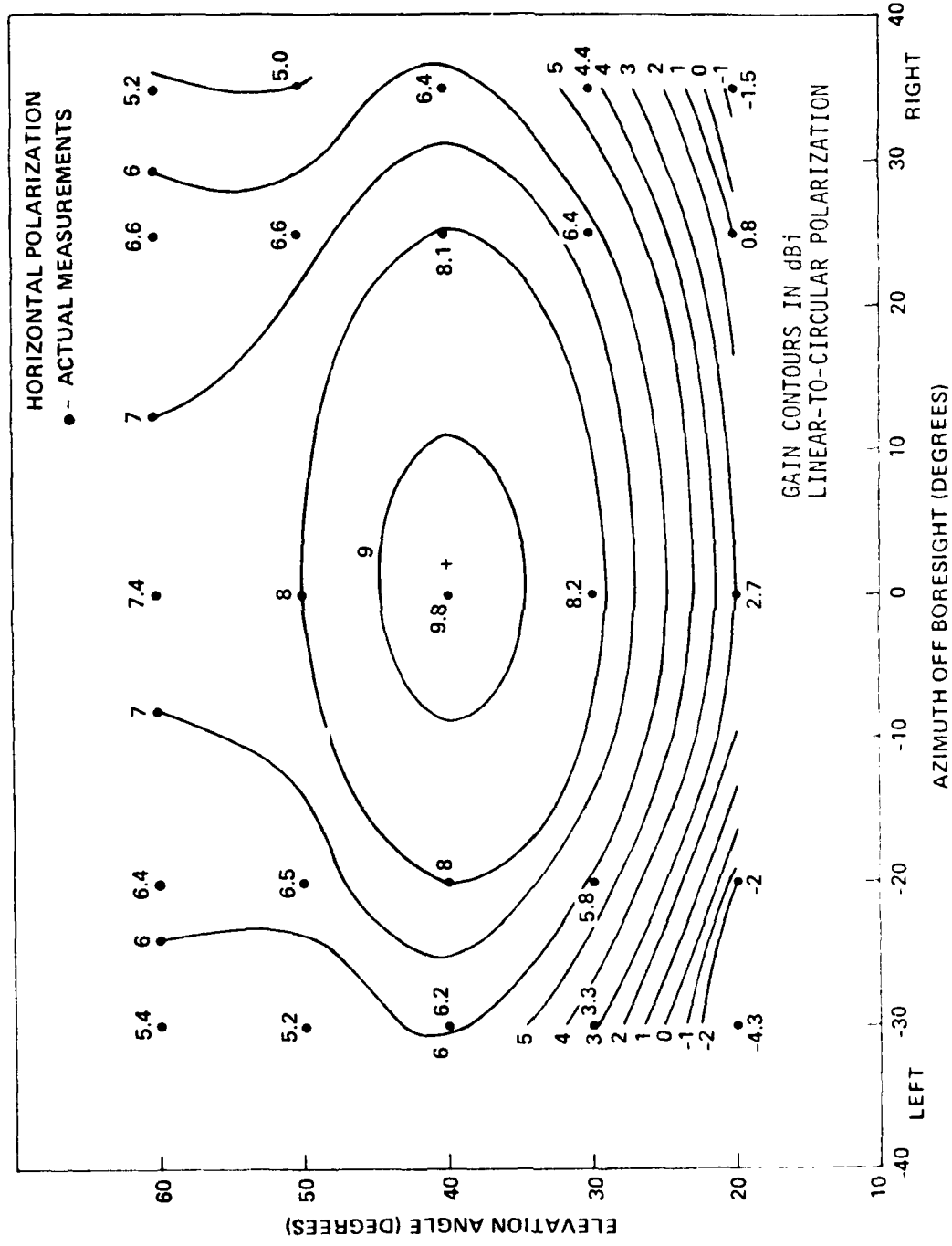
Figure A-9. Gain Contours of Beacon Ground Station Antenna at 98 MHz; Horizontal Polarization
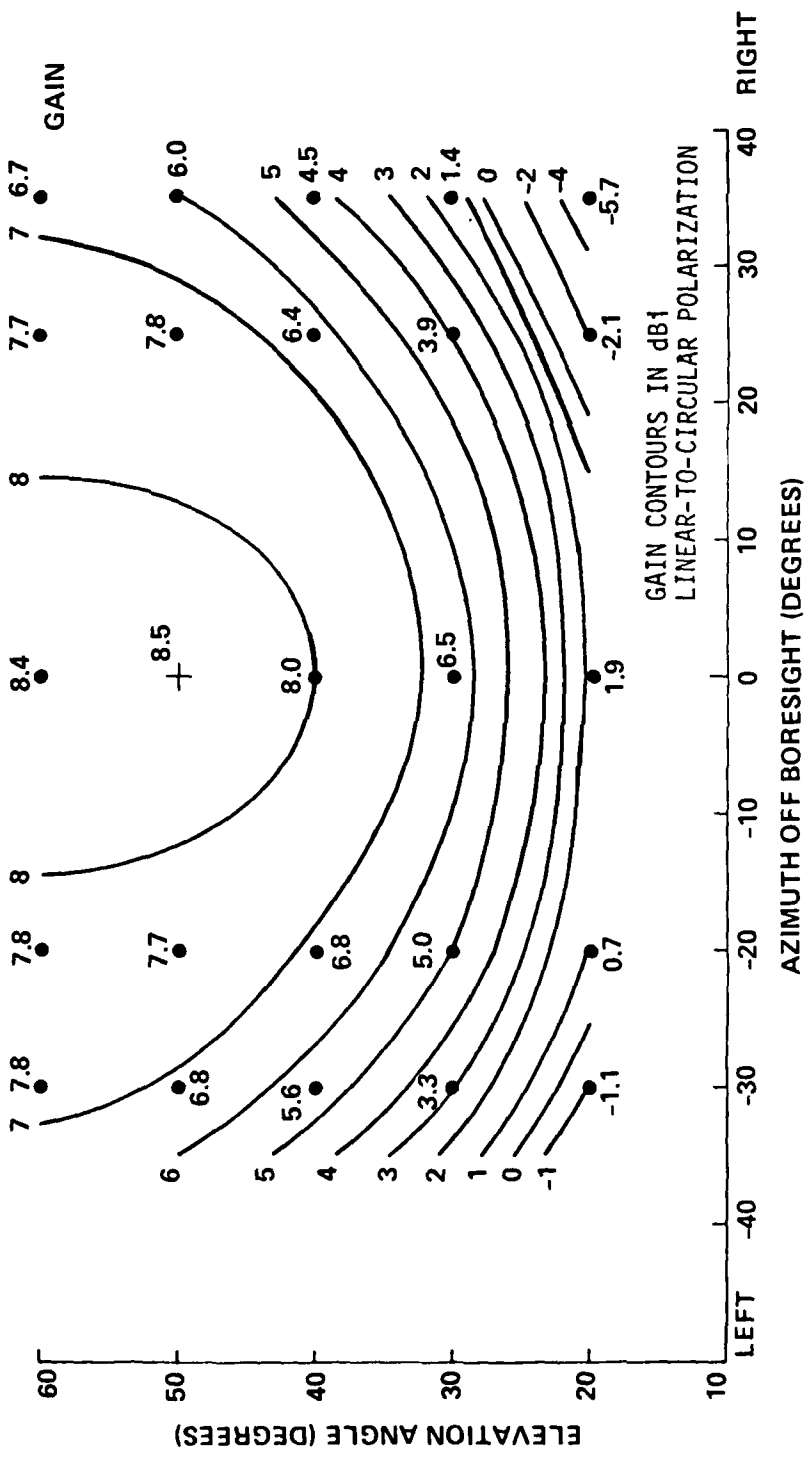
Figure A-10. Gain Contours of Beacon Station Antenna at 98 MHz, Linear-to-Circular Polarization, Vertical Polarization
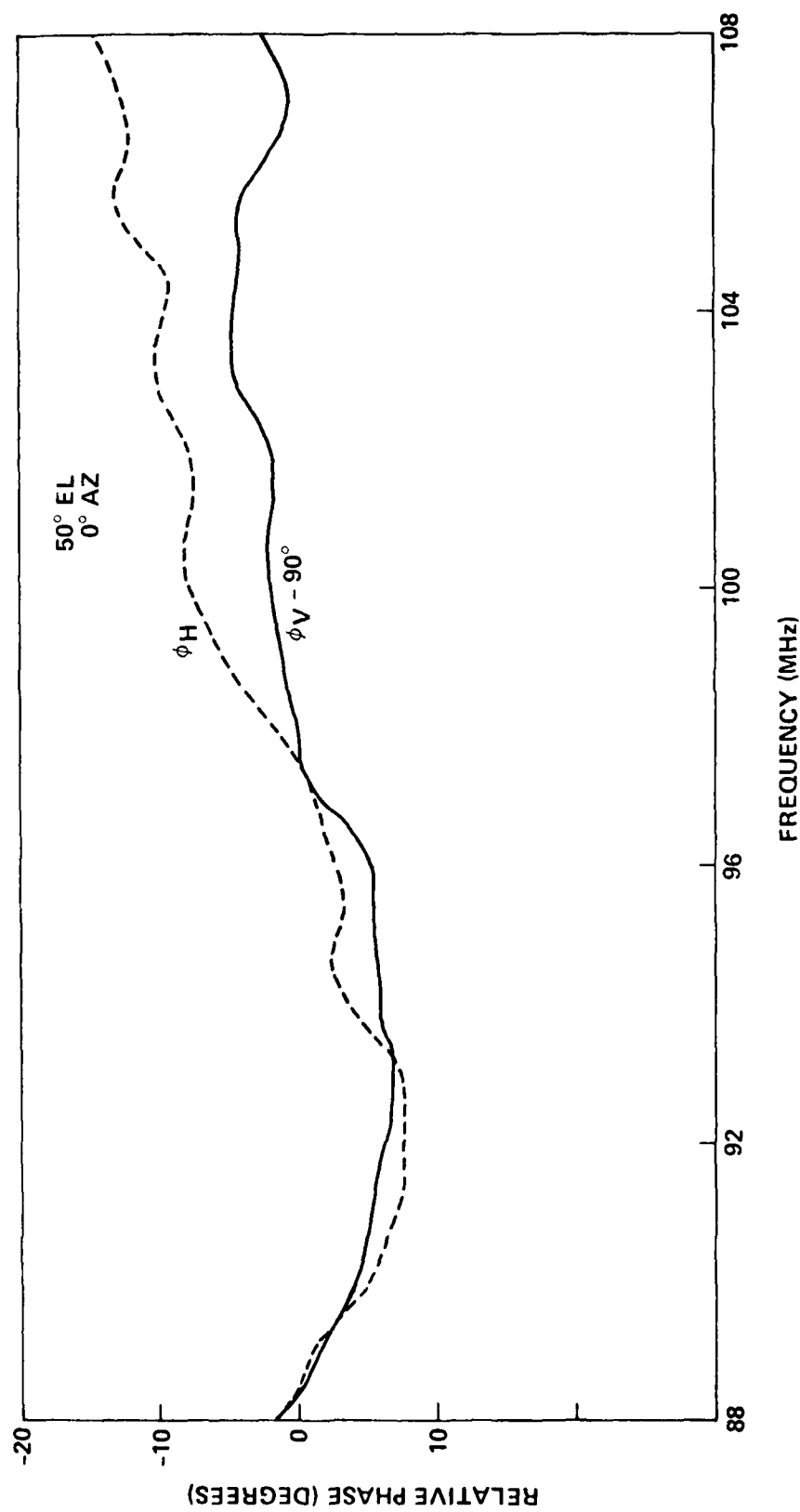
Figure A-11. VHF Receiving Antenna Boresight Phase Versus Frequency
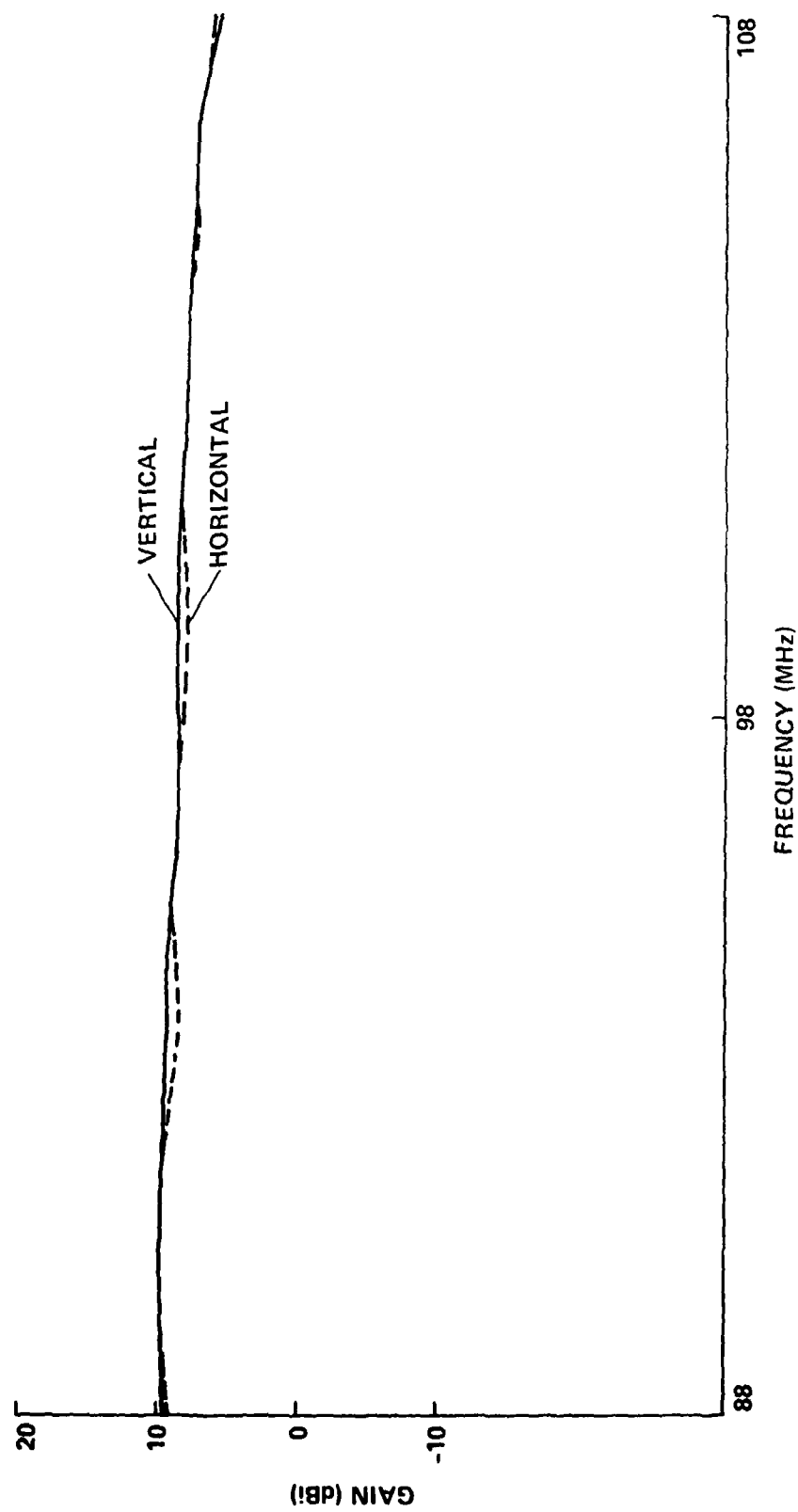
Figure A-12. VHF Receiving Antenna Boresight Gain Versus Frequency
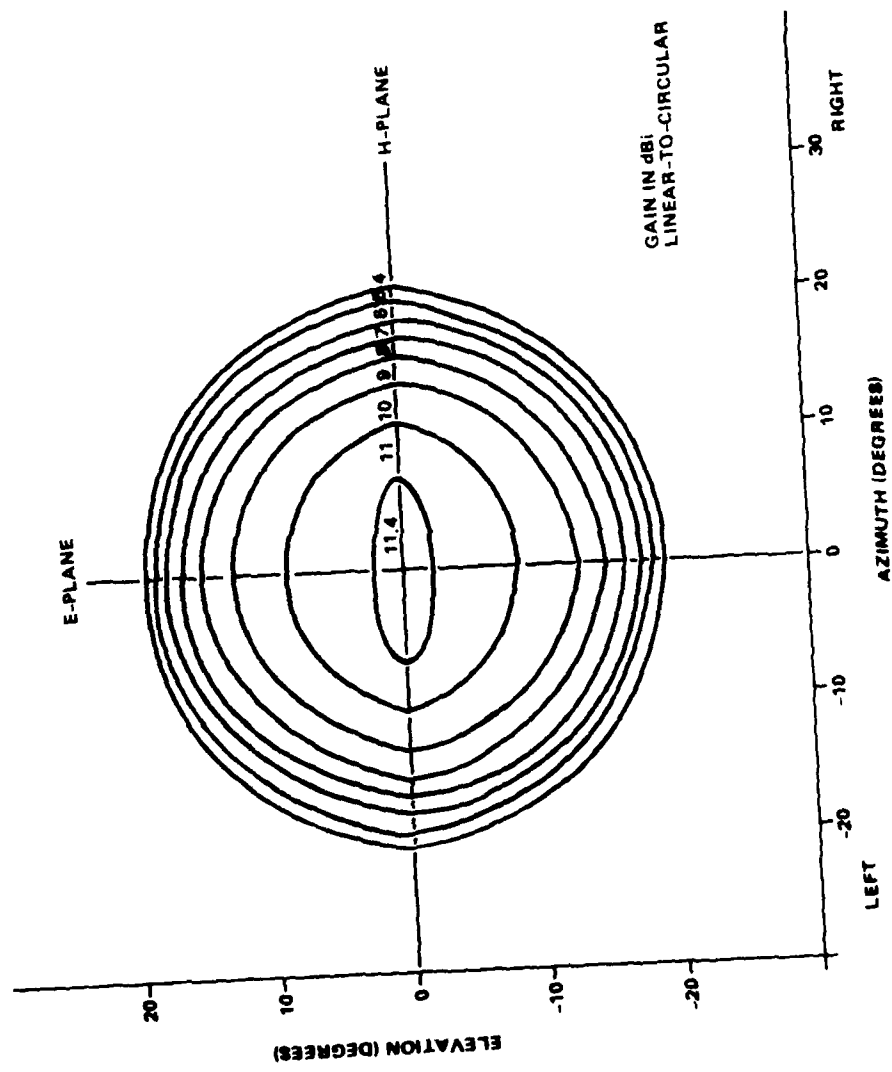
Figure A-13. C-Band Horn Pattern, E- and H-Plane Minimum Gain Contours. E-Plane is Vertical

A-25
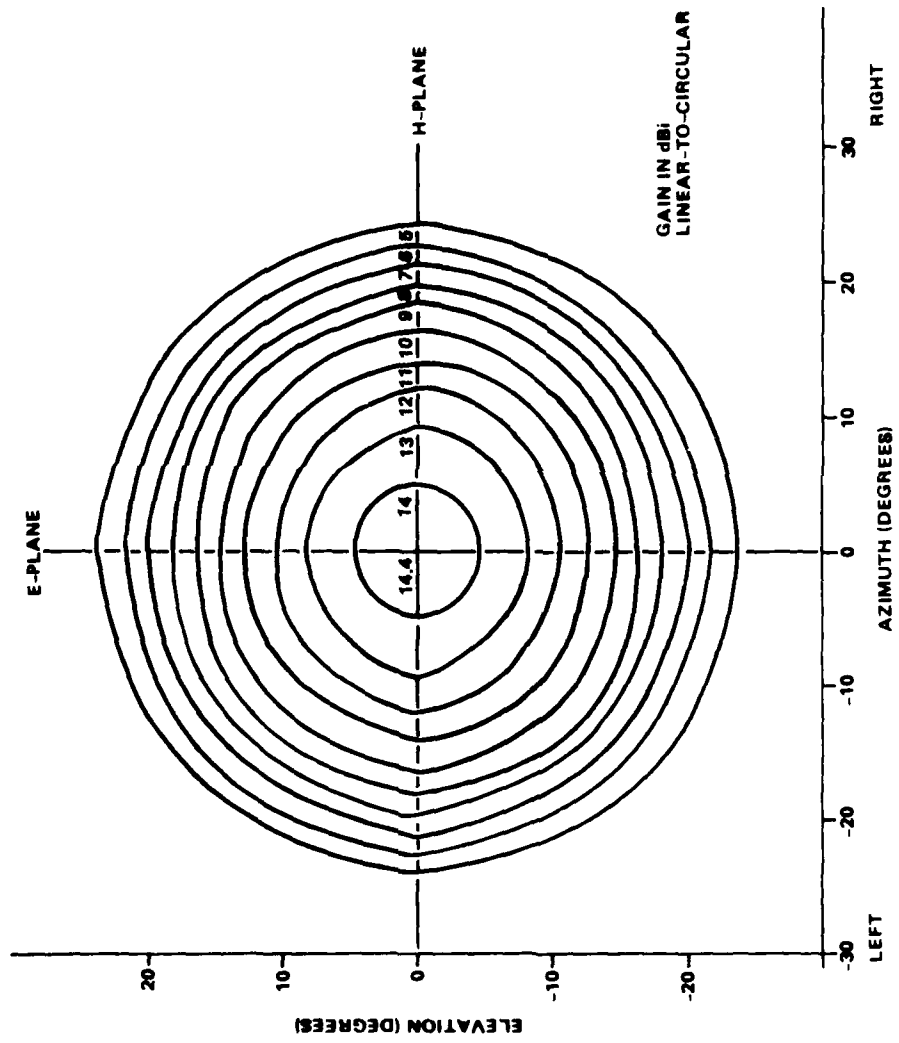
Figure A-14.   C-Band Horn Pattern, E- and H-Plane Maximum
Gain Contours.   E-Plane is Vertical

A-9   LINK CALCULATIONS.

A-9.1   VHF Link Calculations.

A nominal link calculation for the VHF signal from the rocket to a ground receiving site is provided in Table A-2. The local interference environment sets a limit upon the output signal-to-noise ratio. The receiver processing gain is 32.2 dB as measured.

The received signal-to-noise ratio will vary over the rocket trajectory due to the antenna coupling. Further, there will be a fluctuation in signal level due to the Faraday rotation of the signal vector and the corresponding variations in the ground station antenna gain with polarization. Further, the rocket coning will result in a signal variation. Figures A-15 and A-16 show the signal-to-interference ratio at the ground receiving sites of Cape San Blas and St. George Island, respectively, for a nominal trajectory with the VHF antenna pointed at 262 and 267 degrees azimuth, respectively. For this nominal trajectory at Cape San Blas a signal-to-noise ratio of approximately 40 dB is to be expected, whereas at St. George Island a signal-to-noise ratio of approximately 37 dB is to be expected for the non-fading signal near occultation.

Through computer processing a higher signal-to-noise ratio can be achieved. The effective real-time processing bandwidth is approximately 200 Hz. The amount of processing that can be affected in post computer processing is a function of the amount of energy delay. That is, each tap delay will have a relative doppler that is a function of the delay as shown in Figure A-17. Long delay components cannot be processed in as small of a bandwidth as the smaller delay signal components.

Note that the worst case PN signal code acquisition requires a signal-to-interference ratio of -2 dB. As long as this condition is met the

Table A-2. PN System Boresight Link Calculation @ 98 MHz

Transmitter Power	50 dBm	
Rocket Antenna Gain	3 dBi	
Propagation Loss, 310 km	-122 dB	
Receive Gain Max	9.8 dB	Linear-to-Circular
Received Signal Power	-59.2 dBm	
Interference Power in 20 MHz IF BW	-73.2 dBm	Cape San Blas
(Receiver Noise Power	-91 dBm)	
(Mean Galactic Noise Power	-91 dBm)	
S/I in 20 MHz, no fading	14.0 dB	
Processing Gain	32.2 dB	
S/I in 200 Hz BW, no fading	46.2 dB	
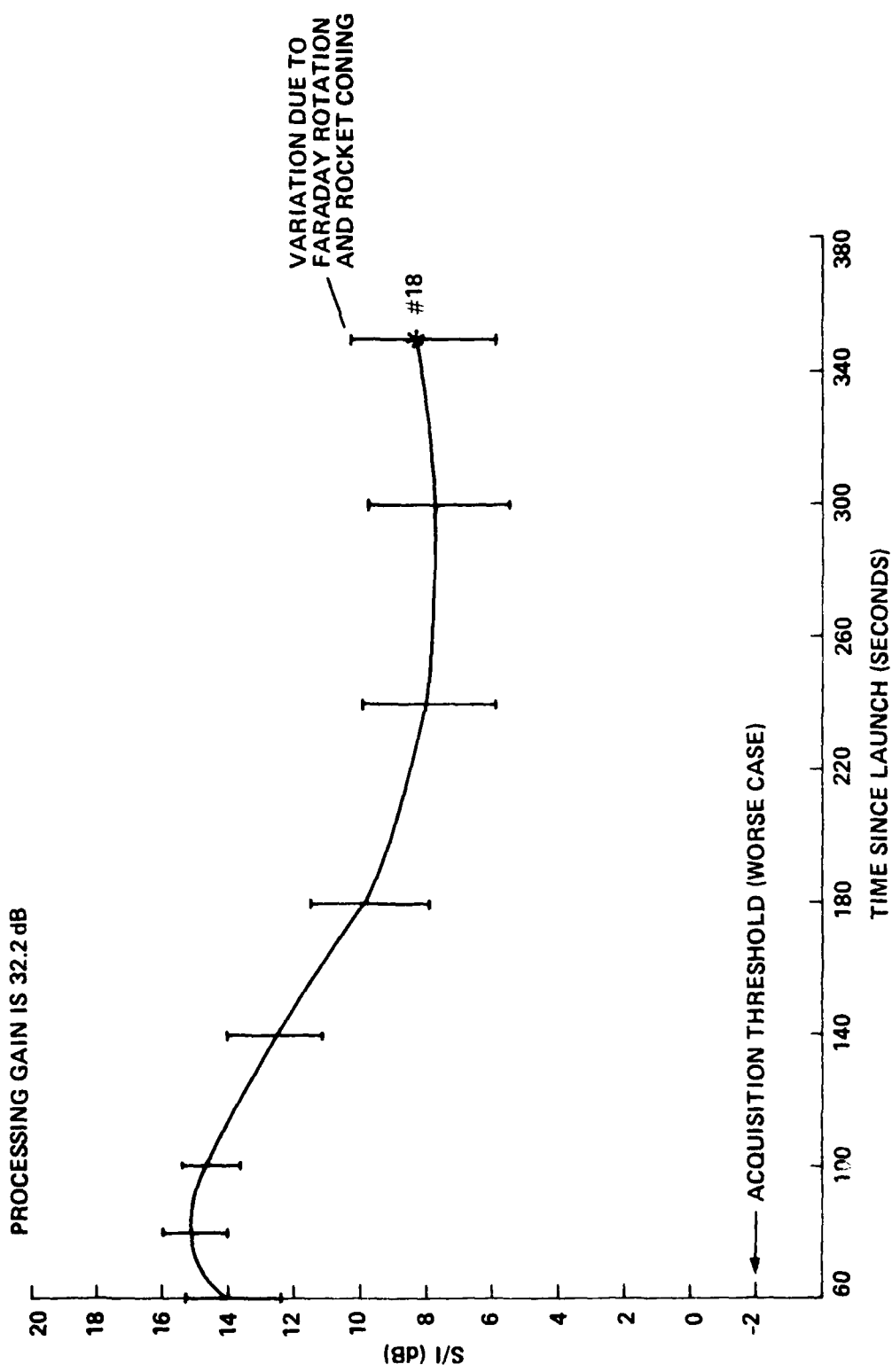
Figure A-15. Signal-to-Interference Ratio Versus Time at Cape San Blas
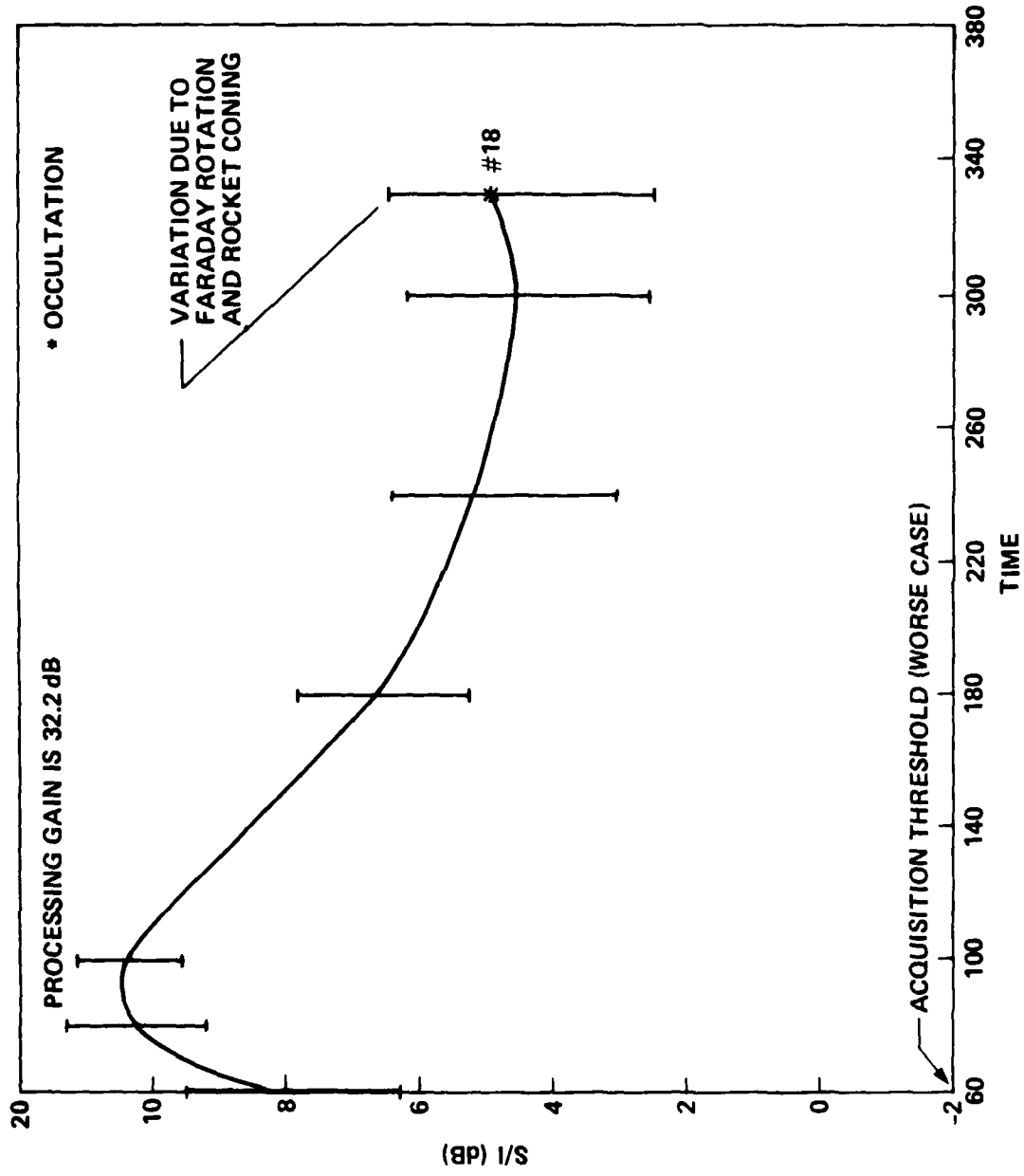
Figure A-16. Signal-to-Interference Ratio Versus Time at St. George Island
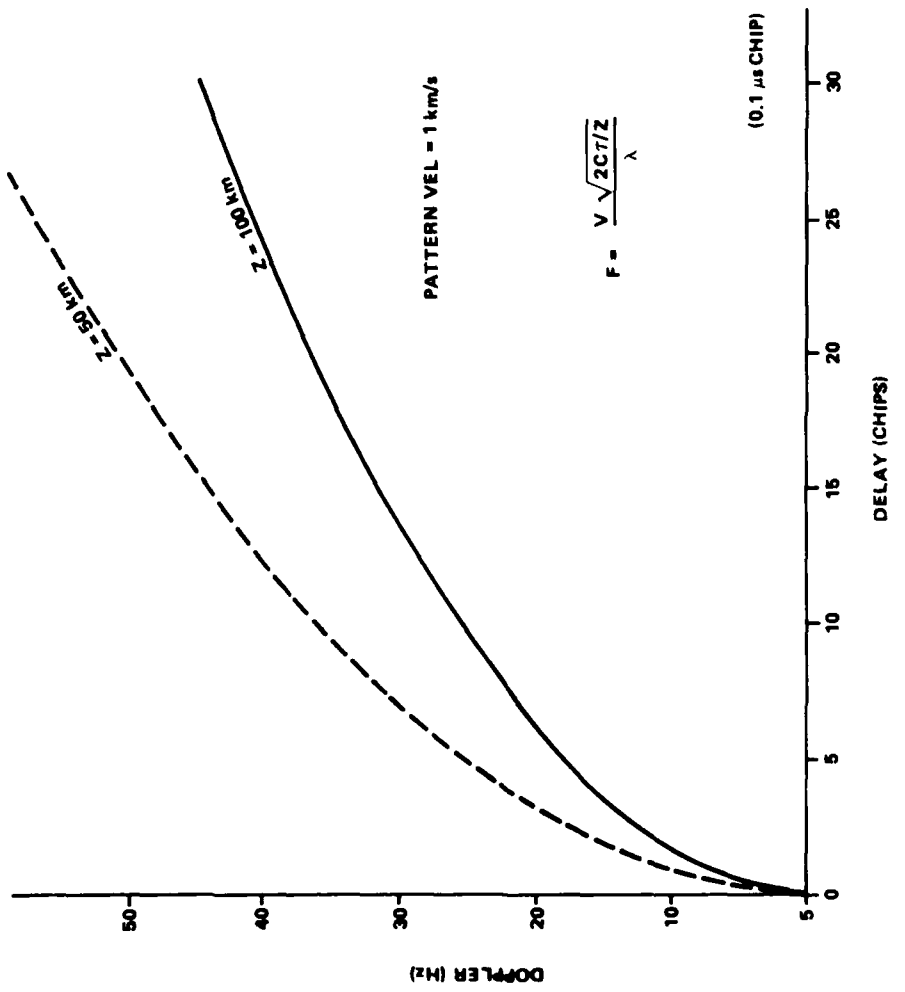
Figure A-17. Relative Doppler Versus Tap Delay at 98 MHz

mean time to acquisition is less than approximately 20 seconds. Under ideal conditions the time to acquisition would be less than 1 second.

A-9.2   C-Band Link Calculations.

The link calculation for the C-band reference system is provided in Table A-3. The maximum loop SNR is estimated to be 30.8 dB near occultation. Figure A-18 shows the signal-to-noise ratio variations over a nominal trajectory. It was assumed that the C-band antenna was maintaining pointing at the rocket while the evaluation angle was held fixed at 50 degrees. Figure A-19 shows the effects of a simultaneous worst case 5 degree elevation and 10 degree azimuth error over the trajectory. Note that the loop SNR is at all times adequate to acquire the C-band phase within a few seconds.

The doppler that must be tracked by the C-band phase tracking system is shown in Figure A-20 for a nominal trajectory.

A-10   INTERFERENCE ENVIRONMENT.

Measurements of the interference environment in the beacon receiving area were made during August 1980. The measurements at C-band showed there were no interferers sufficiently close in frequency to present any problems. The interference environment at VHF is severe and drove the current site placement. Figure A-21 summarizes the total average interference power in the beacon receiver bandwidth of 88 to 108 MHz. It is important to note that the interference power increases as the sun sets. Since the experiment is conducted at sunset, the local environment must be carefully monitored during the experiment time frame to determine that the environment has not changed dramatically. Figure A-22 and A-23 summarize the interference spectrum observed at Cape San Blas and St. George Island, respectively. Essentially no other signals were observed above -95 dBm. The design goal is for the total

A-32

Table A-3. Reference System Boresight Link Calculation

	4.116 GHz	
Transmitter Power, 0.5 W	27 dBm	
Line Losses	1 dB	
Rocket Antenna Gain	0 dBi	Linear Polarization
EIRP	26 dBm	
Propagation Loss	-154.6 dB	310 kilometers
Ground Antenna Gain Max (Boresight)	14.4 dBi	Linear-to-Circular
Received Signal Input Level	-114.2 dBm	
Receiver Noise Density	-174 dBm/Hz	(Conservative)
C/KT	59.8 dB-Hz	
Loop S/N	30.8 dB	(800 Hz BW)

Figure A-18. C-Band Phase Tracking Loop SNR for Optimum Azimuth Tracking from Cape San Blas

FIXED ELEVATION AT $50^{\circ} \pm 5^{\circ}$ ERROR
AZIMUTH TRACKING WITH $\pm 10^{\circ}$ ERROR

VARIATION DUE TO POLARIZATION
ROTATION, ROCKET CONING AND ROLL

OCCULTATION

TIME AFTER LAUNCH (SECONDS)
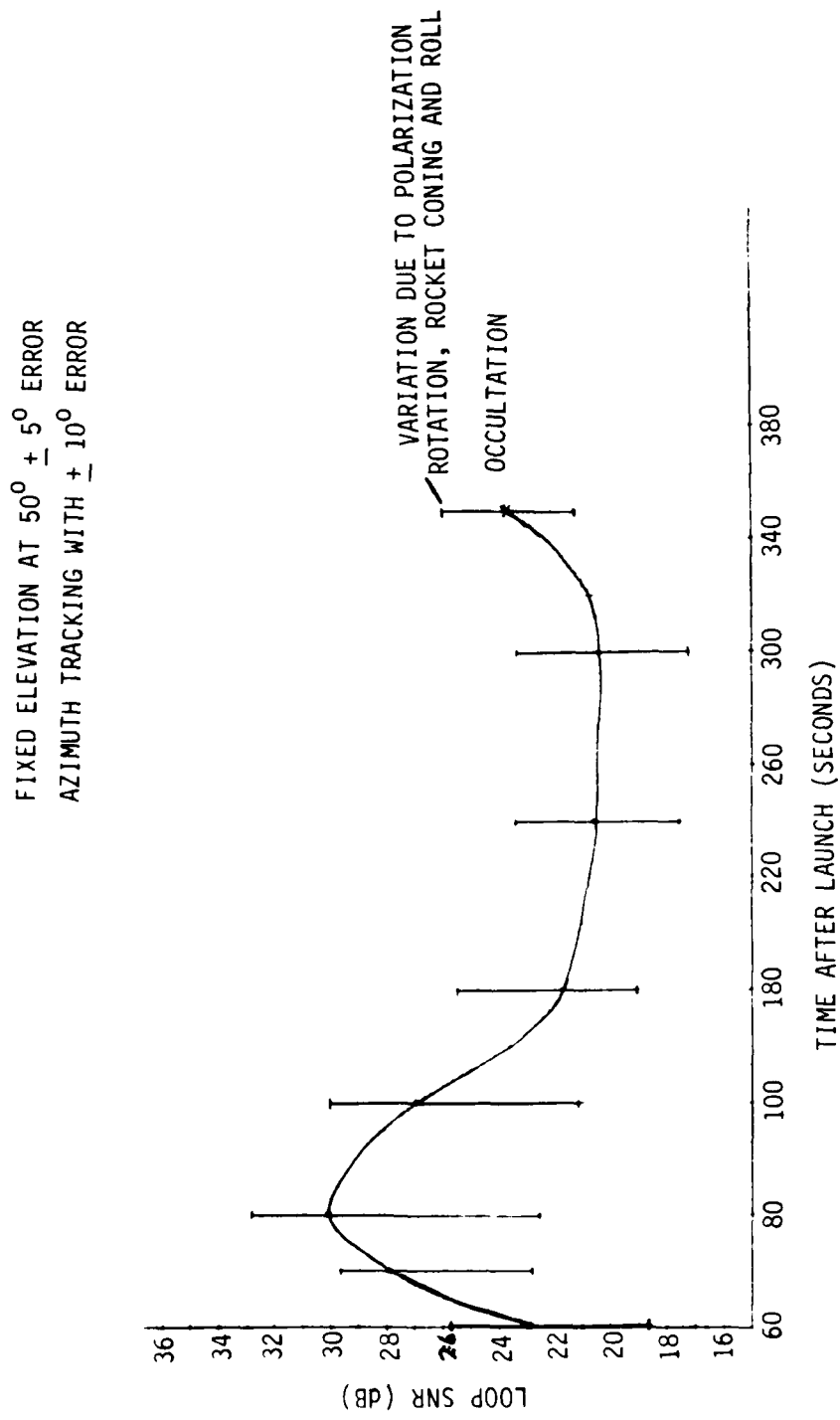
LOOP SNR (dB)

Figure A-19. C-Band Phase Tracking Loop SNR for a Worst Case
5-Degree Elevation and a 10-Degree Azimuth Error
from Cape San Blas
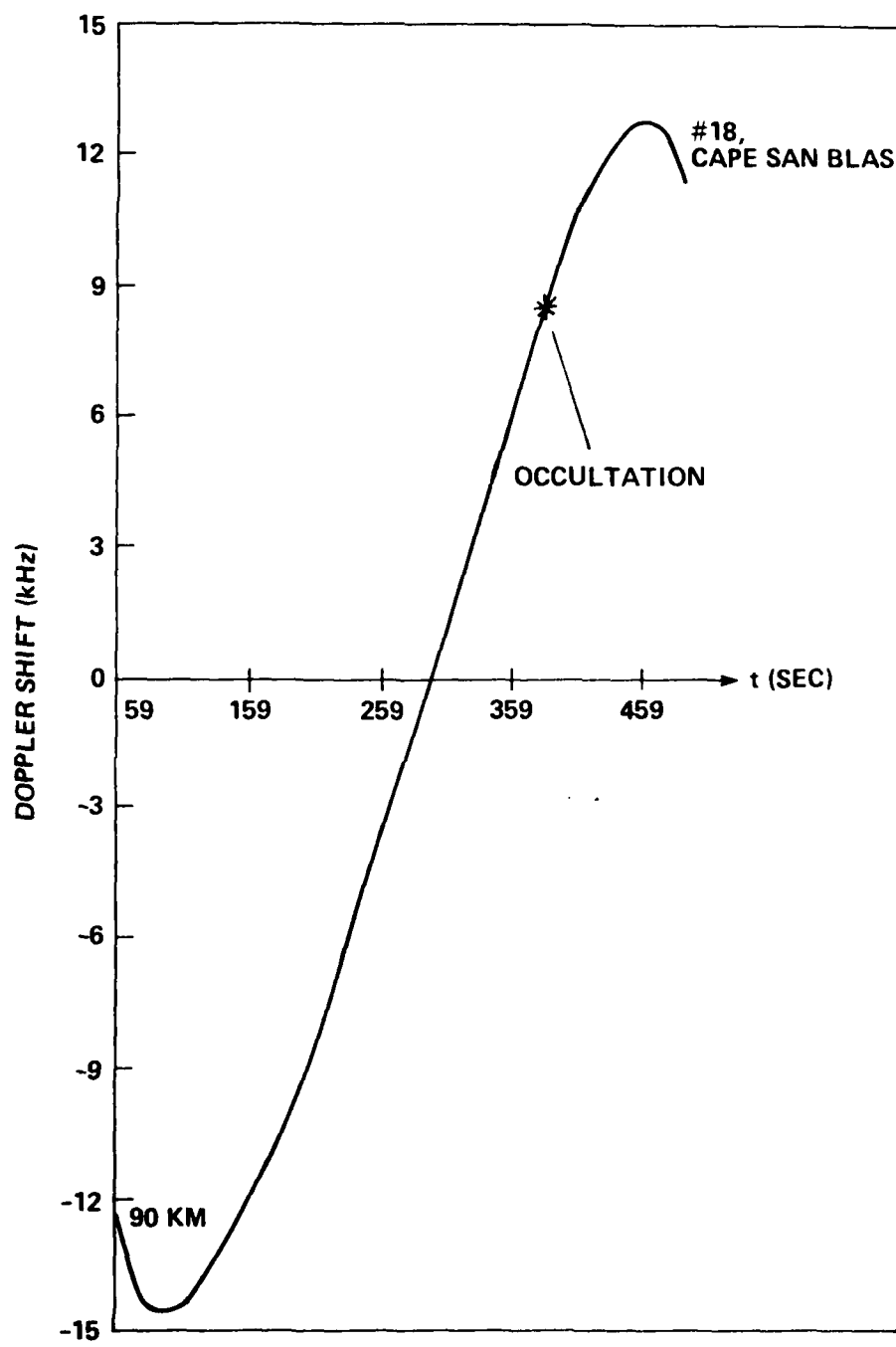
Figure A-20.   Beacon Rocket C-Band Doppler at Cape San Blas

● -1 HOUR AFTER SUNSET
X - DAYTIME

LIVE OAK

TALLAHASSEE

HAMPTON SPRINGS
-75.8 dBm

SCANLON
-69.0 dBm

LIVE OAK POINT
-61.1 dBm

BALD POINT
-61.7 dBm

SOPCHOPPY
-58.6 dBm

CARRABELLE
-58.8 dBm
(-73.5 dBm MIDDAY)

ST. GEORGE ISLAND
-69.6 dBm

TELOGIA
-49.2 dBm

SUMATRA
-48 dBm

BEVERLY
-66.9 dBm

PORT ST. JOE
93.5 MHz

92.5 MHz

D3-A
-73.2 dBm
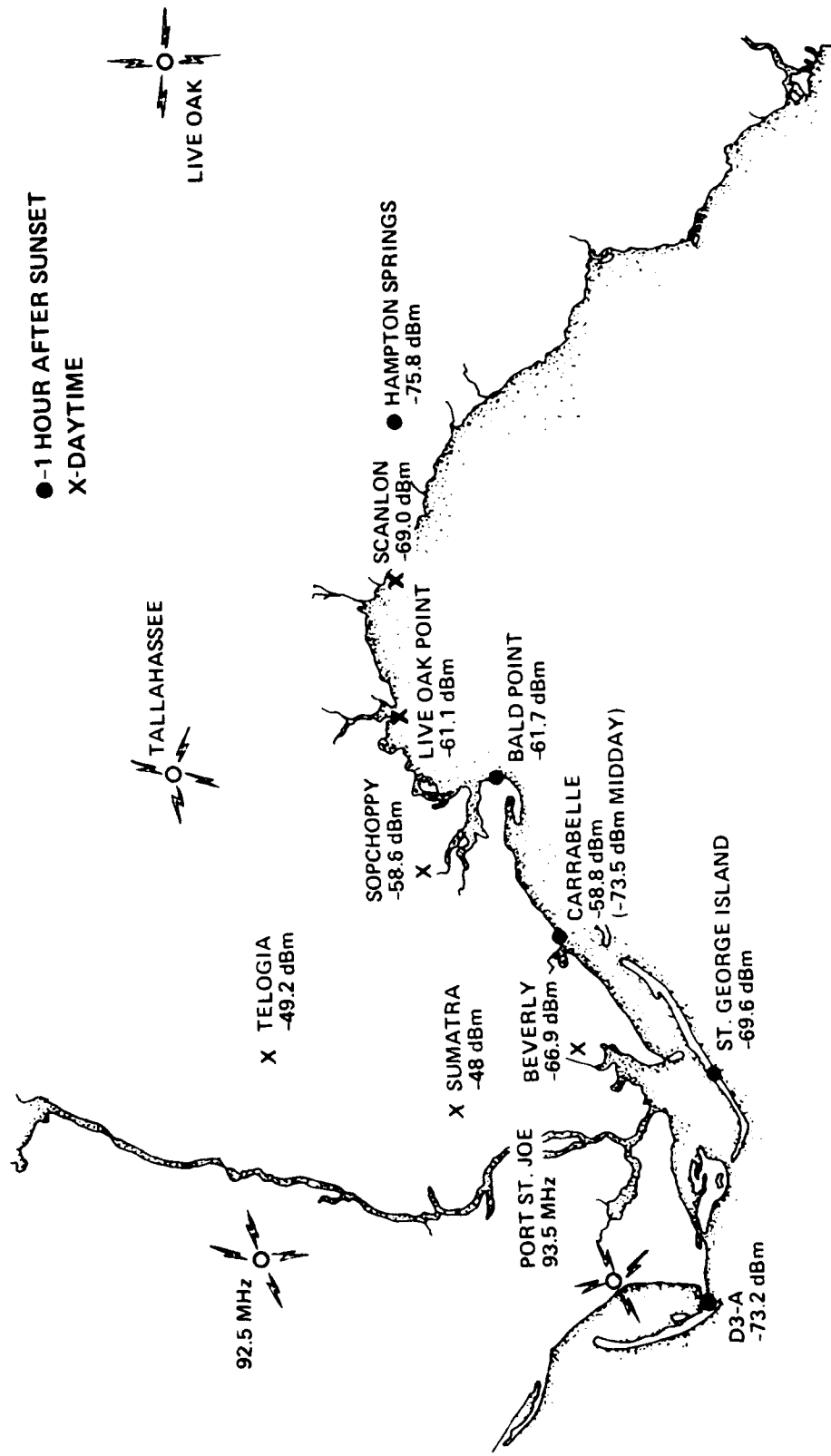
Figure A-21. RFI Measurement Summary, August 1980

A-37
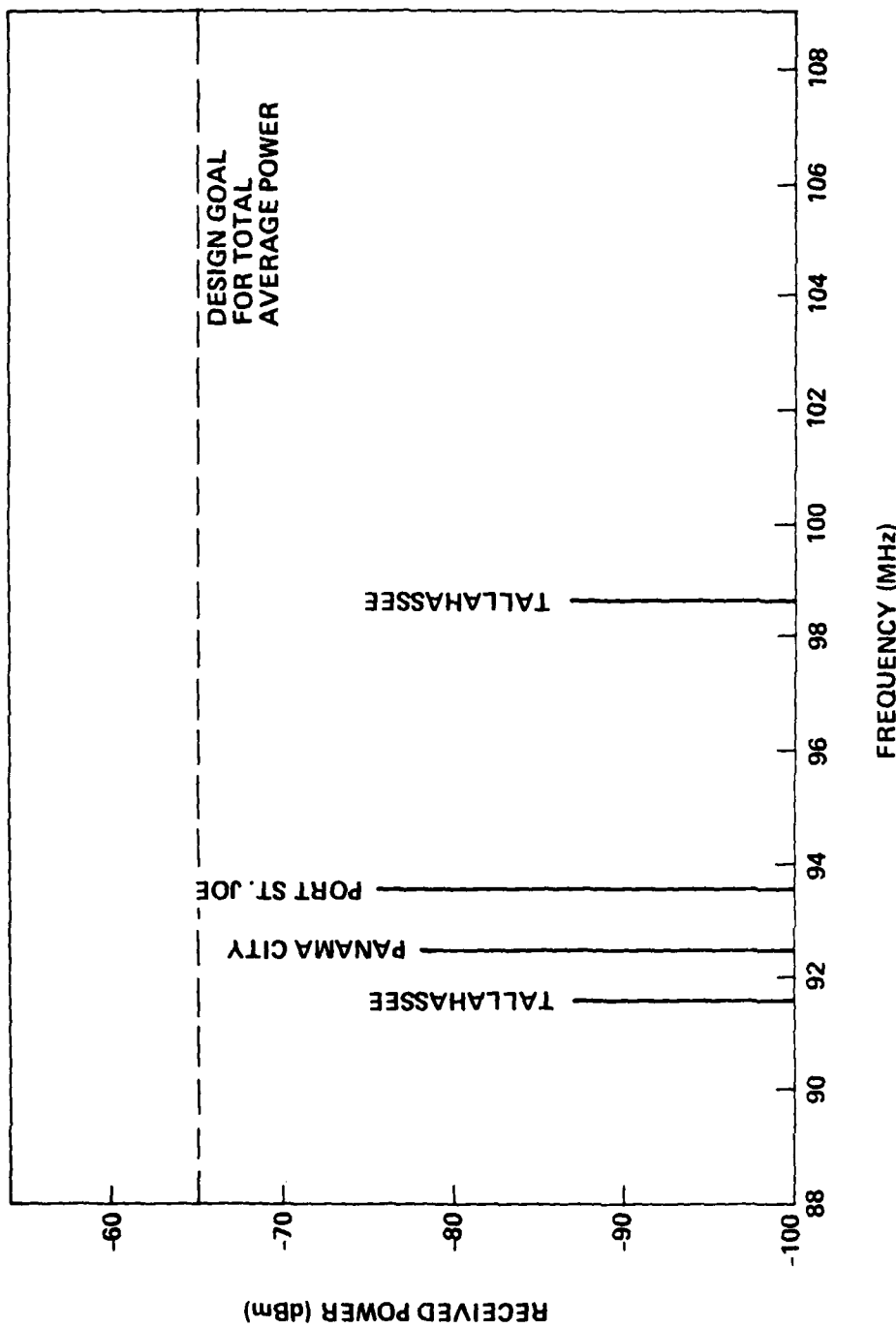
Figure A-22. Interference Spectrum at Sunset at Cape San Blas (D3A), August 1980
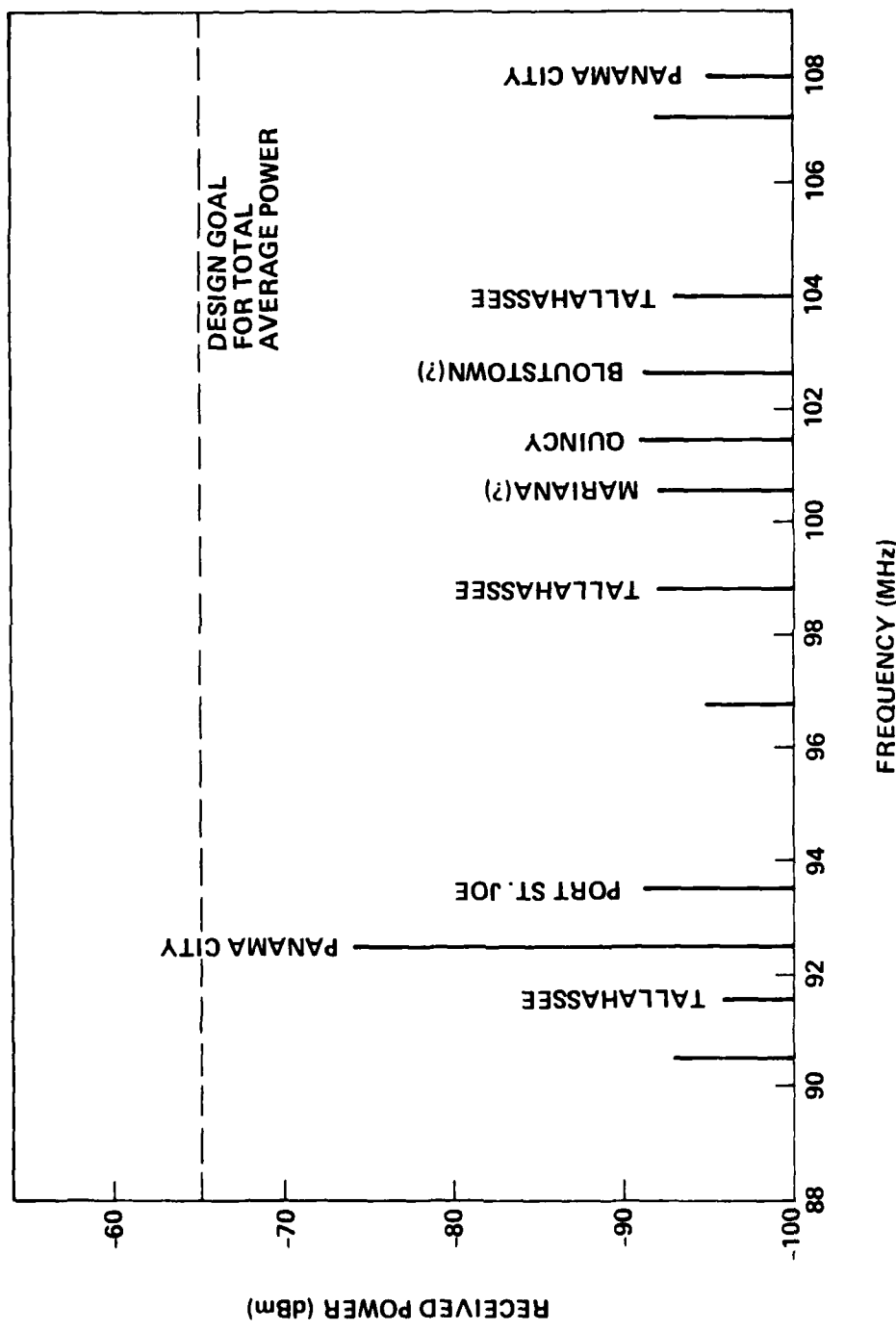
Figure A-23. Interference Spectrum at Sunset at St. George Island, August 1980

A-39

average interference power to be less than -65 dBm. The measured total average interference power was -73.2 dBm at Cape San Blas (D3A) and -69.6 dBm at St. George Island.

A-11   PROCESSING OF THE BEACON DATA.

The processing implemented for quick-look analysis of the beacon data began with the transfer of data from the 1 inch 13 track tape recorded in the field to a 1/2 inch ?-track IBM compatible tape. Because this transfer was between digital formats no sampling or conversion process was applied to the data. This step only involved redefining word sizes and record lengths used for tape storage. The actual procedure followed here is discussed in Section A-11.1.

The first step in preparing the data for analysis is a software initialization routine. Here the data is examined for parity errors and correct frame synchronization. Words in parity error are corrected through interpolation. Synchronization errors, where the actual relation between recorded words and their chip delay is lost, would be more difficult to correct. Fortunately, synchronization errors occurred infrequently and did not affect data over times during occultation. The processed data is sorted into continuous representations of the complex impulse response and stored on disk. It was the magnitude of the disk records that were illustrated in this report. The initialization process is explained more completely in Section A-11.2. Calibration of this data, making use of the calibration sequence recorded before and/ or after the beacon launches, was not done for this quick-look at the data; but is planned during future processing. This calibration will remove the small nonlinearities inherent in the hardware.

A-11.1   Transfer of Beacon Data to Standard Format Tape.

Field collection of the beacon experiment impulse response was made on Sangamo Sabre III digital tape recorders. This recording was done at a tape
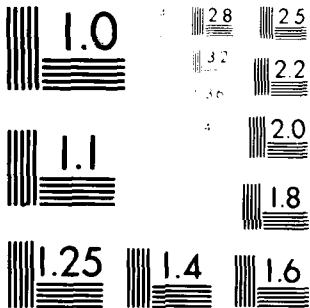
MICROCOPY RESOLUTION TEST CHART

speed of 120 ips in order to accommodate the large volume of information generated. The transfer of this data to a tape format acceptable for analysis by the general computer user is discussed in this section. The transfer is largely a hardware process, though a minicomputer is used for buffering the data before a final transfer to tape. This resultant recording is made on a 9 track tape at a density of 6250 bpi.

A simplified flow diagram of the processing appears in Figure A-24. The transfer hardware accepts three signals from the Sangamo recorder: an 11-bit data word; time code, and a copy of the system clock. The system clock is used as the drive for the transfer hardware. No processing is required of the time code, it is stored in a hardware buffer until a tape record is written, whereupon it is used as the time for that record.

There are two basic purposes behind the operation of the transfer hardware on the data words. Its most important task is the recognition of the synchronization word which signals the beginning of the 180 word data stream. Without this synchronization information it would be impossible to correctly establish where the impulse response occurs within the delay window. These 180 word (90 complex samples) segments represent one measurement cycle of the hardware and are referred to as frames. The frames are transferred to minicomputer memory on a word by word basis for temporary storage. The second basic task performed by the hardware is counting the frames read, accomplished by driving a counter from detection of the sync word. The frame counter is used to control final storage of the data, signalling the computer to create a tape record after the accumulation of 13 frames. An important feature of the hardware lies in its ability to generate its own sync. Once the sync word is detected, the fact that it should occur again after 180 data words can be used to predict the location of its next occurrence. This predicted sync is referred to as the generated sync signal in Figure A-24. Should it occur that sync not be detected over some number of frames, this generated signal can be used to prevent loss of the data.
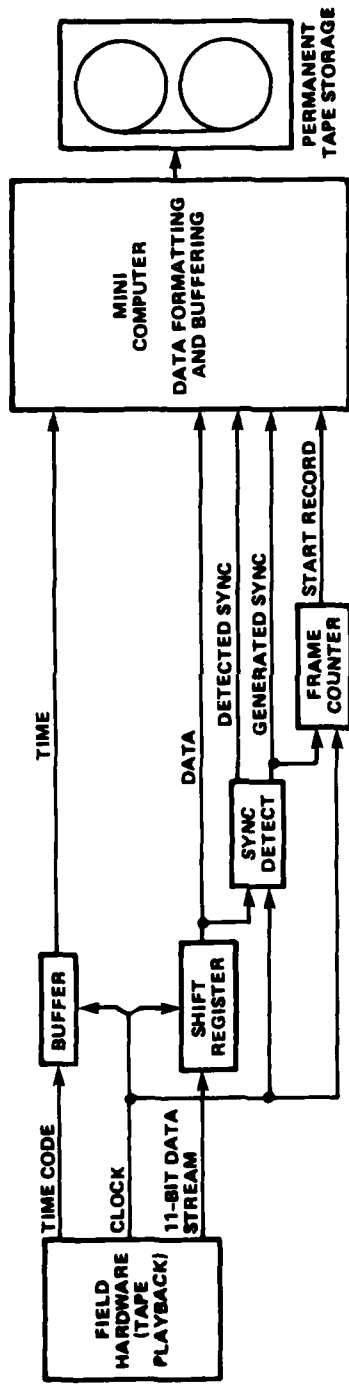
Figure A-24. Transfer of Beacon Data from Field Recording to Standard 9 Track Computer Compatible Tape Format

There are several omissions made from Figure A-24 to preserve clarity. The most important of these are a parity error detector and counter and a set of counters to keep track of synchronization loss and record loss. These quantities are monitored during the transfer operation to detect any problems that might be occurring. No serious difficulties were encountered. Also not shown is the handling of various auxiliary values recorded in the field and transferred to the final tape record. These quantities included the C-band tuning voltage and signal level, the delay offset added to the recorded data, and an overall system status word.

A-11.2   Preliminary Software Processing.

With completion of the transfer of the field recordings to 9-track tape this data could be easily scanned for time periods of interest. The periods about occultation were located and transferred to disk storage. It is those records transferred to disk which were presented in Section 2-3. In part because of data integrity preserved during the measurement, recording, and transfer steps little processing had to be performed on the data prior to presentation in this document. The software processing undertaken is shown in Figure A-25. Due to the low error rate encountered a simple interpolation scheme was employed to correct words found to be in error.

Operation of the software takes place on two levels. An outer loop reads through the new data tape until the record closest to the time of interest is located. This record, representing 13 frames or impulse response recordings, is then passed to an inner program loop. This loop processes the data frame by frame, and when finished with a record creates a disk file. The outer loop then supplies another record to the frame processing section, and this iteration continues until the desired time interval has been processed.
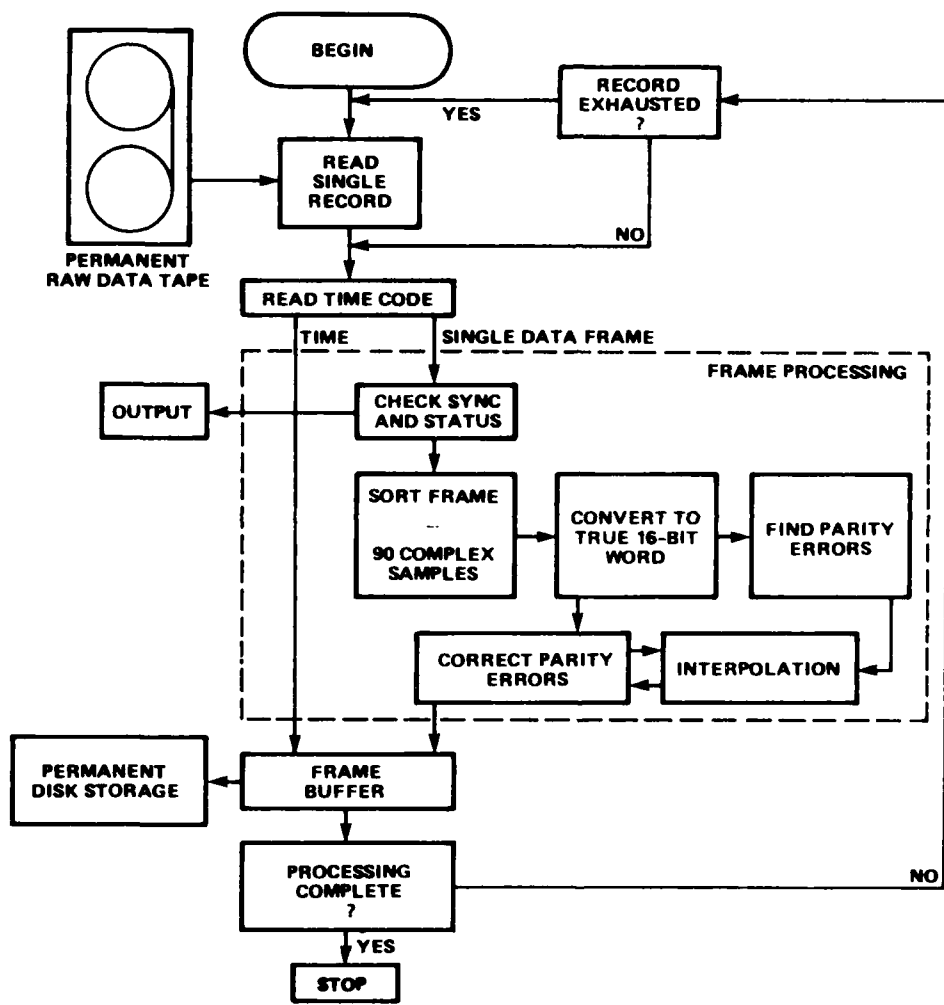
Figure A-25. Preliminary Software Operations on the Beacon Impulse Response

A-44

The inner loop performs both data sorting and correction of parity errors. The need for sorting arises from the hardware steps in computation of the impulse response. This response is computed as nine values spaced in delay 3-1/3 chips, and the process repeated 10 times at 1/3 chip intervals to determine the total form of the response. The first task of the software is to sort the recorded data into a representation of continuous delay.

The second task performed involves searching the data for parity errors. Prior to this search the words, which are still represented as 2's complement integers of 11 bit length with 5 bits of padding, are converted to the 16 bit format valid for machine arithmatic. Each frame is then scanned for parity errors, and the offending words flagged for future correction. Word correction was a simple matter for this data, largely because of the low error rate encountered. Table A-4 presents the error rates experienced. The highest rate was at St. George Island. Another contributing factor allowing a simple error correction scheme is the manner in which the data was recorded. The non-continuous format performs as data interleaving which eliminates serious data losses occurring due to the bursty nature of tape dropouts. Correction of any word found in error is performed by replacing the word with the result of an interpolation between its nearest error free neighbors. This completes the processing undertaken on the data, with the results presented in preceeding sections of this report.

Table A-4. Errors Encountered in Processing the Recorded
Impulse Response Functions

Data Recording		Bit Error Rate (x 10^-6)	Occurrence of Sync Loss
San Blas	Beacon 1	2.5	1
	Beacon 2	3.2	1
St. George	Beacon 1	6.1	0
	Beacon 2	9.6	2

A-46

APPENDIX B

AIRCRAFT EQUIPMENT CONFIGURATION

B-1   CONFIGURATION.

The aircraft equipment configuration to be used during the PLACES
experiment is shown in Figure B-1. Also shown on Figure B-1 are the track
assignments used in recording the data both on the Ampex AR-200 analog tape
recorder and on the 8-channel strip chart recorders.

The format shown for the analog tape recorder is essentially the
same as that used during the STRESS Experiment. The 8-channel strip chart
recorder format is new and is intended to accommodate and display the uplink
fading data together with the downlink data. The display of the K-band video
spectrum is intended to provide a reference as to the status of K-band lock and
it divides the uplink and downlink data on the chart display. The log envelope
output on the uplink tone processor has degraded to the point where it is
believed to be of marginal quality, and thus was not recorded. The aircraft
heading data from the INS is recorded on the analog tape recorder on one of the
standard channels.

The Dorne Margolin antenna is used for the UHF uplink. The uplink
power must be set to a point approximately 6 dB below saturation at the
satellite. This procedure is described in Section B-2.

The Collins Crossed Dipole is used for receipt of the UHF downlink
tone. The downlink tone processor divide ratios and synthesizer settings are
presented in Section B-3.2. The choices vary depending upon which satellite
is used. Likewise, uplink synthesizer and divide ratio are presented there.

The downlink tone and a 1 kHz reference tone (PRE-D + 1 kHz) are sent
over a 500 kHz channel on the Atlantic FLTSATCOM satellite to the CCF. This is
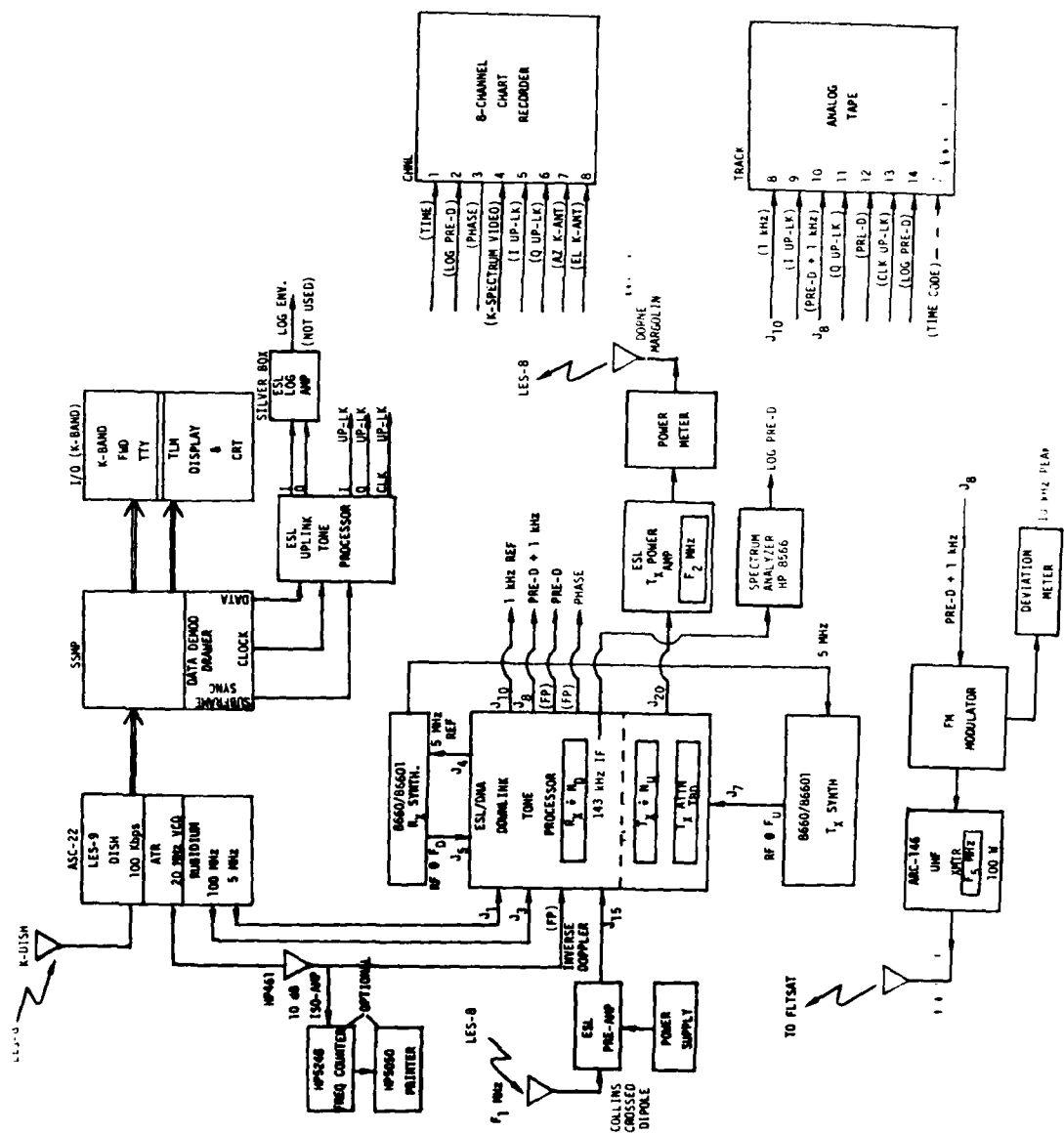
Figure B-1. Aircraft Equipment Configuration

the same signal as is recorded on Track 10 of the analog recorder. It is to be
FM modulated using a 10 kHz peak frequency deviation under non-fading conditions.
Using a 50 kHz IF receive bandwidth at the Eglin ground station, a peak signal
enhancement (focus) of approximately 9.5 dB can be accommodated without distor-
tion. It is important that an AGC not be used at the modulator otherwise long
signal enhancements (focus and defocus) are not accurately reproduced. This
link is discussed further in Section B-4. A blade antenna on the top side of
the aircraft will be used for this link together with the ARC-146 transmitter.
Only approximately 100 watts of the 1 kW available transmitter power is required.

The LES K-band receiver provides the K-band doppler to the downlink
tone processor on a 20 MHz carrier. The K-band receiver also demodulates the
I-Q uplink samples sent down on this K-band link. These samples are output to
the uplink tone processor along with subframe sync and clock data.

B-2   UPLINK TONE POWER SETTING.

This operating point is found by measuring the magnitude of the
uplink I and Q outputs of the uplink tone processor versus the uplink tone
power. The uplink power is then set 6 dB below the point at which the output
signal power (I^2+Q^2) no longer linearly varies with the uplink tone power.
The resulting signal should be close to the point at which the signal-to-noise
ratio in the satellite 75 kHz IF bandwidth is 0 dB. The signal-to-noise ratio
is approximately measured and sent down over the K-band telemetry link to the
command terminal where it is displayed. The calibration procedure described
above is followed prior to each release and immediately following the experiment.

B-3

B-3   LES SATELLITE CONFIGURATION.

B-3.1   LES Satellite Mode Configurations.

Table B-1 lists the modes the LES-8 and LES-9 satellites should be in for the PLACES experiment in the parlance of the LESOC. Since both LES-8 and LES-9 are currently located near 105°W, either satellite is equally good from a geometry standpoint. If it is possible to use the high power mode on LES-9, then much improved data quality would result and it would be preferred. No mode changes are necessary during the experiment unless RFI is encountered. The frequency settings are presented in Section B-3.2.

The proper pointing of the dish antenna may vary as a function of time. If it becomes necessary to repoint the antenna during the experiment, the aircraft notifies the CCF on the air-to-ground link and the CCF contacts the LESOC.

B-3.2   LES Frequency Selection.

Table B-2 lists the frequency pairing used during the experiment. The same downlink (F_1 or F_3) and uplink (F_2 or F_4) frequency pair as used during the ESTHER release should be used with LES-8. The corresponding satellite synthesizer octal and decimal codes are listed for convenience. Likewise, the synthesizer settings (R_x and T_x) for the downlink tone processor are given.

Due to aging of the satellite oscillators and due to frequency set-tability constraints the optimum settings may vary slightly. The preferred setting, of course, is the one that results in the least residual total fre-quency offset error, e.g., on the downlink tone the output should be exactly 500 Hz. The setting on the uplink tone can be checked by noting when the

Table B-1. LES Satellite Configurations for DNA PLACES Experiment

Configuration	UP & DNLK Tone Data	UP & DNLK Tone Data
Satellite	9	8
Lo Rate Data Source	TLM	TLM
Horn Xmit	Lo Rate	Off
Dish Xmit	U	U
UHF Xmit	Synth	Synth
Power	40 or 6 watts	6 watts
WOD #	2	3
DNLK Synth[2]	Stop at F1	Stop at F3
UPLK Synth[2]	Resultant (at F2)	Resultant (at F4)
HOP Int.	200 ms	200 ms
UPLK Ant.	UHF	UHF
BB Demod.	Sampler	Sampler
Data Rate	100 Kbps	100 Kbps
XLK Ant.	Dish	Dish
Dish Ptg.	(30°N, 85.5°W)[1]	(30°N, 85.5°W)[1]

[1]Maintain pointing throughout mission, precise coordinates to be provided day of test.

[2]See Table B-2 for F1, F2, F3, and F4.

Table B-2.   LES-8 Frequency Selection Pairing for Uplink and Downlink Tones Used During PLACES

DOWNLINK

K-Band Source	ih	Freq (MHz)	Doppler Error (Hz)	Satellite Synth Octal	Satellite Synth Decimal	HP 8660 Synth (Hz)	Freq offset error (Hz)
LES-8 Dish 38.04 GHz	152	250.326.591 6	.08	46.0344	1268892	40.784.313	-.35

UPLINK

ih	Resultant Sat. Freq. (MHz)	Satellite Synth Octal	Satellite Synth Decimal	HP 8660 Synth (Hz)	Transmit Freq (MHz)	+ Doppler Correction (Hz)	Uplink Doppler Error (Hz)	Total Freq Offset Error (Hz)			Comments
112	339.644 726 6	0650345	217317	59.823.247	339.644 726 6	+.453	.02	-.03			used during ESTHER
					339.644 726 6	+.453	.00	-.03			improved choice

B-6

uplink I and uplink Q outputs do not change. These can be checked before the aircraft is in flight. The residual doppler error will increase slightly when in flight.

Because the satellite uplink frequency setting is tied to the downlink frequency setting and because only certain pairs result in a small frequency offset error these were precalculated and available in case interference is encountered. If none of these pairings are possible, then the uplink tone can be dropped and a suitable frequency for the downlink tone used. For that reason, several alternate frequencies were also computed for the downlink for which an uplink pair was not possible. Some of these frequencies are sub-optimal from the hardware standpoint.

B-4   REAL TIME RELAY THROUGH FLTSATCOM.

The aircraft fading data was relayed through FLTSATCOM to the B-4 site at Eglin AFB and from there a microwave link to the CCF building for processing as depicted in Figure B-2. The signal format that is sent to the CCF is the same signal format that is recorded on the 662 aircraft. The fading signal is at 500 Hz and is essentially contained within a 10 Hz bandwidth. A 1 kHz reference signal equal in amplitude with the 500 Hz tone under non-fading conditions is sent as a reference to be used by the ground processing software to eliminate any frequency translation errors in the telephone equipment, any slowly varying amplitude and phase variations in the transmission path or on the telephone lines, and any error in the sampling rate of the A/D converter at the ground.

There are two FLTSATCOM satellites in view of the Eglin area, one over the Pacific Ocean at 100°W (Az≈205.2°, El≈52.1° from B-4) and one over the Atlantic Ocean at 23°W (Az≈103.8°, El≈14°). It was preferable to use the Atlantic satellite as the link to the Pacific satellite encounters the same fading as the LES-8/9 UHF tone signal for a 30 to 45 minute period.
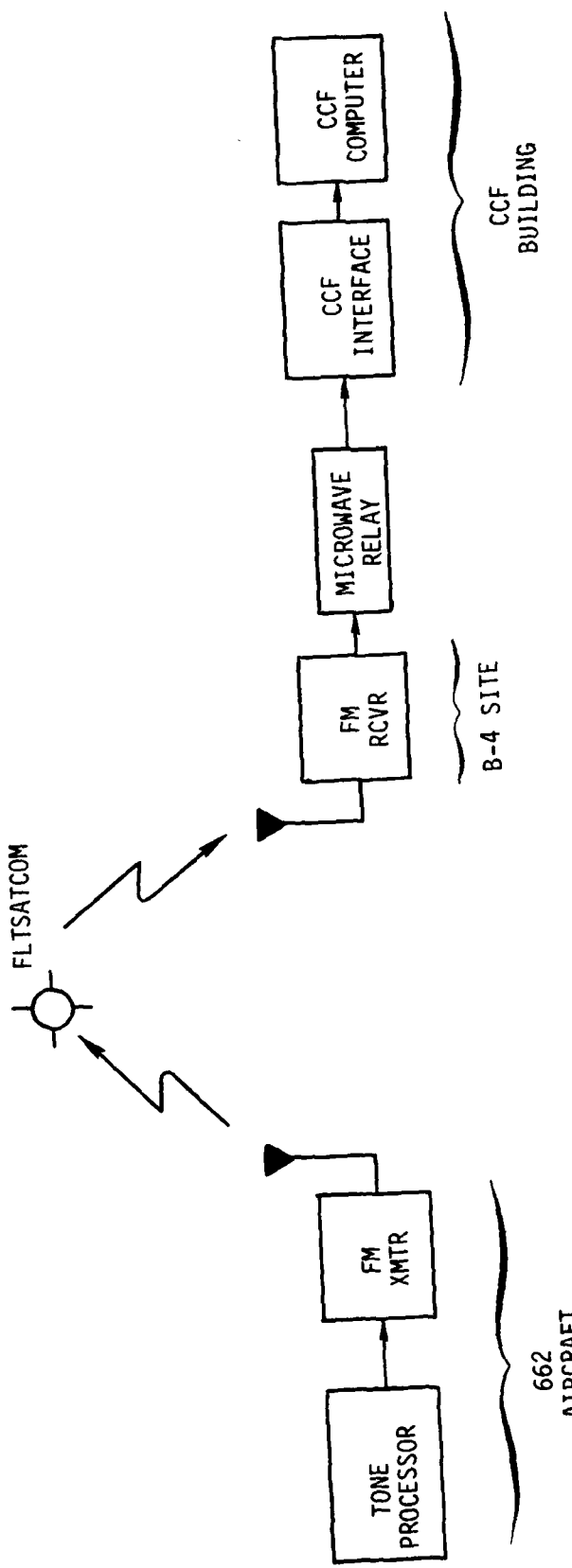
Figure B-2. Real Time Data Relay

The 500 kHz wideband transponder channel was used to support the mission. Table B-3 provides a link calculation for this channel. Approximately 100 watts of power is required at the aircraft (ARC-146) to produce a 12.9 dB carrier-to-noise ratio at the ground receiver which has a 50 kHz IF bandwidth at the input to the FM demodulator. The ground antenna has 10 dBi of gain (circular-to-linear polarization). As indicated there is approximately 6 dB margin available if a 7 kHz peak frequency deviation is provided at the aircraft under non-fading conditions. This was increased to 11 kHz following some early link tests to further improve the signal quality. No AGC was used at the transmitter in order to keep from distorting long signal focus or defocus regions of fading. With a 7 kHz peak frequency deviation under non-fading conditions and a 50 kHz receiver IF bandwidth, a peak signal enhancement (focus) of approximately 9.5 dB can be accommodated without distortion.

B-5   AIRCRAFT EXPERIMENT CONTROL AT THE CCF.

B-5.1   Introduction.

The key to improved data quality are the improved real time aircraft and cloud tracking displays at the CCF in conjunction with the real time display of fading as seen by the aircraft and sent to the CCF via a FLTSATCOM relay link. Additionally, near real time data processing was conducted to ensure the highest possible quality of data results from the aircraft positioning.

B-5.2   Aircraft and Cloud Radar Tracking Data Display at CCF.

A display of the aircraft and barium ion cloud shadow positions are necessary to the experiment in order to vector the aircraft through the barium cloud shadow at the proper azimuth. This display was used primarily by the aircraft controller. The cloud shadow is generally expected to move southeast

Table B-3. Link Calculation for FLTSAT Real Time Relay -
500 kHz Channel

a/c to Satellite   Comments

XMTR Power	20 dBW	Min. required
Antenna Gain	2 dBi	
EIRP	22 dBW	

Space Loss	173.9	@ 296 MHz @ 14 deg. elevation
Polarization Coupling Loss	0.3 dB	
G/T Satellite	-16.7 dB/°K	
Boltzmans Constant^{-1}(K^{-1})	228.6 dB-°K-Hz/W	
C/kT	59.7 dB-Hz	
Inverse Bandwidth	-57.0 dB-Hz	500 kHz Channel
SNR @ Limiter	2.7 dB	
Limiter Gain	2.5 dB	
SNR after Limiter	5.2 dB	

Satellite to B4 Site

EIRP	25.6 dBW	RHCP
Power Sharing Loss	~1.1 dB	No other users
Space Loss	172.9 dB	@ 262 MHz
Polarization Coupling Loss	0.3 dB	
Antenna Gain	10.0 dBi	(13 dBi Linear)
Received Power	-138.7 dBW	
kT	-198.6 dBW/Hz	1000°K Noise Temp
C/kT	59.9 dB-Hz	
Inverse Bandwidth	-47.0 dB-Hz	50 kHz
CNR	12.9 dB	(~6 dB Margin)
FM Improvement	35.7 dB	7 kHz Peak Frequency Dev.
SNR in 1 kHz	48.6 dB	$\approx 3/2 \ (f_d/f_m)^2$

$$(B_{IF}/f_m) \ CNR$$

NOTE:

8 dB CNR gives 31.5 dB SNR
7 dB CNR gives 26.1 dB SNR
6 dB CNR gives 21.6 dB SNR

at 50 to 100 meters per second and presents a moving target to the aircraft controller. The barium cloud is released at 185 kilometers altitude in the ionosphere. The aircraft must be positioned to fly through the shadow at the aircraft altitude (~40,000 feet) cast by the barium cloud to energy coming from the LES-8 satellite which is in a figure-eight orbit near 108°W. The flight path of the aircraft through the shadow is such that the plane flies perpendicular to the projection of the earth's magnetic field lines from the satellite. This geometry sweeps out the striated portion of the barium cloud in the minimum time, improving the system phase stability and provides an easy to interpret propagation geometry. Occasionally the aircraft may be vectored to fly along the field line projections to test the diffusion properties of the plasma along the field lines.

The cloud tracking data (cloud projection point, its drift velocity vector, and field line projection cross) were to be supplied to the CCF through a real time link from the AN/FPS-85 radar.

An ability to compute the current position of the cloud from past data was provided in case the radar lost track of the barium ion cloud. This problem occurred several times during the STRESS experiment in 1977. It was thought possible to track the cloud for 30 minutes or more without the radar by a combination of past data, a future position calculation, and the real time fading data from the aircraft. In actual fact, the real time fading display along with the aircraft location data proved adequate for several hours during GAIL and JAN. At other times it was possible to use the TV track data to position the aircraft.

B-5.3   Real Time Fading Data Display and Relative Aircraft Position.

A real time display was provided at the CCF of the fading signal as received on the aircraft and a corresponding display of the aircraft track with respect to the cloud center. These displays provide a real time history

of fading as a function of the aircraft position relative to the radar cloud track point and thus allow a more precise control of the aircraft.

B-5.4   Display of Barium Cloud Phase Structure.

A display of the cloud phase structure that produced the received fading signal was provided at the CCF as an aid in assessing the behavior of the striation structure in real time. This provides an indication of cloud breakup or bifurcation that could result in the radar tracking one of two objects after a time. Likewise, the character of the striations along various altitude cuts by the propagation path could potentially be assessed in real time and correlated with the received signal. It was though this data would help insure that the aircraft continues to traverse the same striated object from pass to pass and thus, a truer picture of striation evolution will result. The cloud phase structure is obtained by back-propagating the aircraft received signal. Unfortunately, this provied too time consuming to be effectively accomplished in real time. Thus, the back-propagation processing was only occasionally done.

B-5.5   Barium Cloud Ionization Contour Plot.

In order to better ascertain what portion of the cloud the radar is tracking, a static display fo the cloud shape given by an ionization contour was to have been provided to the CCF by the FPS-85 radar. This display it was thought would provide an early indication of tracking difficulties. Unfortunately, the software at the FPS-85 to provide this data was not available in time for the experiment.

B-6   LINK CALCULATIONS.

The link calculations for the downlink UHF tone is provided in Table B-4. The predicted received carrier power-to-noise power density ratio

Table B-4. Link Calculation Downlink Tone to Aircraft

XMTR Power	37.8 dBm	6W
Antenna Gain	9 dB	
EIRP	46.8 dBm	
Space Loss	171.9 dB	@ 245 MHz El=35° R=38,193 km h_s=35,800
Polarization Loss	0.4 dB	3 dB to 3 dB El=50° R=37,091 SL=171.6 dB
Receiver Gain	3 dBi	
Received Power	-122.5 dBm	
Noise Density	-168.6 dBm/Hz	T=1000 degrees
C/kT	46.1 dB-Hz	
Noise Power	-148.6 dBm	100 Hz BW - real time a/c indicator?
a/c Strip Chart SNR	26 dB	Real time on a/c
Noise Power	-156.8 dBm	15 Hz BW Real time @ CCF
SNR	34.2 dB	CCF displays

(C/KT) is computed to be 46.1 dB-Hz. The value measured during the STRESS experiment was 46 to 47 dB and will vary somewhat from pass-to-pass depending on the aircraft antenna coupling to the satellite. The LES-9 satellite potentially at least could be used in a high power mode. This would result in approximately 8 dB higher signal levels at the aircraft.

The real time fading indicator on the aircraft uses the log output of an HP 8566 spectrum analyzer. The detection bandwidth is approximately 100 Hz providing a signal-to-noise ratio of 26 dB on the real time strip-chart display.

The ground processing software at the CCF uses a 15 Hz bandwidth, resulting in approximately 34 dB SNR on the CCF real time displays.

Table B-5 provides a link calculation for the uplink tone. The uplink power level is set to approximately 0 dB SNR at the satellite. The corresponding effective C/KT is approximately 42.8 dB-Hz. During the STRESS experiment the uplink power was set by noting when the satellite output signal power began to compress as the uplink power was increased. The uplink power was then backed off about 8 dB. This would have resulted in a C/KT of approximately 38 dB-Hz at the satellite. A value of around 39 dB-Hz was observed in the ESTHER data.

The real time fading indicators use 256 bit averaging windows on the I and Q data, which corresponds to approximately a 360 Hz bandwidth or 17.2 dB SNR. Post processing the data in 1024 bit windows results in approximately 23 dB SNR. These outputs can be averaged further as necessary.

Table B-6 gives an approximate link calculation for the K-band down-link to the 662 aircraft. This calculation indicates there is approximately 4 dB of margin at the 100 Kbps data rate. A dB or so of implementation loss in the modem along with possible satellite output power degradation over time and potential antenna pointing errors could make this link somewhat marginal.

Table B-5. Link Calculation Uplink Tone Aircraft-to-Satellite

XMTR Power	44.4 dBm	(27.5W) Adj. for 0 dB SNR (100W max)
Antenna Gain	2 dBi	+2 dB
EIRP	46.4 dBm	
Space Loss	175.9 dB	@ 388.4 MHz, 35°E1, R=38,193
Polarization Loss	0.5 dB	+0.5 dB 5 dB to 3 dB
Receiver Gain	10 dBi	+1 dB
Incident Power	-120.0 dB	+2.3 dB
Noise Density	-167.8 dBm/Hz	
C/kT	47.8 dB-Hz	
Noise Power	-120 dBm	+1 dB in 60 kHz
SNR	0 dB	+2.5 dB at input to limiter
$SNR_{AL/samp}$	-5 dB	Simulation results (after limiter and Sampler)
$C/kT_{AL/samp}$	42.8 dB	
SNR	17.2 dB	in 256 bit window (~360 Hz BW) real time
SNR	23.2 dB	in 1024 bit window (~90 Hz BW) post process

Table B-6. Approximate K-band Downlink Calculation

XMTR Power	26.2 dBm	(.4 watt)
Antenna Gain	42.6 dBi	(3' dish)
EIRP	68.8 dBm	
Space Loss	216.0 dB	@ 38 GHz
Receiver Ant. Gain	47.0 dBi	
Received Power	-100.2 dBm	
Noise Power Density	-164.5 dBm/Hz	9.5 dB noise figure
C/kT	64.3 dB-Hz	
Loop SNR	50.3 dB	25 Hz BW
E_b/N_o Required	10.3 dB	10^{-5} BER DPSK
R	50 dB	100 Kbps
C/kT required	60.3 dB/Hz	
Margin	4.0 dB	

The tracking loop SNR is, however, high and thus there is ample margin to loss of phase lock (and thus loss of the downlink tone doppler correction).

B-7   DOWNLINK TONE PROCESSING.

The measurement of phase data on the downlink tone is made possible by phase referencing the UHF tone to signals divided down from the LES-8 or LES-9 100 Kbps K-band doppler signals. The downlink tone fading is measured, recorded and processed in the same manner as during the STRESS Experiment (Reference 3).

Recordings of the downconverted doppler corrected signal is the real time outputs of each flight test. The UHF signal is downconverted to a frequency that is nominally 500 Hz. Recorded on the same FM tape track is a 1 kHz reference tone. The same 1 kHz reference tone is also recorded alone on a separate tape track. Analog tape data is processed after the test in the ESL Tape Center. The analog 500 Hz plus 1 kHz track is 8-bit digitized at a 4K sample per second rate and stored on digital tape for subsequent computer processing. The nominal level of the 500 Hz signal on the tape is equal to the 1 kHz reference signal level during nonfading signal conditions. An IBM 4341 software demodulator program is used to convert the digitized analog data into a format suitable for plot generation and back-propagation. The output of the demodulator software is the amplitude and phase of the envelope of the 500 Hz data sampled at a 100 sample pairs per second rate and formatted into 2048 point files. Plots of the amplitude and phase are generated by a subsequent software routine and are back-propagated.

B-8   UPLINK TONE PROCESSING.

Obtaining data from the aircraft uplink to the LES satellites involved a significant amount of data processing as described in Reference 3. The aircraft transmits signals that are doppler precorrected.

The systems on the satellite which process the UHF uplink tone transmitted from the aircraft are as follows. The signal received at the satellite is amplified by the UHF FRONT END. The DOWNCONVERTER downconverts the signal from UHF to HF. The "SAMPLES" BASEBAND CONVERTER hard limits the signal, downconverts it to baseband, and converts the coherent and quadrature outputs of the baseband downconversions to digital data streams using 1-bit sampling (hard quantizing). The SIGNAL PROCESSOR formats the sample data stream together with synchronization and telemetry data. The formatted data is DPSK modulated and sent via K-band back down the aircraft. The K-dish system must be used to transmit the high data rate required.

The DOWNCONVERTER acts as simple mixer and merely translates the uplink UHF signal down in frequency. The actual DOWNCONVERTER on the satellite is some-what more complex than its name would imply, but the effective translation is the same. The first BPF of the BASEBAND CONVERTER filters the translated signal to a bandwidth of 75 kHz. The hard-limiter system (HL/FIL) hard limits the received signal and filters out the higher frequency components from the hard-limiter output. The signal is then mixed down to baseband with an I-Q mixer. The I arm and Q arm signals are low-pass filtered to a cutoff frequency of 35 kHz before they are 1-bit sampled each at a 50 kilobit per second rate.

The SIGNAL PROCESSOR uses a 50-bit frame format into which the I and Q samples are put. The first bit position is for the SYNC bit which is always a "1" and is conventionally used by the reportback and crosslink demodulators to achieve frame synchronization. The next bit position is dedicated to bits of the forward message. The third and fourth bit positions are dedicated to telem-etry information and the fifth through fiftieth bit positions carry the I and Q samples alternating between I and Q. In the formatting process, some of the I and Q samples from the BASEBAND CONVERTER are dropped in order to accommodate the bits in the 1 through 4 bit positions. Two out of 25 bits are lost from both the I and Q channels in this manner. The effective I and Q data rates are, as a consequence, each decreased to 46 kilobits per second.

This transmitted data stream is to be demodulated and processed at the aircraft for eventual recovery of the inphase and quadrature signals. The technique used in recovering the signals from the hard quantized data relies on the fact that the diffracted field received at the satellite is of a low power, comparable to the received noise power. As each bit in the sample stream is a measure of whether or not the signal plus noise voltage at some instant of time is greater than 0, the summation of a number of these bits over an interval represents a probability estimate of this voltage being greater than 0 within that interval. It is this computed probability that will be used to recover the original I and Q signals. In the aircraft the demodulated data stream is sorted and serially fed into a pair of 256 bit shift registers and UP/DOWN counters. By comparing the delayed bit from the shift register with a current bit from the I/Q sort, the counters generate a running sum of the number of 1's in a 256 bit window. The counter output is then converted once every 2.78 milliseconds to an analog voltage, displayed on strip chart, and FM recorded on analog tape along with time frame data. Computer implemented processing to follow this step treats the recorded data as probability estimates made over the window time frame. At the incoming data rate of 46 Kbits per second this 256 bit window derives its probability estimate from a 5.56 milliseconds window.

At ESL, the recordings of the samples are processed to estimate the propagation parameters of interest by estimating the voltages in the I and Q channels at the satellite. The SYNC bit will be identified and the bits in the first 4 bit positions of the frame will be ignored. The I samples will then be separated from the Q samples, the two streams being used to estimate the coherent and quadrature components of the diffracted signal envelope.

The I and Q samples carry information about the signal amplitude and phase statistically. The tone transmitted by the aircraft is intentionally given a relatively low output power level so that the signal strength at the satellite is about equal to the noise power in the hard limiter - hard quantizer processing

bandwidth. Decisions of the hard quantizer are thereby influenced not only by the signal but also by the noise. The noise is almost independent from sample to sample and influences each decision independently. The signal strength in either the I or Q channel is slowly varying and for this reason the signal influences many consecutive decisions. By noting the trend of the samples over periods when the signal is approximately constant, not only can the presence of the signal be detected, but its strength relative to the noise power can also be evaluated. This fact is the basis of the data reduction scheme used to measure amplitude and phase.

Recovery of the signal can be demonstrated by considering a function of the form:

$$s(t) = A + n(t) . \tag{1}$$

Here A represents the I or Q channel signal and $n(t)$ is the white Gaussian noise of variance σ^2 present in the channel. For the case of concern, I and Q may be taken as constant since the dependency of the barium induced fluctuations on time is much slower than the variation of the noise. Over the 5.56 milliseconds window over which probability is estimated, A is essentially constant. The data obtained for the uplink configuration confirms these assumptions.

As $n(t)$ is a zero mean Gaussian noise process over the processing bandwidth, the probability that $s(t)$ is greater than 0:

$$P[s(t) > 0] = \frac{1}{\sqrt{2\pi\sigma^2}} \int_{-A}^{\infty} e^{-x^2/2\sigma^2} \, dx . \tag{2}$$

If a quantity $\hat{p}$ is now defined as the function of samples in a string of samples (the 256 sample window) that are greater than 0, it will approximate the above probability. The output realized by the up-down counters, scaled by 256, is

this estimate. It remains to implement the inverse of the above equation so that A can be obtained from $\hat{p}$. Rearranging Equation (2) yields:

$$P[s(t) > 0] = \frac{1}{\sqrt{2\pi}} \int_{-\infty}^{A/\sigma} e^{-x^2/2} \, dx$$

equivalently:

$$\hat{p} = \frac{1}{\sqrt{2\pi}} \int_{-\infty}^{A/\sigma} e^{-x^2/2} \, dx \ . \tag{3}$$

Software processing uses Equation (3) to generate a table of values of $\hat{p}$ and A/σ from which the ratio of I or Q to noise variance can be obtained from $\hat{p}$. Noting that this method actually obtains A/σ and that σ is constant, the final amplitudes estimated are seen to be linearly scaled from the actual values. A complete signal processing description can be found in Reference 3.

DISTRIBUTION LIST

DEPARTMENT OF DEFENSE

Defense Nuclear Agcy
ATTN: NAFD
ATTN: STNA
ATTN: RAEE
ATTN: NATD
3 cy ATTN: RAAE
4 cy ATTN: TITL

Defense Technical Info Ctr
12 cy ATTN: DD

Field Command
Defense Nuclear Agcy
ATTN: FCP

Field Command
Defense Nuclear Agcy
Livermore Br
ATTN: FCPRL

Joint Chiefs of Staff
ATTN: C3S
ATTN: C3S, Eval Ofc

Under Secretary of Defense for Rsch & Engrg
ATTN: Strat & Space Sys (OS)

WWMCCS System Engrg Org
ATTN: R. Crawford

DEPARTMENT OF THE ARMY

BMD Advanced Technology Ctr
Department of the Army
ATTN: ATC-T, M. Capps
ATTN: ATC-O, W. Davies

US Army Chemical Sch
ATTN: ATZN-CM-CS

US Army Communications Cmd
ATTN: CC-OPS-W
ATTN: CC-OPS-WR, H. Wilson

US Army Nuclear & Chemical Agcy
ATTN: Lib

US Army Satellite Comm Agcy
ATTN: Doc Con

DEPARTMENT OF THE NAVY

COMSPTEVFOR
Department of the Navy
ATTN: Code 605, R. Berg

Naval Ocean Systems Ctr
ATTN: Code 5322, M. Paulson

Naval Research Lab
ATTN: Code 4780, S. Ossakow

DEPARTMENT OF THE NAVY (Continued)

Office of Naval Rsch
ATTN: Code 420
ATTN: Code 465
ATTN: Code 421

Strategic Systems Proj Ofc
Department of the Navy
ATTN: NSP-43
ATTN: NSP-2141
ATTN: NSP-2722, F. Wimberly

DEPARTMENT OF THE AIR FORCE

Air Force Geophysics Lab
ATTN: OPR, H. Gardiner
ATTN: OPR-1
ATTN: LKB, K. Champion
ATTN: OPR, A. Stair
ATTN: S. Basu
ATTN: PHP
ATTN: PHI, J. Buchau
ATTN: R. Thompson

Air Force Weapons Lab
Air Force Systems Command
ATTN: SUL
ATTN: NTYC
ATTN: NTN

Air Force Wright Aeronautical Lab
ATTN: W. Hunt
ATTN: A. Johnson

Air University Lib
Department of the Air Force
ATTN: AUL-LSE

Air Weather Service, MAC
Department of the Air Force
ATTN: DNXP, R. Babcock

Assistant Chief of Staff
Studies & Analyses
Department of the Air Force
ATTN: AF/SASC, W. Keaus
ATTN: AF/SASC, C. Rightmeyer

Electronic Systems Div
Air Force Systems Command
ATTN: OCT-4, J. Deas

Electronic Systems Div
Air Force Systems Command
ATTN: YSM, J. Kobelski
ATTN: YSEA

Foreign Technology Div
Air Force Systems Command
ATTN: TQTD, B. Ballard
ATTN: NIIS, Lib

DEPARTMENT OF THE AIR FORCE (Continued)

Headquarters Space Div
Air Force Systems Command
        ATTN: SKA, D. Bolin
        ATTN: SKY, C. Kennedy

Headquarters Space Div
Air Force Systems Command
        ATTN: YZJ, W. Mercer

Headquarters Space Div
Air Force Systems Command
        ATTN: E. Butt

Strategic Air Command
Department of the Air Force
        ATTN: DCXT
        ATTN: DCXR, T. Jorgensen
        ATTN: NRT
        ATTN: XPFS
        ATTN: DCX

OTHER GOVERNMENT AGENCIES

Central Intelligence Agcy
        ATTN: OSWR/NED

Department of Commerce
National Bureau of Standards
        ATTN: Sec Ofc for R. Moore

Department of Commerce
Natl Oceanic & Atmospheric Admin
        ATTN: R. Grubb

Institute for Telecomm Sciences
        ATTN: L. Berry
        ATTN: A. Jean
        ATTN: W. Utlaut

DEPARTMENT OF ENERGY CONTRACTORS

EG&G, Inc
        ATTN: J. Colvin
        ATTN: D. Wright

Lawrence Livermore Natl Lab
        ATTN: L-389, R. Ott
        ATTN: L-31, R. Hager
        ATTN: Tech Info Dept Lib

Los Alamos Natl Lab
        ATTN: D. Simons

Sandia Natl Lab
        ATTN: Org 1250, W. Brown

DEPARTMENT OF DEFENSE CONTRACTORS

Aerospace Corp
        ATTN: R. Slaughter
        ATTN: J. Straus
        ATTN: V. Josephson
        ATTN: I. Garfunkel
        ATTN: D. Olsen
        ATTN: T. Salmi
        ATTN: N. Stockwell
        ATTN: S. Bower

DEPARTMENT OF DEFENSE CONTRACTORS (Continued)

University of Alaska
        ATTN: Tech Lib
        ATTN: N. Brown
        ATTN: T. Davis

BDM Corp
        ATTN: T. Neighbors
        ATTN: L. Jacobs

Berkeley Research Assoc, Inc
        ATTN: J. Workman

University of California at San Diego
        ATTN: H. Booker

Charles Stark Draper Lab, Inc
        ATTN: D. Cox
        ATTN: J. Gilmore

Computer Sciences Corp
        ATTN: F. Eisenbarth

Cornell University
        ATTN: M. Kelly
        ATTN: D. Farley, Jr

E-Systems, Inc
        ATTN: R. Berezdivin

ESL, Inc
  4 cy ATTN: J. Marshall
  4 cy ATTN: G. Elston
  4 cy ATTN: W. Solbrig
  4 cy ATTN: J. Lehman

General Electric Co
        ATTN: M. Bortner
        ATTN: A. Harcar

General Research Corp
        ATTN: J. Garbarino
        ATTN: J. Ise, Jr

University of Illinois
        ATTN: Scty Supervisor for K. Yeh

Institute for Defense Analyses
        ATTN: E. Bauer
        ATTN: H. Wolfhard
        ATTN: J. Aein
        ATTN: J. Bengston

International Tel & Tel Corp
        ATTN: Tech Lib
        ATTN: G. Wetmore

JAYCOR
        ATTN: J. Sperling

Johns Hopkins University
        ATTN: T. Potemra

Kaman Tempo
        ATTN: DASIAC
        ATTN: T. Stephens
        ATTN: W. McNamara
        ATTN: W. Knapp

DEPARTMENT OF DEFENSE CONTRACTORS (Continued)

M.I.T. Lincoln Lab
    ATTN: D. Towle

Mission Research Corp
    ATTN: S. Gutsche
    ATTN: R. Bogusch
    ATTN: R. Hendrick
    ATTN: R. Kilb
    ATTN: F. Fajen
    ATTN: Tech Lib
    ATTN: D. Sappenfield

Mitre Corp
    ATTN: G. Harding
    ATTN: C. Callahan
    ATTN: A. Kymmel
    ATTN: B. Adams

Mitre Corp
    ATTN: J. Wheeler
    ATTN: M. Horrocks
    ATTN: W. Hall
    ATTN: W. Foster

Pacific-Sierra Rsch Corp
    ATTN: H. Brode

Pennsylvania State University
    ATTN: Ionospheric Rsch Lab

Physical Dynamics, Inc
    ATTN: E. Fremouw

Physical Research, Inc
    ATTN: R. Deliberis

R & D Associates
    ATTN: R. Lelevier
    ATTN: C. Greifinger
    ATTN: B. Gabbard
    ATTN: M. Gantsweg
    ATTN: R. Turco
    ATTN: W. Wright
    ATTN: W. Karzas
    ATTN: F. Gilmore
    ATTN: H. Ory
    ATTN: P. Haas

R & D Associates
    ATTN: B. Yoon

Rand Corp
    ATTN: E. Bedrozian
    ATTN: C. Crain

Science Applications, Inc
    ATTN: L. Linson
    ATTN: C. Smith
    ATTN: D. Hamlin
    ATTN: E. Straker

SRI International
    ATTN: R. Leadabrand
    ATTN: R. Livingston
    ATTN: D. Neilson
    ATTN: J. Petrickes
    ATTN: C. Rino
    ATTN: G. Price
    ATTN: R. Tsunoda
    ATTN: A. Burns
    ATTN: M. Baron
    ATTN: G. Smith
    ATTN: W. Chesnut
    ATTN: W. Jaye

Sylvania Systems Gp
    ATTN: R. Steinhoff

Technology International Corp
    ATTN: W. Boquist

Tri-Com, Inc
    ATTN: D. Murray

Utah State University
    ATTN: J. Dupnik
    ATTN: K. Baker
    ATTN: L. Jensen

DATE FILMED

2-8